

CARDIFF
UNIVERSITY

PRIFYSGOL
CAERDYDD

**Investigation of No-load and on-load performance of a
model three-phase transformer core operating under
sinusoidal and PWM voltage excitation**

By

Nabiel Mahmoud Dgali

Thesis submitted in fulfilment of the requirement for the degree
of Doctor of Philosophy

Wolfson Centre for Magnetics

School of Engineering, Cardiff University

Acknowledgments

The work was carried out at the Wolfson Centre for Magnetic Technology, Department of Electrical and Electronic Engineering, Cardiff University. And thanks to Dr Fatih Anayi for readily allowing me the use of the facilities of the Department.

I wish to express my profound gratitude to my supervisor, Dr Fatih Anayi for his guidance, assistance, encouragement and his vast knowledge and skills in many areas, and his advice during the period of my research.

Besides my supervisor, I would like to express my special thanks to Dr Yevgen Melikhov for his advice during the course of my study. And thank the other members of Wolfson Centre, Dr Philip Anderson and Dr Turgut Meydan for their advice and comments at all levels of my research. I would also like to thank Mrs Christine Lee, Mrs Aderyn Reid, Ms Jeanette C Whyte, in research office and Mr Denley Slade and David Billings in electronic workshop and Mr Steve Mead, Mr Malcolm Seaborne, Mr Andrew Rankmore and Mr Mal lyall in mechanical workshop for taking time out from their busy schedule to help and support my project during my study in Cardiff University.

Finally, my greatest thanks go to my family, for their unconditional love, support and encouragement in whole my life.

Summary

The iron losses in transformer laminated cores is higher than the nominal losses of the material itself by a factor known as the building factor. Reduction of the building factor of a transformer core is as important as the improvement of the basic properties of the material. In this investigation grain oriented 100 kVA three-phase distribution transformer core was investigated in order to obtain detailed study of losses. The core used in this study has overall dimensions of 540 mm in length and 520 mm in width. The core was built of 120 laminations as single joint three lamination per stacking layer with length of overlap shift of 3 mm and density of 7650 kg/m^3 . The core has the [011] [100] texture which is known as the Goss texture or Cube-on edge texture. This study considers four aspects of losses and localised magnetostriction on transformer core.

Firstly, the power loss under sinusoidal and PWM excitation in the three-phase transformer core which was made up of 3% silicon Highly Grain-Oriented material (HGO) was measured. Also, the power loss of Epstein strips at various flux density and frequencies was measured. In addition, localised and overall flux density distributions in depth under sinusoidal and PWM excitation conditions in the transformer core at core flux densities of 0.4T, 0.6T and 1.0T under load and no-load conditions were measured.

Secondly, the effect of the clamping pressure on overall and localised power loss was determined under sinusoidal and PWM voltage excitations. The results showed that the loss under PWM voltage excitation increased by 10-30% as the flux density is increased. Further, the shape of the excitation voltage as well as the switching frequency spectrum and modulation index values also played a major role in the power loss.

Thirdly, the influence of localised magnetostriction on the three-phase transformer core was investigated under sinusoidal and PWM voltage excitations by measuring the mechanical strain distribution in the transformer core under different peak flux densities. The investigation showed that increasing the peak flux density from 0.4T to 1.0T increased localised magnetostriction where the largest localised magnetostriction was obtained at the T-joints.

Investigation of No-load and on-load performance of a model three-phase transformer core operating under sinusoidal and PWM voltage excitation

Finally, using MATLAB environment comparisons have also been made between the results obtained from sinusoidal and PWM inverter. These results showed that the localised and overall power loss increased considerably under PWM voltage excitation. Comparisons have also been made between practical core and the simulated model magnetic core results. These results showed that lower power losses occurred under simulated results because the model core had zero flux leakage.

List of Abbreviation and Nomenclatures

Abbreviations

B	Flux density
CGO	Conventional grain oriented
DAQ	Data acquisition
H	Magnetic field
HGO	High permeability grain oriented
L	Length
LDR	Laser scribed domain refined
M	Magnetization
PWM	Pulse width modulation
RMS	Root mean square
RD	Rolling direction
SST	Single strip/ sheet tester
TD	Transvers direction
THD	Total harmonic distortion
V	Voltage

Subscripts

x	Variables in the RD
y	Variables in the TD

Symbols

ϕ	Flux density
ϕ_{pk}	Peak flux density
μ	Permeability

Investigation of No-load and on-load performance of a model three-phase transformer core operating under sinusoidal and PWM voltage excitation

K_h	Hysteresis loss constant
l	Sample length
Δl	Change in length
m	Flux density of the material
μ_o	Permeability of free space
M	Magnetisation
M_s	Saturation magnetisation
M_r	Remnant magnetisation
N_s	Number of step laps
N_1, N_2	Number of turns of the primary and secondary windings
P_{ave}	Average power loss per cycle
P_{cl}	Loss due to eddy currents in electrical steel laminations
P_h	Loss due to hysteresis in electrical steel laminations
P_{ex}	Excess loss in electrical steel lamination
P_s	Specific power loss
P_x	Specific power loss component along RD
P_y	Specific power loss component along TD
P_{total}	Overall power loss
R_s	Shunt resistance
R_o	Strain gauge resistance
t	Time
V_1, V_2, V_3	Secondary phase voltage in 3-phase, 3-limb, transformer core
V_{rms}	Root mean square value of the secondary voltage

Investigation of No-load and on-load performance of a model three-phase transformer core operating under sinusoidal and PWM voltage excitation

V^2_{rms}	Overall <i>rms</i> voltage
$V_{rms}(1st)$	Fundamental voltage harmonic components
V_{av}	Average value of the secondary voltage
$V_{control}$	Amplitude of Sinusoidal signal
V_{tri}	Amplitude of carrier voltage signal
σ	Conductivity of magnetic core
d	Thickness of the lamination sheet
m_a	Modulation index
m_f	Frequency modulation ratio
N_{m^2}	Clamping pressure
E_λ	Saturated magnetostriction
ϵ_L, ϵ_T	Young's module in the rolling and transvers direction
χ	Magnetic susceptibility
λ	Magnetostriction
λ_{rd}	Magnetostriction in the RD
λ_{td}	Magnetostriction in the TD
ϵ	Strain

Table of contents

Declaration.....	ii
Acknowledgments.....	ii
Summary	iii
List of Abbreviation and Nomenclatures	v
Table of contents	xvi
List of figures	xviii
List of tables.....	xxv
1. Introduction.....	1
1.1.1 Parameters of magnetic field.....	1
1.1.2 Ferromagnetic and non-ferromagnetic materials	2
1.1.3 Short survey of ferromagnetism.....	3
1.1.4 Basic properties	4
1.2 Transformer core materials	5
1.2.1 Development of silicon-iron alloys	6
1.2.2 Coatings	8
1.2.3 Stress sensitivity.....	8
1.2.4 Mechanical stress	9
1.3 Transformer core design and coating.	9
1.3.1 Transformer cores corner joints	13
1.3.2 Cross-section of transformer cores.....	15
1.3.3 Flux density harmonics	17

Investigation of No-load and on-load performance of a model three-phase transformer core operating under sinusoidal and PWM voltage excitation

1.3.4	Core performance.....	17
1.4	Power loss in silicon-iron transformer cores.....	17
1.4.1	Power loss due to core materials.....	18
1.4.2	Power loss due to construction of the cores.....	18
1.4.3	Magnetostriction in ferromagnetic material.....	18
1.4.4	Previous related work.....	21
1.4.5	Aims of the Investigation.....	22
CHAPTER 2	24
2.	Type of the transformer core materials.....	24
2.1.1	Grain oriented steel.....	24
2.1.2	Non- oriented steel.....	24
2.1.3	Laser scribed domain refined (LDR).....	25
2.2	Transformer theory and performance.....	26
2.2.1	Overall flux density measurement under sinusoidal excitation.....	28
2.2.2	Overall flux density measurement under PWM voltage excitation.....	30
2.2.3	Fundamental theory of localised power loss measurement in transformer cores.....	31
2.2.4	Total iron losses using loss separation criteria.....	32
2.3	Hysteresis losses.....	33
2.3.1	Eddy current losses.....	35
2.3.2	Anomalous loss.....	36
2.3.3	Theory of estimates of iron loss components using loss separation criteria.....	38
2.3.4	Flux density distribution.....	39
2.4	Overall flux density distribution under sinusoidal voltage excitation.....	40

Investigation of No-load and on-load performance of a model three-phase transformer core operating under sinusoidal and PWM voltage excitation

2.4.1	Overall flux density distribution under PWM voltage excitation	43
2.4.2	Field and flux measurement method	45
2.4.3	Magnetic field measurement	45
2.4.4	H -coil construction and calibration	45
CHAPTER 3		48
3.	Pulse width modulation (PWM).....	48
3.1.1	Modulation index	49
3.1.2	Switching frequency.....	49
3.1.3	Voltage source inverter	50
3.1.4	Current source of PWM inverter.....	51
3.2	Magnetizing current variation under PWM voltage excitation	52
3.2.1	Magnetizing current variation under sinusoidal voltage excitation	57
3.2.2	Comparison of the results	62
3.2.3	Effect of switching frequency on overall flux density	64
3.3	Overall power losses under sinusoidal waveform.....	67
3.3.1	Setup of the measurement of overall power loss	67
3.3.2	Effect of clamping pressure	74
3.3.3	Analysis and discussion	75
3.3.4	Order harmonic content with a change in peak flux density.....	75
CHAPTER 4		78
4.	Experimental apparatus and measuring technique	78
4.1.1	Core geometry	78
4.1.2	Type of joints	80
4.1.3	Support and clamping	80

Investigation of No-load and on-load performance of a model three-phase transformer core operating under sinusoidal and PWM voltage excitation

4.2	Localised flux density calculation	83
4.2.1	Localised flux density measurement	84
4.2.2	Construction and positioning of search coils	85
4.2.3	Calibration and testing of search coils	85
4.2.1	Measurement preparation	86
4.3	Measurement results of localised power loss	88
4.3.1	Comparison of the results	107
4.3.2	Localised power loss obtained in the outer limb of the model three-phase transformer core with various peak flux densities	108
4.3.3	Localised power loss obtained in the middle limb of the model three-phase transformer with various peak flux densities	112
4.3.4	Comparison between localised power loss obtained in the middle of the outer and central limbs of the model three-phase transformer core with various peak flux densities	115
4.3.5	Localised power loss obtained in the limb corner joints of the model three-phase transformer core with various peak flux densities	116
4.3.6	Localised power loss obtained in the yoke corner joints of the model three-phase transformer core with various peak flux densities	118
4.3.7	Comparison between localised power loss obtained in the limb and yoke corner joints of the model three-phase transformer core with various peak flux densities	121
4.3.8	Localised power loss obtained in the yoke- 45° joints with various peak flux densities	122
4.3.9	Localised power loss obtained in the limb T joints with various peak flux densities	126
4.3.10	Comparison between power loss obtained in the limb and yoke T joints with various peak flux densities	129

Investigation of No-load and on-load performance of a model three-phase transformer core operating under sinusoidal and PWM voltage excitation

4.3.11	Influence of modulation index and switching frequency on total power loss in three-phase transformer core.	131
4.3.12	Analysis and discussion	133
CHAPTER 5		134
5.	Introduction	134
5.1.1	Magnetostriction λ	134
5.1.2	Domain wall and spontaneous magnetostriction.....	135
5.1.3	Saturation magnetostriction	136
5.1.4	Transformer noise	137
5.2	Winding noise.....	137
5.2.1	Fans and pump noise	137
5.2.2	Magnetic core vibration	137
5.2.3	Core construction and design	137
5.2.4	Magnetostriction characteristic under applied field.....	138
5.3	Method used to measure magnetostriction	139
5.3.1	Piezoelectric displacement transducer	139
5.3.2	Linear variable differential transformer	140
5.3.3	Capacitive displacement sensors.....	141
5.3.4	Laser Doppler techniques.....	141
5.4	Pro foils strain gauges	142
5.4.1	Three-wire strain gauge rosettes pre-wired.....	143
5.4.2	Strain data logger	144
5.4.3	Strain gauge sample preparation	146
5.4.4	Magnetostriction calculation.....	152
5.5	Investigation of localised magnetostriction within transformer core.....	153

Investigation of No-load and on-load performance of a model three-phase transformer core operating under sinusoidal and PWM voltage excitation

5.5.1	Stress	158
5.5.2	Stress calculation.....	158
5.5.3	Noise and vibration phenomena in transformer core	159
5.5.4	Influence of magnetic flux density on transformer core magnetostriction and vibration.....	160
5.6	Core vibration and sound level measurement (SPL).....	160
5.6.1	Analysis and Discussion	161
5.6.2	Localised magnetostriction under PWM and sinusoidal voltage excitation in three-phase transformer core in horizontal position.....	161
5.6.3	Localised magnetostriction under PWM and sinusoidal voltage excitation in three-phase transformer core in vertical position.....	164
CHAPTER 6		166
6.	Measurement with the Epstein Frame.....	166
6.1.1	Single Strip Tester measurement	168
6.1.2	Power loss in electrical steel based on two-term formula.....	172
6.1.3	Power loss in electrical steel based on three-term formula.....	173
6.2	Loss separation using extrapolation method based on the two-term formulation.....	173
6.2.1	Loss separation using extrapolation method based on the three-term formulation.....	174
6.2.2	Experimental results under PWM voltage excitation at 0.4 T	175
6.2.3	Experimental results under PWM voltage excitation at 1.0 T	178
6.2.4	Experimental results under sinusoidal voltage excitation at 0.4T.....	180
6.3	Experimental results under sinusoidal voltage excitation at 1.0 T	182
6.3.1	Comparison of the results	186
7.	CHAPTER 7	187

Investigation of No-load and on-load performance of a model three-phase transformer core operating under sinusoidal and PWM voltage excitation

7.1.1	MATLAB block diagram contents.....	187
7.1.2	Simulation under sinusoidal voltage excitation	188
7.1.3	Simulation under PWM voltage excitation	190
7.1.4	Total harmonic distortion under sinusoidal voltage excitation	192
7.2	Total Harmonic Distortion, THD under PWM Voltage Excitation	194
7.2.1	Total harmonic contents with a change in switching frequency	197
7.2.2	Harmonic analysis	199
7.2.3	Power loss analysis	200
7.2.4	Specific losses with a change in PWM modulation index	202
7.2.5	Total losses with a change in PWM switching frequency	204
7.2.6	Summary	206
CHAPTER 8	207
8.	Conclusion and suggestion for future work	207
8.1.1	Conclusion	207
8.1.2	Suggestion for future work.....	209

List of figures

Fig. 1-1 Domain pattern under magnetizing process.....	3
Fig. 1-2 Hysteretic magnetisation of grain oriented electrical steel [4].....	5
Fig. 1-3 Schematic diagram of square orientation.....	7
Fig. 1-4 Effect of stress on domain pattern	8
Fig. 1-5 Different cores structures.....	10
Fig. 1-6 Forms of cores built from wound strips. (a) Single-phase core type. (b) Single-phase shell type. (c) Three-phase core type	11
Fig. 1-7 (a,b) Three phase transformer core with involute legs and Symmetrical magnetic system	12
Fig. 1-8 Square joint.....	13
Fig. 1-9 350/550 Miter joint.....	13
Fig. 1-10 Mitred corners.....	14
Fig. 1-11 Step-lap joint	14
Fig. 1-12 450 Mitre joints	15
Fig. 1-13 Cross sectional area of transformer core – limbs.....	16
Fig. 1-14 Magnetic domain wall in ferromagnetic materials	19
Fig. 1-15 Effect of magnetostriction (a) zero field (b) applied field	20
Fig. 2-1 Ideal single-phase transformer core [3]	26
Fig. 2-2 Positions of the localised search coils.....	39
Fig. 2-3 Position of the reference search coils	41
Fig. 2-4 Variation of the induced voltage against time under sinusoidal waveform in the transformer limb at 0.4T	42
Fig. 2-5 Variation of the induced voltage against time under sinusoidal waveform in the transformer yoke at 0.4T.....	42

Investigation of No-load and on-load performance of a model three-phase transformer core operating under sinusoidal and PWM voltage excitation

Fig. 2-6 variation of the overall flux density against time (ms) before the integrator circuit	43
Fig. 2-7 variation of the overall flux density against time (ms) after integrator circuit	43
Fig. 2-8 Schematic diagram of solenoid system.....	46
Fig. 2-9 Voltage vs magnetic field with assign value of flux density	47
Fig. 3-1 . PWM waveform generators [3]	48
Fig. 3-2 Three-phase PWM inverter voltage configuration circuit [4].....	50
Fig. 3-3 Schematic diagram of controlled current S1, S2 Switch. L: Inductance R: Resistor [1]	51
Fig. 3-4 Block diagram for measuring magnetising current	52
Fig. 3-5 Variation of magnetizing current at 0.3T in the outer limb with assigned values of switching frequency.....	53
Fig. 3-6 Variation of magnetizing current at 0.3T in the middle limb with assigned values of switching frequency.....	53
Fig. 3-7 Variation of magnetizing current at 0.4T in the outer limb with assigned values of switching frequency.....	54
Fig. 3-8 Variation of magnetizing current at 0.4T in the central limb with assigned values of switching frequency.....	54
Fig. 3-9 Variation of magnetising current at 0.7T in the middle limb with assigned values of switching frequency.....	55
Fig. 3-10 Variation of magnetising current at 0.7T in the outer limb with assigned values of switching frequency.....	56
Fig. 3-11 Variation of magnetising current under three-phase variac under no-load condition at 0.3T	59
Fig. 3-12 Variation of magnetising current under three-phase variac under load condition at 0.3T	59
Fig. 3-13 Variation of magnetising current under sinusoidal voltage excitation under no-load Condition at 0.4T	60
Fig. 3-14 Variation of magnetising current under sinusoidal voltage excitation under Load Condition at 0.4T	60

Investigation of No-load and on-load performance of a model three-phase transformer core operating under sinusoidal and PWM voltage excitation

Fig. 3-15 Variation of magnetising current under sinusoidal voltage excitation under no-load Condition at 0.7T	61
Fig. 3-16 Variation of magnetising current under sinusoidal voltage excitation under load Condition at 0.7T	61
Fig. 3-17 Overall induced voltage under PWM voltage excitation (no-load conditions) with switching frequency varied from 2 to 3 kHz at different peak flux density (T).....	65
Fig. 3-18 Overall induced voltage under PWM voltage excitation (load conditions) with switching frequency varied from 2 to 3 kHz at different peak flux density (T).....	65
Fig. 3-19 Overall induced voltage under PWM voltage excitation (load conditions) with switching frequency varied between 8, 12, 16 kHz at different peak flux density (T)	66
Fig. 3-20 Overall induced voltage under PWM voltage excitation (load conditions) with switching frequency varied between 12, 16 kHz at different peak flux density (T)	66
Fig. 3-21 Overall power loss measurement system.....	68
Fig. 3-22 Overall power loss at clamping pressure of 0 N/m^2 under no-load condition at different flux densities.....	69
Fig. 3-23 Overall power loss at clamping pressure of 8 N/m^2 under no-load condition at different flux densities.....	69
Fig. 3-24 Overall power loss at clamping pressure of 15 N/m^2 under no-load condition at different flux densities	70
Fig. 3-25 Overall power loss at clamping pressure of 27 N/m^2 under no-load condition at different flux densities.....	70
Fig. 3-26 Overall power loss at clamping pressure of 0 N/m^2 under load condition at different flux densities.....	72
Fig. 3-27 Overall power loss at clamping pressure of 8 N/m^2 under Load Condition at different flux densities.....	72
Fig. 3-28 Overall power loss at clamping pressure of 15 N/m^2 under load condition at different flux densities.....	73

Investigation of No-load and on-load performance of a model three-phase transformer core operating under sinusoidal and PWM voltage excitation

Fig. 3-29 Overall power loss at clamping pressure of 27 N/m ² under load condition at different flux densities.....	73
Fig. 4-1 (a) Dimension of the middle limb. (b) Dimensions of the outer limb (c) Dimensions of the yoke.....	79
Fig. 4-2 Three-phase transformer core	80
Fig. 4-3 Photograph of magnetising and associated measurement system.....	82
Fig. 4-4 Block diagram of virtual instrument for calculating magnetic flux density	87
Fig. 4-5 Locations of localised search coils in the outer limb	91
Fig. 4-6 Locations of the search coils in the outer limb corner joint, rolling (R) and transvers Directions (T).....	94
Fig. 4-7 Locations of the search coils in the outer yoke corner joint, rolling (RD) and transfer directions (TD).....	97
Fig. 4-8 Locations of the search coils in the middle limb	100
Fig. 4-9 Locations and direction of the search coils in the T-joint.....	103
Fig. 4-10 Locations and directions of the search coils in the T-joint R and T directions.....	106
Fig. 4-11 Comparison of localised power loss under sinusoidal and PWM voltage excitations (No-load condition) at the center of the outer limb at various peak flux densities (T), 50 Hz.	111
Fig. 4-12 Comparison of localised power loss under sinusoidal and PWM voltage excitations (Load condition) at the center of the outer limb at various peak flux densities (T), 50 Hz.	111
Fig. 4-13 Comparison of localised power loss under sinusoidal and PWM voltage excitation (No-load condition) central limb at various peak flux densities (T), 50 Hz	114
Fig. 4-14 Comparison of localised power loss under sinusoidal and PWM voltage excitation (Load condition) central limb at various peak flux densities (T), 50 Hz	114
Fig. 4-15 Comparison of localised power loss under sinusoidal and PWM voltage excitation (No-load condition) at limb corner joints at various peak flux densities (T), 50 Hz.	117

Investigation of No-load and on-load performance of a model three-phase transformer core operating under sinusoidal and PWM voltage excitation

Fig. 4-16 Comparison of localised power loss under sinusoidal and PWM voltage excitation (Load condition) at limb corner joints at various peak flux densities (T), 50 Hz.	118
Fig. 4-17 Comparison of localised power loss under sinusoidal and PWM voltage excitation (no-load condition) at yoke corner joints at various peak flux densities (T), 50 Hz.....	120
Fig. 4-18 Comparison of localised power loss under sinusoidal and PWM voltage excitation (Load condition) at various peak flux densities (T), 50 Hz.	121
Fig. 4-19 Comparison of localised distribution of power loss under sinusoidal and PWM voltage excitation (No-load condition) at various peak flux densities (T), 50 Hz	124
Fig. 4-20 Comparison of localised power loss under sinusoidal and PWM voltage excitation (Load condition) at various peak flux densities (T), 50 Hz	124
Fig. 4-21 Comparison of localised power loss under sinusoidal and PWM voltage excitation (No-load condition) at limb T-joints at various peak flux densities (T), 50 Hz.....	128
Fig. 4-22 Comparison of localised power loss under sinusoidal and PWM voltage excitation (Load condition) at limb T-joints at various peak flux densities (T), 50 Hz.....	128
Fig. 4-23 Total power loss under PWM voltage excitation with assigned value of modulation index at f_s 3 kHz.....	131
Fig. 4-24 Total power loss under PWM voltage excitation with assigned value of modulation index at f_s 2 kHz.....	132
Fig. 4-25 Total power loss under PWM voltage excitation with assigned value of modulation index at f_s 1 kHz.....	132
Fig. 5-1 Mechanism of magnetostriction	135
Fig. 5-2 Domain walls rotate to the applied field	138
Fig. 5-3 Magnetostriction measurement systems using piezoelectric transduces technique	139
Fig. 5-4 Schematic diagram of LVDT.....	140
Fig. 5-5 Block diagram of a laser doppler velocimeter	141
Fig. 5-6 Pro Foil strain gauge used to Measure magenetostriction	142

Investigation of No-load and on-load performance of a model three-phase transformer core operating under sinusoidal and PWM voltage excitation

Fig. 5-7 Shows 3-Wire Strain Gauge Rosettes Pre-wired	143
Fig. 5-8 Strain gauges measurement system	145
Fig. 5-9 Strain gauges measurement connection	147
Fig. 5-10 Positions of pro foil strain gauges selected position	148
Fig. 5-11 Positions of three-wire strain gauges Roesttes pre-wired	149
Fig. 5-12 Position of the robber placed around Pro-foil strain gauges	151
Fig. 5-13 Position of the robber placed around three- wire strain gauges Rosettes pre-wired	151
Fig. 5-14 Three-phase magnetic flux density waveforms [20].....	159
Fig. 6-1 Epstein frame and double overlapped joints	166
Fig. 6-2 Schematic diagram of computer-controlled Single Strip Tester (SST).....	169
Fig. 6-3 Measurement system of single strip tester	170
Fig. 6-4 Single strip tester	171
Fig. 6-5 Specific power loss per cycle versus square root of frequency at 0.4T under PWM voltage excitation.....	176
Fig. 6-6 Eddy current and hysteresis loss per cycle versus frequency (Hz) at 0.4T under PWM voltage excitation.....	177
Fig. 6-7 Specific power loss per cycle versus root of frequency at 1T under PWM voltage excitation	179
Fig. 6-8 Eddy current and hysteresis loss per cycle versus frequency (Hz) at 1T under PWM voltage excitation.....	179
Fig. 6-9 Specific power loss per cycle versus square root of frequency at 0.4T under sinusoidal voltage excitation.....	181
Fig. 6-10 Eddy current and hysteresis loss per cycle versus frequency (Hz) at 0.4T under sinusoidal voltage excitation	182

Investigation of No-load and on-load performance of a model three-phase transformer core operating under sinusoidal and PWM voltage excitation

Fig. 6-11 Specific power loss per cycle versus square root of frequency at 1T under sinusoidal voltage excitation.....	184
Fig. 6-12 Eddy current and hysteresis loss per cycle versus frequency (Hz) at 1T under sinusoidal voltage excitation	185
Fig. 7-1 Sinusoidal voltage excitation circuit under load condition	188
Fig. 7-2 Sinusoidal voltage excitation circuit under no-load condition.....	189
Fig. 7-3 PWM voltage excitation circuit under load condition	190
Fig. 7-4 PWM voltage excitation circuit under no-load condition	191
Fig. 7-5 Harmonic order content of primary current for sinusoidal supply voltage under no-load condition with different peak flux density (T)	192
Fig. 7-6 Harmonic order content of primary current for sinusoidal supply voltage under on-load condition with different peak flux density (T)	193
Fig. 7-7 Harmonic order content of primary voltage for sinusoidal supply voltage under no-load condition with different peak flux density (T)	193
Fig. 7-8 Harmonic order content of primary voltage for sinusoidal supply voltage under on-load condition with different peak flux density (T)	194
Fig. 7-9 Harmonic order content of primary current for PWM supply voltage under on-load condition with different peak flux density (T)	195
Fig. 7-10 Harmonic order content of primary current for PWM supply voltage under no-load condition with different peak flux density (T)	195
Fig. 7-11 Harmonic order content of secondary voltage for PWM supply voltage under on-load condition with different peak flux density (T)	196
Fig. 7-12 Harmonic order content of secondary voltage for PWM supply voltage under no-load condition with different peak flux density (T)	196
Fig. 7-13 Harmonic order contents of primary current for PWM supply voltage under on-load condition at switching frequency 3 kHz.....	197

Investigation of No-load and on-load performance of a model three-phase transformer core operating under sinusoidal and PWM voltage excitation

Fig. 7-14 Harmonic order contents of secondary voltage for PWM supply voltage under on-load condition at switching frequency 3 kHz.....	197
Fig. 7-15 Harmonic order contents of primary current for PWM supply voltage under on-load condition at switching frequency 5 kHz.....	198
Fig. 7-16 Harmonic order contents of secondary voltage for PWM supply voltage under on-load condition at switching frequency 5 kHz.....	198
Fig. 7-19 Overall power loss of three-phase transformer core supplied by sinusoidal and PWM waveforms with change in the peak flux density (T) at 50 Hz at $M_i= 0.5$ and $F_s= 3\text{kHz}$	201
Fig. 7-20 Total power losses of the three-phase transformer core supplied by PWM waveform with change in the modulation index at 3kHz switching frequency.....	202
Fig. 7-21 Total power losses of the three-phase transformer core supplied by PWM waveform with change in the modulation index at 2kHz switching frequency.....	203
Fig. 7-22 Total power losses of the three-phase transformer core supplied by PWM waveform with change in the modulation index at 1 kHz switching frequency.....	203
Fig. 7-23 Total power loss of the three-phase transformer core with change in switching frequency at constant modulation index of 0.5	204
Fig. 7-24 Total power loss of the three-phase transformer core with change in switching frequency at constant modulation index of 0.7	205
Fig. 7-25 Total power loss of the three-phase transformer core with change in switching frequency at constant modulation index of 1.0	205

List of tables

Table 2-1 Overall voltage calculation of desired peak flux density under sinusoidal excitation	29
Table 2-2 overall voltage calculation of desired peak flux density under PWM excitation	31
Table 2-3 saturation value of some material [3,5,6]	34
Table 2-4 Induced B (<i>rms</i>) in the reference search coil	41
Table 2-5 Variation of fundamental components of overall flux density in the limbs and yokes	44
Table 2-6 Output voltage and current from solenoid core	47
Table 3-1 Current required for desired flux density under no-load condition	58
Table 3-2 Current Required for Desired Flux Density under Load Condition	58
Table 3-3 Overall Power under No-load condition	68
Table 3-4 Overall power loss under load condition	71
Table 6-1 Power loss per cycle under PWM voltage excitation at 0.4 T at different magnetising frequencies	175
Table 6-2 Measured and total power loss component of Epstein size lamination under PWM voltage excitation at 0.4T with different magnetising frequencies	177
Table 6-3 Power loss per cycle under PWM voltage excitation at 1.0 T at different magnetising frequencies	178
Table 6-4 Measured and total power loss component of Epstein size lamination under PWM voltage excitation at 1.0 T with different magnetising frequencies	178
Table 6-5 Power loss per cycle under sinusoidal voltage excitation at 0.4 T at different magnetising frequencies	180
Table 6-6 Specific and total power loss of an Epstein size lamination under sinusoidal voltage excitation at 0.4T and different magnetising frequencies	180
Table 6-7 power loss per cycle at 1.0 T at different magnetising frequencies	183
Table 6-8 Specific and total power loss of an Epstein size lamination under sinusoidal voltage excitation at 1.0 T at different magnetising frequencies	183

CHAPTER 1

1. Introduction

Electrical steels are the most considered material in terms, of studying magnetic power loss performance under a particular peak flux density and magnetising frequency of 50 and 60 Hz. Magnetic permeability and magnetostriction of electrical steel is also considered as important properties. In this chapter fundamental terms in magnetic materials, magnetising process, magnetic power loss mechanisms in electrical steel, developing of transformer design and related issues have been discussed.

1.1.1 Parameters of magnetic field

The parameters of a magnetic field are the magnetic field strength, H, magnetic flux density, B, and magnetisation, M.

The magnetic field strength (H) is measured in amperes per meter ($\frac{A}{m}$). Magnetic field is the force which produces, or is associated with the magnetic induction at that point [1]. The magnetic flux density (B) is measured in Weber per meter square ($\frac{W}{m^2}$) or Tesla is a vector quantity that determines the induced *e.m.f.* The relationship between H and B in air is written as:

$$B = \mu_0 H \quad \dots (1.1)$$

Where μ_0 is the permeability of free space ($\mu_0 = 4\pi \times 10^{-7} \text{ H/m}$)

The magnetization, M, is measured in Weber per square meter (W/m^2) or Tesla (T) the three quantities relationships are,

$$B = \mu_0 (H + M) \quad \dots (1.2)$$

The magnetization (M) at any point in a magnetic field is a vector lying in the same direction as H at that point is directly proportional to the magnetic intensity within the material thus,

$$M = \chi H \quad \dots (1.3)$$

Where χ is the magnetic susceptibility of the material and is in turn a function of H . Substituting Eq. (1.3) in Eq. (1.2) and putting $1 + \chi = \mu_r$ where μ_r is the relative permeability, we get:

$$B = \mu_0 (H + M) = \mu_0 H + \mu_0 M$$

$$B = \mu_0 H + \mu_0 \chi H = \mu_0 H (1 + \chi) = \mu_0 \mu_r H \quad \dots (1.4)$$

μ_r in Electromagnetic units for free space is equal to 1. Magnetic circuit is usually solved in term of (B) and H, where M is seldom used, but when necessary, its value can be found from equation (1.3).

1.1.2 Ferromagnetic and non-ferromagnetic materials

Magnetic properties of all materials are divided into three types: diamagnetic, paramagnetic and ferromagnetic.

Diamagnetic materials are: copper, gold, silver and bismuth which have relative permeability (μ_r) slightly less than unity (for bismuth it is 0.99983). Their magnetic response is in opposition to the applied magnetic field.

Paramagnetic materials are: aluminium, platinum and manganese which have relative permeability (μ_r) slightly greater than unity (for platinum it is 1.00036). These materials exhibit weaker magnetisation (M) whose direction is aligned towards the magnetic field.

Ferromagnetic materials are: iron, cobalt and nickel those which have high values of relative permeability, up to 10^4 or even 10^6 .

In electrical engineering it is suffice to class all materials simply as ferromagnetic or non-ferromagnetic. The former includes materials of relative permeability many times greater than unity while the latter has relative permeability practically equal to unity. (μ_r) is used to classify the magnetic materials.

1.1.3 Short survey of ferromagnetism

Ferromagnetic materials are composed of many small regions or domains, each displaying a net magnetization [2], even under no external magnetic field magnetic domains line up. The magnetization vector of each domain point in a direction which depends on the elastic stresses present inside a given material and its crystal structure. As shown in Fig. 1-1 (A) under ordinary conditions the vectors of the individual domains re-directed at random and cancel their magnetic moment, thus leaving the samples as a whole with no resultant magnetization. When an external magnetic field is applied as shown in Fig. 1-1 (B) the domains become re-arranged, producing a net magnetization along the applied field. Continue to increase the applied magnetic field the spontaneous (M_S) rotate all domains in sample into one direction so the sample reach the saturation point as shown in (C). Owing to this, the resultant magnetic induction becomes many times greater than the applied magnetic field (by hundred or even hundred thousand times) [3].

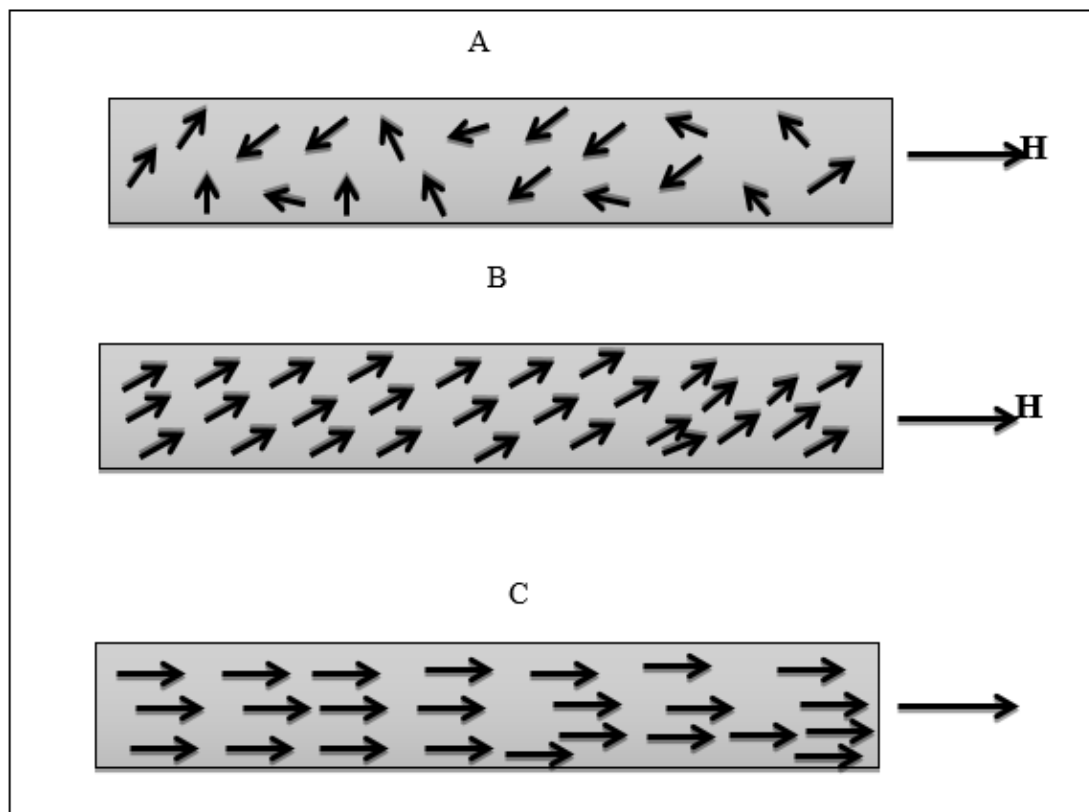


Fig. 1-1 Domain pattern under magnetizing process

Investigation of No-load and on-load performance of a model three-phase transformer core operating under sinusoidal and PWM voltage excitation

The most advantageous state for ferromagnetic materials is such that it is subdivided into many domains with their magnetic moments anti-parallel to one another. Then the total magnetostatics energy of the system will be a minimum.

1.1.4 Basic properties

The magnetic properties of ferromagnetic materials are conveniently represented by drawing curves of B against H. As shown in these are magnetization curves and hysteresis curves.

Ferromagnetic materials exhibit a hysteresis between the magnetic induction and the applied magnetic intensity [4] the phenomenon of hysteresis is analogous to mechanical inertia. This is due to the friction occurring in the domain wall. When external magnetic field applied net magnetisation in the material is not zero. This occurs by the movement of the domain wall to the direction of the applied field point 1 (red dots between point f and point b).

Increasing the applied field during the magnetisation domain walls rotate out of the easy axes of magnetisation into the direction of the applied field and reach the saturation value point (a). Since the domain is being moved from its original position to new a position this leads to production of magneto – static energy. For a material which has never been magnetized (virgin state), many cycles of magnetization may be required before a closed loop is obtained, the one obtained for H_{max} is referred to as the major hysteresis loop, and the material is said to be cyclically magnetized.

When the applied magnetising field is removed, the magnetic induction always lags behind the change in the applied H the magnetic induction is still near its saturation value point (b) remnant flux density. In order to reduce B to zero, a negative field called the coercive force must be applied point (c).

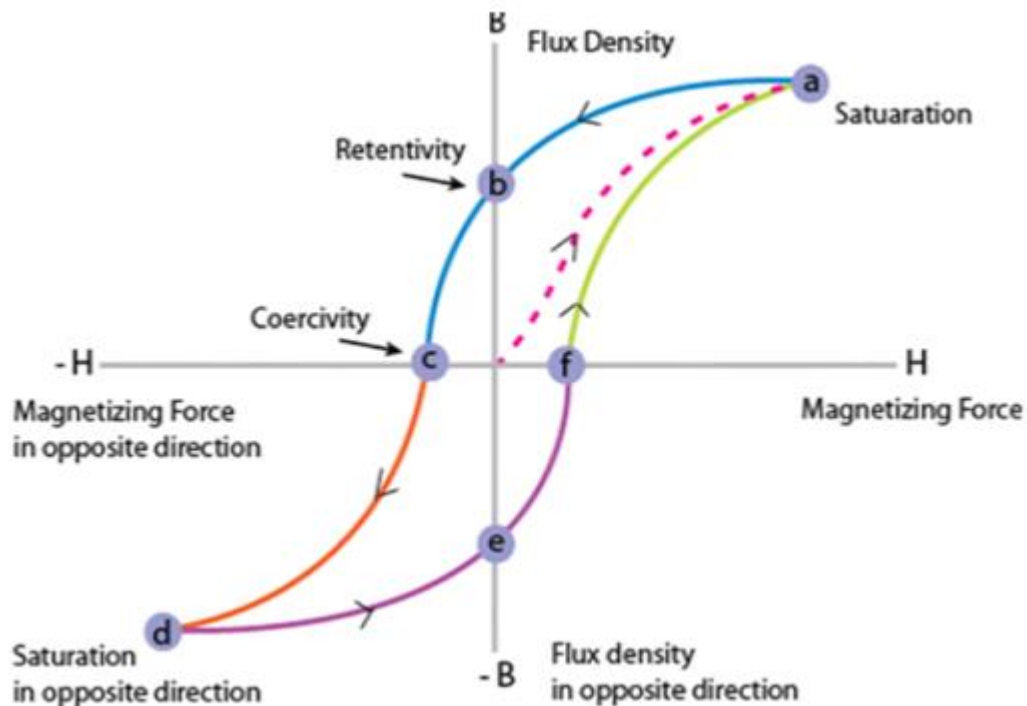


Fig. 1-2 Hysteretic magnetisation of grain oriented electrical steel [4]

1.2 Transformer core materials

There are essentially two main grades of electrical steels for use in power transformer: grain-oriented steel and non-oriented steel.

Non-oriented steels offer magnetic properties in a primarily random pattern with respect to the direction of rolling. An oriented material refers to the materials crystal structure with magnetic properties substantially better in the direction of rolling [5].

Two different grades are supplied by the manufacture, non-oriented non-silicon steel and non-oriented silicon steel, Both types of material can be supplied either fully processed or semi-processed. Semi-processed with or without a stress-relief annealing. Non-oriented electrical steels are made to final thickness of 0.35 mm, 0.50 mm or 0.65 mm. For special application, 1.0 mm thick laminations may be used. Non-oriented Si-Fe steel contains a range of silicon from about 0.5% to 3.2%. Adding silicon to the steel increase the resistivity and decrease the permeability of the steel and result in lower eddy current losses but increase the hysteresis losses if the amount of the steel exceeds 3.5%, the steel cannot be rolled in acceptable direction.

Investigation of No-load and on-load performance of a model three-phase transformer core operating under sinusoidal and PWM voltage excitation

Grain oriented 3% silicon steel used to build transformer cores and large rotating machines because it has very low iron losses. Moreover, the losses of the best grain-oriented steel are about 70% less than the best grades of non-oriented electrical steel.

In general, oriented electrical steels are more expensive than non-oriented steel but offer substantially better magnetic properties. For example, under certain conditions, the difference in the exciting currents for a favourable direction and an unfavourable direction in grain-oriented steels may be more than 20 times greater than the difference in case of the non-oriented steel [6].

1.2.1 Development of silicon-iron alloys

Early transformer cores were built using solid iron cores. In 1882 Hadfield observed the adding silicon to high purity steel can improve the coercive force and permeability which was accidentally produced [7].

Since 1903 silicon-iron alloys have been used in transformer cores and many research works have been carried out to reduce the core losses, minimise the eddy current and increase the permeability of the material. Silicon content of the steel is 3.2% by weight if the silicon is higher than 3.2% the steel become brittle and hard to assemble. However, the losses are now are approximately one third of what they were in 1910. In addition to improvement in power loss, there were great savings in space.

In 1934 the greatest drop in core loss was achieved by Goss [8] with the invention of ((Grain-Oriented Silicon Steel)). This process including heat treatment and cold rolling product. These treatments have been used to cultivation desired grain texture with a direction of easy magnetization parallel to the rolling direction, the magnetization should be in this direction, since in the transvers direction the loss is about three times greater [9].

Other method were developed [10, 11] to control the crystallization by processing silicon-iron sheet with certain purities, so that both rolling and transvers directions have easy magnetization and low loss (Four Square or Cube orientation (010) [100]). Fig. 1-3 progress in commercial production was also made [12, 13]. Various

Investigation of No-load and on-load performance of a model three-phase transformer core operating under sinusoidal and PWM voltage excitation

impurities which were used to control the recrystallization texture are: oxygen, sulphur, vanadium nitride and aluminium nitride [14].

Other method recently introduced is laser scribed domain refined (LDR) this method reducing the width of magnetic domain by laser irradiation process, this process reduce heat in the sheet.

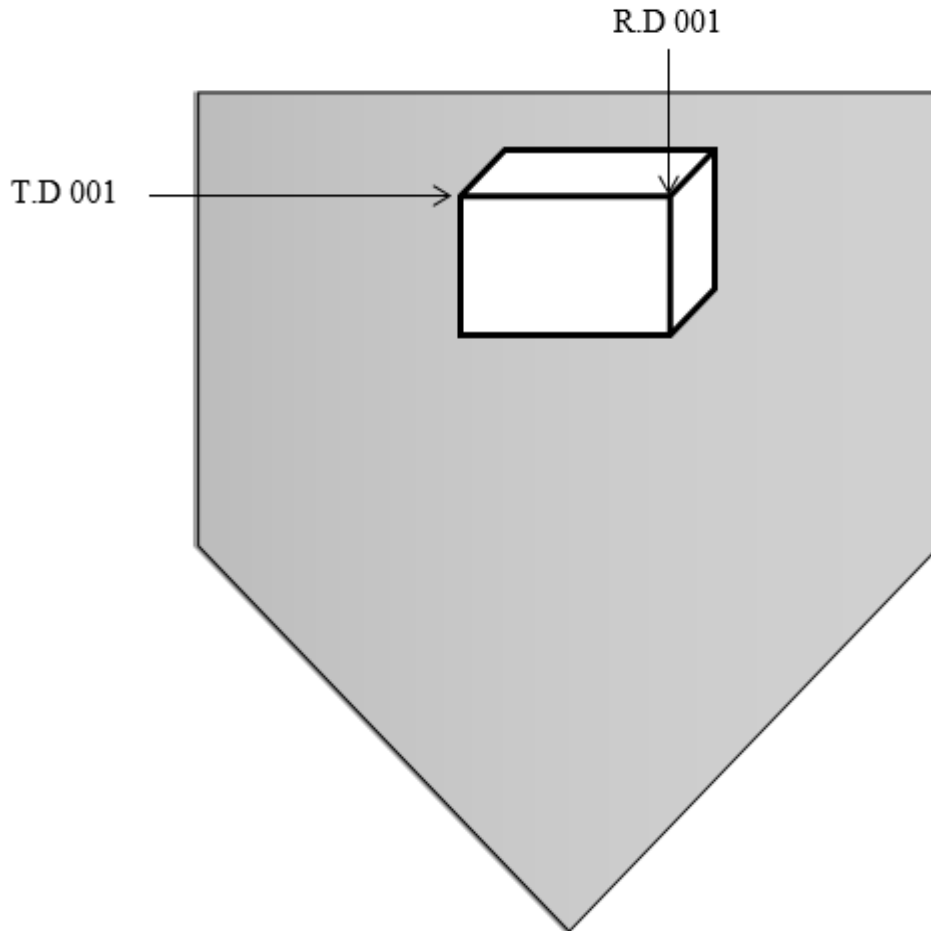


Fig. 1-3 Schematic diagram of square orientation

1.2.2 Coatings

Transformer laminations are coated on either side with thin layer of insulating coating [15] these coating helps to provide electrical insulation between the adjacent laminations and also prevent corrosion. On the other hand, coating produce stress and increase the core mass weight. Coatings can be made of inorganic material, a mixture of inorganic and organic materials. The typical coating thickness varies between $2\ \mu\text{m}$ to $5\ \mu\text{m}$.

1.2.3 Stress sensitivity

The magnetic properties of Goss-oriented steel are sensitive to stress. The effects of compressive stress along the rolling direction have been investigated by several authors [16] [17].

Corner and Mason [18] have shown that the increase in power loss is due to the change of the ideal ((bar domain)) which becomes difficult to magnetize and needs extra magnetization.

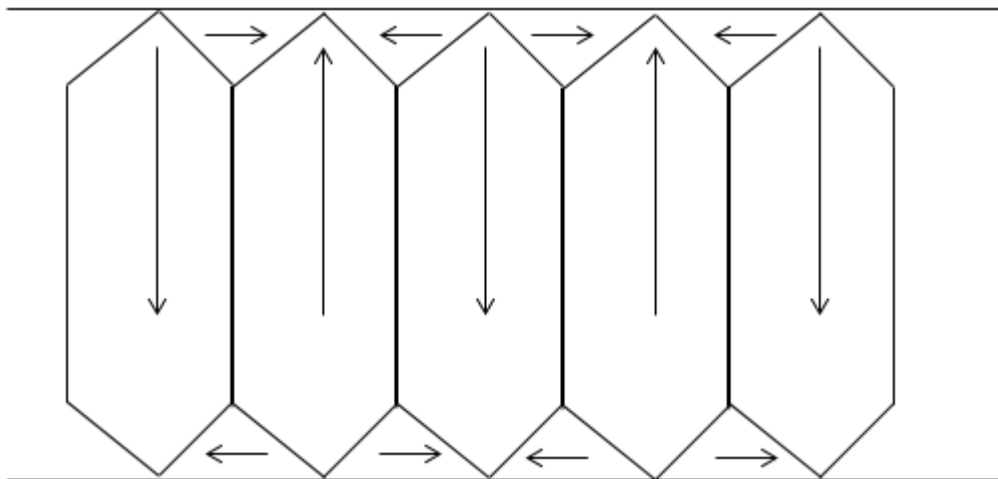


Fig. 1-4 Effect of stress on domain pattern

When stress is applied to the transformer core, some of the domain walls will be slightly misaligned. However, this domain movement is the primary generator of magnetostriction in the core. In commercial production this sensitivity of the steel to

compression has been overcome by using insulating coating which keeps the material under tension.

1.2.4 Mechanical stress

In the transformer cores, stresses are present, and it is very difficult to eliminate them. These stresses are presented due to:

- (1) Waviness of the laminations
- (2) Bending induced by the weight of the laminations
- (3) Clamping force
- (4) Temperature gradients due to non-uniform distribution of flux density

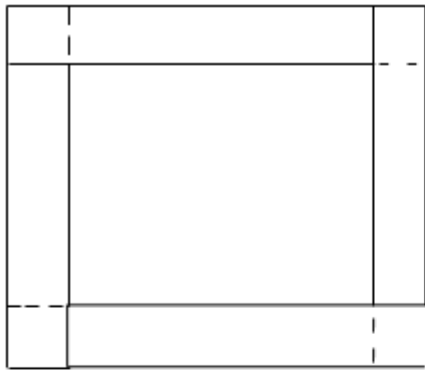
The effect of stress results in increasing power losses in transformer core [19]. In general, compressive stresses are the main causes of increasing power losses.

1.3 Transformer core design and coating.

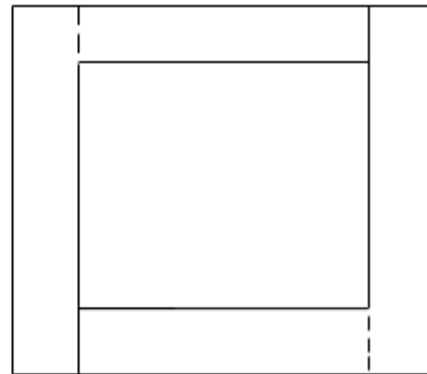
Laminated core

Transformer cores are always built of strip cut or punched from sheets of grain-oriented steel. Different core structures are generally used as shown in Fig. 1-5 yokes and limbs joints are always overlapped thus minimising the air gaps introduced into the magnetic circuit. All these cores are assembled by stacking the laminations and when completed, the core is clamped, and the upper yokes are removed. Then pre-wound coils slipped into place and the top yoke is built again in its previous place. The core is held together to avoid vibration and noise [6].

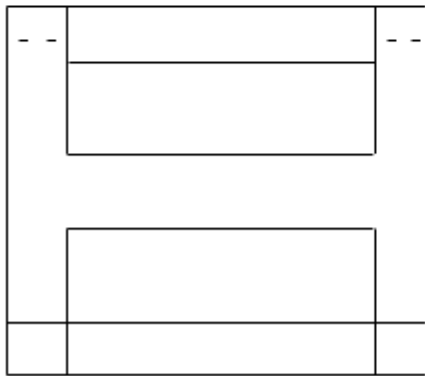
Investigation of No-load and on-load performance of a model three-phase transformer core operating under sinusoidal and PWM voltage excitation



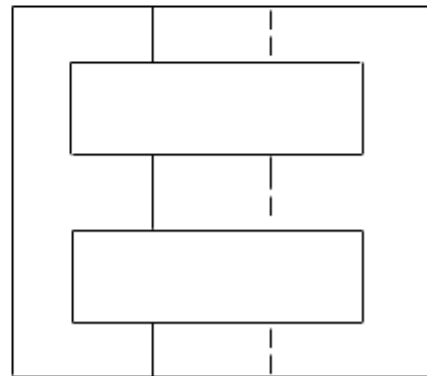
I Core



L Core



H and I Cores



E Core

Fig. 1-5 Different cores structures

Wound core

In order to direct the flux to flow in one direction, wound core was introduced. These types of core consist of spirals of silicon-iron strip wound by a machine. Then the core is annealed to relieve stress induced by the bending of the sheet. This type of cores can be used for single and three phase system, wound core build as core-type and shell type Fig. 1-6 shows types of cores.

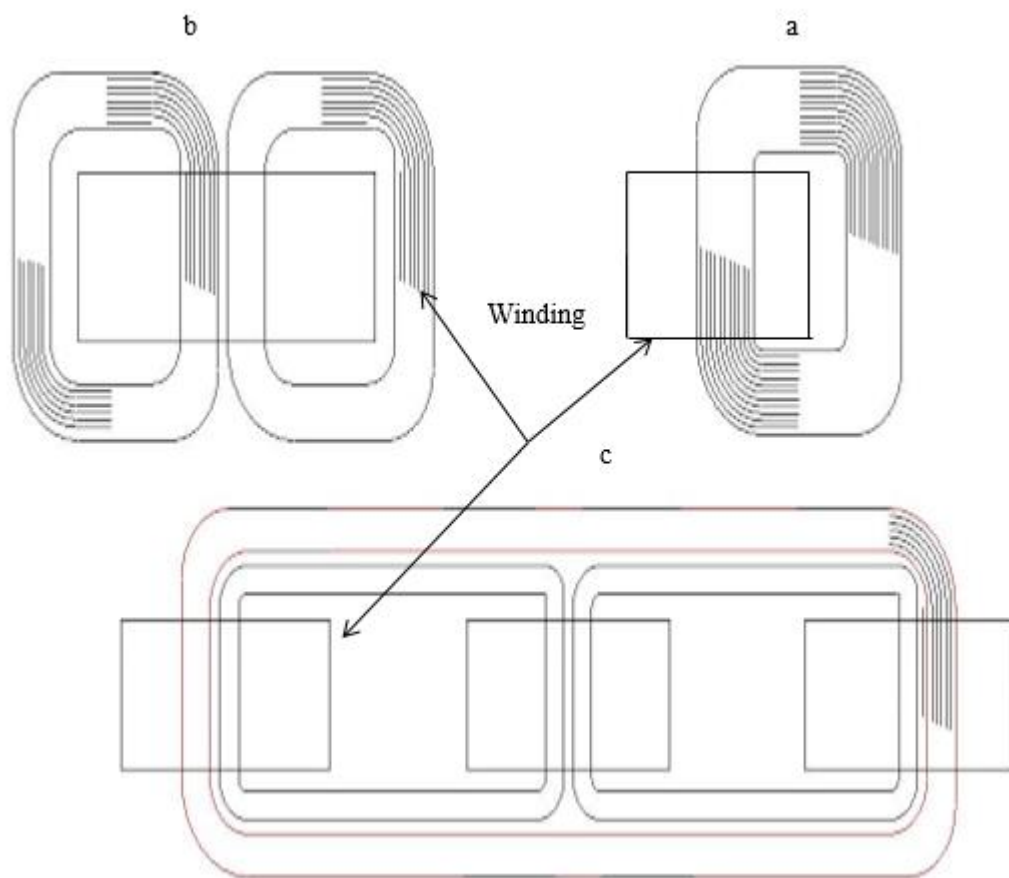


Fig. 1-6 Forms of cores built from wound strips. (a) Single-phase core type. (b) Single-phase shell type. (c) Three-phase core type

Investigation of No-load and on-load performance of a model three-phase transformer core operating under sinusoidal and PWM voltage excitation

Involute core

The first system had three limbs arranged uniformly in three plants along the circumference of the yoke. The limbs are constructed in an involute curve forming a thick-walled tube. Finally, core is formed by using triangular yokes at the top and bottom. These cores are stress-relief annealed and are held together by means of screws through the limbs as shown in Fig. 1-7. Experiment has been carried out on involute core, it was found that the instantaneous fluxes in the limbs differ 120° , and the flux in the yoke is less than the maximum flux in the limb by a factor of $\sqrt{3}$.

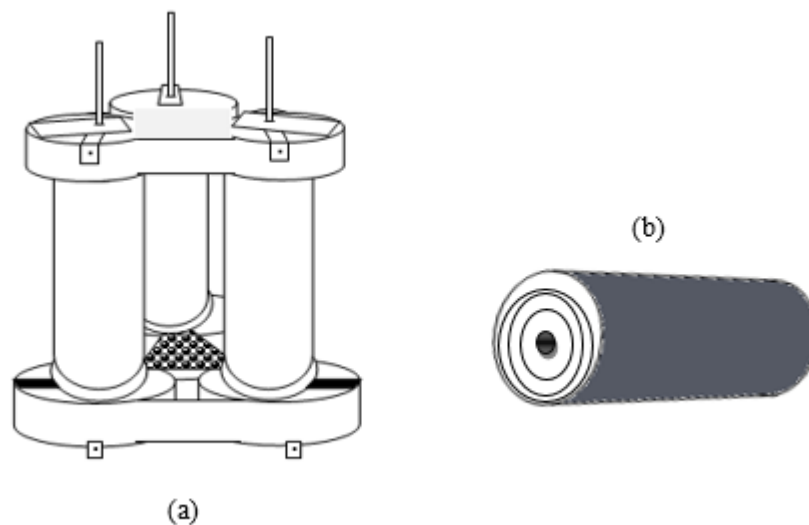


Fig. 1-7 (a,b) Three phase transformer core with involute legs and Symmetrical magnetic system

1.3.1 Transformer cores corner joints

Transformer core built up using various types of joints [20], [21]. Fig. 1-8 to Fig. 1-12 show transformer core joints. These joints link the limbs and the yokes. Nevertheless, as transformer joints introduce air gapes, hence flux concentration, cross fluxes, normal fluxes and rotational fluxes occur. The combination of these effects increases the undesirable power loss [22].

Stacking singles layers ensures minimum air gaps at the corner joints and T-joints because each layer is accurately positioned. This is more difficult with two layers stacked together and almost impossible with three layers. Also having two or three layers stacked in the same way causes increased joint losses, since the flux losses increase significantly and hence the eddy current losses increase.

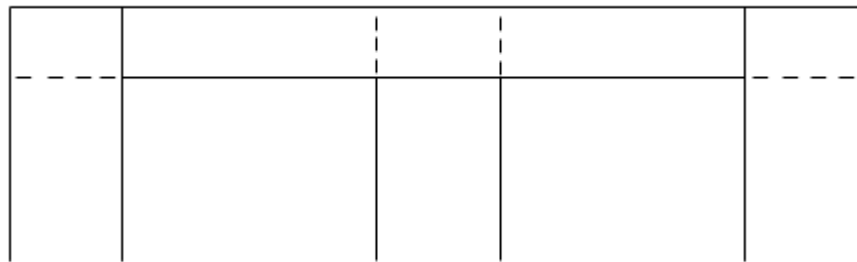


Fig. 1-8 Square joint

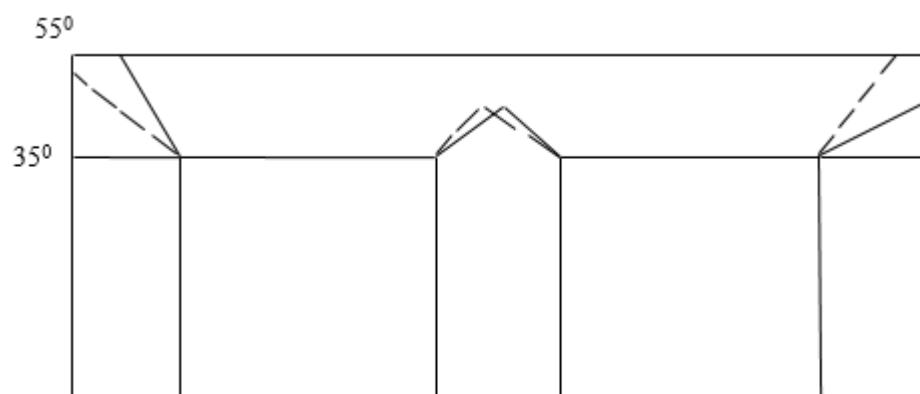


Fig. 1-9 350/550 Miter joint

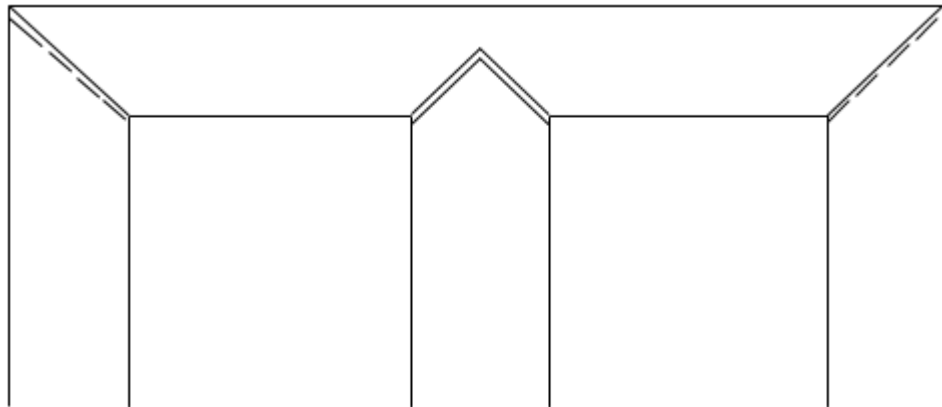


Fig. 1-10 Mitred corners

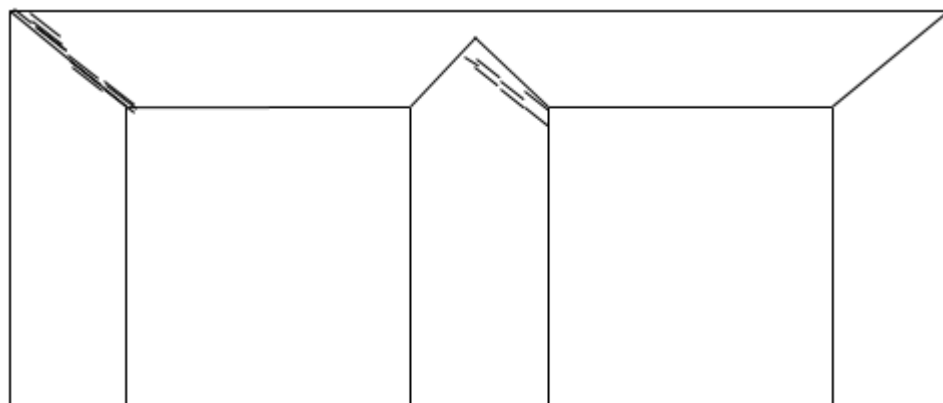


Fig. 1-11 Step-lap joint

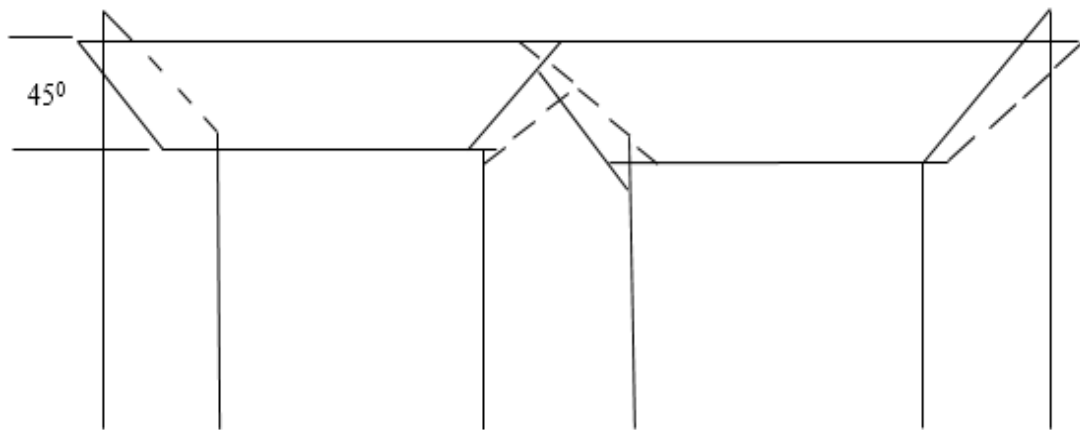


Fig. 1-12 450 Mitre joints

1.3.2 Cross-section of transformer cores

Transformer cores are built with different type of cross-sectional area, for example cores build with rectangular cross-section as shown in Fig. 1-13 (A). This type of cross section can be used for a small size transformer. Because it is wasteful to use magnetizing coils for rectangular cross-sections. So square cores maybe used as shown in Fig. 1-13 (B). But considerable amount of useful space is still wasted so a common improvement on square core is to employ cruciform core as shown in Fig. 1-13(C), which demands at least two sizes of core strips [23]. However, for large transformer core cross-section, more steps are used as shown in Fig. 1-13(D).

Investigation of No-load and on-load performance of a model three-phase transformer core operating under sinusoidal and PWM voltage excitation

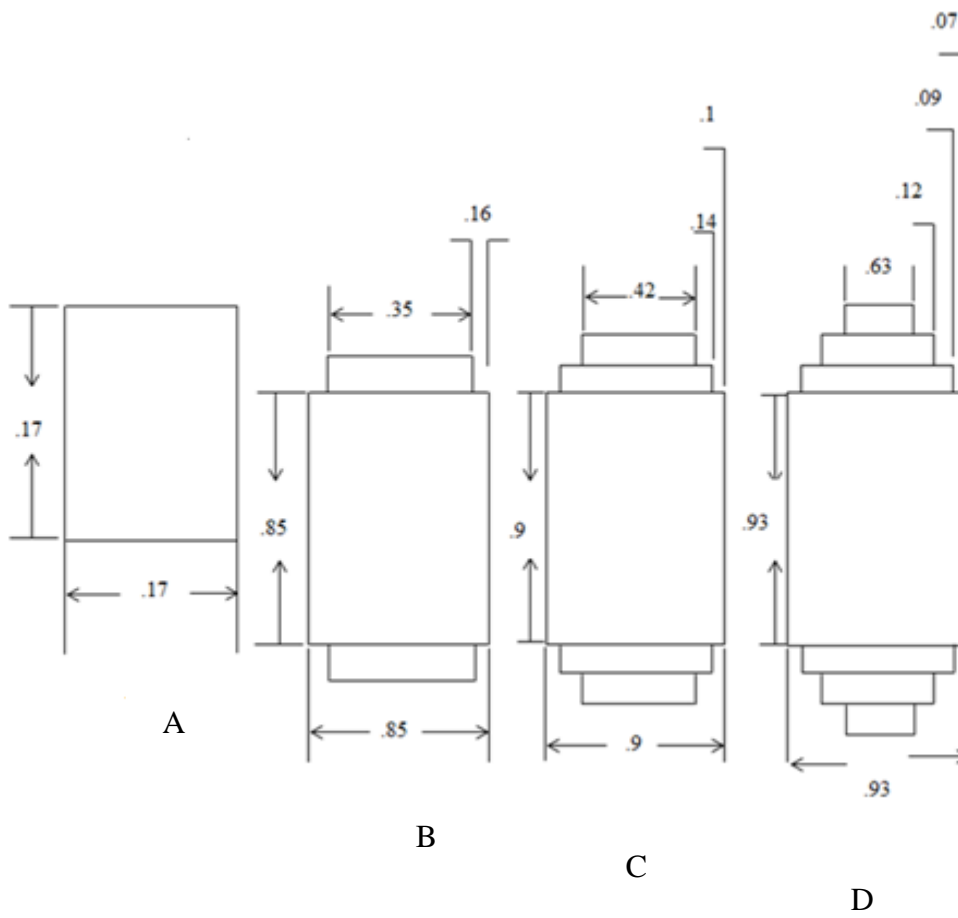


Fig. 1-13 Cross sectional area of transformer core – limbs

1.3.3 Flux density harmonics

The overall flux density in transformer core is sinusoidal, but it is distorted in individual layers [24]. In general harmonic mainly occur in the saturated regions such as T-joint area [25]. However, circulating harmonics have also been experimentally found in the limbs and yokes of transformers [26]. It is extremely difficult to calculate the power losses due to harmonics.

1.3.4 Core performance

The first transformer was built in (1885) and the most important development was initiated after the grain-oriented steel was made available for use in 1941 [27]. Early experiments were carried out to compare the performances of the grain-oriented steel with non-oriented silicon steel. It was found that the use of grain-oriented steel resulted in approximately 20% reduction of core weight and 10 to 15% reduction of iron losses.

In 1922 [28] the most extensive research carried out in recent years were an investigation of magnetic distribution of three and single phase transformer laminations, flux distribution and power loss in the mitred overlap and T-joints, flux paths and flux transfer mechanism and measurements of rotating flux.

1.4 Power loss in silicon-iron transformer cores

When transformer core energised, alternating magnetizing current flows in the core and this results in electrical power dissipated in form of heat within the cores [29].

This loss can be looked at as a result of two components, one due to the material and the other due to the construction of the core.

1.4.1 Power loss due to core materials

Loss occurred due to the material is considered to be two types: hysteresis loss and eddy current loss. Static hysteresis loss is the energy lost when magnetizing the material around its magnetization loop and it is affected by its chemical composition and the methods used in processing it [30].

Eddy current loss occurs when the material is magnetized in an alternating field, and it is influenced by the electrical resistivity of the material and the thickness of the lamination.

1.4.2 Power loss due to construction of the cores

Additional losses are introduced when building transformer core. These losses are due to mechanical stresses, flux density harmonics, presence of joints, air gaps and mechanical stresses.

In transformer core stresses are present and it is very difficult to eliminate them. These stresses are introduced due to waviness of lamination, bending caused by the weight of laminations, clamping forces and temperature gradients due to non-uniform distribution of flux density [31].

1.4.3 Magnetostriction in ferromagnetic material

The magnetic moment in ferromagnetic material lie in one direction. This alignment leads to a strong interaction in magnetic domain as shown in Fig. 1-14. Hence, ferromagnetic material can exhibit net magnetisation without applied external magnetic field.

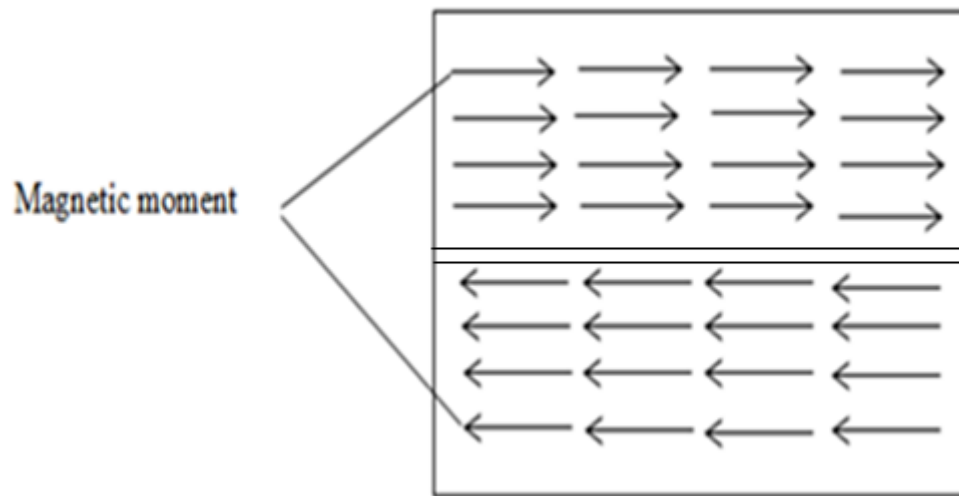


Fig. 1-14 Magnetic domain wall in ferromagnetic materials

First effect of the magnetostriction on ferromagnetic material was observed by Jule [30]. If a low value of external magnetic field is applied to these domains, few domains will change their direction to the applied field in order to balance the internal field to zero.

A second effect occurs during the magnetisation when increasing the external applied magnetic field, these domains will rotate into the direction of the applied field. However, removing the external applied field forces the domain wall to move from its original position to a new position and will not return to its original position due to the domain wall pinning and due to the impurities of the material. Therefore, any rearrangement of the domains result in changing the shape of the material. Fig. 1-15 b [32]. This change in magnetic domain induces strain in the material, and results in change in the magnetostrictive strain, $\Delta\lambda$. The magnetostrictive strain can be positive or negative depends on the material properties and applied magnetic field. If the length of the material increased under external magnetic field this called positive magnetostriction.

Changes occurred in the material can be calculate using equation:

Investigation of No-load and on-load performance of a model three-phase transformer core operating under sinusoidal and PWM voltage excitation

$$\lambda = \frac{\delta L}{L} \quad (1.5)$$

Where δL is the change in length and L is the original length of the material

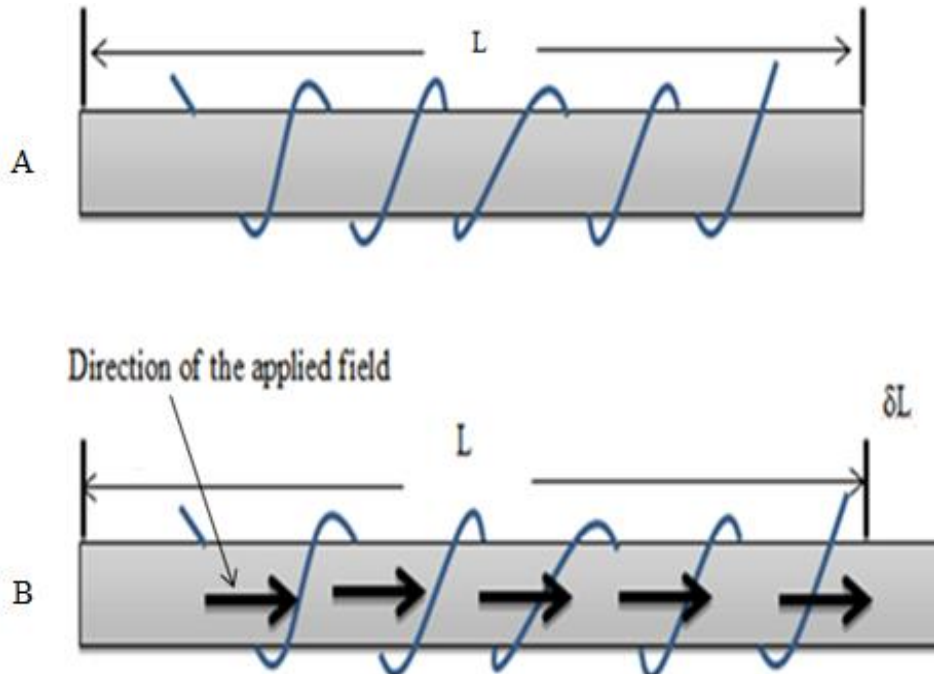


Fig. 1-15 Effect of magnetostriction (a) zero field (b) applied field

1.4.4 Previous related work

There has been huge number of research studies carried out on transformer core losses, core magnetostriction and core harmonic distribution under sinusoidal and PWM voltage excitations.

Boglietti, Ferraris and Lazzari [29], measured power losses under sinusoidal and PWM excitations using wound grain oriented transformer core. They found that PWM caused higher power losses than sinusoidal. This increasing of the losses was due to the high eddy current caused by PWM inverter.

Moses and Tutkun [33] investigated harmonic components under PWM and sinusoidal and they found that total harmonic distortion (THD) was higher under PWM. This was due to the complex flux waveform.

Basak and Moses [34], investigated the relationship between losses caused by low harmonics order in the three-phase transformer core, they found that losses were higher in the joints and the harmonic distortion was a major cause of power losses.

Basak and Abdul Qader [35] investigated (THD) in the three-phase transformer core with high magnetising range, they found that the largest third and fifth harmonic components were found in the central limb.

Neurath [36] has measured localised magnetostriction using displacement transducers

In 1966 Brownsey [37] measured fundamental component of magnetostriction using ceramic displacement transducer.

Anderson [38] has measured peak to peak magnetostriction in Epstein strip using piezoelectric accelerometer.

1.4.5 Aims of the Investigation

Transformer represents the largest capital investment in the distribution section of a power system and provides the best opportunity to make them more efficient whenever possible. Since power is transformed from the generation station to the consumer, the accumulative losses are significant, although transformer consume the majority of a nation's electricity and are the primary movers of manufacturing industry, efficiently designed and built transformer core have resulted in significant economic and productivity benefits, both to manufacturing industry and to the nation as a whole. One of the most common electrical machines is the transformer, which is universally highly used for industrial applications although there is a difficulty of power loss and core noise.

The research about core loss began very early on in the life of the power transformer. The improvement of the performance of such cores has come from improving basic magnetic properties of core material and the advance in the production techniques providing purer material with strong directional properties The efficient performance of a transformer core not only depends on the quality of the material but also on the core design. Some relevant work have been carried out previously but only when transformer is energised through three- phase inverter under no-load condition.

In the present work, an attempt has been made on practical transformer core and on the model cores to obtain deep knowledge of the flux behaviour. Moreover, studies about localised power losses and stress and also the effect of clamping pressure on losses under both on-load and no-load conditions, when transformer energised via three-phase sinusoidal and PWM voltage excitation were performed. Within this knowledge overall power loss of magnetic cores can be reduced and more efficient transformer can be developed.

Moreover, increased environmental concern has called for low acoustic noise produced by transformers. It is known that energy supply systems have undergone some major changes due to the growing role of power electronic techniques in the grid through power flow conditioners and converters of electricity. Therefore, transformers subjected to PWM voltage excitation are becoming more common; assessment and improvement in the performance of transformers under PWM

Investigation of No-load and on-load performance of a model three-phase transformer core operating under sinusoidal and PWM voltage excitation

voltage excitation are increasingly prominent. This research project aims to investigate the no-load and on-load performance of a model three-phase, three-limb laminated transformer core, assembled from high permeability grain oriented steel (HGO), operating under sinusoidal and PWM voltage excitations. Also, the main aims of the investigation can be summarised as follows:

- a). To measure localised magnetostriction of grain-oriented, 3% silicon electrical steel in the form of three-phase transformer, using strain gauge method, to compare and analyse the measurement results under sinusoidal and PWM voltage excitations, and also to explain mechanical resonance phenomena in material subjected to PWM voltage excitation.
- b). To measure the total iron losses and localised flux density within the laminations in transformer core joints using a computerised measurement system, to estimate localised rotational and planar eddy-current losses under sinusoidal and PWM voltage excitations, and to obtain a better understanding of the influence of modulation index and switching frequency.
- c). To measure localised bending effects and strain of the same model transformer core, to compare and analyse the measurement results under sinusoidal and PWM voltage excitations, and also to explain the magneto-mechanical resonance phenomenon of the core under PWM voltage excitation.
- d). To make an analysis of the results in order to draw general conclusions as to the effect of PWM waveforms on loss, strain and flux distribution and quantify the expected effect on transformer core efficiency in general.

CHAPTER 2

2. Type of the transformer core materials

Transformer core material is the significant part which may be made from various types of electrical steel dependent on the type of the transformer. It is also dependent on the cost of the electrical steel for example, in induction motors, the stator cores are usually made from non-oriented steel to minimise the magnetic losses in the core. On the other hand, transformer core is usually built from grain-oriented steel and grain-oriented steel with laser scribed domain refined material to minimise the core losses.

2.1.1 Grain oriented steel

The most important magnetic material used in large quantities in transformers and sometimes in large rotating machines, is grain-oriented silicon steel which is produced in different grades with their qualities assessed by iron losses. Therefore, the use of grain-oriented steel is to reduce the production of iron losses. The losses of the best oriented steel are about 70% less than the best grades of non-oriented steel.

Introduction of silicon into iron result in two important effects, firstly it decreases the permeability of the material and second, it increases the resistivity. Therefore, reducing eddy current loss. On the other hand, the presence of a large amount of silicon in steel result in reducing the saturation magnetisation and it also makes the steel harder and more brittle. In order to obtain optimum Si-Fe alloys, the silicon content should not exceed 5%. [39]

2.1.2 Non- oriented steel

Non-oriented steels are very nearly isotropic. Their magnetic and mechanical properties are approximately the same in all directions in the sheet. Two different grades of this material are supplied non-oriented non-silicon steel and non-oriented silicon steel. In the case of non-oriented steel when material is rolled, some degree of texture is usually produced. Therefore, in non-oriented silicon steel both losses and permeability are lower than non-oriented non-silicon steel. The non-oriented silicon steels contain a range of silicon from about 0.5% to about 3.2% to increase the

Investigation of No-load and on-load performance of a model three-phase transformer core operating under sinusoidal and PWM voltage excitation

resistivity of the steel. If the concentration of silicon is higher than 3.5%, the steel cannot be rolled in acceptable conditions. Hence, the amount of silicon rarely exceeds 3.2%. Permeability of the steel increases through making the steel purer and the grain size larger. Electrical steel with the large grain size result in lower eddy current losses but higher hysteresis loss.

2.1.3 Laser scribed domain refined (LDR)

The LDR is another material used to build transformer core and it was developed to reduce core loss of the high permeability grain-oriented material (HGO) by reducing the width of magnetic domains through means of laser irradiation. However, the laser irradiation produces stress in the lamination which then creates discontinuous domain structure. And this leads to increase of magnetostriction in the transformer core. [40]

2.2 Transformer theory and performance

Ideal transformer was always chosen to study the theory of the transformer. Fig. 2-1 shows ideal single-phase transformer core, having primary and secondary windings N_1 and N_2 respectively, wound around ferromagnetic core.

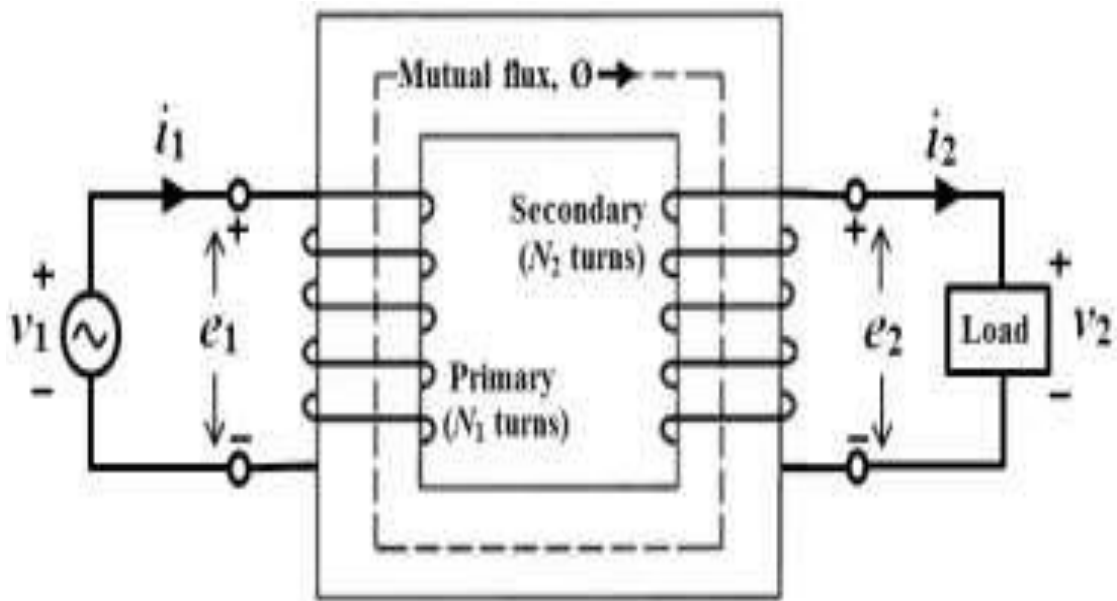


Fig. 2-1 Ideal single-phase transformer core [3]

Investigation of No-load and on-load performance of a model three-phase transformer core operating under sinusoidal and PWM voltage excitation

Therefore, the voltage induced in primary winding is equal to the voltage induced in secondary winding, the relationship between primary and secondary windings known as numbers of turns ration defined as:

$$\frac{V_1}{V_2} = \frac{N_1}{N_2} \times \frac{I_1}{I_2} \quad [41] \quad (2.1)$$

Where V_1 and V_2 are the primary and secondary voltages, N_1 and N_2 are the number of turns, and I_1 and I_2 are the primary and secondary currents,

Measuring flux density in ideal core using Faraday's law

$$e = \frac{-d\phi}{dt} \quad [41] \quad (2.2)$$

Where ϕ is the flux in Webers (Wb) and equal to $\bar{B} \cdot d\bar{S}$

Since no flux leakage in the ideal transformer core hence the instantaneous *e.m.f* in secondary winding N_2 is equal to

$$e_2 = N_2 \frac{d\phi}{dt} \quad [2] \quad (2.3)$$

Therefore, the induced *e.m.f* in the secondary winding by the flux variations is given by.

$$e_2(t) = N_2 \frac{d\phi}{dt} \quad [2] \quad (2.4)$$

As the flux is flowing continuously and changing its direction around the core, so to find the flux density at any point of the core flux density could be found as:

$$B(t) = \frac{\phi(t)}{A} \quad [2] \quad (2.5)$$

Where A is the cross-sectional area of the core from equations (2.4) and (2.5) it can be seen that

Investigation of No-load and on-load performance of a model three-phase transformer core operating under sinusoidal and PWM voltage excitation

$$e_2(t) = N_2 \frac{d\phi(t)}{dt} = N_2 A \frac{dB(t)}{dt} \quad [2] \quad (2.6)$$

By using the above definition, the instantaneous flux density can be expressed as

$$B(t) = \frac{1}{N_2 A} \int e_2(t) dt \quad [41] \quad (2.7)$$

2.2.1 Overall flux density measurement under sinusoidal excitation

When the core is excited under sinusoidal waveform, the flux as function of time is given by

$$\phi(t) = \phi_{pk} \sin \omega t \quad [41] \quad (2.8)$$

Where ϕ_{pk} is the peak flux, and ω is the angular frequency ($2\pi f$), then the secondary induced voltage in the transformer core is given by:

$$e_2(t) = N_2 \frac{d\phi(t)}{dt} = \omega N_2 \phi_{pk} \cos \omega t \quad [41] \quad (2.9)$$

Therefore, the *rms* value of the secondary induced *e. m. f* is given by

$$e_{rms} = \frac{2\pi}{\sqrt{2}} f N_2 \phi_{pk} = 4.44 f N_2 \phi_{pk} \quad [41] \quad (2.10)$$

For an alternating and sinusoidal variation of flux density

$$B(t) = B_{pk} \sin \omega t \quad [41] \quad (2.11)$$

Where B_{pk} is the peak value of the core flux density, by introducing equations (2.5) and (2.9), it can be shown that

$$e_2(t) = \omega N_2 A B_{pk} \cos \omega t \quad [41] \quad (2.12)$$

So that the *rms* value of the secondary induced *e. m. f* is also given by

$$e_{rms} = 4.44 f N_2 A B_{pk} \quad [41] \quad (2.13)$$

Investigation of No-load and on-load performance of a model three-phase transformer core operating under sinusoidal and PWM voltage excitation

In order to determine the average value of the secondary induced voltage over a period of time,

$$e_{av} = \frac{2}{T} \int_0^{T/2} e_2(t) dt \quad [41] \quad (2.14)$$

Hence the average secondary induced voltage can be calculated from

$$e_{av} = 4f N_2 A B_{pk} \quad [41] \quad (2.15)$$

Hence, for desired core flux density B_{max} the corresponding induced voltage in the reference search coil could be calculated using the equation (2.13). Moreover, equation (2.15) can be used under sinusoidal voltage excitation. For this work, equation 2.13 was used to determine the level of excitation of the core. Table 2-1 shows the required voltage to obtain desired flux density 0.4T, 0.6T and 1Tesla. Therefore, the induced voltages in the search coil were measured using a Fluke 8050A Digital Multimeter type 8050A which had accuracy better than $\pm \frac{1}{4}$ %. The overall flux density could therefore be set to within $\pm 1 \frac{1}{4}$ %.

Table 2-1 Overall voltage calculation of desired peak flux density under sinusoidal excitation

B/Tesla (T)	e/ Volt
0.4	33.3
0.6	49.95
1	83.25

2.2.2 Overall flux density measurement under PWM voltage excitation

Power loss was measured under load and no-load conditions, in order to monitor the induced voltage in the search coil both localised and overall. Integrator was used to convert the voltage into magnetic flux density so that the induced voltage will be sine waveform.

Due to the distortion generated by the PWM waveform, power loss induced in the transformer core will be higher than those when transformer core is energised by sinusoidal waveform. Using the fundamental equation in electromagnetism the PWM waveform must be defined analytically, as PWM voltage waveform is a discrete function therefore the definition can be given in a half cycle:

$$v(t) = \begin{cases} V \sum \tau_i \neq 0 \\ 0 \sum \tau_i = 0 \end{cases} \quad [42] \quad (2.16)$$

Where $\sum_1^n \tau_i$ are sum of pulse widths in a half cycle and V is the inverter output voltage. Therefore, the instantaneous flux density can be obtained from Faraday's law in discrete form as:

$$B(t) = -\frac{1}{NA} \int v(t) dt \approx \frac{v}{NA} \sum \tau_i \quad [42] \quad (2.17)$$

Where N is the number of turns and A is the cross-sectional area. When flux density approaches its maximum at one cycle it can be expressed by:

$$B_m = \frac{V}{2NA} \sum \tau_i \quad [T] \quad [42] \quad (2.18)$$

Equation (2.18) was used to set desired value of the peak flux density in the transformer core. Table 2.2 shows the required voltage to obtain desired flux density 0.4T, 0.6T and 1Tesla. However, in order to obtain the peak magnetic flux density in transformer core it is important to know the number of turns in the overall search coil and it is usual to use the middle limb as reference. Nevertheless, search coil must be

Investigation of No-load and on-load performance of a model three-phase transformer core operating under sinusoidal and PWM voltage excitation

placed in the middle of the limb where the amount of flux flowing is highly through that area. Second parameter that must be known is the core cross sectional area.

Table 2-2 overall voltage calculation of desired peak flux density under PWM excitation

B/Tesla (T)	e/ (volt)
0.4	150
0.6	250
1.0	350

2.2.3 Fundamental theory of localised power loss measurement in transformer cores

Power losses instantaneously dissipated in a single point of transformer cores lamination under one dimensional magnetisation can be expressed by:

$$P(t) = \int_v [H(t) \frac{\partial B(t)}{\partial t}] dv + \frac{1}{\sigma} \int_v (\frac{\partial H(t)}{\partial z})^2 dv \text{ [w]} \quad [42] \quad (2.19)$$

Where $H(t)$ is the instantaneous magnetic field strength, $\frac{\partial B}{\partial t}$ is partial differentiation of the flux density with time, dv is the differentiation of the volume, σ is conductivity of magnetic core material and $\frac{\partial H(t)}{\partial z}$ is partial differentiation of the magnetic field strength with one dimension of the transformer core. Hence, averaged power loss over one cycle can be obtained from:

$$P_{average} = \frac{1}{T} \int_0^T \left(\int_v H(t) \frac{\partial B(t)}{\partial t} dv + \frac{1}{\sigma} \int_v (\frac{\partial H(t)}{\partial z})^2 dv \right) dt \text{ [W]} \quad [42] \quad (2.20)$$

Investigation of No-load and on-load performance of a model three-phase transformer core operating under sinusoidal and PWM voltage excitation

By re-arranging equation (2.20) averaged total power losses can be expressed as:

$$P_{averaged} = \frac{1}{T} \int_0^T \int_v H(t) \frac{\partial B(t)}{\partial t} dv dt + \frac{1}{T} \int_0^T \int_v \frac{1}{\sigma} \left(\frac{\partial H(t)}{\partial z} \right)^2 dv dt \text{ [W]} \quad [42] \quad (2.21)$$

If magnetic field strength and magnetic flux density are assumed to be uniform within volume v , that is magnetic field strength and magnetic flux density change with only time, then $\left(\frac{\partial H(t)}{\partial z} \right)$ will be zero and $\frac{\partial B(t)}{\partial t}$ will be defined as $\frac{dB(t)}{dt}$. Hence,

averaged total power loss under one dimensional magnetisation can be written as:

$$P_{total} = \frac{v}{m} \frac{1}{T} \int_0^T \left[H(t) \frac{dB(t)}{dt} \right] dt \quad \text{[W/kg]} \quad [42] \quad (2.22)$$

Where v , m , T , $H(t)$ and $dB(t)/dt$ are volume of the magnetic core, mass of the material, magnetisation period, instantaneous magnetic field strength and the rate of change of flux density with time respectively.

2.2.4 Total iron losses using loss separation criteria

Recently, several methods have been approached to calculate total iron losses under PWM waveform such as (Amar) [42] shows to predict total iron losses under PWM excitation in Epstein strips using separation method. Dividing iron losses into three parts which are hysteresis losses, eddy current losses and excess losses, total iron losses under PWM voltage excitation can be expressed by:

$$P_{tot} = P_h + \frac{2}{3} \frac{\sigma d^2}{m} \frac{B_m^2}{\sum \tau_i} + \frac{4\sqrt{2\sigma G V_0 A}}{M} \frac{B_m^{1.5}}{(\sum \tau_i)^{0.5}} \quad \text{[W/kg]} \quad [42] \quad (2.23)$$

Where P_h is hysteresis loss, σ is conductivity of the material d is the thickness of the lamination sheet G is a dimensionless coefficient. Total power loss under PWM excitation is dependent on the total number of pulses in a half cycle for example as the pulses increase losses decrease. However, in order to show the difference

Investigation of No-load and on-load performance of a model three-phase transformer core operating under sinusoidal and PWM voltage excitation

between frequency dependent total loss under PWM and sinusoidal excitations iron losses under sinusoidal excitation can be expressed as:

$$P_{tot} = P_h + \frac{\sigma\pi^2 d^2}{6m} B_m^2 f^2 + \frac{\sqrt{2\sigma G V_0} A}{m} B_{pk}^{1.5} f^{1.5} \quad [\text{W/kg}] \quad [42] \quad (2.24)$$

Where f is the magnetising frequency. The form factor coefficient of PWM voltage is ratio of the form factor of the PWM voltage and sinusoidal voltage, $F_c = 2/(\pi \sqrt{f \sum \tau_i})$. If the dynamic losses in equation (2.24) are multiplied by this term under the condition of the PWM voltage excitation with respect to sinusoidal voltage excitation (where F_c is 1) the total iron losses under PWM voltage excitation rewritten as:

$$P(f)_{tot} = P_h + \frac{41}{\pi^2 \sum \tau_i} \frac{P_{cl}^{\sin(f)}}{f} + \frac{2}{\pi} \frac{P_{ex}^{\sin(f)}}{\sqrt{\sum \tau_i} \sqrt{f}} \quad [\text{W/kg}] \quad [42] \quad (2.25)$$

Where P_h is the hysteresis loss, P_{cl} is eddy current losses, and P_{ex} is the excess losses respectively. Moreover, as the number of pulses per half cycle is the most important parameter in the PWM which influences the power loss to increase, this can be controlled by control voltage frequency and the carrier frequency. If the ratio of these two frequencies is large then the number of pulses will be high. Therefore, the losses are expected to decrease.

2.3 Hysteresis losses

As shown in Fig. 1-2 hysteresis loss is proportional to the area enclosed by the loop hysteresis losses occur in ferromagnetic material such as iron or steel. For example,

When ferromagnetic material is subjected to external magnetic field the hysteresis loop will appear, it is also known as B-H loop or B-H curve [43]. When a low external magnetic field is applied to magnetise a pure specimen of ferromagnetic material it will result in changing the material properties as some of domain walls will follow in the direction of the applied field and some will direct to random

Investigation of No-load and on-load performance of a model three-phase transformer core operating under sinusoidal and PWM voltage excitation

direction. When the external field is increased, all domain walls will align into the applied field. However, when the external applied field is removed, domain walls will not return to their first pattern so induced magnetising element will remain in the material because ferromagnetic material have high coercivity that is hard to demagnetise. A coercive field has to be applied to bring the saturation value (M_0) to zero. If the external field increased again, magnetic path will follow into the negative side of the curve and hence one full cycle has been obtained which is proportional to the power losses per one cycle[44].

Table 2-3 saturation value of some material [3,5,6]

Saturation value of the material	
Material	Saturation magnetisation. M_0 [T]
Iron	2.15
Cobalt	1.78
Nickel	0.60
3% silicon Iron	2.03

There are several methods that have been developed to study hysteresis losses, such as Jiles Atherton [44] method and Preisach method. Each method is based on different estimation, for example Jiles Atherton studied the physical mechanisms in ferromagnetic materials such as (magnetic domains, domain wall pattern and pinning sites). Whereas, Preisach method is known as the mathematical method disregarding the physical background. However, they are adapted methods for predicating the hysteresis loss. Steinmetz method has also been used to calculate hysteresis losses. His method depends on the peak flux density and experimental coefficients. Using Steinmetz method, hysteresis losses can be written as:

$$P_h = k B_m^n \quad [W] \quad [42] \quad (2.27)$$

Investigation of No-load and on-load performance of a model three-phase transformer core operating under sinusoidal and PWM voltage excitation

Where k and n are experimental constants which are dependent on the magnetic material. Therefore, by substituting equation (2.18) into equation (2.27), hysteresis loss can be written as:

$$P_h = k \left(\frac{V}{2NA} \right) \sum \tau_i \quad [W] \quad [42] \quad (2.28)$$

By the identification of the unknown constant for the magnetic material tested under the PWM voltage waveform in an electromagnetic circuit, hysteresis losses can be predicted using equation (2.28).

2.3.1 Eddy current losses

Eddy current loss component is proportional to the magnetising frequency and is dependent on the thickness of the lamination. If the lamination is thick and has small grain oriented, exciting current is low to give peak flux density, as the transformer core is made from conducting material and when the core is energised, alternating flux flows through the core. This flux will induce an electromotive force (*emf*) voltage according to Farady's law.

This induced voltage causes currents to circulate through the magnetic core according to Ohm's law. These "eddy currents" produce heat in the core and as a result power loss takes place in the core. The eddy current loss under PWM excitation can be calculated by:

$$P_{cl} = \frac{\sigma d^2 f}{(12m) T} \int_0^T (dB/dt)^2 dt \quad [W/kg] \quad [42] \quad (2.29)$$

Where σ is conductivity of the material, m is density of the material, d is the thickness of the lamination and $\frac{dB}{dt}$ is the rate of changing flux density with changing time, as the rate of changing flux under PWM excitation is constant and equal to $\frac{V}{NA}$ in half cycle. However, when the output voltage of the inverter is not zero by replacing $\frac{V}{NA}$ with $\frac{dB}{dt}$ in equation (2.29) eddy current loss can be expressed as:

$$P_{cl}(f, \sum \tau_i) = \frac{2}{3} \frac{\sigma d^2}{m} \frac{B_m^2}{\sum \tau_i} f \quad [\text{W/kg}] \quad [42] \quad (2.30)$$

As the eddy current loss under PWM excitation depend on number of pulses in half a cycle and the magnetising frequency. Hence in order to decrease eddy current losses under PWM excitation the number of pulses per half cycle should be made high, this is obtained by increasing the carrier frequency modulation index as well as choosing a thinner material.

2.3.2 Anomalous loss

When external magnetic field is applied to a transformer core, domain walls start moving and obeying the external field by rearrange themself toward the external field. This domain wall motion leads to increase excess loss. According to (Bertotti), excess losses are the difference between the measured total losses and the sum of hysteresis losses and eddy current losses and can be expressed as:

$$P_{ex} = h_e \frac{dB}{dt} \quad [\text{W/m}^3] \quad [45] \quad (2.31)$$

Where h_e is the damping field generated by the excess eddy currents. It also assumed that the change of magnetisation is accomplished, at a given time t through the reversal of n_x active regions, so called “magnetic objects” randomly placed in the sample cross section.

As the lamination of the transformer core made with the fine material, domain walls strongly associated together so magnetisation process will thus proceed according to the distribution of the domain walls will produce dynamic balance between the external filed and the domain walls that can be expressed as; induction rate $\frac{dB}{dt}$ and eddy current counter-fields. Any variation of $\frac{dB}{dt}$ entails a variation in such a balance, on the basis of the analysis developed through equation (2.22), Hence, the excess damping field can be defined as:

$$h_e = \sigma G S \frac{dB}{dt} \frac{1}{n_x(t)} \quad [\text{A/m}] \quad [45] \quad (2.32)$$

Investigation of No-load and on-load performance of a model three-phase transformer core operating under sinusoidal and PWM voltage excitation

$$n_x(t) = \frac{h_e}{V_o} \quad [45] \quad (2.33)$$

Where σ is the conductivity of the materials A is the cross-sectional area and G and V_o were determined from the previous experiments carried out by Bertotti. They were found to be 0.1356 and 0.15 A/m for 3% Grain-oriented and 0.1356 and 0.12 A/m for 3% Non-oriented laminations respectively [45]. By combination of equations (2.32) and (2.33) the instantaneous excess power loss can be expressed by

$$P_{ex} = \frac{\sqrt{\sigma G V_o A}}{m} \frac{1}{T} \int_0^T \left| \frac{dB}{dt} \right|^{1.5} dt \quad [\text{W/kg}] \quad [45] \quad (2.34)$$

If $\frac{dB}{dt}$ is replaced with $\frac{v}{NA}$ then equation will be rewritten as

$$P_{ex} = \frac{4\sqrt{2\sigma G V_o A}}{m} \frac{B_m^{1.5} f^{1.5}}{(\sum \tau_i)^{0.5}} \quad [\text{W/kg}] \quad [45] \quad (2.35)$$

Determined σ, A, G and V_o from the magnetic material excess losses under PWM voltage waveform can be calculated from equation (2.35). Nevertheless, all these equations can be used to predict total iron losses under PWM voltage excitation in grain oriented or non-oriented electrical steel.

2.3.3 Theory of estimates of iron loss components using loss separation criteria

The total iron loss can be divided into three groups using loss separation criteria which can be expressed as:

$$P = K_h f + K_{ed} f^2 + P_{an}(f) \quad [45] \quad (2.36)$$

Where K_h is the hysteresis loss constant, K_{ed} is the eddy current loss constant and P_{an} is the anomalous loss which is frequency dependent dividing equation 2.36 by the magnetising frequency we obtain

$$\frac{P}{f} = K_h + K_{ed} f + \frac{P_{an}(f)}{f} \quad [45] \quad (2.37)$$

In order to determine K_h , the total loss is measured at different frequencies at constant peak flux density and then the measured total power loss is divided by the magnetising frequency in each case.

Estimates of loss components can be also obtained using Bertotti's model. The general Bertotti's model can be written as a frequency dependent function of form

$$P_b = K_{hb} f + K_{edb} f^2 + K_{exb} f^{3/2} \quad [\text{W/kg}] \quad [45] \quad (2.38)$$

Where K_{hb} is the hysteresis loss constant, K_{edb} is the eddy current loss constant and K_{exb} is the anomalous loss constant. Dividing both sides by f we can obtain specific loss per cycle which can be written as:

$$\frac{P_b}{f} = K_{hb} + K_{edb} f + K_{exb} f^{1/2} \quad [45] \quad (2.39)$$

Where K_{hb} is the hysteresis loss per cycle, $K_{edb} f$ is the classical eddy current per cycle and $K_{exb} f^{1/2}$ is the excess loss per cycle respectively.

2.3.4 Flux density distribution

Flux density distribution will be examined in great details throughout the cores. Both overall and localised flux densities were measured. One layer of the core lamination was removed and prepared to study localised distribution at T-sections, corner sections, and in the middle of the limbs and the yokes as shown in Fig. 2-2. Overall flux density of the core was also studied through the limb and yoke as shown in Fig. 2-3. The effect of clamping pressure and the variation of magnitude and phase angles of flux density will be examined in great details.

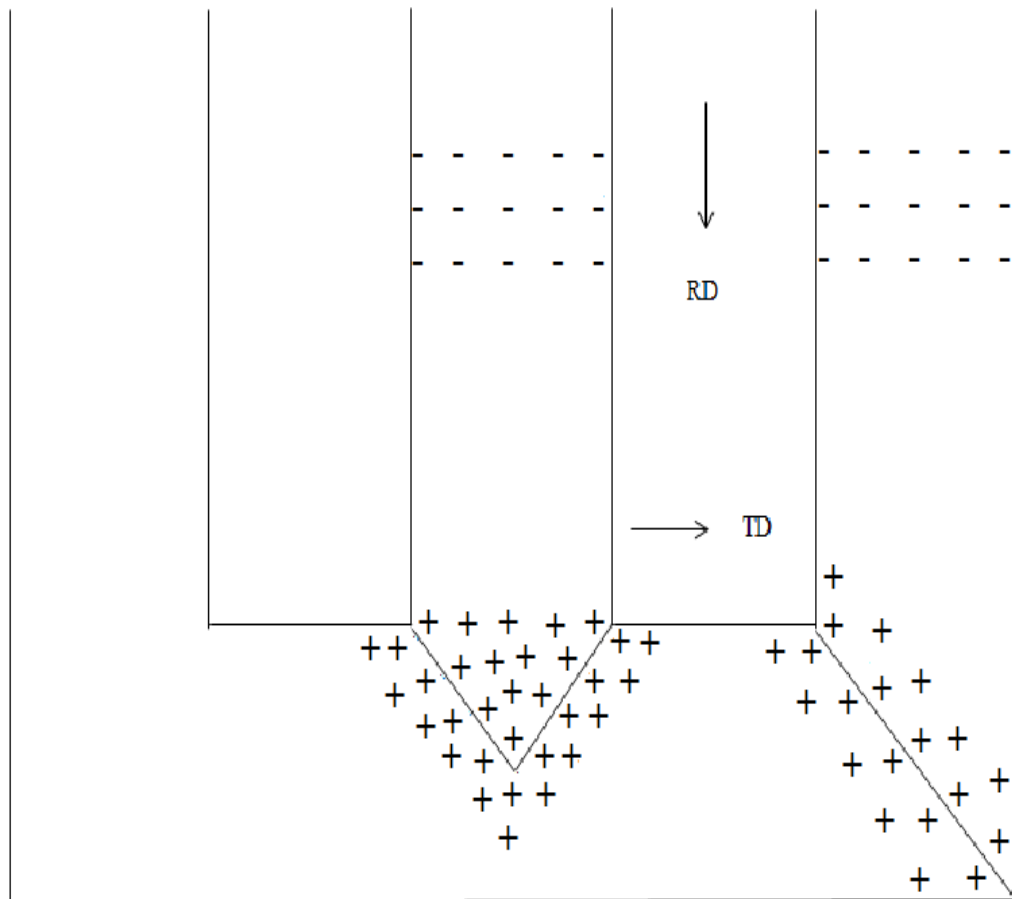


Fig. 2-2 Positions of the localised search coils

2.4 Overall flux density distribution under sinusoidal voltage excitation

In order to measure overall flux density distribution in transformer core, search coil technique was used which is also known as reference search coil technique. Two search coils were wound around the limb and yoke Fig 2-3 illustrates the positions of the search coils. The width of the limb was 0.0075 cm and that of the yoke. The core was energised over a range of different peak flux densities of 0.4T, 0.6T and 1.0T. Study of the overall flux density distribution has been obtained over every range of magnetising peak flux density for example at 0.4 T, under load condition the flux density in the yoke was 1.5% higher than that of the limb. Whereas, at 0.6 T, the flux density in the yokes had a value of 1.6% higher than that in the limb. However, when the core was energised at 1.0T, flux density in the limbs was 2% higher than this in the yoke.

It can be observed that energising the core at higher level of flux density 1.0T, the overall flux density in the yokes started to decrease and became lower than that of the limb. Whereas when the core energised at 0.4T and 0.6T, flux density in the yoke was higher than that in the limb. Furthermore, measurements of the overall flux density were taken under load and no-load conditions, and results have shown those overall flux densities are close to each other under load and no-load conditions. Fig. 2-4 shows overall flux density in the limb and Fig. 2-5 shows overall flux in the yoke when the core was energised at 0.4T. Table 2.4 summarise overall B_{rms} distribution in the three-phase transformer core.

Investigation of No-load and on-load performance of a model three-phase transformer core operating under sinusoidal and PWM voltage excitation

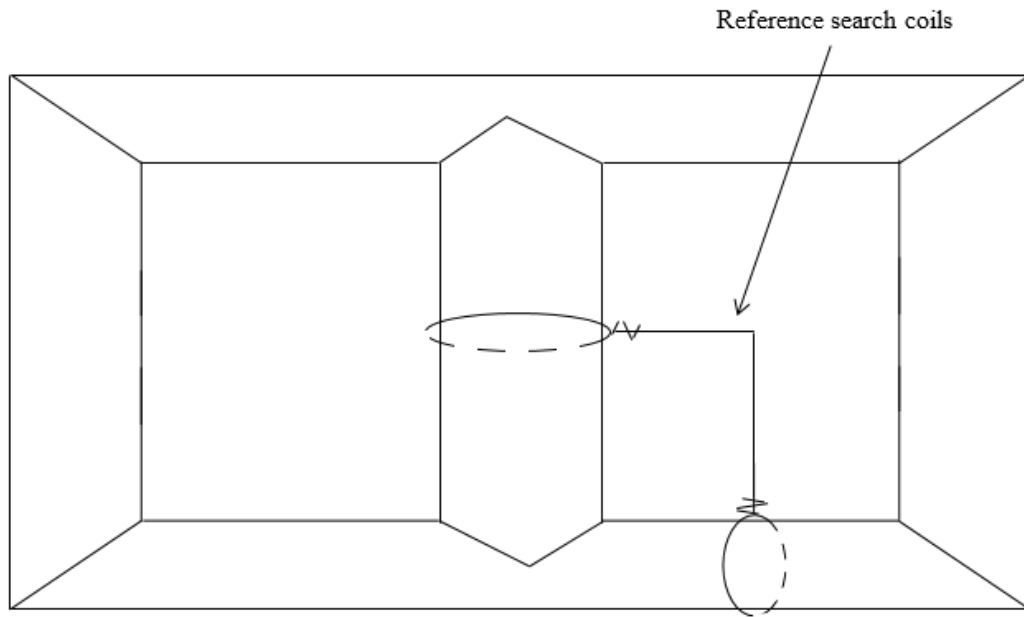


Fig. 2-3 Position of the reference search coils

Table 2-4 Induced B (*rms*) in the reference search coil

B_{peak} (T)	Limb (mV)	Yoke (mV)	Percentage
0.4	5.91	6.00	1.5%
0.6	9.03	9.18	1.6%
1.0	10.58	10.35	2%

Investigation of No-load and on-load performance of a model three-phase transformer core operating under sinusoidal and PWM voltage excitation

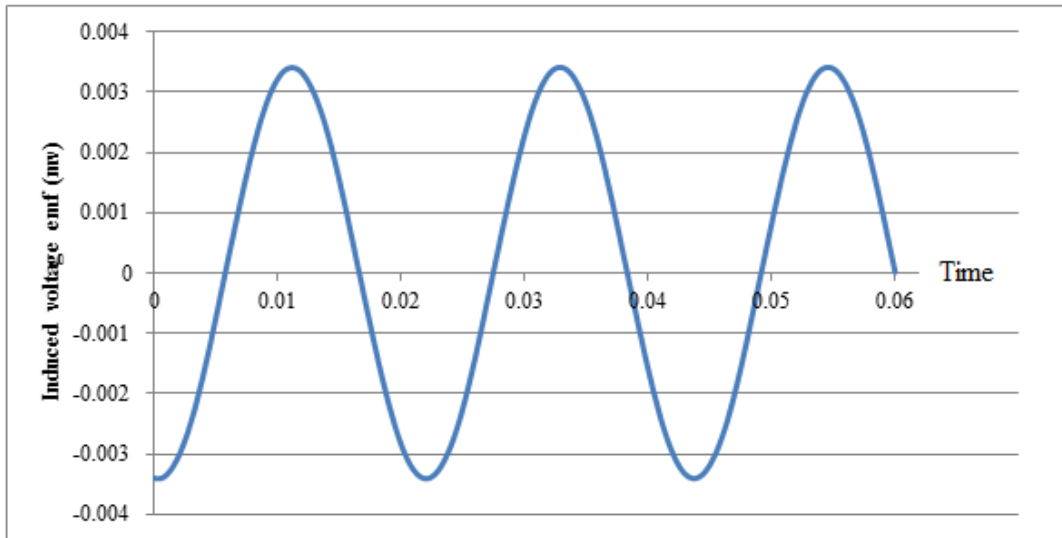


Fig. 2-4 Variation of the induced voltage against time under sinusoidal waveform in the transformer limb at 0.4T

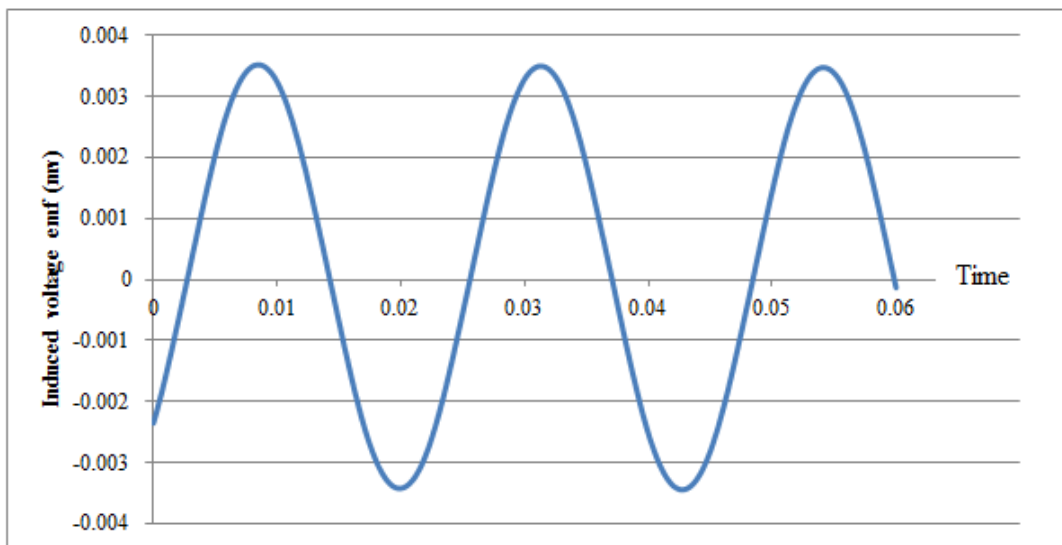


Fig. 2-5 Variation of the induced voltage against time under sinusoidal waveform in the transformer yoke at 0.4T

Investigation of No-load and on-load performance of a model three-phase transformer core operating under sinusoidal and PWM voltage excitation

2.4.1 Overall flux density distribution under PWM voltage excitation

In order to adjust output voltage of the inverter integrator circuit must be implemented to change pulse signal to sine signal. Fig. 2-6 is showing voltage signals before integrator circuit and Fig. 2-7 shows PWM signal after integration. However, when transformer core was energised by PWM voltage waveform, transformer core was subjected to additional losses due to PWM flux distortion.

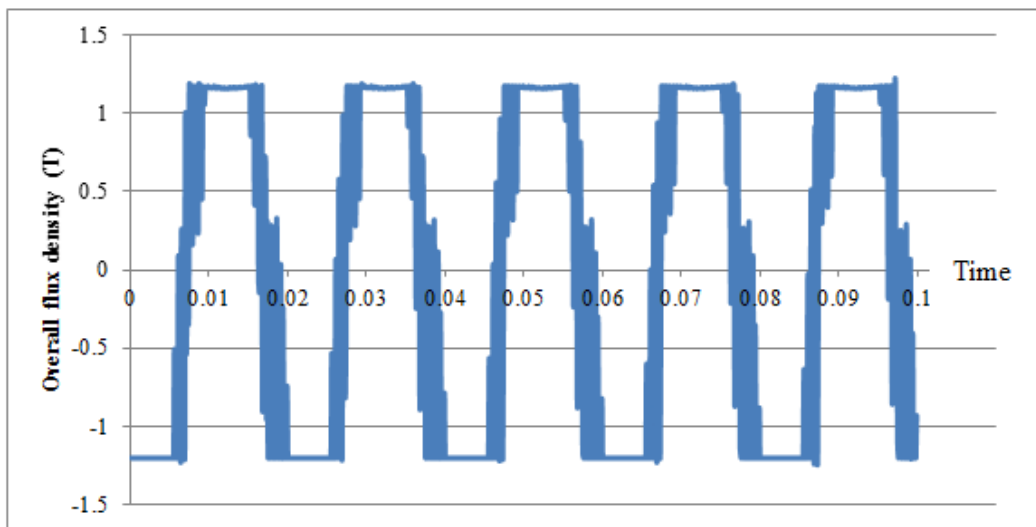


Fig. 2-6 variation of the overall flux density against time (ms) before the integrator circuit

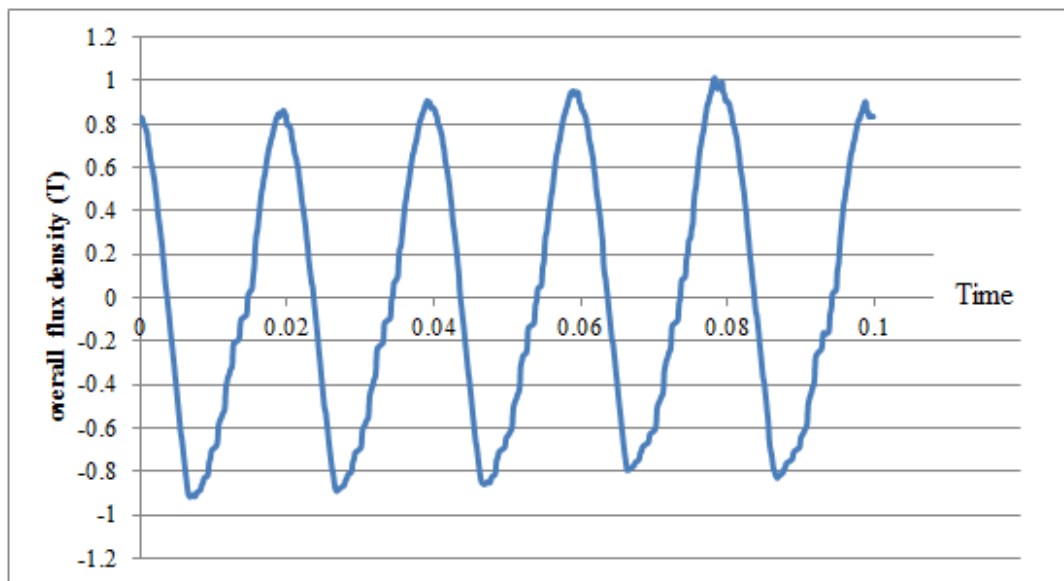


Fig. 2-7 variation of the overall flux density against time (ms) after integrator circuit

Investigation of No-load and on-load performance of a model three-phase transformer core operating under sinusoidal and PWM voltage excitation

Instantaneous PWM has spikes on its waveform. At high switching frequencies, the PWM has less distortion because of the increase in the number of pulses per cycle.

When the core fed by PWM voltage excitation at 0.4 T, under load condition the flux in the limb was 11% higher than that in the yoke. However, when the flux density was increased to 0.6 T, flux density in the limb was 6% higher than that of the yoke. Further increase in the peak flux density to 1.0 T, flux density in the limb was higher than those of the yoke by a factor of 10%.

It could be noticed that the flux density in the limb was higher than those of the yoke when the core energised under 0.4 T, 0.6T and 1.0 T. Similar results were obtained under no-load condition.

Flux density in the limb was always higher than those in the yoke at all magnetising levels and that has led to higher temperature rise in the limbs rather than that in the yoke. Temperature gradients could also occur in areas near the joint producing stresses in the laminations, table 2.5 summarise overall *rms* occurred in the limb and in the yoke.

Table 2-5 Variation of fundamental components of overall flux density in the limbs and yokes

Core excitation B_{peak} (T)	Limb (T)	Yoke (T)	Percentage
0.4	0.42	0.37	11%
0.6	0.73	0.68	6%
1.0	1.10	0.98	10%

2.4.2 Field and flux measurement method

In order to measure localised power loss it was required to measure magnetic field and so the measurement technique was decided upon the requirement need.

2.4.3 Magnetic field measurement

For the measurement of magnetic field induction, it was decided to use a conventional search coil method. The search coils of 0.1mm wound around a common non-magnetic former and then number of search coil was chosen to one turn for both X and Y directions.

2.4.4 H -coil construction and calibration

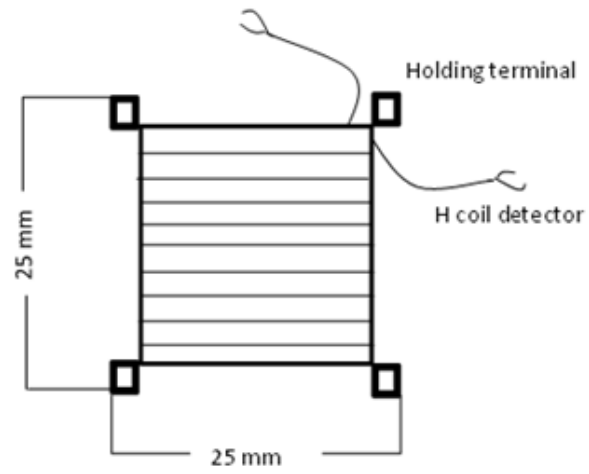
The H-coil was made from enamelled copper wire, wound around a common non-magnetic former with precise dimensions of (25 mm X 25 mm X 0.3 mm). The number of turns of the coil and the diameter of the wire were 500 turns and 0.1 mm respectively. Many turns of H -coils were wound to produce a large *e. m. f* proportional to dH/dt , to produce a high signal to noise ratio. Fig 2-8a. The H-coil was calibrated in a range of known sinusoidal magnetic field produced inside a 1.15 m long, 729 turns uniformly wound air cored solenoid with 1.5 mm wire diameter. H-coil was positioned at the centre of the solenoid core, where the magnetic field is uniform and constant. The H – coil calibration set up used is shown in Fig. 2-8a and 2-8b the output voltage V_o form the H coil was measured for different magnetising currents. Equation 2.37 was used to calculate the field strength H values for different magnetising currents. Graphs of H versus V_o were plotted. Output signal form the H and V_o coil was connected to a “Fluke 115 true *rms* multi-meter” for the processing of magnetic signal [46].

$$H = \frac{NI}{L} \quad (2.37)$$

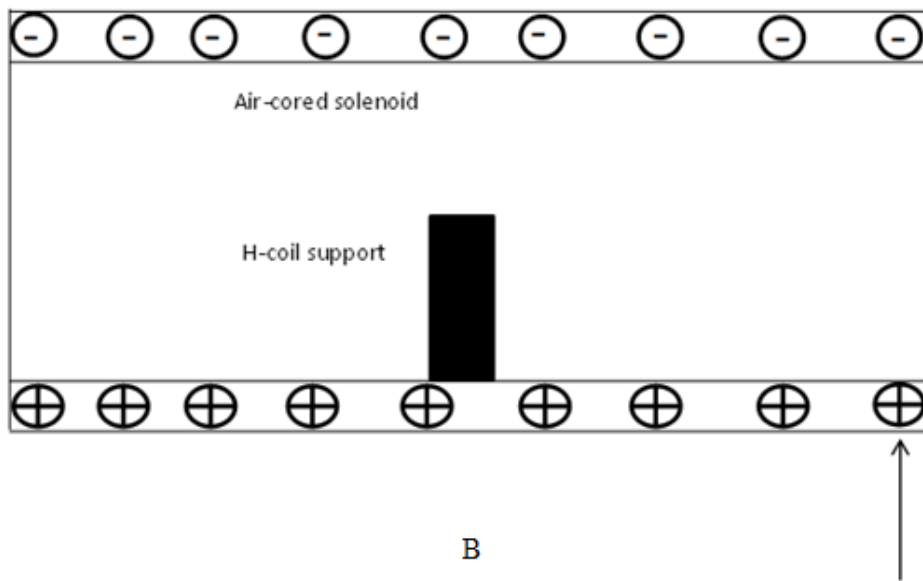
Where N = number of turns in the magnetising winding

I, L = magnetising current and mean magnetic path length respectively

Investigation of No-load and on-load performance of a model three-phase transformer core operating under sinusoidal and PWM voltage excitation



A



B

Fig. 2-8 Schematic diagram of solenoid system

Investigation of No-load and on-load performance of a model three-phase transformer core operating under sinusoidal and PWM voltage excitation

Table 2-6 Output voltage and current from solenoid core

Applied voltage V	I . amp	Detected voltage V_{rms} (mV)	$H = \frac{NI}{L}$ A/m
24	3.28	15.2	2079
33	4.47	21.9	2833
58	7.94	24.5	5033

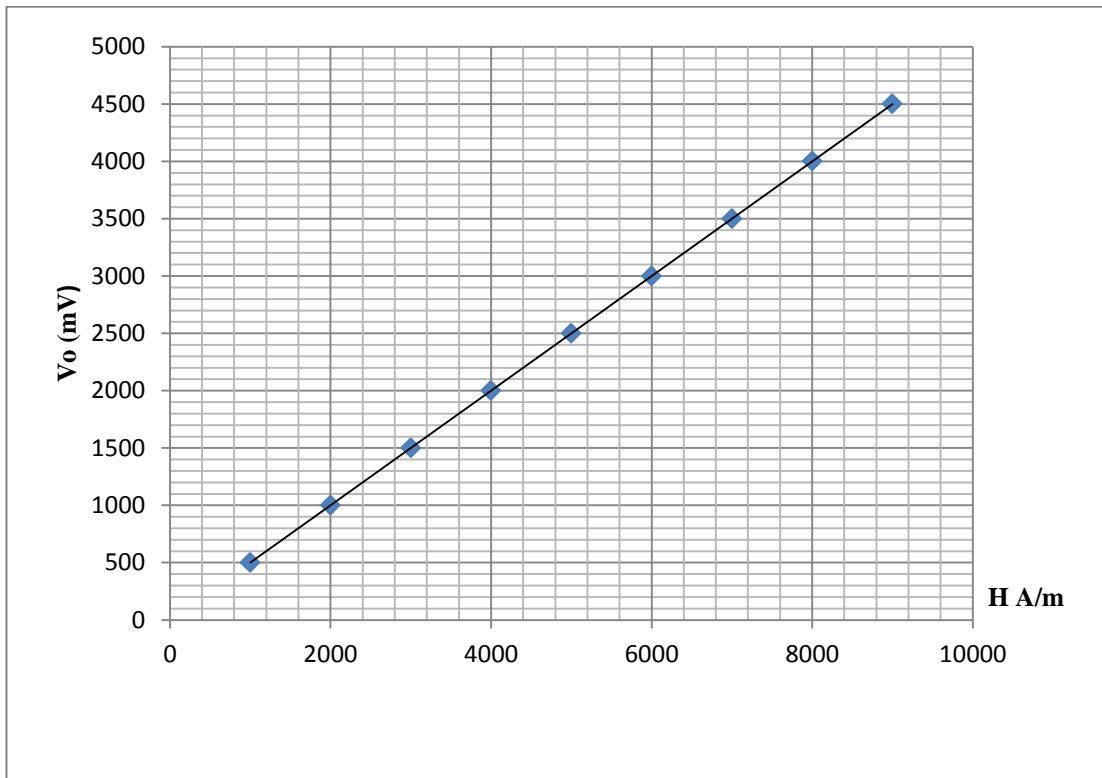


Fig. 2-9 Voltage vs magnetic field with assign value of flux density

CHAPTER 3

3. Pulse width modulation (PWM)

Historically AC motors have fixed frequency which is 50 Hz or 60 Hz. Developments in the technology of power electronics have provided inverters with different voltage and different frequency level usually in the range between 0 to 500 Hz. Three-Phase static converters (PWM), are usually used in commercial and domestic applications which are found in air conditioners, dryers, and many other applications [47, 48]

The output voltage of (PWM) is obtained by comparing a reference voltage waveform usually sinusoidal and carrier voltage waveform, usually triangular (Fig 3.1). Reference voltage frequency usually in the range 0 to 100 Hz, and the carrier voltage is usually between 1 kHz to 22 kHz. PWM has two parameters which determine its output performance, modulation index and switching frequency.

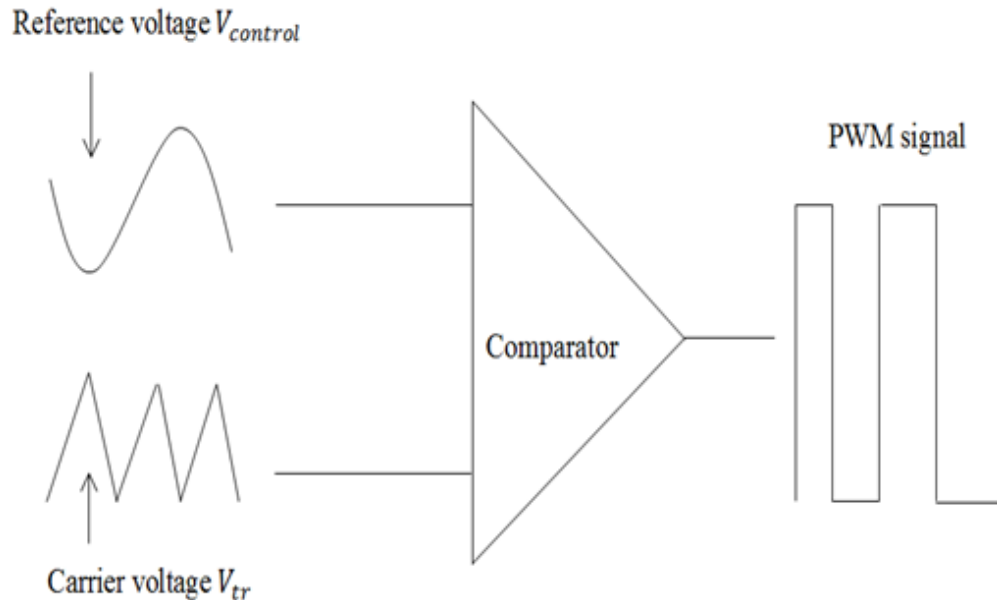


Fig. 3-1 . PWM waveform generators [3]

3.1.1 Modulation index

Modulation index and its range is one significant parameters that determines the output voltage of the PWM inverter. The amplitude of the fundamental frequency component $V_{control}$ of the output voltage varies linearly with modulation index provided that modulation index range is between 0 and 1. Therefore, range of the modulation index from 0 to 1 is referred to as linear range. However, if the modulation index is larger than 1.0 the peak value of $V_{control}$ exceeds the peak value of $V_{carrier}$ and this will cause large harmonic contents in the PWM output voltage.

Modulation index defined as:

$$m_a = \frac{V_{control}}{V_{carrier}} \quad (3.1)$$

Where $V_{control}$ is the sinusoidal signal and V_{tri} is the carrier voltage signal as shown in Fig. 3-1. Then the output voltage will depends on the circuit configuration [49]

3.1.2 Switching frequency

PWM has two frequency components which are switching frequency f_s and fundamental frequency. The inverter switching frequency f_s is generally kept constant with triangular waveform $V_{carrier}$. Whereas, the fundamental frequency f is used to modulate the switch duty ratio and is kept constant with $V_{control}$ sinusoidal voltage signal. The ratio between switching frequency f_s and fundamental frequency f is defined as frequency modulation ratio m_f and equal to:

$$m_f = \frac{f_s}{f} \quad (3.2)$$

It is desirable to use as high a switching frequency as possible. Moreover, switching losses with the inverter increase proportionally with the switching frequency because of the relative ease in filtering harmonic [49]. It is also desirable to use as high a switching frequency as possible because of the advantages of no audible noise with switching frequency of 20 kHz or greater than 20 kHz [50].

3.1.3 Voltage source inverter

The three-phase inverters consist of three legs, one leg for each phase and are commonly used to supply three-phase loads as shown in Fig. 3-2. Each phase voltage has 120° phase angle between them, therefore the conduction sequence is given as: S_6S_1 , S_1S_2 , S_2S_3 , S_3S_4 , S_4S_5 , S_5S_6 and S_6S_1 . The output voltage is independent of the output load current since one of the two switches in each leg is on at any instant [49].

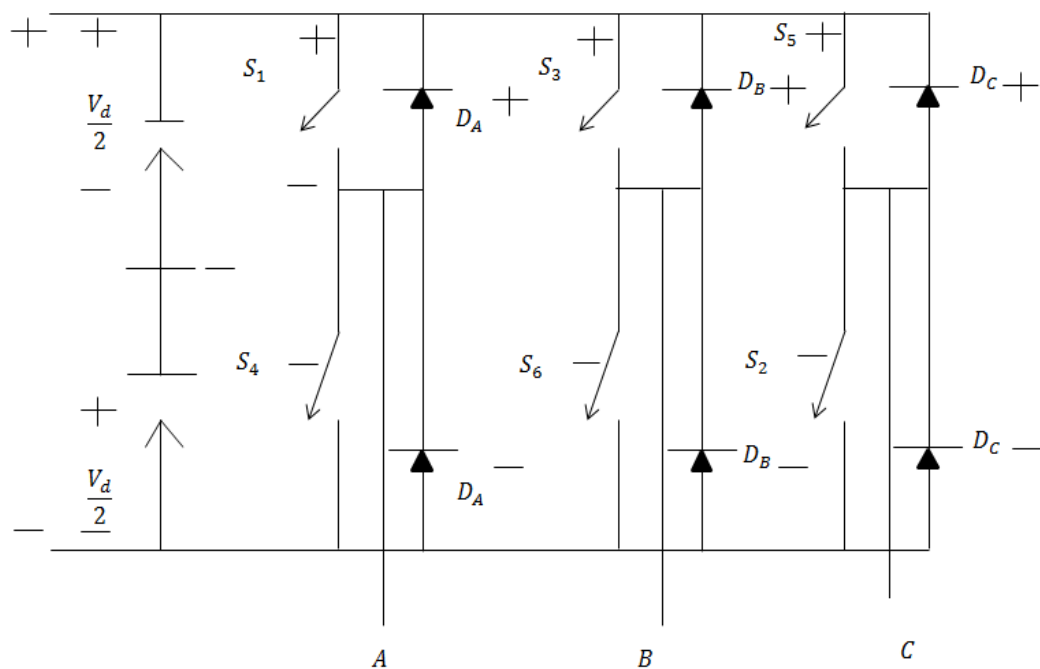


Fig. 3-2 Three-phase PWM inverter voltage configuration circuit [4]

3.1.4 Current source of PWM inverter

One important parameter of the PWM inverter that has been studied in this section is its use as current supply source. The PWM inverter consists of three elements (thyristors, capacitors, and diodes). To control three-phase current circulation each thyristor is used to switch the current element on by firing a pulse on its gate whereas capacitors and diodes are used to turn the current off. The force commutation circuit works in such a way that firing an incoming thyristor automatically commutates the outgoing thyristor. This force is known as auto sequential commutation. Fig. 3-3 shows circuit diagram of controlled current [49]

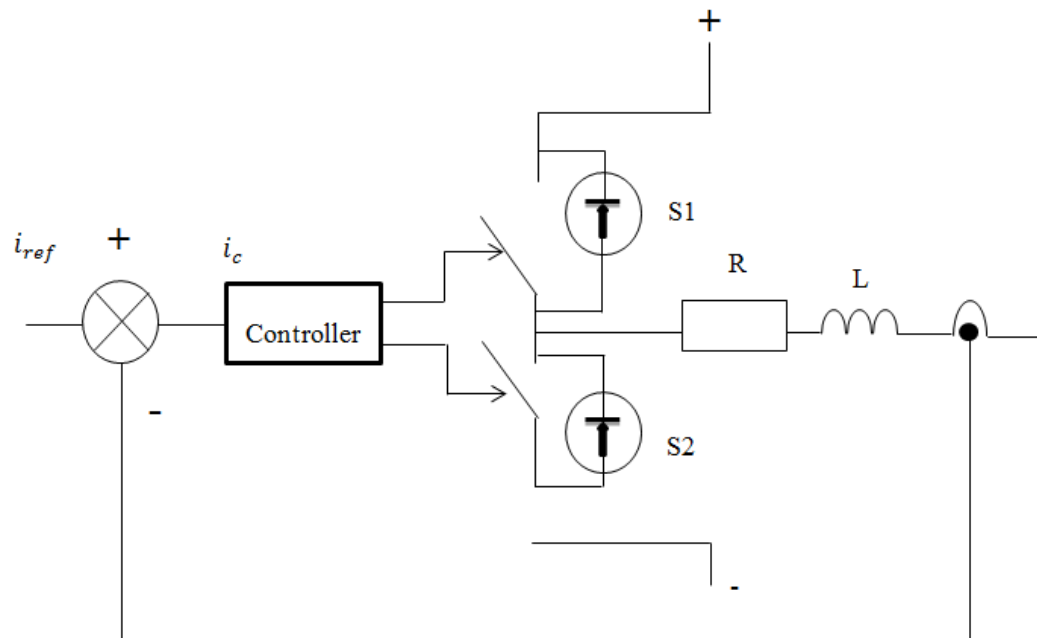


Fig. 3-3 Schematic diagram of controlled current S1, S2 Switch. L: Inductance R: Resistor [1]

3.2 Magnetizing current variation under PWM voltage excitation

In order to detect the current flowing in the three-phase inverter, three $1\ \Omega$ power resistors were coupled parallel to the three-phase inverter. The outputs of the resistors were connected to the DAQ card. Detection of each phase current signal was taken through “Lab-View” programme. The core was energised over different range of peak flux density 0.3T , 0.4T and 0.7T respectively. During the measurements, switching frequency was varied in the range of $2\ \text{kHz}$, $3\ \text{kHz}$, $12\ \text{kHz}$ and $16\ \text{kHz}$. Measurements were taken under load condition and transformer was connected in star configuration. Fig. 3-4 shows block diagram for measuring magnetising current.

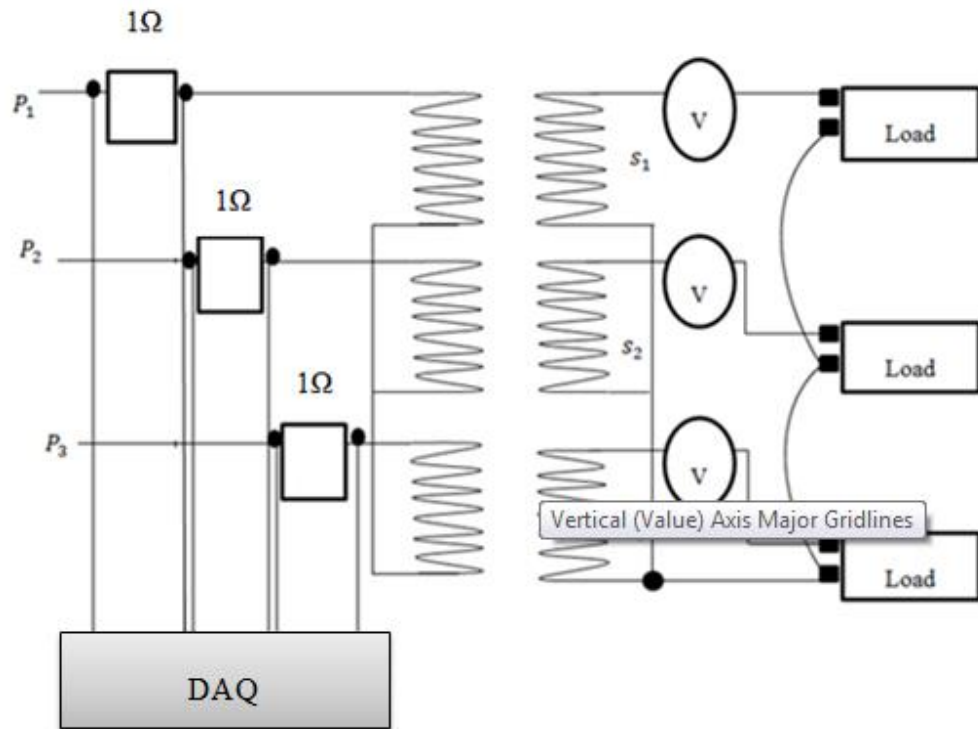


Fig. 3-4 Block diagram for measuring magnetising current

Investigation of No-load and on-load performance of a model three-phase transformer core operating under sinusoidal and PWM voltage excitation

Fig. 3-5 shows variation of the magnetizing currents with flux density in the outer limb under PWM voltage excitation with assigned value of switching frequency. To obtain a flux density of 0.3T at switching frequency of 2 kHz and 3 kHz, the current required was 0.1144amps. Whereas, at switching frequency of 3 kHz, current needed was 0.1108amps. However, for the middle limb current needed at switching frequency 2 kHz and 3 kHz were 0.1087amps and 0.1062amps respectively, as shown in Fig. 3-6.

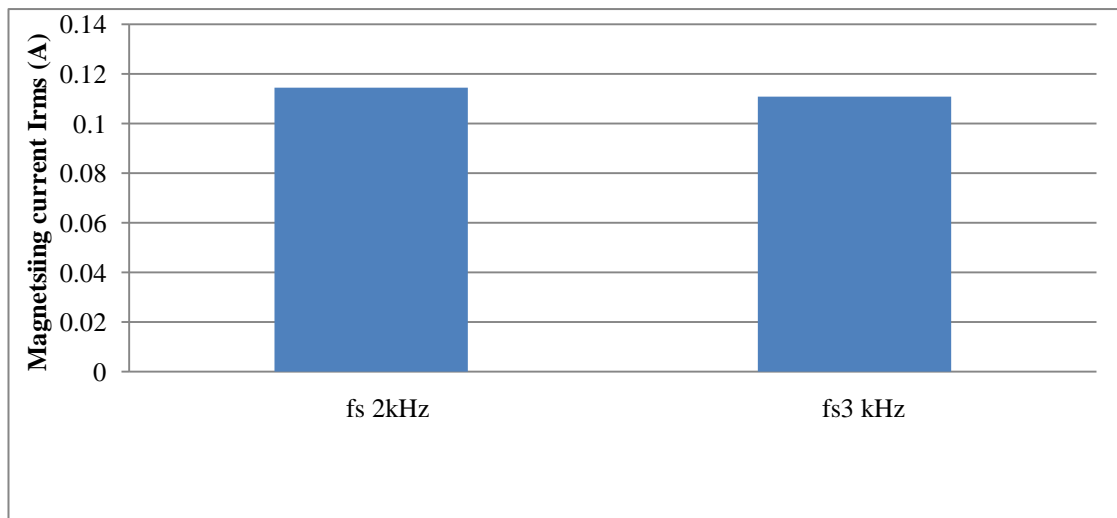


Fig. 3-5 Variation of magnetizing current at 0.3T in the outer limb with assigned values of switching frequency (kHz)

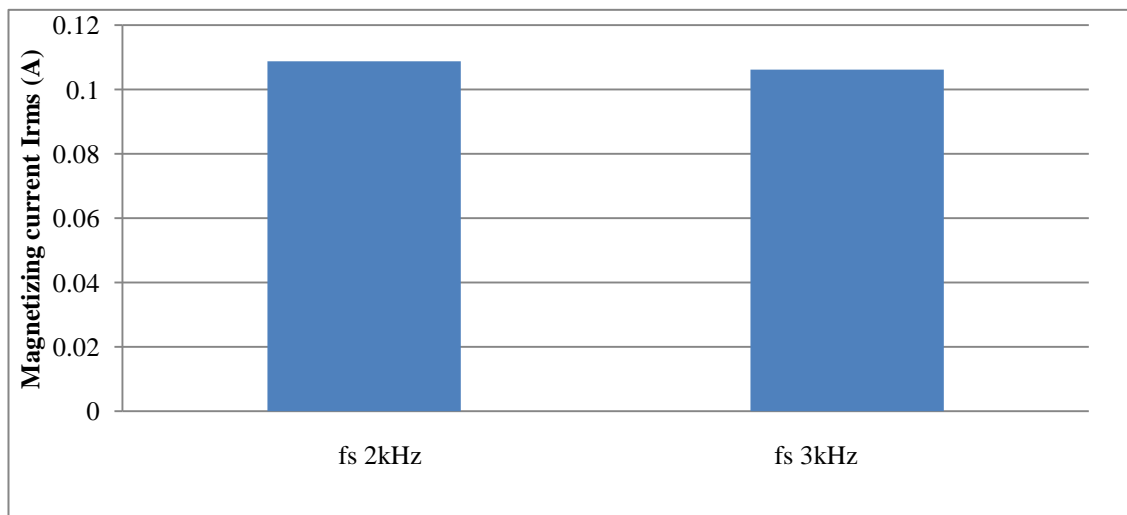


Fig. 3-6 Variation of magnetizing current at 0.3T in the middle limb with assigned values of switching frequency (kHz)

Investigation of No-load and on-load performance of a model three-phase transformer core operating under sinusoidal and PWM voltage excitation

When the peak flux density was increased to 0.4T current needed in the outer limb at switching frequency 2 kHz was 0.139amps. Whereas, at switching frequency 3 kHz current needed was 0.1164amps as shown in figure 3-7. However, for the middle limb current needed at switching frequency 2 kHz was 0.112amps and for 3 kHz current required was 0.1091amps as shown in Fig. 3-8 respectively.

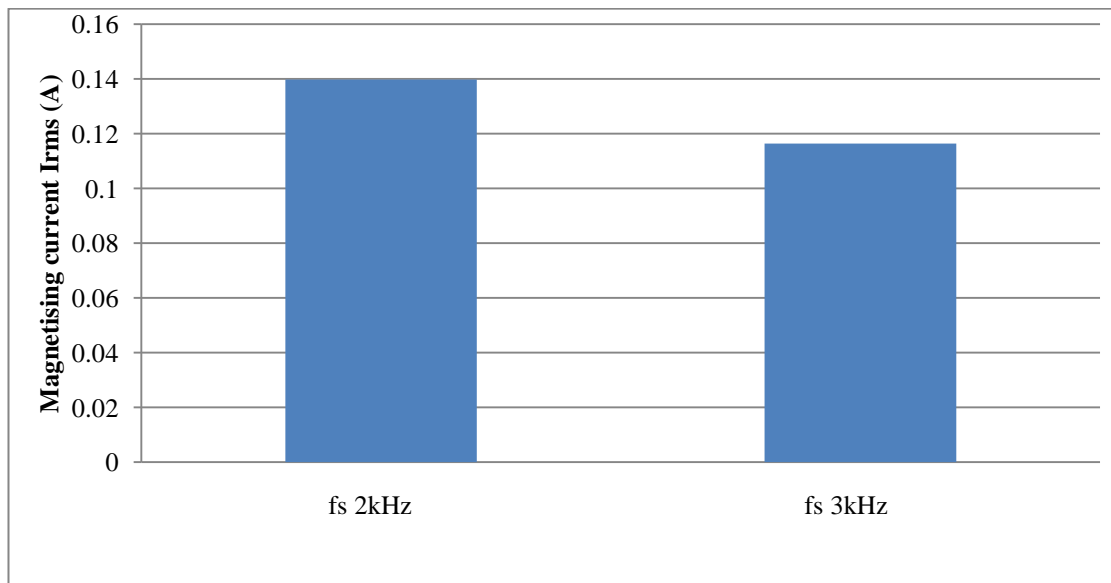


Fig. 3-7 Variation of magnetizing current at 0.4T in the outer limb with assigned values of switching frequency (kHz)

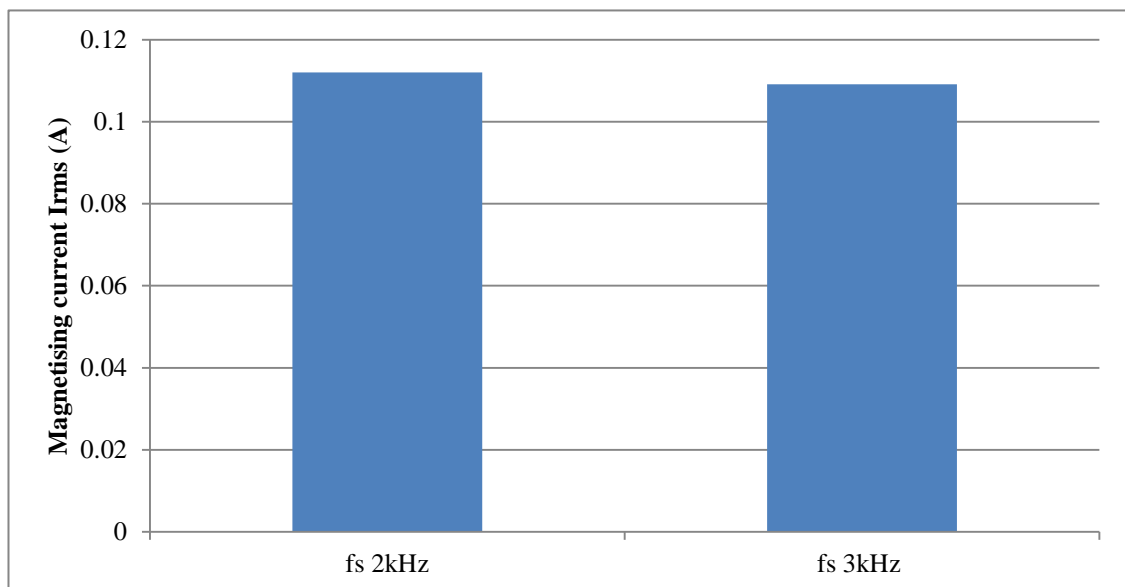


Fig. 3-8 Variation of magnetizing current at 0.4T in the central limb with assigned values of switching frequency (kHz)

Investigation of No-load and on-load performance of a model three-phase transformer core operating under sinusoidal and PWM voltage excitation

When the switching frequency was increased to 16 kHz and 12 kHz to obtain flux density of 0.7T current required in the middle limb was 0.1833 amps and 0.1869 amps respectively as shown in Fig. 3-9.

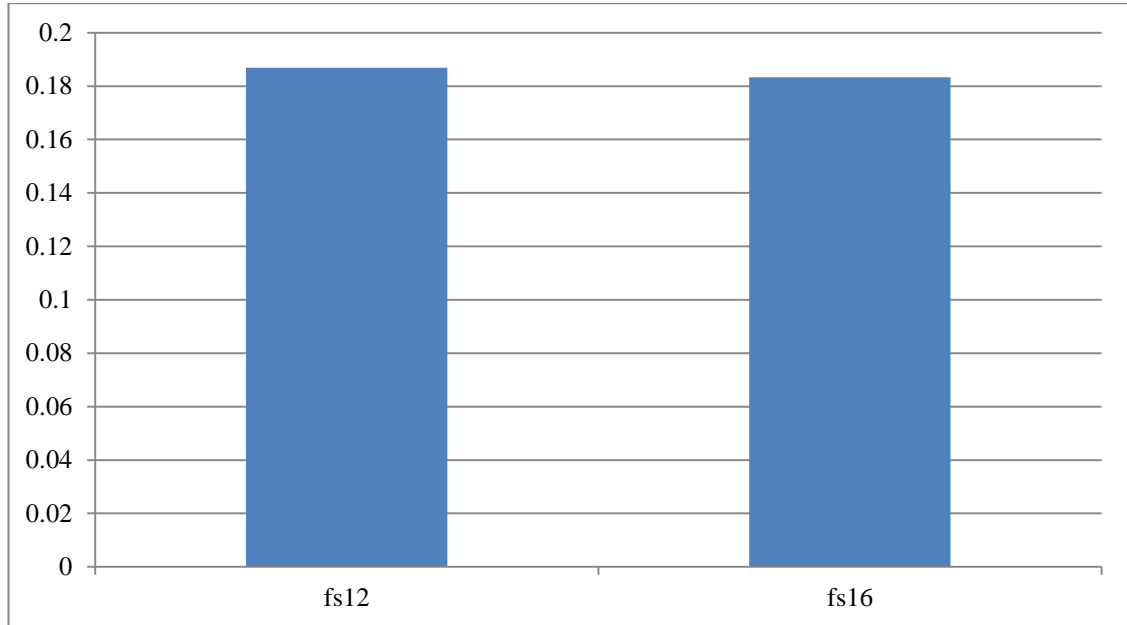


Fig. 3-9 Variation of magnetising current at 0.7T in the middle limb with assigned values of switching frequency (kHz)

Fig. 3-10 illustrates the current needed in the outer limb to obtain flux density of 0.7T at switching frequencies 16 kHz and 12 kHz were 0.1854amps and 0.1887amps respectively.

Investigation of No-load and on-load performance of a model three-phase transformer core operating under sinusoidal and PWM voltage excitation

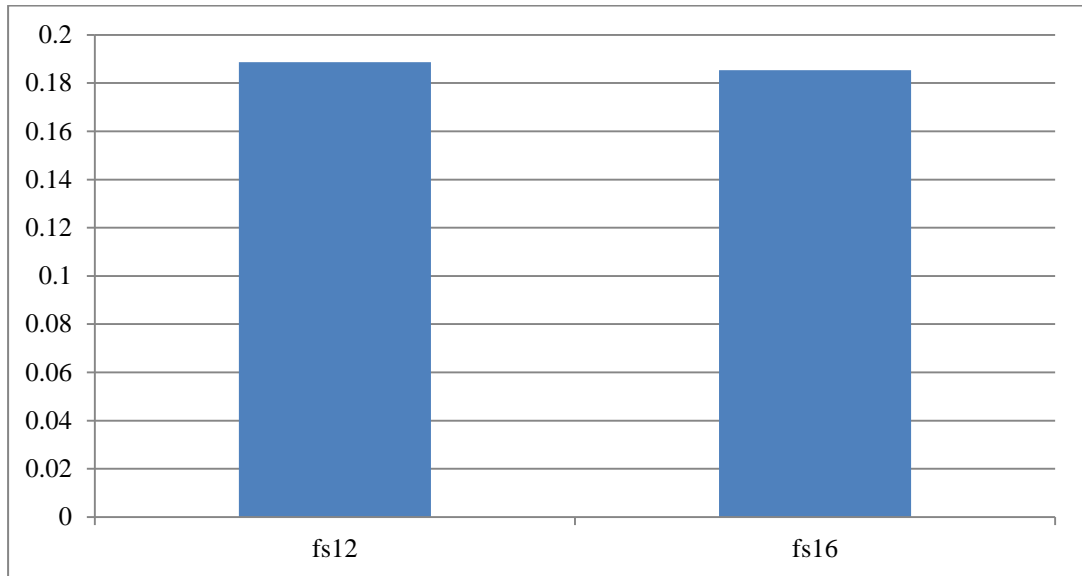


Fig. 3-10 Variation of magnetising current at 0.7T in the outer limb with assigned values of switching frequency (kHz)

Therefore, at all magnetizing levels at low switching frequency (f_s) PWM waveform requires more current than that at high switching frequency. Nevertheless, at low switching frequency audible noise is high and that will lead to increased vibration in the transformer core. Hence, magnetostriction will increase the advantages of increasing switching frequency to 16 kHz or greater is the absence of audible noise.

3.2.1 Magnetizing current variation under sinusoidal voltage excitation

Digital power analyser was used to study the variation of the magnetising current. When the core was excited via three-phase variacs, measurements were taken under load and no-load conditions. Table 3.1 and table 3.2 show current needed to obtain desired value of the peak flux density 0.3 T, 0.4 T and 0.7 T. In the outer and central limb and Fig. 3-11 to Fig. 3-16, shows the variation of magnetizing current with peak flux density in an outer and central limb.

To obtain a peak value of 0.3 T under no-load condition, currents required in the outer and central limb were 0.095A and 0.074A respectively. Whereas, currents required at 0.3 T peak flux density in the outer and central limbs under load condition were 0.4663A and 0.3879A respectively. However, increasing the flux density to 0.4 T under no-load condition currents required in the outer and central limb were 0.120A and 0.094A respectively. Furthermore at 0.4 T under load condition currents required in the outer and central limb were 0.5869A and 0.5093A respectively. Further increasing the peak flux density to 0.7T under no-load condition current required in the outer limb was 0.201A. Whereas, in the central limb current required was 0.187A. On the other hand, under load condition at 0.7 T currents required in the outer and middle limb were 1.4804A and 1.2738A respectively.

Investigation of No-load and on-load performance of a model three-phase transformer core operating under sinusoidal and PWM voltage excitation

Table 3-1 Current required for desired flux density under no-load condition

$B_{\rho\rho}$	Outer Limb I_{rms} (Amp)	Central Limb I_{rms} (Amp)	Outer Limb I_{rms} (Amp)
0.3T	0.095	0.074	0.095
0.4T	0.120	0.094	0.120
0.7T	0.201	0.187	0.201

Table 3-2 Current Required for Desired Flux Density under Load Condition

$B_{\rho\rho}$	Outer Limb I_{rms} (Amp)	Central Limb I_{rms} (Amp)	Outer Limb I_{rms} (Amp)
0.3T	0.466	0.387	0.466
0.4T	0.586	0.509	0.586
0.7T	1.480	1.273	1.480

Investigation of No-load and on-load performance of a model three-phase transformer core operating under sinusoidal and PWM voltage excitation

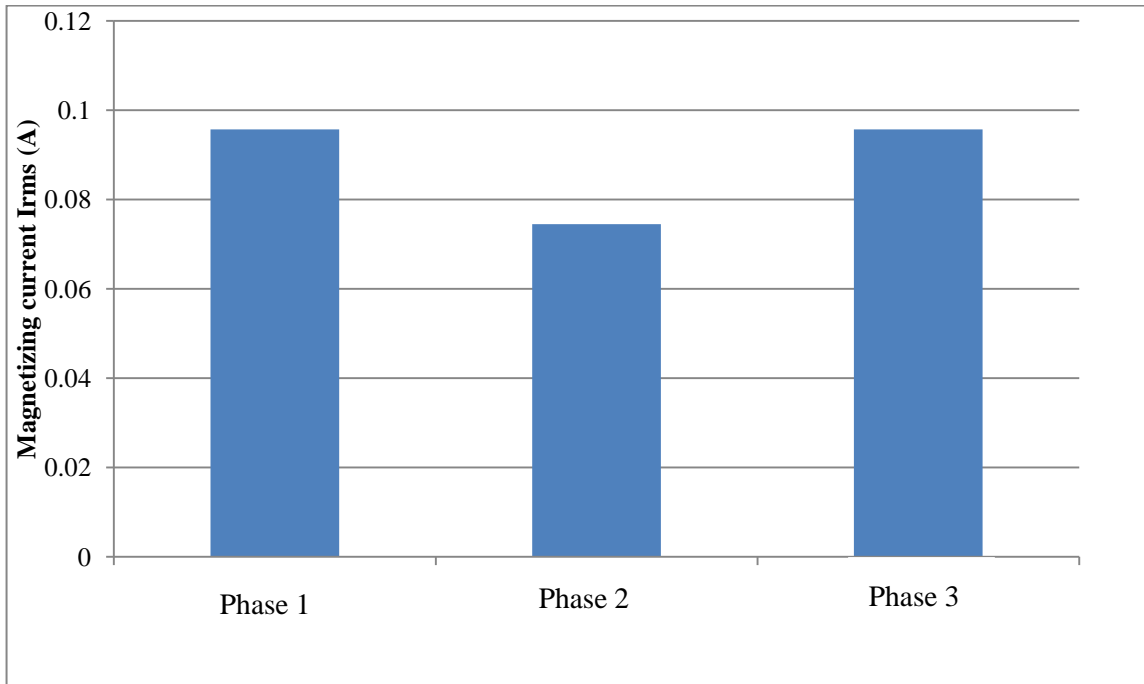


Fig. 3-11 Variation of magnetising current under three-phase variac under no-load condition at 0.3T

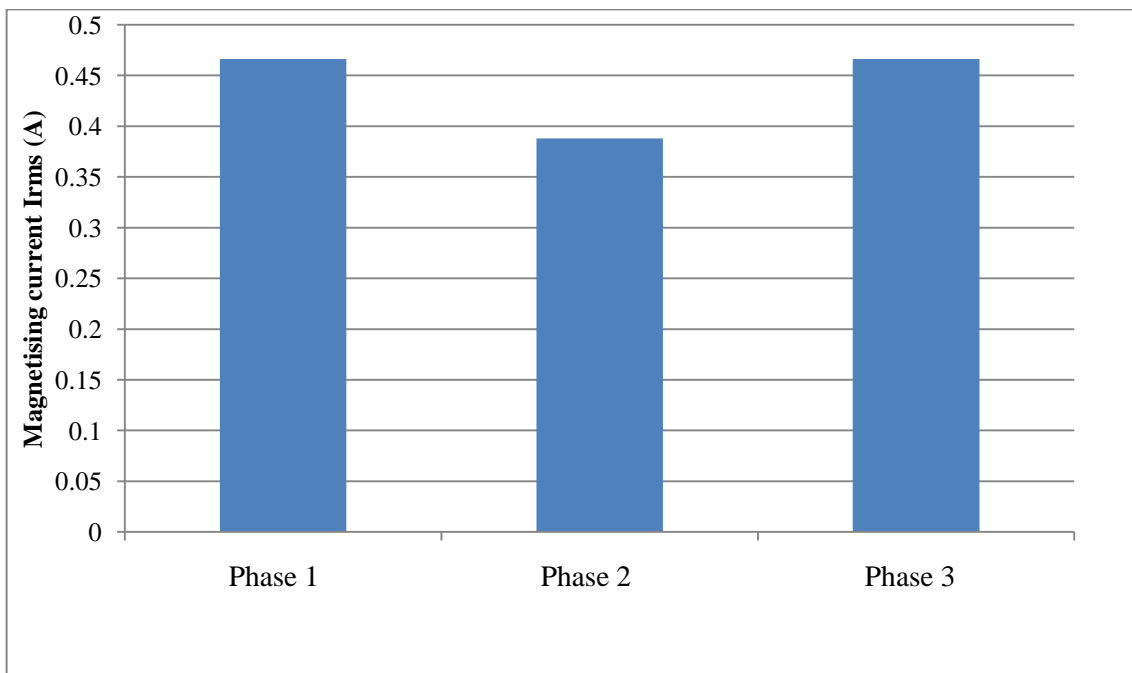


Fig. 3-12 Variation of magnetising current under three-phase variac under load condition at 0.3T

Investigation of No-load and on-load performance of a model three-phase transformer core operating under sinusoidal and PWM voltage excitation

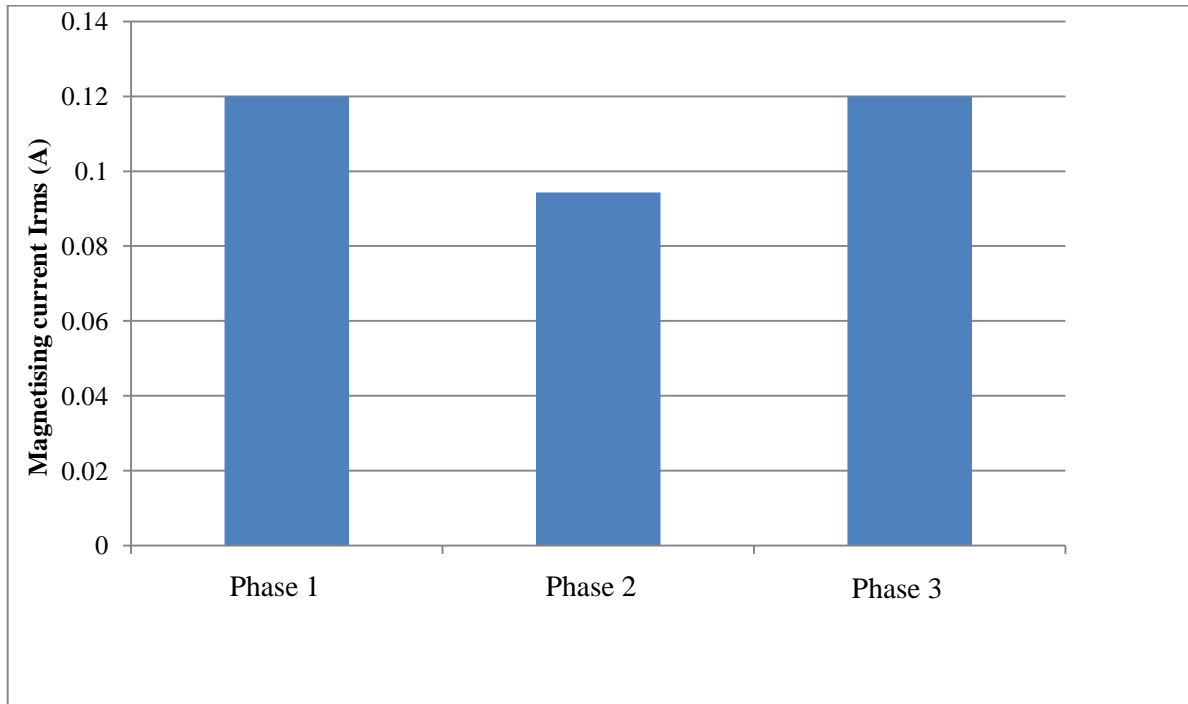


Fig. 3-13 Variation of magnetising current under sinusoidal voltage excitation under no-load Condition at 0.4T

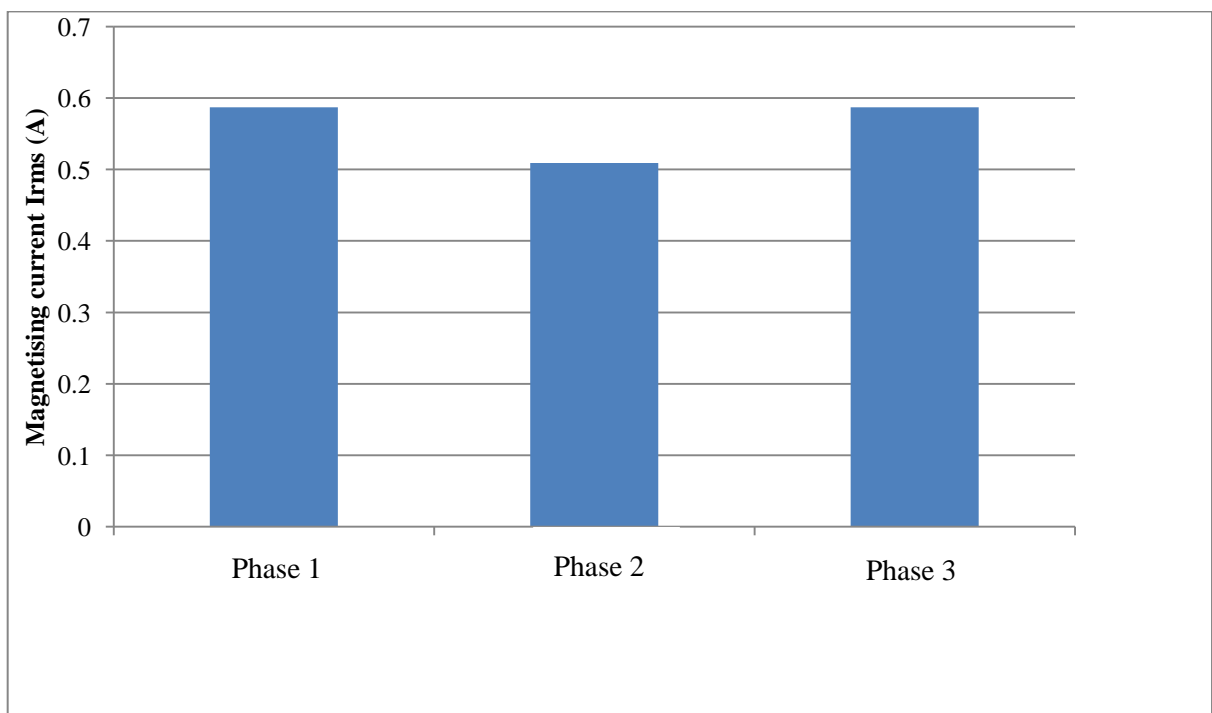


Fig. 3-14 Variation of magnetising current under sinusoidal voltage excitation under Load Condition at 0.4T

Investigation of No-load and on-load performance of a model three-phase transformer core operating under sinusoidal and PWM voltage excitation

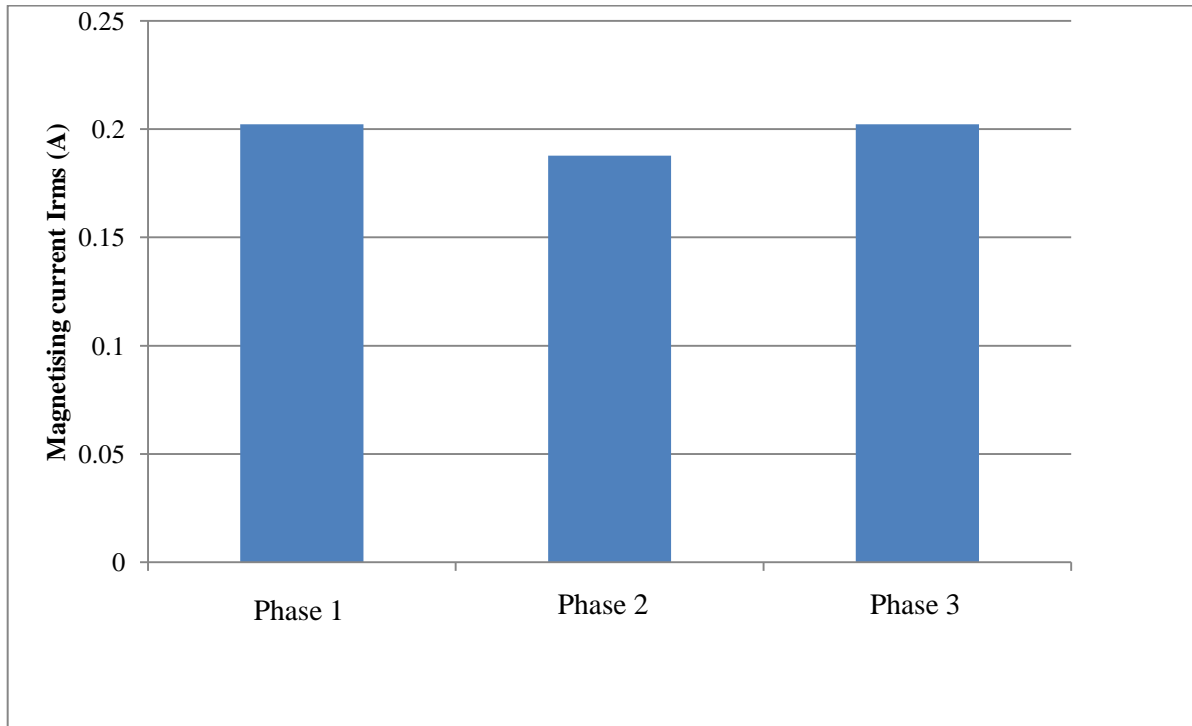


Fig. 3-15 Variation of magnetising current under sinusoidal voltage excitation under no-load Condition at 0.7T

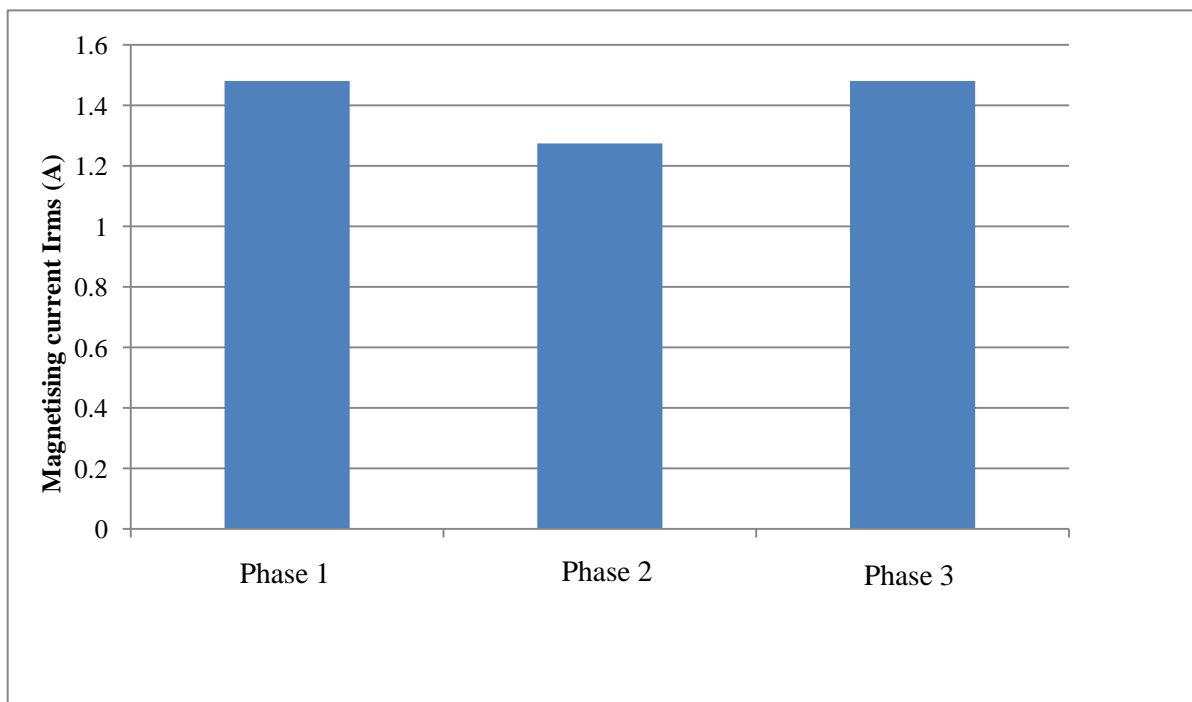


Fig. 3-16 Variation of magnetising current under sinusoidal voltage excitation under load Condition at 0.7T

Investigation of No-load and on-load performance of a model three-phase transformer core operating under sinusoidal and PWM voltage excitation

Therefore, at all levels of magnetizations under both conditions, currents in the outer limbs of the Three-phase transformer core were higher than those in the central limb at 0.3T, 0.4T and 0.7T in the range of 68% to 97%, this was due to the asymmetry of the magnetic path.

3.2.2 Comparison of the results

As it has been shown in Fig. 3-5 to Fig. 3.10, under PWM voltage excitation at low switching frequency, current is higher than those at high switching frequency. However, comparing the result obtained under both PWM and sine waveform, current variation at 0.3T was higher under sinusoidal excitation than those under PWM excitation in the outer and central limb.

At 0.3 T in the other limb, current variation under PWM excitation was higher than those under sinusoidal excitation by the factor of 83%. Furthermore, at the middle limb current variation under PWM excitation was higher by the factor of 68%.

Increasing the flux to 0.4 T, current variation under PWM excitation was higher than sinusoidal excitation in the outer limb by 86%, whereas in the central limb it was higher under sinusoidal by the factor of 83%.

At 0.7 T, current variations under PWM excitation recorded higher value than those under sinusoidal excitation, in the outer limb it was higher by the factor of 92%. Whereas in the central limb it was again higher by the factor of 97%. Comparison of the measurement result is shown in table 3.3.

Investigation of No-load and on-load performance of a model three-phase transformer core operating under sinusoidal and PWM voltage excitation

Table 3.3 Comparison of the Current measurements under sinusoidal and PWM voltage excitation in the central and outer limb of the module Three-phase transform core

B_{pk} T	Sin waveform		PWM waveform		Percentage	
	Outer	Central	Outer	Central	Sin	PWM
0.3	0.095	0.074	0.1144	0.1087	22%	4%
0.4	0.120	0.097	0.139	0.112	19%	19%
0.7	0.201	0.187	0.1887	0.1869	6%	0.9%

It could conclude that under all magnetising level variation current under PWM excitation was higher than those under sinusoidal excitation. However, agreement has been obtained from these experiments. Under all level of magnetising current under both sinusoidal and PWM voltage excitation outer limb shows higher value than the central limb this was due to the asymmetry of the magnetic path.

3.2.3 Effect of switching frequency on overall flux density

One significant parameter that determines the output voltage of the PWM inverter is a switching frequency. Switching frequency and its effect on overall flux density distribution has been studied in detail throughout this work. Switching frequency was varied in the range 2 kHz, 3 kHz, 8 kHz, 12 kHz, and 16 kHz. Single turn search coil was wound around the limb and around the yoke and then single measurement was taken separately for each switching frequency. Transformer core was energised with different peak flux density 0.4T, 0.6T and 1.0T. Measurements were taken under load and no-load conditions using “Lab-View” program as shown in chapter 4. Fig. 4-4.

When transformer core energised at peak flux density of 0.4T under no-load condition at switching frequency f_s 2 kHz, the overall induced voltage was $5.627mV$. Increasing the switching frequency f_s to 3 kHz, overall induced voltage was $5.126mV$. Energising the core with the same peak flux density of 0.4T under load condition at switching frequency f_s 2 kHz, overall induced voltage was found to be $6.486mV$, while increasing the switching frequency to 3 kHz, overall induced voltage was $5.417mV$,

Energising the core with 0.6T under no-load condition at switching frequency f_s 3 kHz overall induced voltage was $7.158mV$, decreasing the switching frequency f_s to 2 kHz overall induced voltage was $8.056mV$. However, when measurements were taken under load condition at $f_s = 2$ kHz and $f_s = 3$ kHz overall induced voltage was $6.486 mV$ and $9.475 mV$.

Increasing the energising flux to 1.0T under no-load condition at f_s 16 kHz, overall induced voltage was $13.343mV$, reducing the switching frequency to 12 kHz, overall induced voltage was $13.577mV$. However, when the core was energised at same peak flux density under load condition at switching frequency of 16 kHz, overall induced voltage was $13.039mV$, decreasing the switching frequency to 12 kHz, overall induced voltage was $13.135 mV$. Further decrease of the switching frequency to 8 kHz, resulted in having an overall induced voltage of $13.425 mV$,

Investigation of No-load and on-load performance of a model three-phase transformer core operating under sinusoidal and PWM voltage excitation

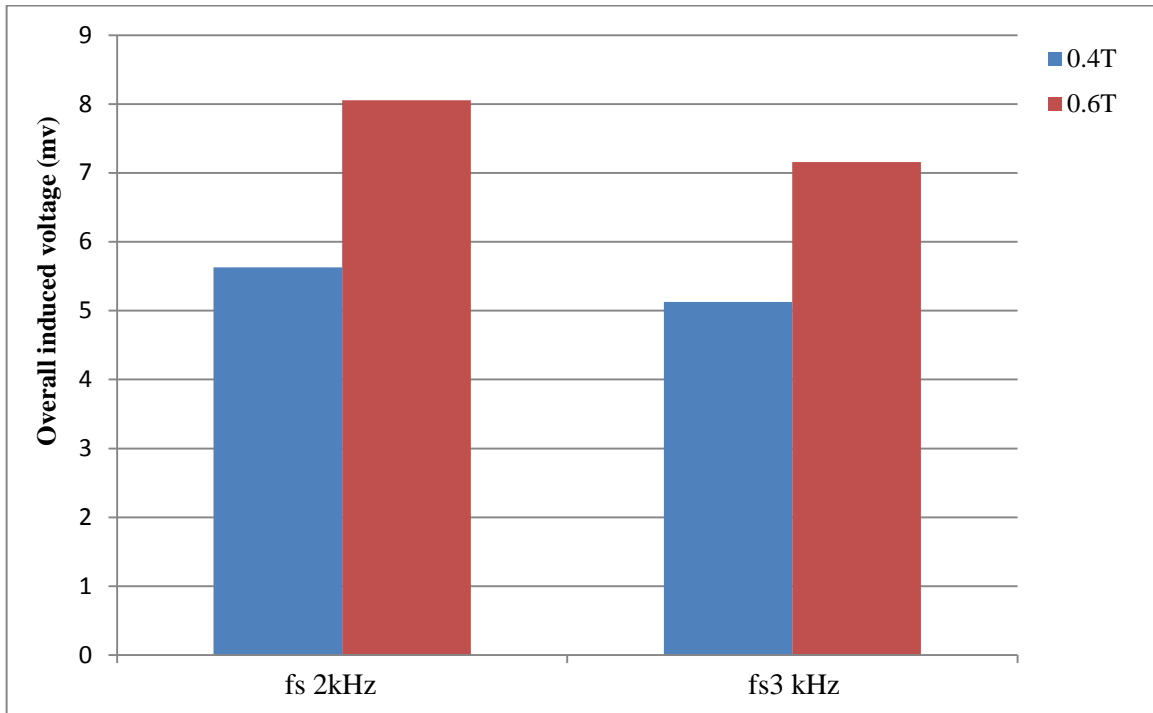


Fig. 3-17 Overall induced voltage under PWM voltage excitation (no-load conditions) with switching frequency varied from 2 to 3 kHz at different peak flux density (T)

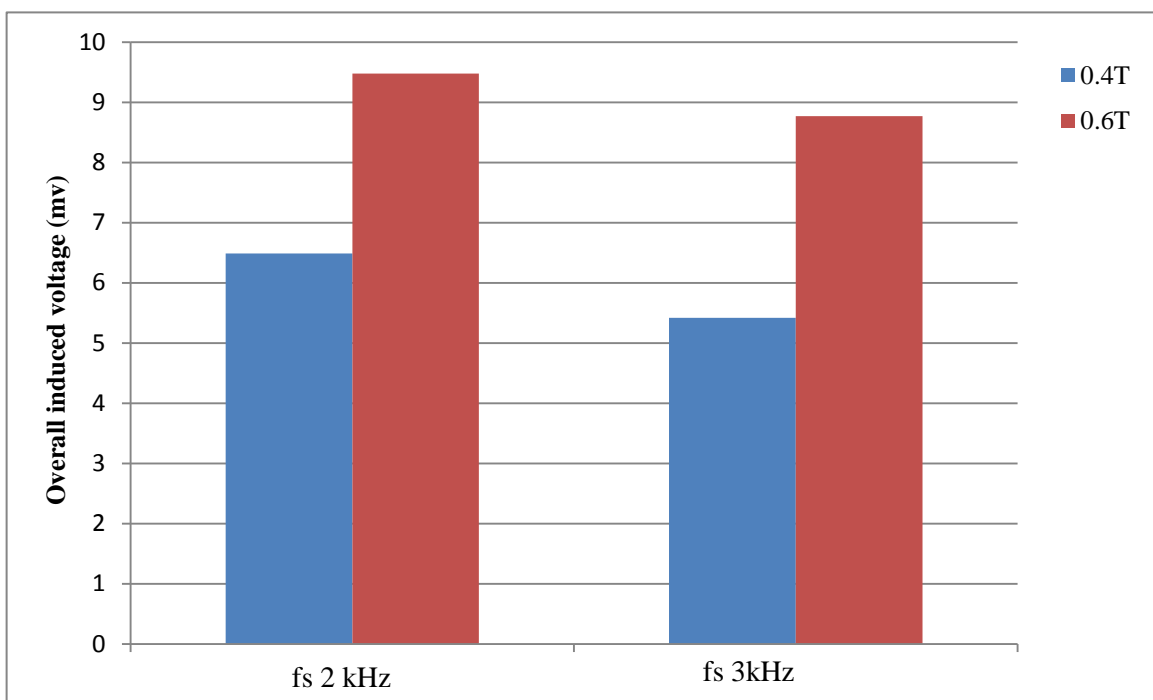


Fig. 3-18 Overall induced voltage under PWM voltage excitation (load conditions) with switching frequency varied from 2 to 3 kHz at different peak flux density (T)

Investigation of No-load and on-load performance of a model three-phase transformer core operating under sinusoidal and PWM voltage excitation

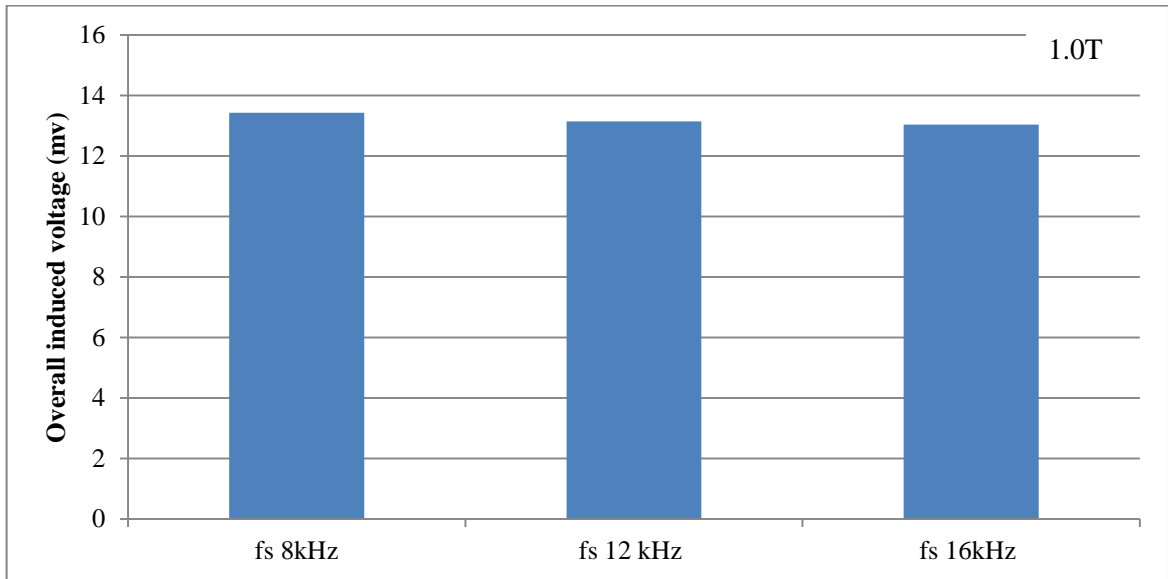


Fig. 3-19 Overall induced voltage under PWM voltage excitation (load conditions) with switching frequency varied between 8, 12, 16 kHz at different peak flux density (T)

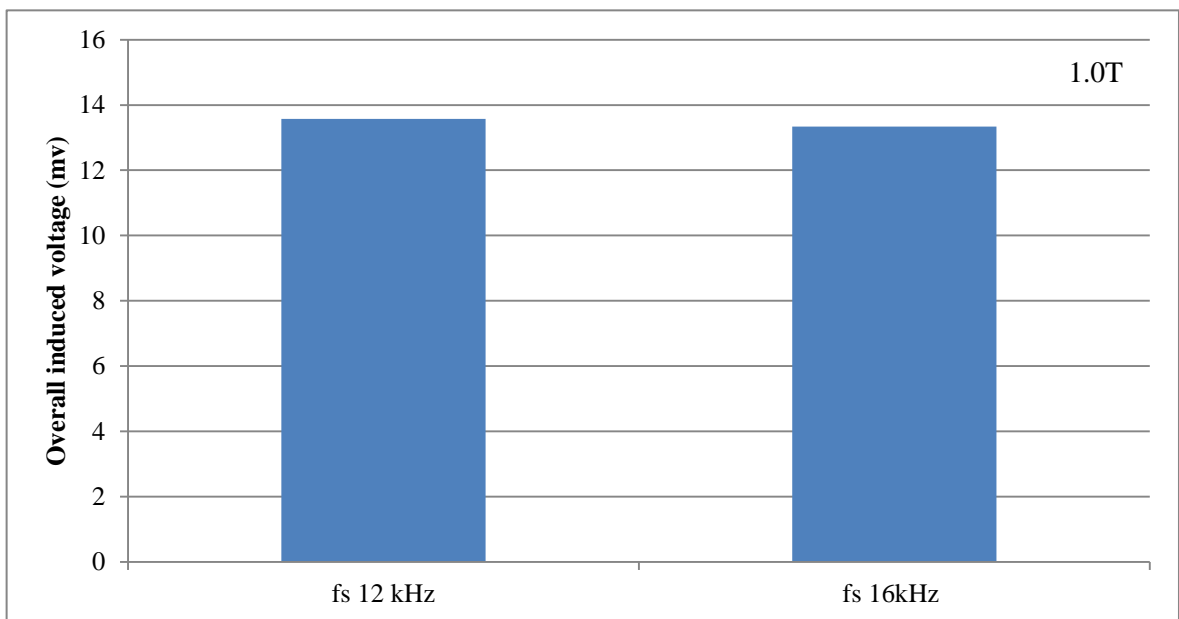


Fig. 3-20 Overall induced voltage under PWM voltage excitation (load conditions) with switching frequency varied between 12, 16 kHz at different peak flux density (T)

Therefore, at all magnetising levels, the induced voltages under low switch frequencies were higher than those at high switch frequency.

3.3 Overall power losses under sinusoidal waveform

Three-phase power analyser “Norma D6000 (S/N: ND 58172 RR)”, was set to measure total power losses under sinusoidal voltage excitation under load and no-load conditions. Torque wrench was used to select desired clamping pressure on the core which was varied in the range of (0, 8, 15, and 27 N/m²). Moreover, overall flux density was varied respectively in the range of (0.3T, 0.4T and 1T). Total power loss formula used was:

$$P_{total} = I_O \cdot U \cdot \cos \varphi \quad (3.3)$$

Where I is the current and U is the voltage. In this experiment the number of turns of the primary and secondary windings were 50 each. In other word, the turn ratio of this transformer is equal to one. Hence, since the number of turns of the primary and secondary are the same ($N_p=N_s$), the induced voltage in the secondary winding is equal to the voltage on the primary winding ($V_s = V_p$). In the power analyser measurement system, primary current (I_p) and secondary voltage (V_s) of the transformer were used.

3.3.1 Setup of the measurement of overall power loss

Fig. 3-21, shows a picture of the measuring system which includes three single-phase variacs with star connection, used to magnetise the transformer core. A digital multi-meter was used to measure the output voltage of the single turn search coil and a digital three-phase power analyser was used to measure the overall power loss. The transformer core is made by highly grain-oriented material HGO and the laminated core was compressed together with three non-magnetic clamping bars. The total mass of the core was 96.1 ± 0.01 kg. The primary and secondary windings were all connected in star- star (λ - λ) configurations. Tables 3.3 to 3.4 and graphs 3.22 to 3.30 shows the total power losses under load and no-load conditions

Investigation of No-load and on-load performance of a model three-phase transformer core operating under sinusoidal and PWM voltage excitation

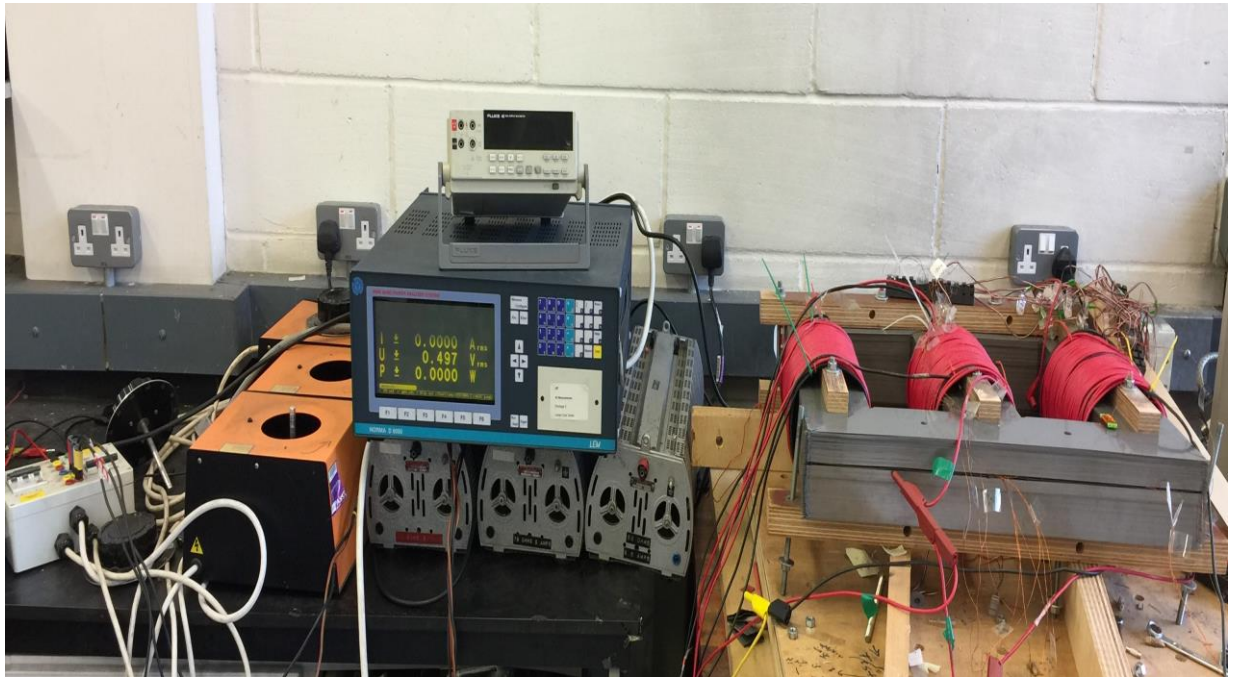


Fig. 3-21 Overall power loss measurement system

Table 3-3 Overall Power under No-load condition

B_{pk} (T)	Clamping pressure (N/m^2)	P_{total} W/kg
0.4	0	0.41
	8	0.45
	15	0.47
	27	0.48
0.6	0	0.57
	8	0.78
	15	0.87
	27	0.88
1	0	1.22
	8	1.24
	15	1.19
	27	1.18

Investigation of No-load and on-load performance of a model three-phase transformer core operating under sinusoidal and PWM voltage excitation

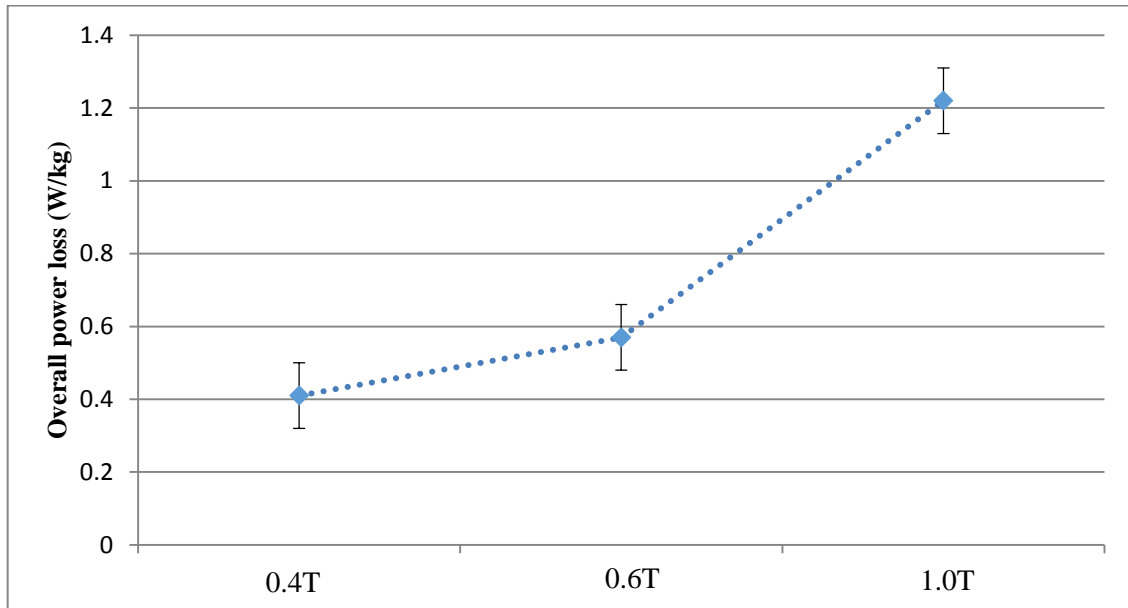


Fig. 3-22 Overall power loss at clamping pressure of 0 N/m^2 under no-load condition at different flux densities

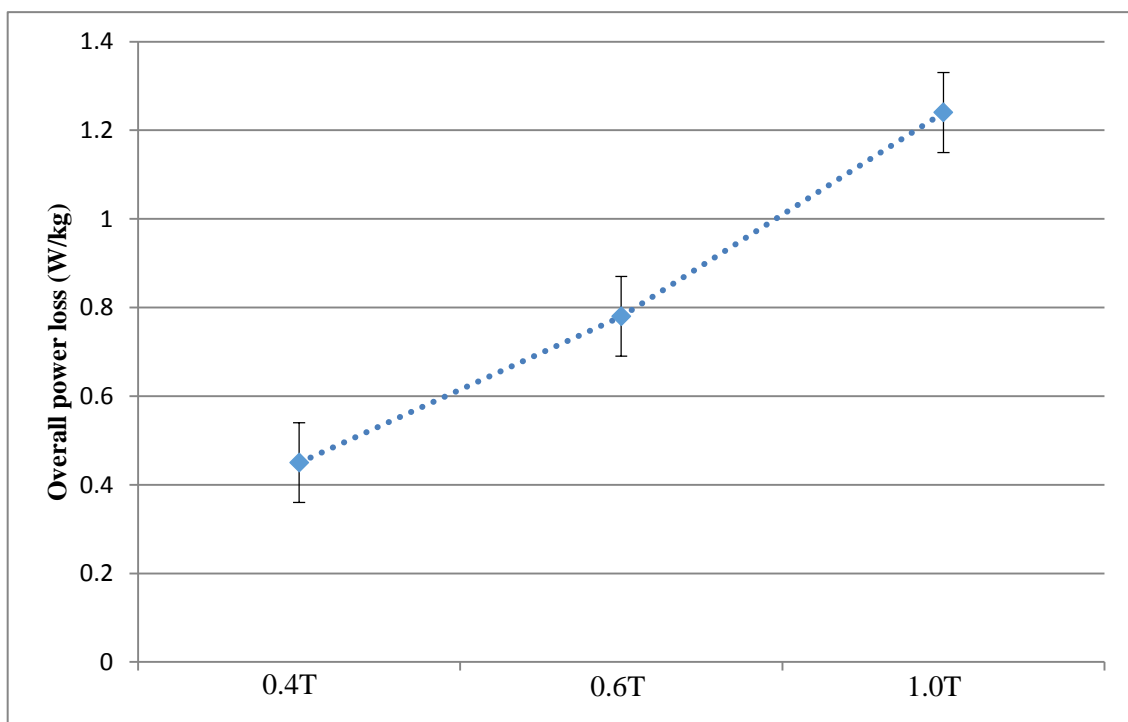


Fig. 3-23 Overall power loss at clamping pressure of 8 N/m^2 under no-load condition at different flux densities

Investigation of No-load and on-load performance of a model three-phase transformer core operating under sinusoidal and PWM voltage excitation

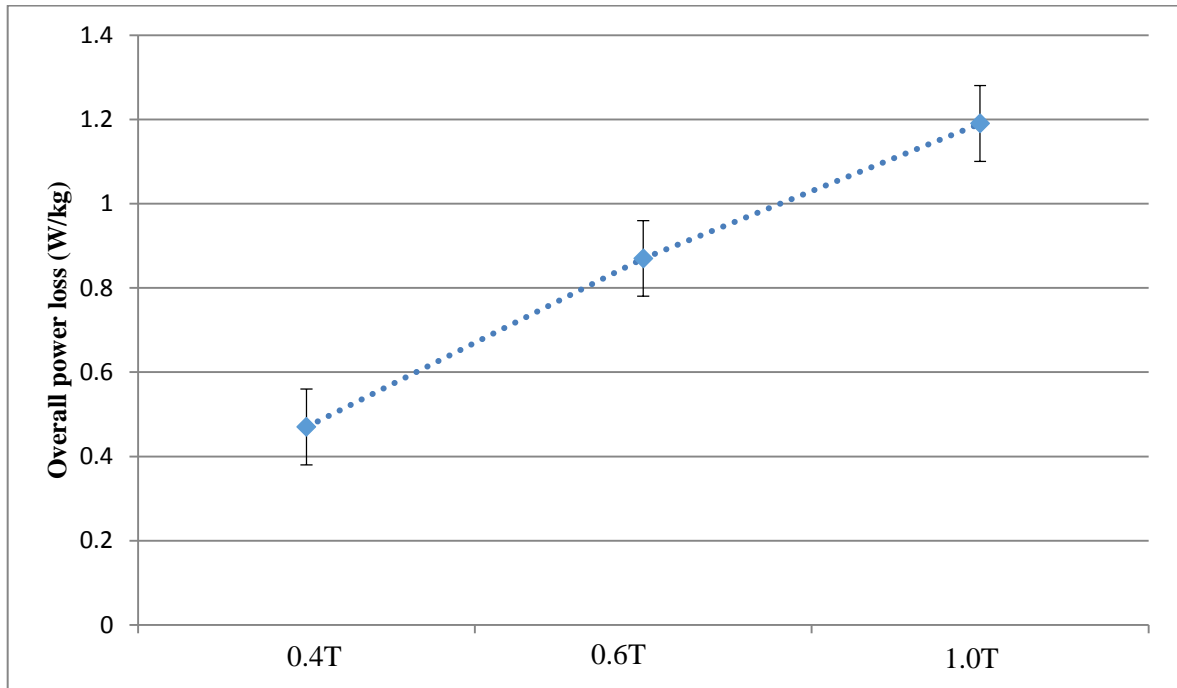


Fig. 3-24 Overall power loss at clamping pressure of 15 N/m² under no-load condition at different flux densities

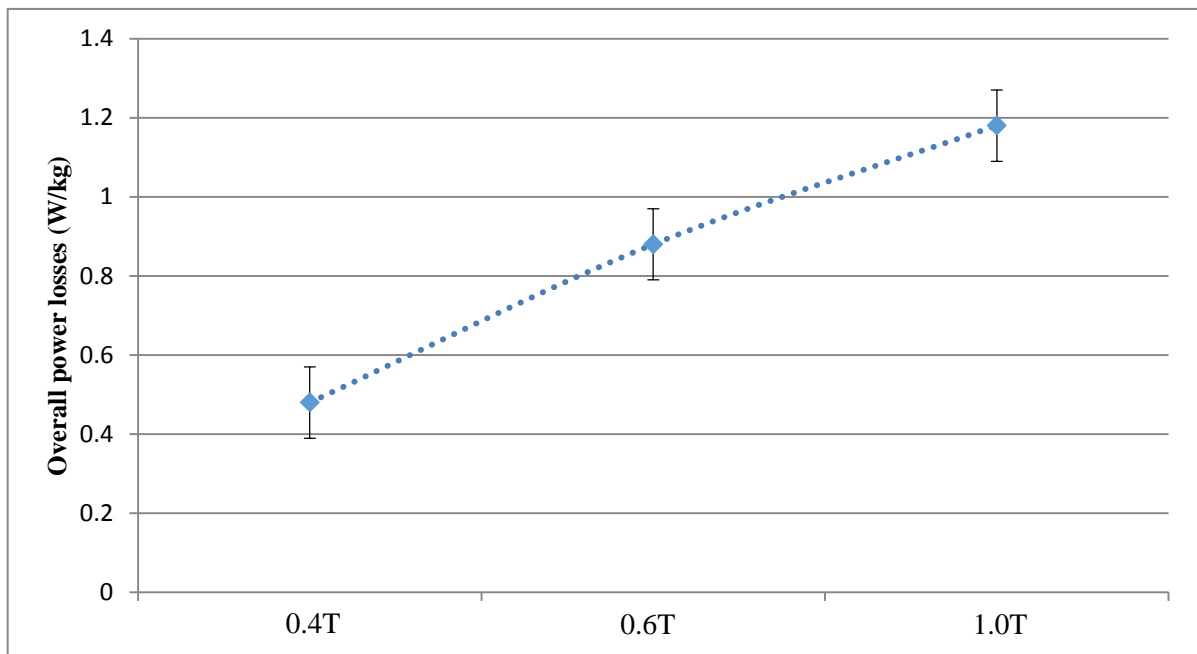


Fig. 3-25 Overall power loss at clamping pressure of 27 N/m² under no-load condition at different flux densities

Investigation of No-load and on-load performance of a model three-phase transformer core operating under sinusoidal and PWM voltage excitation

Table 3-4 Overall power loss under load condition

B_{pk} (T)	Clamping pressure (N/m^2)	P_{total} W/kg
0.4	0	0.51
	8	0.54
	15	0.56
	27	0.57
0.6	0	0.77
	8	0.82
	15	0.91
	27	0.92
1	0	1.20
	8	1.34
	15	1.17
	27	1.16

Investigation of No-load and on-load performance of a model three-phase transformer core operating under sinusoidal and PWM voltage excitation

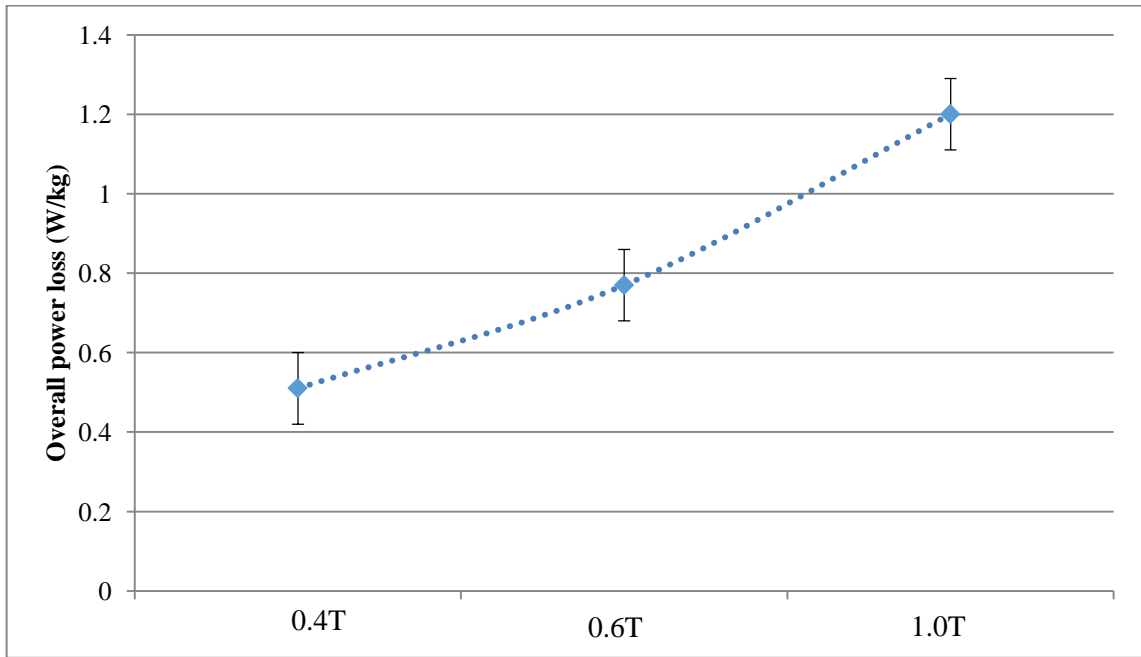


Fig. 3-26 Overall power loss at clamping pressure of 0 N/m² under load condition at different flux densities

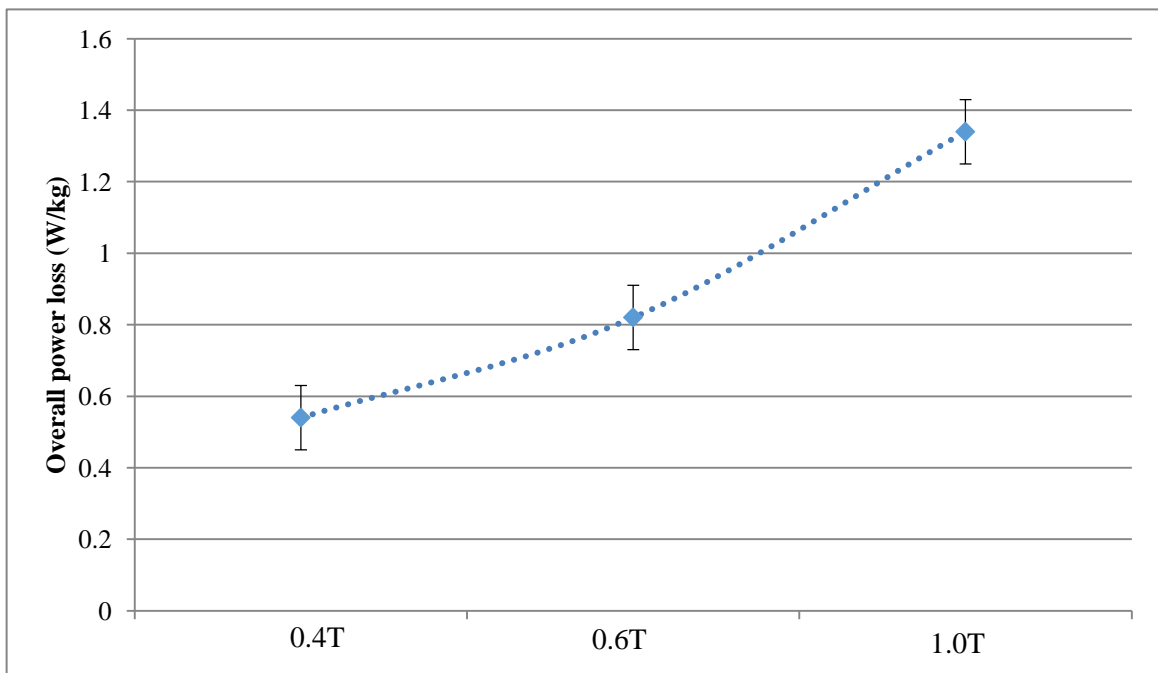


Fig. 3-27 Overall power loss at clamping pressure of 8 N/m² under Load Condition at different flux densities

Investigation of No-load and on-load performance of a model three-phase transformer core operating under sinusoidal and PWM voltage excitation

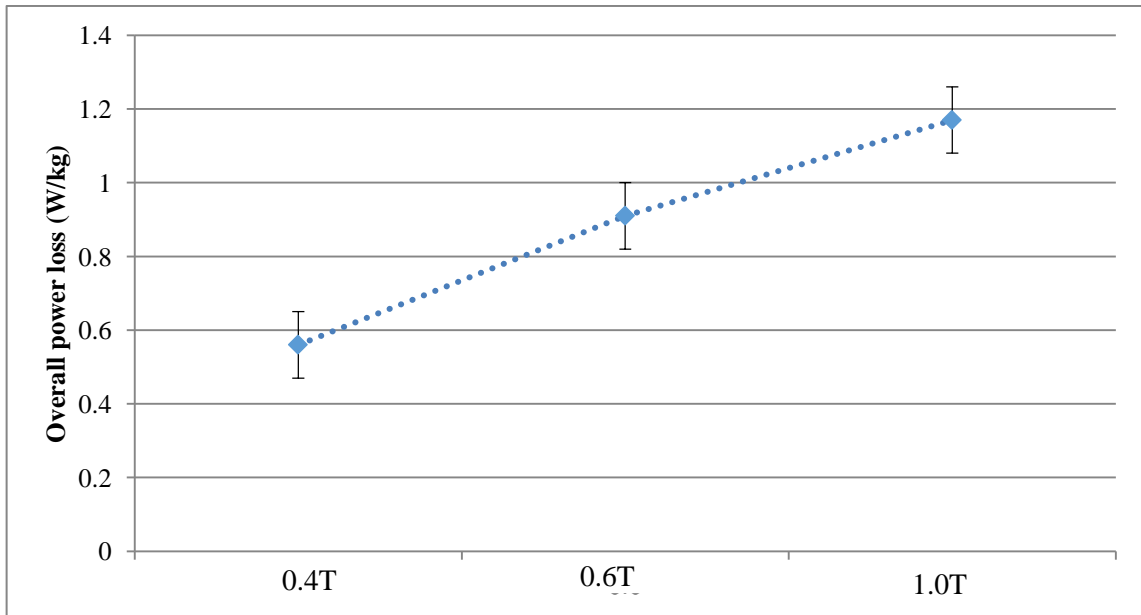


Fig. 3-28 Overall power loss at clamping pressure of 15 N/m^2 under load condition at different flux densities

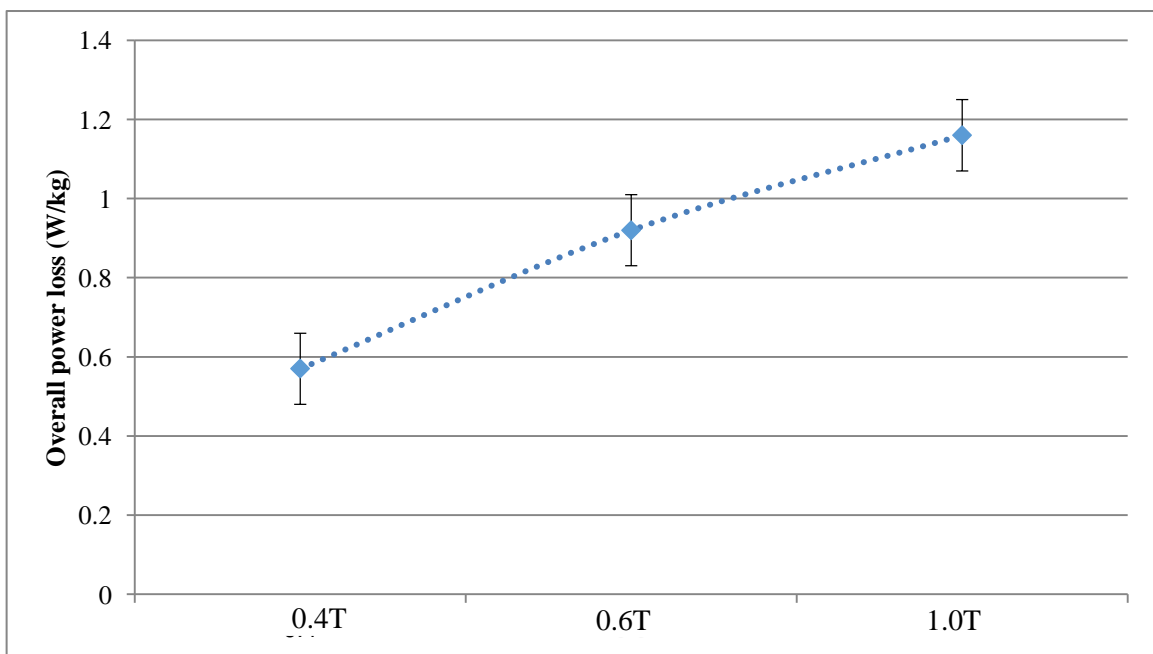


Fig. 3-29 Overall power loss at clamping pressure of 27 N/m^2 under load condition at different flux densities

3.3.2 Effect of clamping pressure

Pro Dial torque wrench was used to set desired clamping pressure on the transformer core, the effect of the clamping torque was monitored on three-phase power analyser “Norma D6000 (S/N: ND 58172 RR)”. When the clamping pressure was changed from zero to 8N/m^2 , its effect at low flux density was to increase the exciting current by 1.3% to keep the flux density constant. At the higher clamping pressure of 15N/m^2 further increase of 3.8%, was required to maintain same flux density. On the other hand, when the core was operated at 1.0T the exciting current had to be reduced with increasing clamping pressure. A reduction of 2.6% was observed with the clamping pressure increased from zero to 8N/m^2 .

The effect of clamping pressure on power loss is shown in tables 3.3 and 3.4 and Fig. 3-22 to Fig. 3-29. At low magnetic flux density, an increase of power was observed. At high flux density of 1.0T, a reduction in power loss was obtained under load and no-load conditions as shown in tables 3.3 and 3.4.

So it could be concluded that, at higher flux density and higher clamping pressure, power loss decreased. That may be due to the fact that higher pressure improves flux transfer in the corner and at T-joint regions by reducing interlaminar gaps and hence reduces the loss in the joints.

3.3.3 Analysis and discussion

As it has been shown in the tables 3.3 and 3.4 at all level of peak flux densities and under all levels of clamping pressure, overall power losses were higher under load condition than that under no-load condition.

At 0.4T 0 N/m², the variation in power losses was higher under load condition than no-load condition by 19%. Increasing the clamping pressure to 8 N/m², the variation in overall power loss was higher by 16% under load condition. Further increase in clamping pressure to 15 N/m² again overall power loss was higher by 16%. More increasing of clamping pressure, power losses variation was kept a same percentage difference.

Hence, it could be concluded that, the effect of varying clamping pressure on power loss as shown in Fig. 3-22 to Fig. 3-29 an increasing of power loss was observed when the clamping pressure was increased from 0 M/m² to 8 M/m². However, further increasing of clamping pressure from 15 N/m² to 27 N/m². Power losses decrease.

3.3.4 Order harmonic content with a change in peak flux density

Harmonic content of the primary current for peak flux densities of 0.4T and 1.0T was examined. The result of the primary current from a sinusoidal excitation can be seen in Fig 3.30. With change in core peak flux density. The harmonic components of the secondary voltage waveform from sinusoidal supply can be seen in Fig. 3.31 the harmonic existing in the primary current from the two peak flux densities excited from PWM source can be seen in Fig 3.32. The harmonic from the secondary PWM voltage waveform can be seen in Fig 3.33

Investigation of No-load and on-load performance of a model three-phase transformer core operating under sinusoidal and PWM voltage excitation

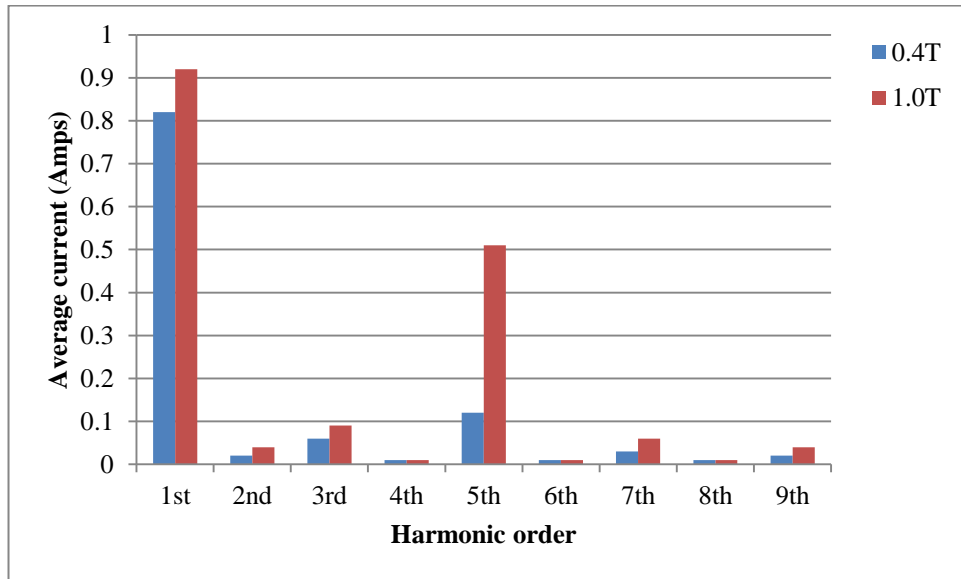


Fig. 3-30 Harmonic content of sinusoidal primary current at peak flux densities of 0.4T and 1.0T

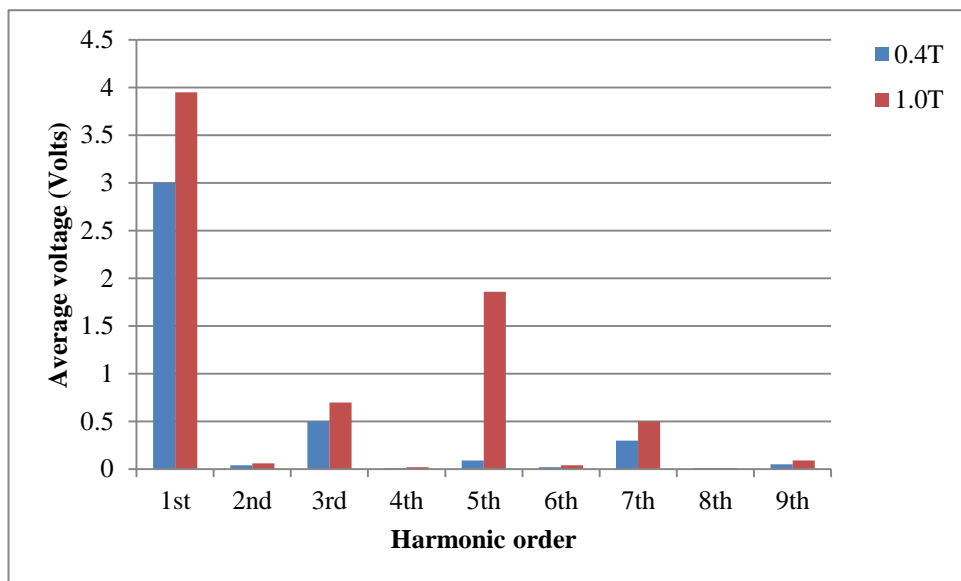


Fig. 3-31 Harmonic content of sinusoidal secondary voltage at peak flux densities of 0.4T and 1.0T

Investigation of No-load and on-load performance of a model three-phase transformer core operating under sinusoidal and PWM voltage excitation

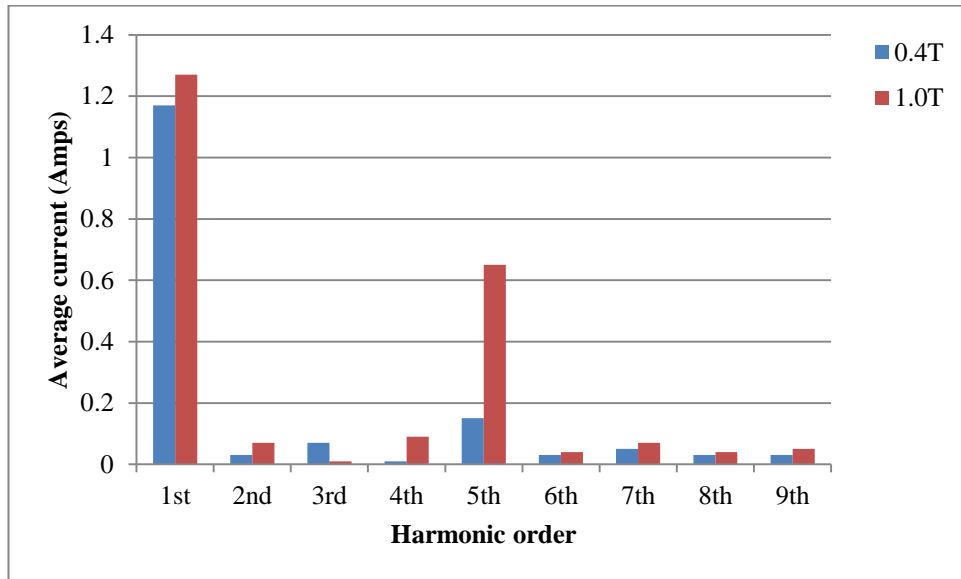


Fig. 3-32 Harmonic content of PWM primary current at peak flux densities of 0.4T and 1.0T

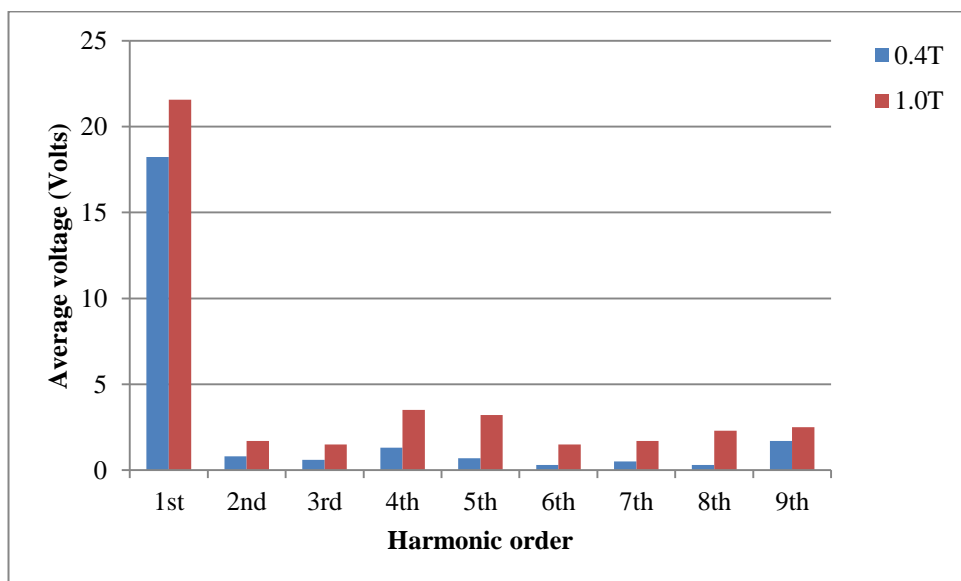


Fig. 3-33 Harmonic content of PWM secondary voltage at peak flux densities of 0.4T and 1.0T

CHAPTER 4

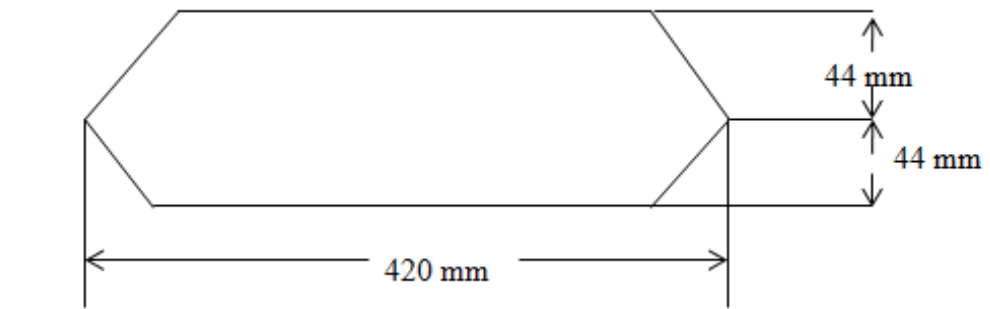
4. Experimental apparatus and measuring technique

The apparatus comprised a 100 kVA, three-phase transformer core with associated instrumentation to measure flux density, power loss and localised mechanical stress within the core.

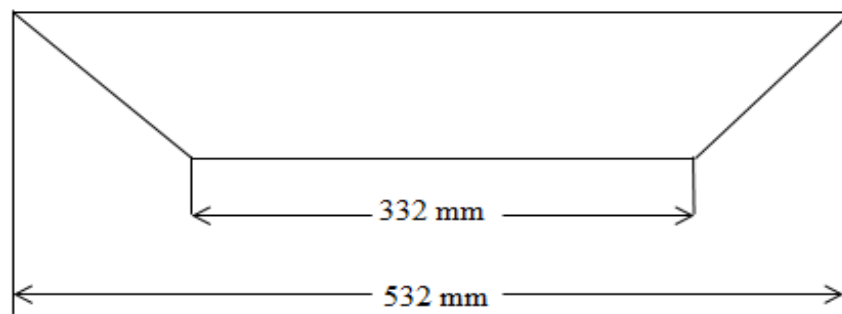
4.1.1 Core geometry

In order to investigate the core losses and mechanical stress under sinusoidal and PWM excitations, experiments were carried out on high permeability grain oriented (HGO) [51], three-phase 100 kVA transformer core. The core was built with single step lap configuration with lamination of 100 mm wide, 0.3 mm thick and density of 7650 kg/m^3 . Overlap shift of 3 mm, the core has been used with three laminations per stacking layer having [011] [100] texture, these are known as Goss texture. The laminations are coated with insulating materials on both sides to provide good electrical insulation and improve the texture of the material. Fig 4-1a, 4.1b and 4.1c show the overall dimensions of the core [40].

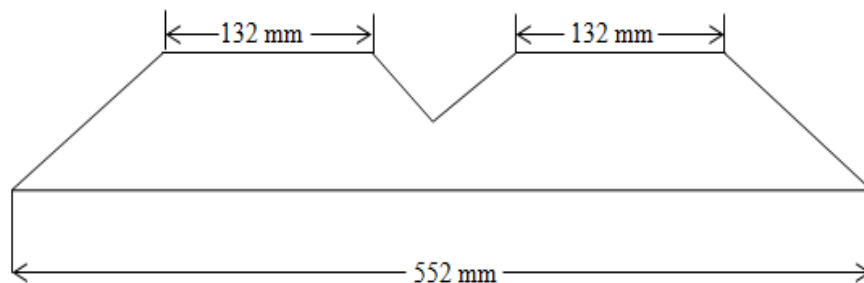
Investigation of No-load and on-load performance of a model three-phase transformer core operating under sinusoidal and PWM voltage excitation



(a)



(b)



(c)

Fig. 4-1 (a) Dimension of the middle limb. (b) Dimensions of the outer limb (c) Dimensions of the yoke

Investigation of No-load and on-load performance of a model three-phase transformer core operating under sinusoidal and PWM voltage excitation

4.1.2 Type of joints

The popular $45^{\circ} - 90^{\circ}$ joint was employed at the T-section and the 45° mitred overlap joints were used at the corners.

4.1.3 Support and clamping

The core was built carefully to avoid air gaps in the joints. It was placed horizontally on stiff wooden table. Fig. 4-2 shows each limb and yoke of the core has two holes and two circular slots. The diameter of the holes was 1 cm and slot length was 1.1cm. Transformer was then clamped by three wooden clamps in the limb $37\text{cm} \times 3\text{cm}$ and two wooden clamps in the yoke with four holes $65\text{cm} \times 5\text{cm}$. Wooden clamp was place over and underneath limb and yokes to avoid any bending. Fibre reinforced plastic bolts inserted through the slot. Torque wrench was used to apply desired clamp force onto the core.

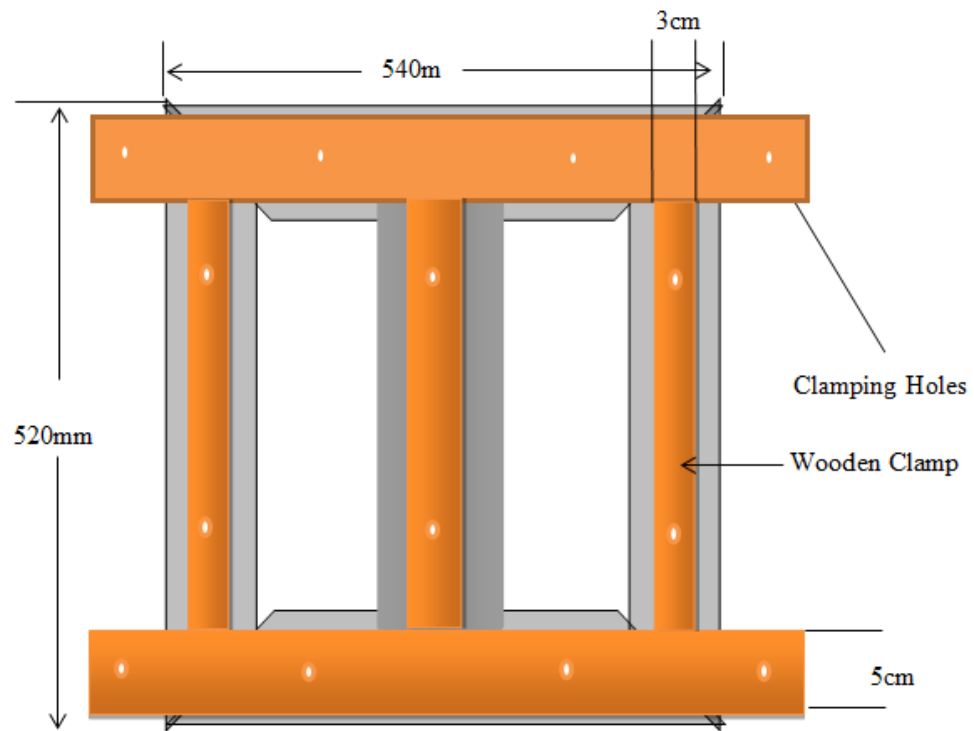


Fig. 4-2 Three-phase transformer core

Investigation of No-load and on-load performance of a model three-phase transformer core operating under sinusoidal and PWM voltage excitation

The photograph of the apparatus shown in Fig. 4-3 was used to magnetize the core, transformer was energised under sinusoidal waveform and PWM waveform.

When the core was fed by three-phase sinusoidal supply voltage was stepped down through three cascaded variacs. Three variacs, were used to give desired peak flux density and to balance the secondary induced voltage.

Additional fine control adjustment was achieved by power analyser. Three primary and secondary windings were connected to a precision digital power analyser “NORMA D6000 Wide-Band Power Analyser System”. Digital oscilloscope was used to record secondary induced voltage.

However, under PWM voltage excitation primary winding was connected to the output of the inverter and the output voltage of the inverter was adjusted through the front panel of the inverter. Transformer winding has 50 turns of PVC coated copper wire with voltage rating of 600 V and 2.5 mm^2 cross-sectional area. The windings were connected in star configuration.

Under sinusoidal and PWM voltage excitation each limb of the core energised to peak flux density B_{peak} of 0.4T, 0.6T and 1T, under load and no-load conditions.

Investigation of No-load and on-load performance of a model three-phase transformer core operating under sinusoidal and PWM voltage excitation

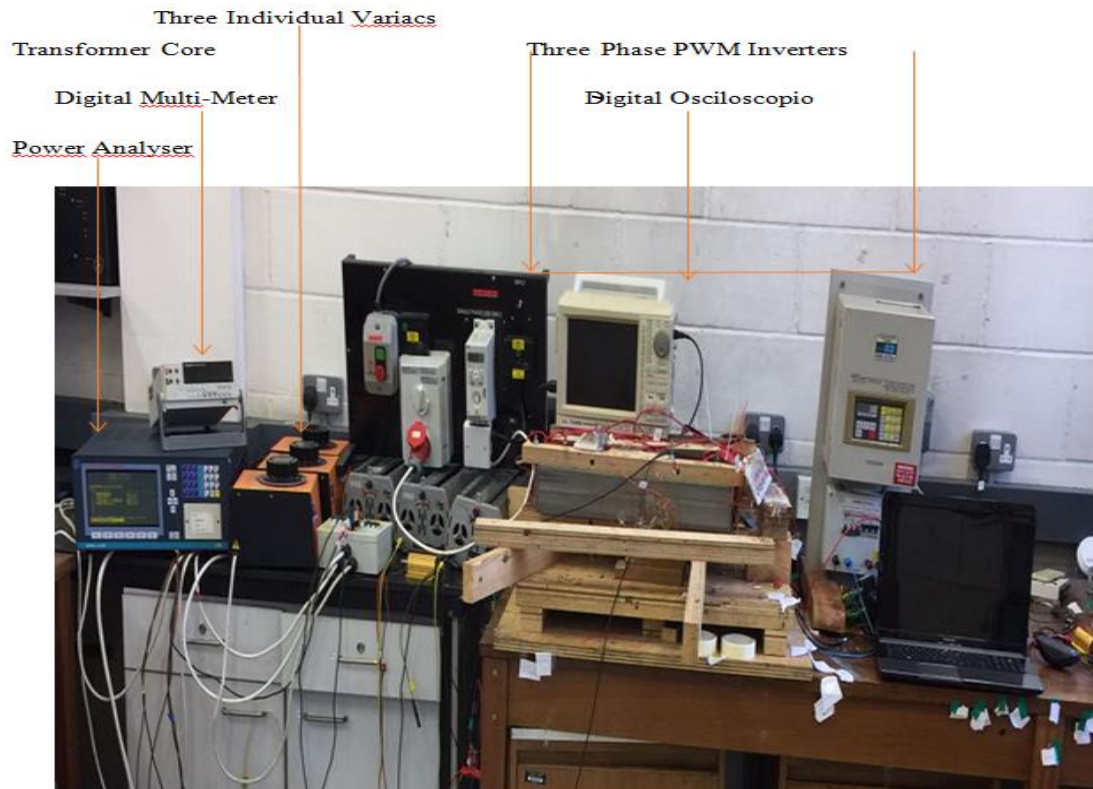


Fig. 4-3 Photograph of magnetising and associated measurement system

4.2 Localised flux density calculation

In order to measure localised flux density within the transformer core, array of search coils were wound on individual laminations as shown in Fig 4.9 to Fig 4.14. Single turn search coils were placed in the rolling and in the transverse directions (RD and TD) to detect the instantaneous flux density component at any instant of time in any direction. The output of the search coil is connect to the DAQ card by means of twisted search coils leads and then the output signal from the DAQ card is connected to the Lab-View programme as shown in fig 4-8. Each detected signal has its magnitude and angle with respect to the reference direction.

Equations (4.1) and (4.2) express the instantaneous induced voltages in the localised search coil in the rolling and transverse directions.

$$e_t(t) = -A_t \frac{dB_t(t)}{dt} \quad (4.1)$$

$$e_r(t) = -A_r \frac{dB_r(t)}{dt} \quad (4.2)$$

Where e_r and e_t are the induced voltage in the rolling and transverse directions respectively, B_r and B_t are the flux density in the rolling and transverse directions respectively. A_r and A_t are cross-sectional area in the rolling and transverse directions respectively. The instantaneous component of flux density can be obtained by integrating equations (4.1) and (4.2)

The magnitude of the induced flux density $|B(t)|$, vectored sum of the $|B_t(t)|$ and $|B_r(t)|$ at any instant in time, can be found as.

$$|B(t)| = [B_r^2(t) + B_t^2(t)]^{1/2} \quad (4.3)$$

This equation can be used to calculate the instantaneous component of the localised flux density under sinusoidal and PWM waveform [52].

4.2.1 Localised flux density measurement

Transformer core was energised by three-phase PWM inverter and by three-phase sinusoidal supply. Measurements were taken separately for each condition.

Search coil technique was used to measure a peak value of localised flux density passing through a given cross-sectional area. In order to obtain the most accurate result out of the measurement, the area should not be very small because small cross sectional area results in very low induced voltage [53], which can be effected by noise and cause a distortion in the induced voltage waveform. In order to avoid any distortion in the induced voltage waveform, the size of a cross-sectional area was chosen as 1 cm on both rolling (RD) and transvers (TD) directions. Fig. 4-7 to Fig 4-12.

In order to precisely locate the search coil upon test laminations, all the positions of the locations were marked on the tested lamination. 0.3 mm holes were drilled using drill “Dremel Model 850”. Polyester-coated 0.3mm wire was threaded through the holes and then each search coil leads were twisted tightly. Both sides of drilled holes were insulated using a thin layer of spray varnish in order to protect the insulation of the search coil wires and avoid short circuits between the lamination and the coil. At each stage of search coil construction, a test was carried out using ohmmeter to check for wire breakage or short circuit between the lamination and the search coil.

4.2.2 Construction and positioning of search coils

For the measurement of localised flux densities, single-turn search coils were constructed by threading 0.3mm diameter enamelled copper wire through holes in the laminations. The holes were 0.3mm in diameter, were accurately located and drilled very slowly to avoid any localised stresses building up around the holes. The holes were lightly countersunk on both sides of the lamination to avoid any damage to the enamel coated wire. The test laminations were placed in large 3-zone Retort furnace and then heat up to 800⁰C to relief stress induced in the lamination during drilling process. After threading the search coils through the holes each pair of search coil leads were twisted tightly together to avoid pick-up of any stray flux.

A large number of search coils were placed in the laminations located in the middle of the core to obtain comprehensive localised flux measurements [54]. Another set of search coils (reference coils) were wound around the limbs and yokes of the core. These search coils were used to measure overall flux density.

4.2.3 Calibration and testing of search coils

Calibration of the localised search coils was carried out by measuring accurately their lengths. A sample from each area under investigation was picked up at random. The maximum variation in length was found to be $\pm 5\%$. The deviation of the search coil axes from the rolling and transverse directions were marked with a tape.

All localised search coils were tested for continuity, insulation and connection. The insulation of the search coil was determined when the core was in demagnetized state by multimeter leads. The detected voltage of the multimeter recorded as reference to ensure that the ends of the search coil are working in the right order. However, induced generated signal in the search coil was measured by lab view.

4.2.1 Measurement preparation

The most two common techniques for measuring flux density is search coil technique and needle probe technique. The method employed to measure localised flux density in this work was search coil technique which was first discovered by Brailsford and Mazza and others [31].

To measure the localised flux density, holes were drilled in the middle of the laminations and near to the corner and T-joint where the flux changes its direction. Single-turn search coils were wound to record dB/dt in the tested areas [42]. Core was build and then single-turn search coil was wound around the yoke and limb to measure overall flux density distribution. Fig. 4-3.

The output voltages from each search and reference coils were fed to the “Fluke 8050A Digital Multimeter” where their *rms* values were compared with labview signals. The latter were fed to the DAQ card type module “NI USB” with a sampling rate of 250 kS/s and then to the personal computer where measurements were taken.

Localised flux density distribution was measured by means of winding an array of single-turn search coils on individual laminations. Localised flux densities were measured in both RD-directions and TD directions. Therefore, search coils were wound at right angles to each other at each point.

The magnitude and relative phase, in time, of voltage induced in the search coils were measured and from these, the magnitude and direction of the flux density vectors in space at individual points were determined. The magnitude and the direction of the overall flux density at each test point of the lamination at any instant in time were calculated by means of the formula:

$$B_{total} = \sqrt{(B_{x1})^2 + (B_{y1})^2} \quad [53] \quad (4.4)$$

Where B_x is the localised flux vector in the rolling direction and B_y is the flux vector in transverse direction. The induced voltages in the search coils were measured using following system illustrated in Fig. 4-4.

Investigation of No-load and on-load performance of a model three-phase transformer core operating under sinusoidal and PWM voltage excitation

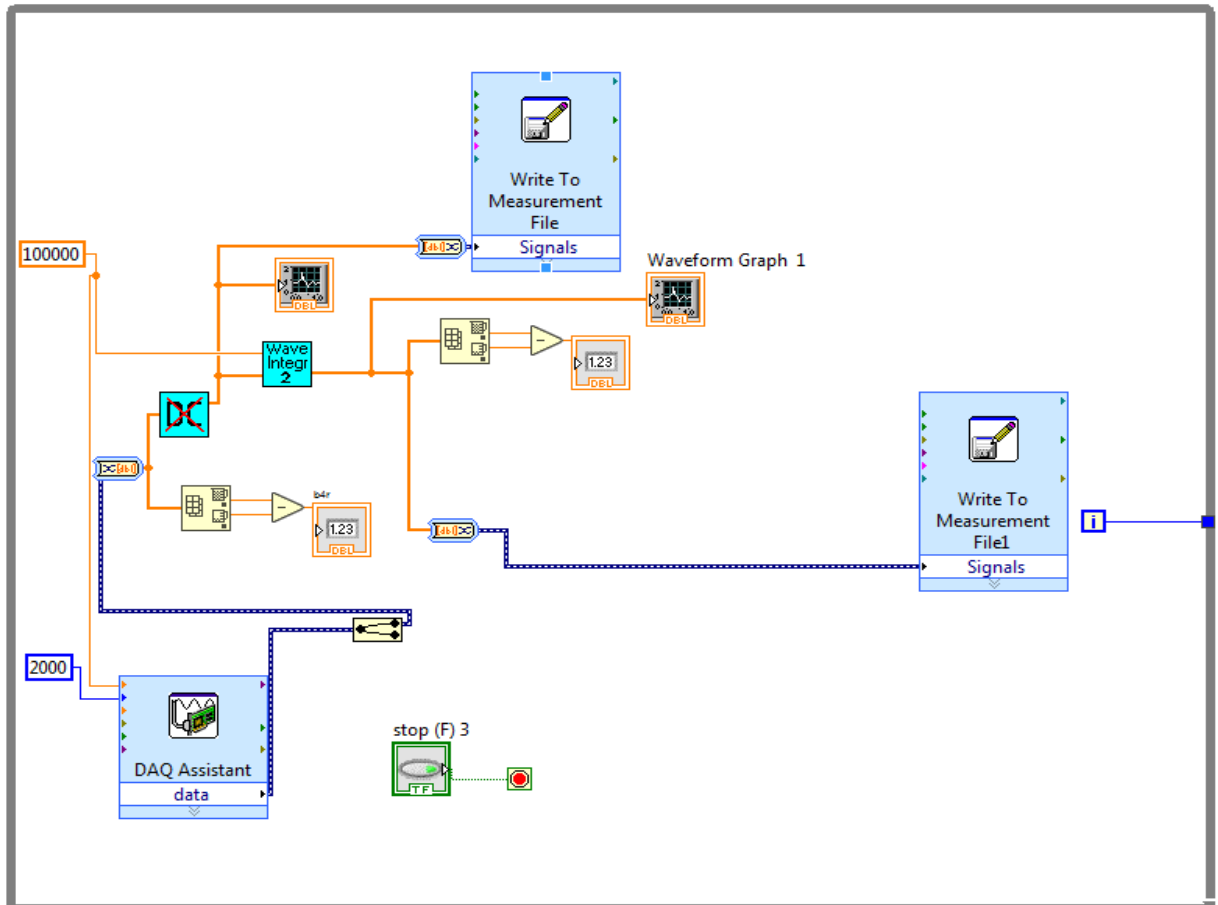


Fig. 4-4 Block diagram of virtual instrument for calculating magnetic flux density

4.3 Measurement results of localised power loss

Investigation on the localised power loss has been carried out when the core energised by sinusoidal and PWM voltage excitation. Measurements were taken under load and no-load conditions. Localised power loss measurements were taken at peak flux density of 0.4T, 0.6T and 1.0T so comparison between localised power loss under sinusoidal and PWM voltage excitation can be made. Equation 4.4 was used to obtain localised power loss measurement.

During the measurement process, the overall accuracy of localised power loss was affected by several parameters such as calculating the cross-sectional area of search coils and data acquisition process was found with the accuracy of ± 1 of full scale voltage. All localised power loss under sinusoidal and PWM voltage excitation was measured at 50 Hz magnetising frequency. Table 4.1 to table 4.24 shows localised power loss measurement under sinusoidal and PWM voltage excitation under load and no-load conditions.

Investigation of No-load and on-load performance of a model three-phase transformer core operating under sinusoidal and PWM voltage excitation

Table 4-1 Measurements of the localised power loss (W/kg) in the outer limb under sinusoidal voltage excitation no-load condition with various peak flux densities

Core excitation B_{peak} (T)	Localised power loss (W/kg) at different positions						
	Position 1	Position 2	Position 3	Position 8	Position 11	Position 12	Position 13
0.4	0.33	0.26	0.26	0.23	0.26	0.36	0.37
0.6	0.38	0.36	0.32	0.27	0.30	0.38	0.43
1.0	0.65	0.65	0.64	0.55	0.59	0.66	0.66

Table 4-2 Measurements of the localised power loss (W/kg) in the outer limb under sinusoidal voltage excitation load condition with various peak flux densities

Core excitation B_{peak} (T)	Localised power loss (W/kg) at different positions						
	Position 1	Position 2	Position 3	Position 8	Position 11	Position 12	Position 13
0.4	0.37	0.35	0.31	0.31	0.31	0.39	0.39
0.6	0.47	0.46	0.45	0.40	0.41	0.59	0.59
1.0	0.71	0.72	0.68	0.69	0.68	0.76	0.77

Investigation of No-load and on-load performance of a model three-phase transformer core operating under sinusoidal and PWM voltage excitation

Table 4-3 Measurements of the localised power loss (W/kg) in the outer limb under PWM voltage excitation no-load condition with various peak flux densities

Core excitation B_{peak} (T)	Localised power loss (W/kg) at different positions						
	Position 1	Position 2	Position 3	Position 8	Position 11	Position 12	Position 13
0.4	0.41	0.35	0.33	0.29	0.31	0.39	0.42
0.6	0.46	0.43	0.41	0.35	0.37	0.44	0.53
1.0	0.71	0.69	0.63	0.62	0.63	0.71	0.72

Table 4-4 Measurements of the localised power loss (W/kg) in the outer limb under PWM voltage excitation load condition with various peak flux densities

Core excitation B_{peak} (T)	Localised power loss (W/kg) at different positions						
	Position 1	Position 2	Position 3	Position 8	Position 11	Position 12	Position 13
0.4	0.45	0.43	0.43	0.37	0.35	0.45	0.46
0.6	0.59	0.56	0.51	0.48	0.53	0.59	0.61
1.0	0.83	0.75	0.79	0.71	0.73	0.82	0.85

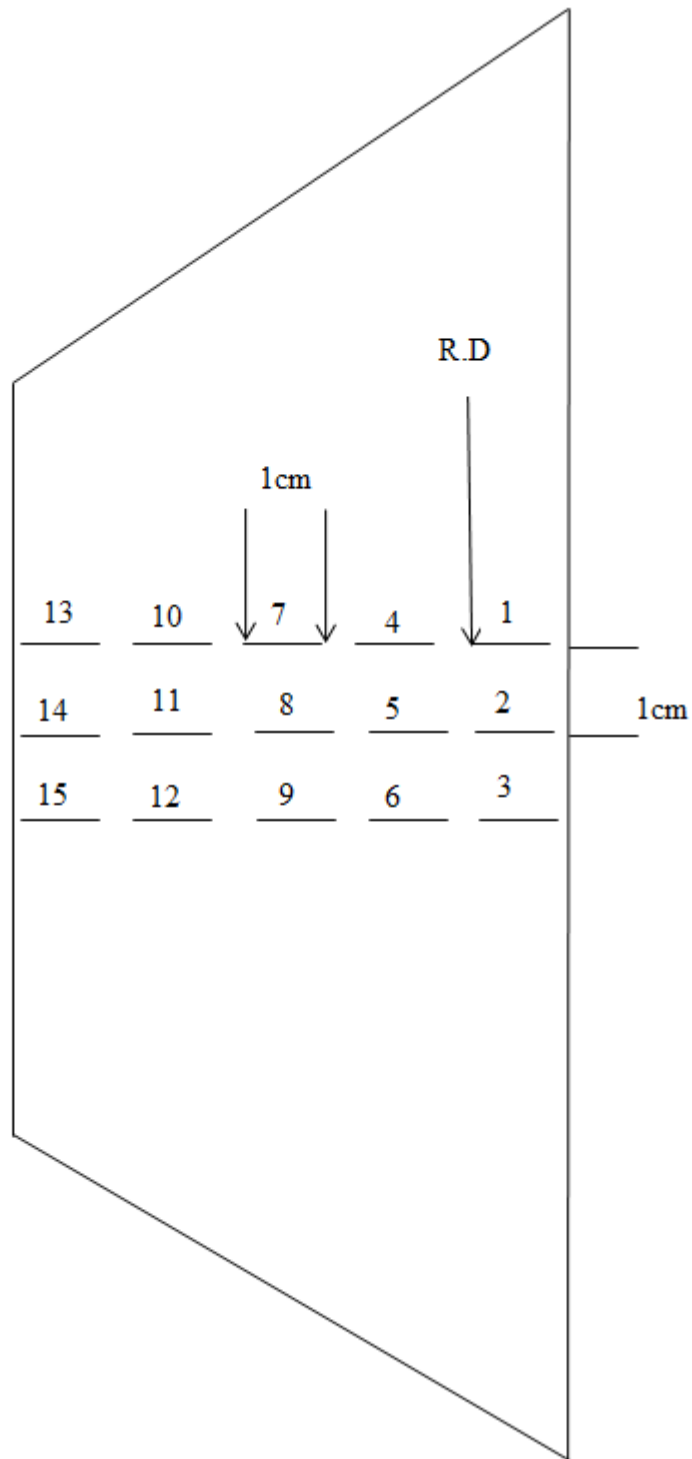


Fig. 4-5 Locations of localised search coils in the outer limb

Investigation of No-load and on-load performance of a model three-phase transformer core operating under sinusoidal and PWM voltage excitation

Table 4-5 Measurements of the localised power loss (W/kg) in the corner joint under sinusoidal voltage excitation no-load condition with various peak flux densities

Core excitation B_{peak} (T)	0.4	0.6	1.0
Search coil positions	Localised power loss at different excitation (W/kg)		
1	0.73	0.86	1.94
2	0.56	0.86	1.26
6	0.43	0.48	0.79
9	0.68	0.85	1.55
10	0.43	0.66	0.86
15	0.53	0.84	1.15

Table 4-6 Measurements of the localised power loss (W/kg) in the corner joint under sinusoidal voltage excitation load condition with various peak flux densities

Core excitation B_{peak} (T)	0.4	0.6	1.0
Search coil positions	Localised power loss at different excitation (W/kg)		
1	0.79	1.87	2.77
2	0.75	1.56	2.39
6	0.48	0.95	1.11
9	0.77	1.69	2.56
10	0.69	1.13	1.28
15	0.71	1.51	2.16

Investigation of No-load and on-load performance of a model three-phase transformer core operating under sinusoidal and PWM voltage excitation

Table 4-7 Measurements of the localised power loss (W/kg) in the corner joint under PWM voltage excitation no-load condition with various peak flux densities

Core excitation B_{peak} (T)	0.4	0.6	1.0
Search coil positions	Localised power loss at different excitation (W/kg)		
1	0.93	2.74	3.97
2	0.79	2.69	3.93
6	0.58	1.47	2.16
9	0.86	2.69	3.93
10	0.68	1.50	3.81
15	0.75	1.97	3.85

Table 4-8 Measurements of the localised power loss (W/kg) in the corner joint under PWM voltage excitation load condition with various peak flux densities

Core excitation B_{peak} (T)	0.4	0.6	1.0
Search coil positions	Localised power loss at different excitation (W/kg)		
1	0.97	3.77	5.76
2	0.85	3.49	4.36
6	0.63	1.66	3.81
9	0.98	3.67	5.43
10	0.79	2.61	4.07
15	0.86	2.67	4.16

Investigation of No-load and on-load performance of a model three-phase transformer core operating under sinusoidal and PWM voltage excitation

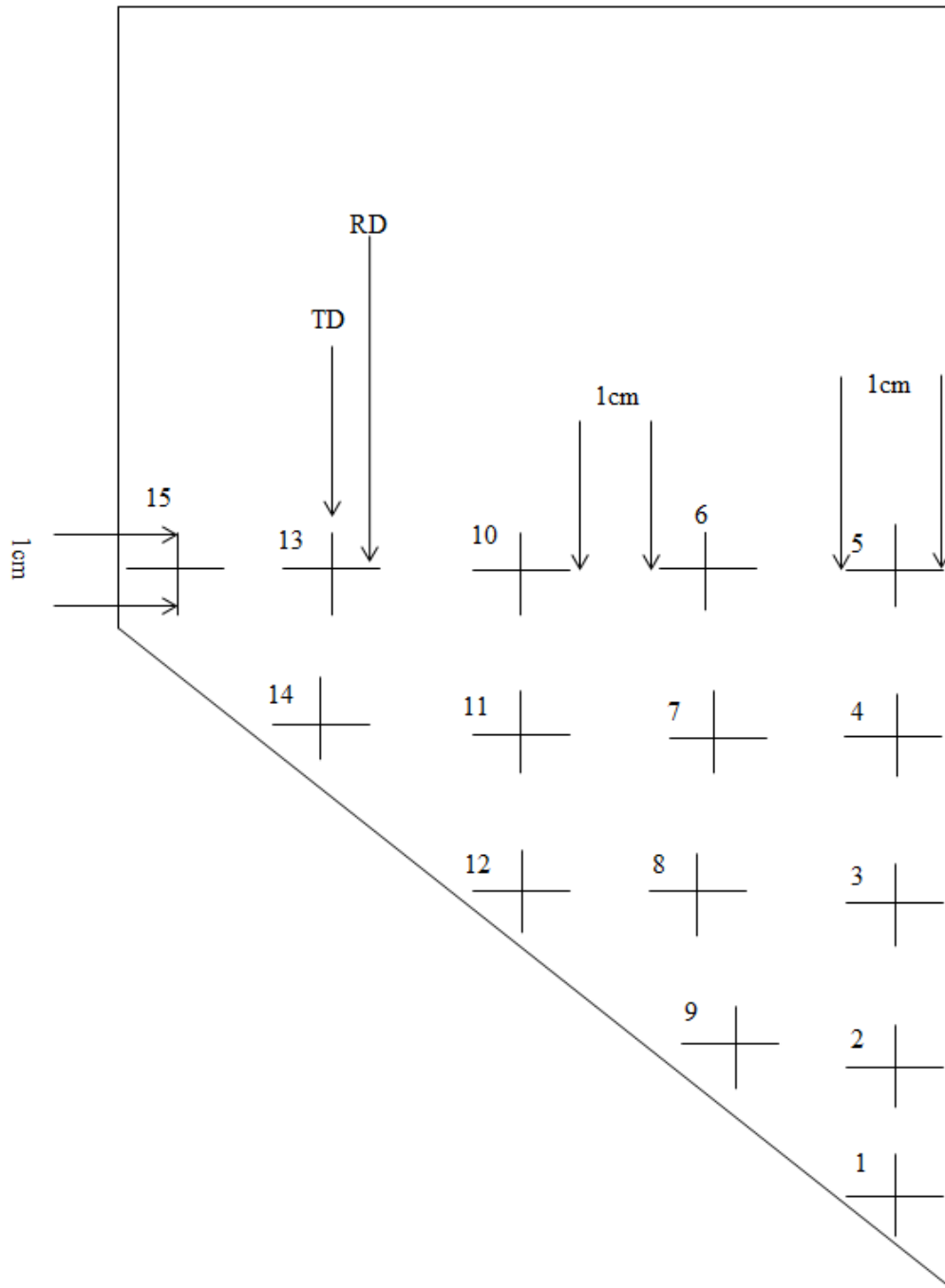


Fig. 4-6 Locations of the search coils in the outer limb corner joint, rolling (R) and transvers (T) Directions (T)

Investigation of No-load and on-load performance of a model three-phase transformer core operating under sinusoidal and PWM voltage excitation

Table 4-9 Measurements of the localised power loss (W/kg) in the corner yoke joint under sinusoidal voltage excitation no-load condition with various peak flux densities

Core excitation B_{peak} (T)	0.4	0.6	1.0
Search coil positions	Localised power loss at different excitation (W/kg)		
1	0.58	0.74	1.87
2	0.50	0.65	0.81
6	0.58	0.71	1.38
9	0.43	0.57	0.72
10	0.54	0.67	0.92
15	0.57	0.68	1.21

Table 4-10 Measurements of the localised power loss (W/kg) in the corner yoke joint under sinusoidal voltage excitation load condition with various peak flux densities

Core excitation B_{peak} (T)	0.4	0.6	1.0
Search coil positions	Localised power loss at different excitation (W/kg)		
1	0.65	1.52	1.82
2	0.44	0.93	1.26
6	0.57	1.51	1.59
9	0.34	0.84	1.09
10	0.56	1.13	1.33
15	0.57	1.19	1.33

Investigation of No-load and on-load performance of a model three-phase transformer core operating under sinusoidal and PWM voltage excitation

Table 4-11 Measurements of the localised power loss (W/kg) in the corner yoke under PWM voltage excitation no-load condition with various peak flux densities

Core excitation B_{peak} (T)	0.4	0.6	1.0
Search coil positions	Localised power loss at different excitation (W/kg)		
1	0.68	1.86	3.17
2	0.54	1.12	2.29
6	0.65	1.77	2.98
9	0.44	0.93	2.11
10	0.65	1.32	2.83
15	0.64	1.67	2.98

Table 4-12 Measurements of the localised power loss (W/kg) in the corner yoke joint under PWM voltage excitation load condition with various peak flux densities

Core excitation B_{peak} (T)	0.4	0.6	1.0
Search coil positions	Localised power loss at different excitation (W/kg)		
1	0.78	2.68	3.93
2	0.64	1.79	2.30
6	0.75	2.19	3.15
9	0.63	1.17	2.13
10	0.65	1.82	2.47
15	0.67	1.93	2.58

Investigation of No-load and on-load performance of a model three-phase transformer core operating under sinusoidal and PWM voltage excitation

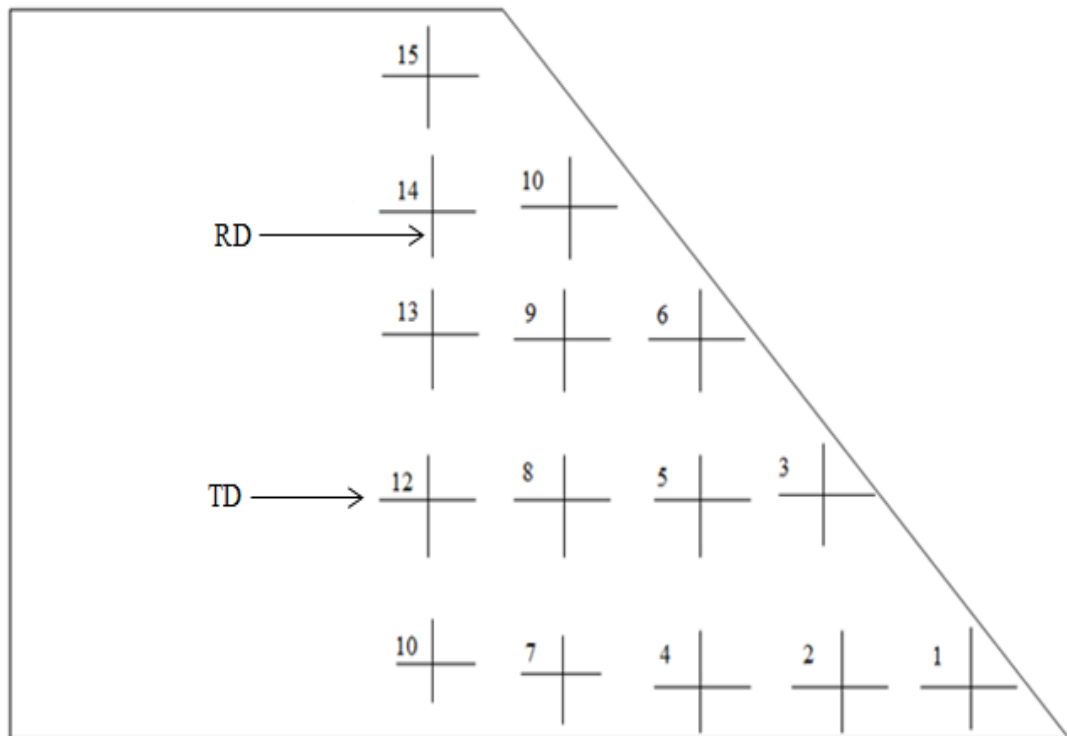


Fig. 4-7 Locations of the search coils in the outer yoke corner joint, rolling (RD) and transfer directions (TD)

Investigation of No-load and on-load performance of a model three-phase transformer core operating under sinusoidal and PWM voltage excitation

Table 4-13 Measurements of the localised power loss (W/kg) in the middle limb under sinusoidal voltage excitation no-load condition with various peak flux densities

Core excitation B_{peak} (T)	Localised power loss (W/kg) at different positions						
	Position 1	Position 2	Position 3	Position 8	Position 11	Position 12	Position 13
0.4	0.43	0.38	0.38	0.33	0.36	0.37	0.43
0.6	0.53	0.41	0.41	0.36	0.38	0.38	0.45
1.0	0.82	0.82	0.76	0.71	0.71	0.76	0.82

Table 4-14 Measurements of the localised power loss (W/kg) in the middle limb under sinusoidal voltage excitation load condition with various peak flux densities

Core excitation B_{peak} (T)	Localised power loss (W/kg) at different positions						
	Position 1	Position 2	Position 3	Position 8	Position 11	Position 12	Position 13
0.4	0.46	0.39	0.38	0.35	0.36	0.36	0.43
0.6	0.63	0.45	0.47	0.42	0.42	0.45	0.45
1.0	0.92	0.87	0.87	0.80	0.82	0.86	0.89

Investigation of No-load and on-load performance of a model three-phase transformer core operating under sinusoidal and PWM voltage excitation

Table 4-15 Measurements of the localised power loss (W/kg) in the middle limb under PWM voltage excitation no-load condition with various peak flux densities

Core excitation B_{peak} (T)	Localised power loss (W/kg) at different positions						
	Position 1	Position 2	Position 3	Position 8	Position 11	Position 12	Position 13
0.4	0.49	0.46	0.46	0.38	0.41	0.53	0.56
0.6	0.61	0.56	0.59	0.47	0.48	0.74	0.79
1.0	0.89	0.80	0.87	0.86	0.80	0.85	0.90

Table 4-16 Measurements of the localised power loss (W/kg) in the middle limb under PWM voltage excitation load condition with various peak flux densities

Core excitation B_{peak} (T)	Localised power loss (W/kg) at different positions						
	Position 1	Position 2	Position 3	Position 8	Position 11	Position 12	Position 13
0.4	0.56	0.77	0.56	0.57	0.53	0.82	0.72
0.6	0.73	0.86	0.77	0.76	0.67	0.97	0.95
1.0	1.04	1.04	0.97	0.95	0.95	1.08	1.06

Investigation of No-load and on-load performance of a model three-phase transformer core operating under sinusoidal and PWM voltage excitation

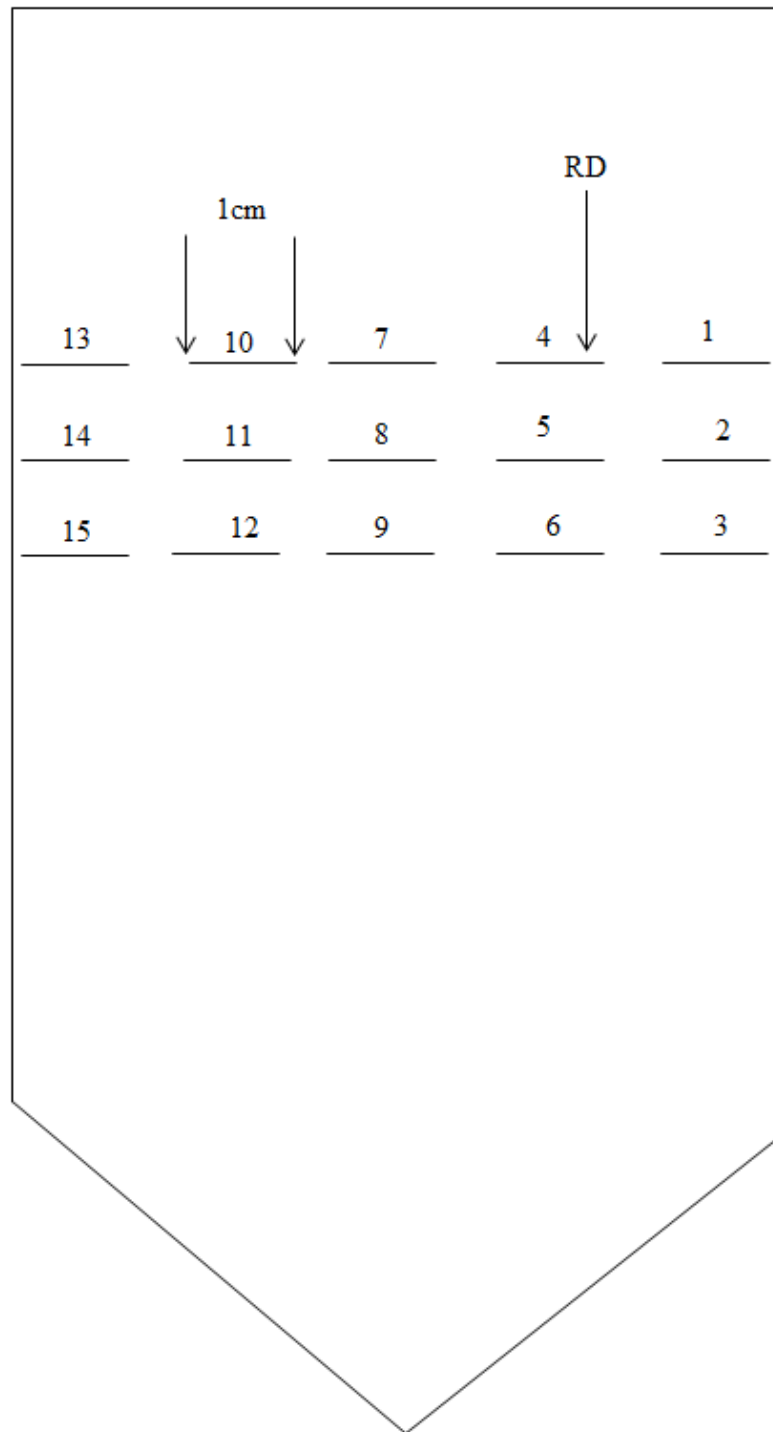


Fig. 4-8 Locations of the search coils in the middle limb

Investigation of No-load and on-load performance of a model three-phase transformer core operating under sinusoidal and PWM voltage excitation

Table 4-17 Measurements of the localised power loss (W/kg) in the yoke T-joint under sinusoidal voltage excitation no-load condition with various peak flux densities

Core excitation B_{peak} (T)	0.4	0.6	1.0
Search coil positions	Localised power loss at different excitation (W/kg)		
1	0.46	0.69	0.92
3	0.37	0.52	0.73
5	0.42	0.63	0.80
8	0.45	0.65	0.84
10	0.41	0.57	0.70
13	0.42	0.59	0.75
16	0.33	0.53	0.70

Table 4-18 Measurements of the localised power loss (W/kg) in the yoke T-joint under sinusoidal voltage excitation load condition with various peak flux densities

Core excitation B_{peak} (T)	0.4	0.6	1.0
Search coil positions	Localised power loss at different excitation (W/kg)		
1	0.46	0.74	1.30
3	0.39	0.56	0.75
5	0.45	0.68	1.00
8	0.45	0.66	1.17
10	0.43	0.66	0.76
13	0.42	0.64	0.85
16	0.36	0.58	0.73

Investigation of No-load and on-load performance of a model three-phase transformer core operating under sinusoidal and PWM voltage excitation

Table 4-19 Measurements of the localised power loss (W/kg) in the yoke T-joint under PWM voltage excitation no-load condition with various peak flux densities

Core excitation B_{peak} (T)	0.4	0.6	1.0
Search coil positions	Localised power loss at different excitation (W/kg)		
1	0.63	0.91	1.38
3	0.44	0.76	1.14
5	0.54	0.80	1.25
8	0.63	0.87	1.35
10	0.47	0.85	1.17
13	0.45	0.83	1.30
16	0.45	0.74	1.10

Table 4-20 Measurements of the localised power loss (W/kg) in the yoke T-joint under PWM voltage excitation load condition with various peak flux densities

Core excitation B_{peak} (T)	0.4	0.6	1.0
Search coil positions	Localised power loss at different excitation (W/kg)		
1	0.69	1.73	2.90
3	0.49	0.87	1.97
5	0.62	1.26	2.25
8	0.68	1.65	2.30
10	0.48	1.29	2.17
13	0.53	1.23	1.96
16	0.47	0.83	1.19

Investigation of No-load and on-load performance of a model three-phase transformer core operating under sinusoidal and PWM voltage excitation

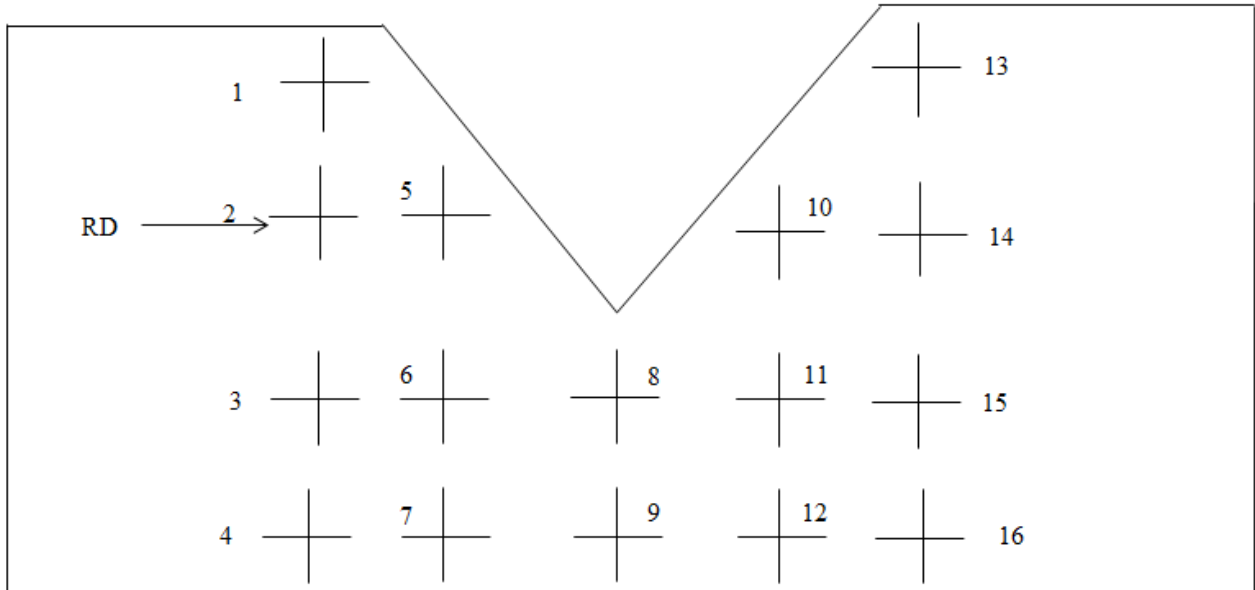


Fig. 4-9 Locations and direction of the search coils in the T-joint

Investigation of No-load and on-load performance of a model three-phase transformer core operating under sinusoidal and PWM voltage excitation

Table 4-21 Measurements of the localised power loss (W/kg) in the limb T-joint under sinusoidal voltage excitation no-load condition with various peak flux densities

Core excitation B_{peak} (T)	0.4	0.6	1.0
Search coil positions	Localised power loss at different excitation (W/kg)		
1	0.48	0.87	0.96
3	0.42	0.77	0.96
5	0.35	0.58	0.84
8	0.37	0.63	0.83
10	0.39	0.72	0.84
13	0.50	0.87	0.99
14	0.41	0.74	0.89

Table 4-22 Measurements of the localised power loss (W/kg) in the limb T-joint under sinusoidal voltage excitation load condition with various peak flux densities

Core excitation B_{peak} (T)	0.4	0.6	1.0
Search coil positions	Localised power loss at different excitation (W/kg)		
1	0.67	1.31	1.71
3	0.58	0.90	1.64
5	0.35	0.67	1.02
8	0.36	0.73	1.22
10	0.53	0.88	1.61
13	0.67	1.36	1.96
14	0.53	0.88	1.35

Investigation of No-load and on-load performance of a model three-phase transformer core operating under sinusoidal and PWM voltage excitation

Table 4-23 Measurements of the localised power loss (W/kg) in the limb T-joint under PWM voltage excitation no-load condition with various peak flux densities

Core excitation B_{peak} (T)	0.4	0.6	1.0
Search coil positions	Localised power loss at different excitation (W/kg)		
1	0.68	1.83	2.41
3	0.62	1.76	2.22
5	0.54	1.10	1.24
8	0.54	1.22	1.35
10	0.55	1.41	1.90
13	0.80	1.98	2.73
14	0.56	1.57	1.98

Table 4-24 Measurements of the localised power loss (W/kg) in the limb T-joint under PWM voltage excitation load condition with various peak flux densities

Core excitation B_{peak} (T)	0.4	0.6	1.0
Search coil positions	Localised power loss at different excitation (W/kg)		
1	0.76	1.83	2.69
3	0.75	1.79	2.61
5	0.54	1.13	1.94
8	0.54	1.40	2.19
10	0.64	1.57	2.59
13	0.86	1.98	2.82
14	0.68	1.74	2.30

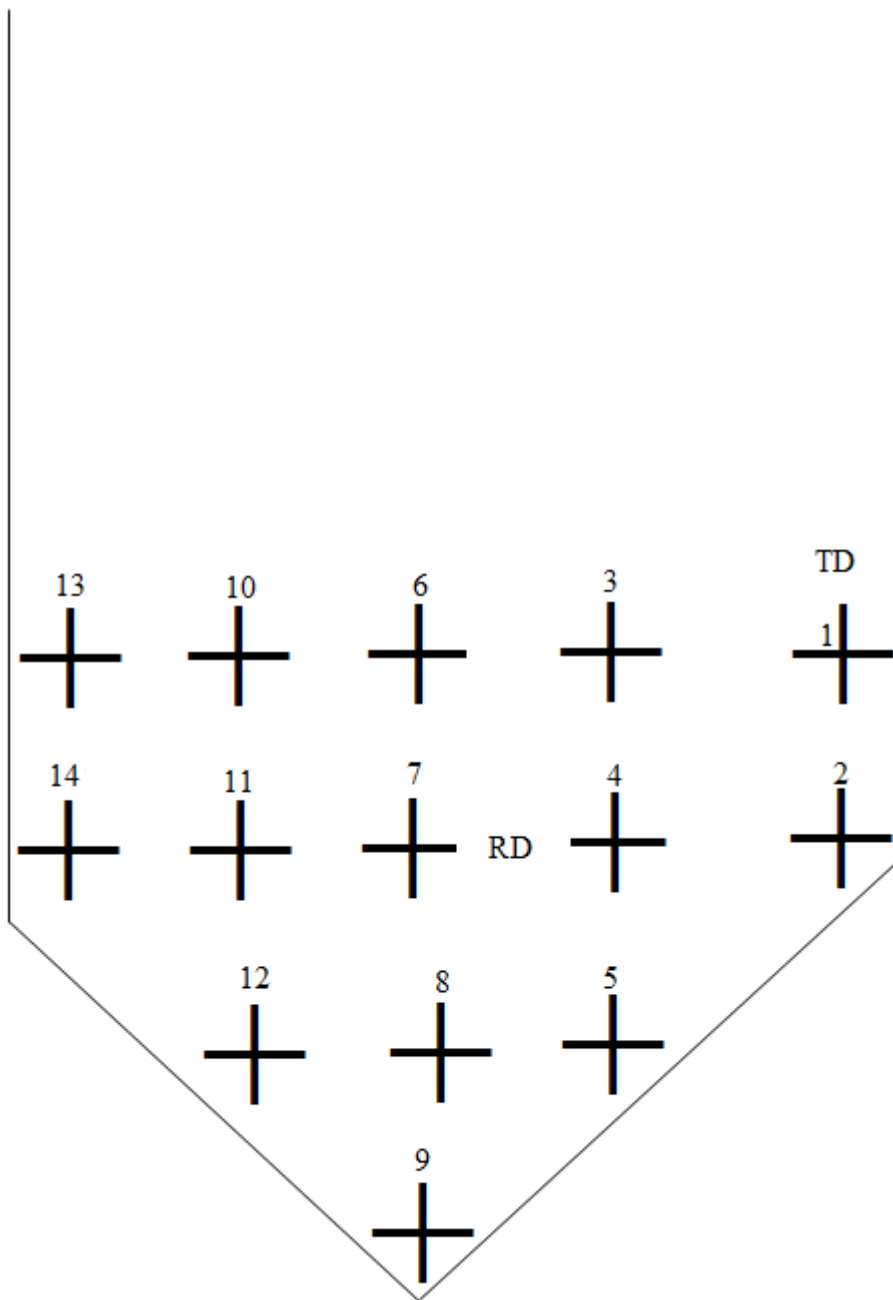


Fig. 4-10 Locations and directions of the search coils in the T-joint R and T directions

4.3.1 Comparison of the results

Localised power losses were obtained under sinusoidal and PWM voltage waveforms, Tables 4.1, 4.2, 4.3 and 4.4. Show measurements of the localised power loss in the middle of the outer limb. As shown in Fig. 4-5, results were obtained from 15 regions at different peak flux densities of 0.4T, 0.6T and 1.0T. Measurement under load condition shows higher localised power loss than that under no-load condition, under both sinusoidal and PWM waveforms. Results have shown that more localised power loss flow in the middle of the limb than that close to the edge.

At the corner limb joints as the flux flow in two directions, search coils were placed in two orthogonal axes, which are known as rolling and transvers directions (RD) and (TD). Fig. 4-6. At all magnetisation, peak flux density result was obtained from 15 regions. Tables 4.5, 4.6, 4.7 and 4.8 show the magnitude of the localised power loss was higher under load condition. It can be seen that search coils close to cutting edges have shown higher localised power loss than search coils away from the cutting edge.

At yoke corner joints Fig. 4-7, shows localised power loss in 15 regions the magnitude of the localised power loss was obtained in tables 4.9, 4.10, 4.11 and 4.12 which have shown higher localised power loss near the cutting edge as the flux jumps to the next layer. This is because large flux flows in both RD and TD directions changing its direction from limb to yoke.

At the central limb Fig. 5-8, shows localised power loss in 15 regions tables 4.13, 4.14, 4.15, and 4.16 at all magnetising peak flux densities all 15 search coils have reached their saturation value.

At the T-joint yoke joint Fig. 4-9, tables 4.17, 4.18, 4.19 and 4.20 show localised power losses in 16 regions, when the core is energised under sinusoidal and PWM loads and no-load conditions, all 16 regions have reach their saturation value.

At the T-joint limb joint Fig 4-10, tables 4.21, 4.22, 4.23 and 4.24 have shown localised power loss in 14 regions. The results have shown higher power loss near the joints which are close to the cutting edges than that away from the cutting edges. This shows that there is more flux concentration in these regions and the magnitude

Investigation of No-load and on-load performance of a model three-phase transformer core operating under sinusoidal and PWM voltage excitation

of the resultant flux density under both sinusoidal and PWM excitations are varied. More details about the results obtained are discussed in 5.5 analysis and discussion.

4.3.2 Localised power loss obtained in the outer limb of the model three-phase transformer core with various peak flux densities

The efficient operation of power transformer core depends to a large extent on the design of the joints between their limbs and yokes. In the three-phase, three-limb core, the most complex joints are the T-joints. At the intersection of the centre limb and yokes the joint should be constructed to give mechanical stability to the core and to be magnetically efficient. Table 4-1 to table 4-24 show localised power loss under sinusoidal and PWM voltage excitations. Transformer core was energised under sinusoidal and PWM voltage excitations at 50 Hz frequency. In order to study the localised power losses occurred in transformer core under sinusoidal and PWM waveforms, equal level of the peak flux density was applied to the core at 0.4 T, 0.6 T and 1.0 T. Localised Measurements were taken in the limbs, yoke, corner and T-joint of the transformer core.

As the flux flows in one direction in the middle of the lamination, search coils embedded on a test lamination in the rolling direction to record localised flux passing through the selected areas as shown in Fig. 4-5. During measurements of localised loss under sinusoidal and PWM voltage excitation, the average value of localised power loss was found to be almost the same under both load and no-load conditions.

Firstly, when the core was energised under sinusoidal waveform at peak flux density of 0.4T under load and no-load conditions, tables 4-1 and 4-2 show the highest localised power loss was recorded to be in search coil positions 13, 12 and 1. And the smallest was found to be in search coil positions 3, 11 and 8. So localised search coil position 13 has shown the largest value of localised power loss under load and no-load conditions. Moreover, smallest values of localised power losses were varied to be at different search coil positions.

Same result was obtained when the core was energised at peak flux density of 0.4 T under PWM voltage excitation, under load and no-load conditions, tables 4-3 and 4-

Investigation of No-load and on-load performance of a model three-phase transformer core operating under sinusoidal and PWM voltage excitation

4. Highest localised power loss value was found to be in search coil positions 13, nevertheless smallest value was found to be varied between search coils 3, 11 and 8.

Comparing the result obtained during the measurement process under sinusoidal and PWM voltage excitations under load and no-load conditions, tables 4-1, 4-2, 4-3 and 4-4, agreement of the result was obtained in search coil position 13 which has shown the highest value of localised power loss. Comparing the result obtained when the core was energised under sinusoidal and PWM voltage excitations, at peak flux density of 0.4 T under load condition under PWM voltage excitation all search coil have shown larger value of localised power loss nevertheless some search coils have not reached their saturation value under both excitation conditions.

Increasing the energising flux density to 0.6T, under sinusoidal waveform load and no-load conditions, the highest localised power loss values were found to be in search coil positions 13, 12 and 1, and the smallest value of localised power losses were found to be in search coils positions 3, 11 and 8.

When transformer core energised with PWM voltage excitation at 0.6T under load and no-load conditions, search coils positions 13, 12 and 1 have recorded the highest value of localised power loss. And the rest of the search coils have recorded almost same value of localised power loss.

Comparing the result obtained at 0.6T under PWM with the result obtained under sinusoidal voltage excitation under load and no-load conditions, agreement of the result was obtained in search coil position 13 which have shown the highest value of localised power loss under both energising conditions.

Increasing the energising flux to 1.0T, under sinusoidal waveform load condition, search coil positions 13, 12, and 1 recorded the highest value of localised power loss, whereas search coil positions 3, 11 and 8 have shown the lowest value of localised power loss. However, when the core energised under no-load condition all 15 search coils have shown almost a same values of localised power loss distribution.

When the core energised by PWM voltage excitation at peak flux density 1.0 T under no-load condition search coil positions 13, 12 and 1 have shown the highest value of localised power loss but they have not reach their saturation value. Whereas, the rest

Investigation of No-load and on-load performance of a model three-phase transformer core operating under sinusoidal and PWM voltage excitation

of the search coils have shown almost a same value. However, energising the core under load condition search coil positions 13, 12, and 1 have shown the highest value of localised power loss, whereas search coil positions 3, 11 and 8 have shown the lowest value of localised power loss.

Comparing the result obtained under PWM with the result obtained under sinusoidal voltage excitation under load conditions. The highest value of localised power losses was agreed to be find in search coil positions 13 and 12. Moreover, the smallest value of localised power loss was varied. Energising the core under no-load condition, largest and smallest value of localised power losses were agreed to be in positions 13 and 12. Fig. 4-11 shows the variation of localised power loss under sinusoidal and PWM voltage excitations under no-load condition, And Fig. 4-12. shows the variation of localised power loss under sinusoidal and PWM voltage excitations under load condition. Both measurements were taken at 50 Hz. Highest values of tables 4-1, 4-2, 4-3. And 4-4 were chosen as reference.

Investigation of No-load and on-load performance of a model three-phase transformer core operating under sinusoidal and PWM voltage excitation

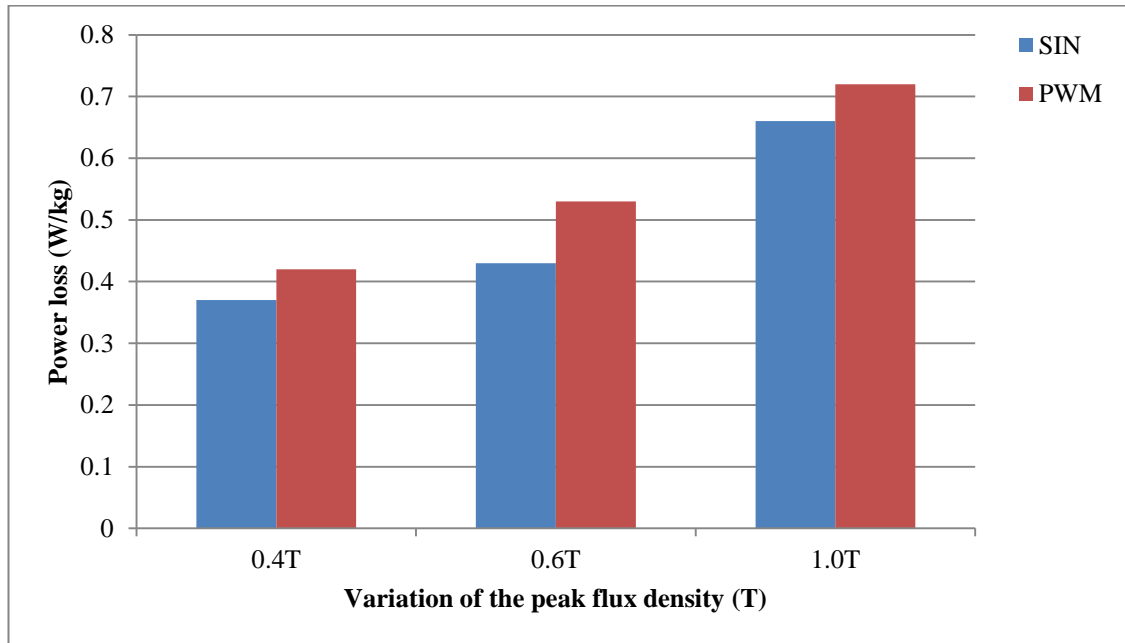


Fig. 4-11 Comparison of localised power loss under sinusoidal and PWM voltage excitations (No-load condition) at the center of the outer limb at various peak flux densities (T), 50 Hz.

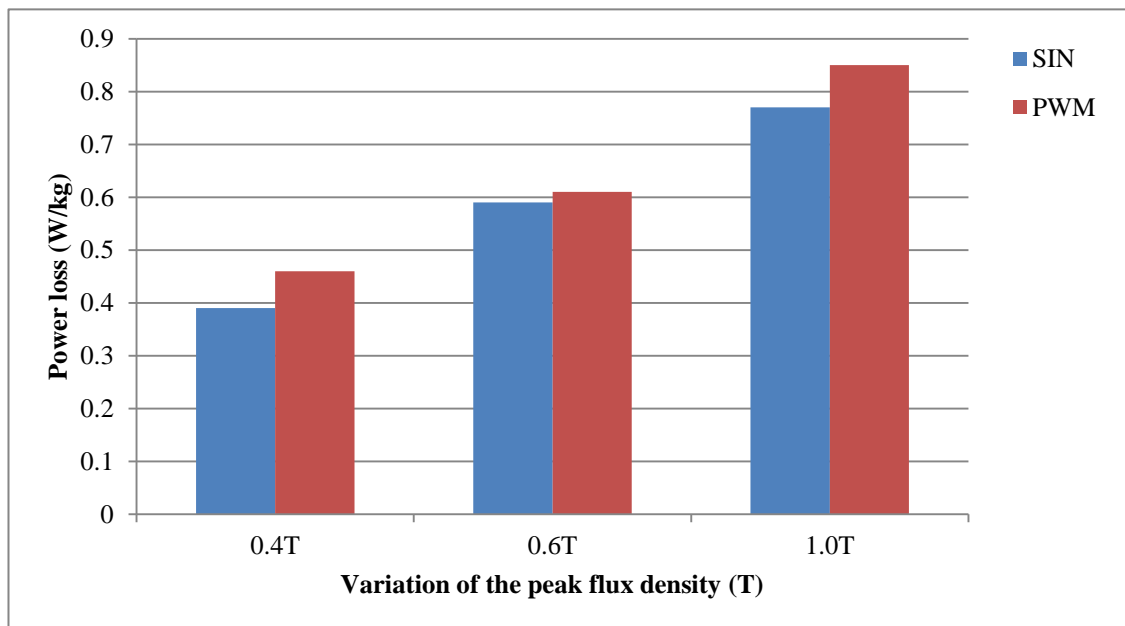


Fig. 4-12 Comparison of localised power loss under sinusoidal and PWM voltage excitations (Load condition) at the center of the outer limb at various peak flux densities (T), 50 Hz.

Investigation of No-load and on-load performance of a model three-phase transformer core operating under sinusoidal and PWM voltage excitation

From Fig. 4-11, 4-12, it could be concluded that localised power losses when the core was energised under sinusoidal and PWM waveforms under no-load condition at peak flux densities of 0.4T and 0.6T have increased under PWM excitation by factors of 11%, and 18% respectively. However, when the core was energised under load condition, localised power losses have increased under PWM excitation by factors of 15% and 3% respectively. Increasing the energising induction to 1.0T, localised power loss under PWM voltage excitation has increased under no-load condition by a factor of 8%, whereas when the core was energised under load condition localised power loss has increased under PWM waveform by a factor of 9%.

4.3.3 Localised power loss obtained in the middle limb of the model three-phase transformer with various peak flux densities

In order to study the localised distribution of power loss in central limb of three-phase transformer core, search coils were positioned in the centre of the lamination in the rolling direction (RD), where the flux is mainly flowing in the rolling direction. Fig. 4-8 shows the positions of localised search coils and tables 4-13, 4-14, 4-15 and 4-16 show the magnitude of localised power losses in the central limb of three-phase transformer.

Energising the core under sinusoidal voltage excitation under no-load and load conditions at peak flux density 0.4T, search coil positions 1 and 13 have reached their saturation value, whereas. When the core was energised at peak flux density of 0.4T under PWM wave excitation under no-load and load conditions, all 15 search coils have reached their saturation value and recorded the highest localised power loss.

Comparing the results obtained under PWM voltage excitation with the results obtained under sinusoidal voltage excitation under no-load conditions at peak flux density of 0.4T, the highest value of localised power loss was recorded in search coil position 1 and it was 6% higher under PWM voltage excitation. Whereas, when the core energised under load condition the variation of localised power loss had a value of 21 % higher under PWM waveform.

Investigation of No-load and on-load performance of a model three-phase transformer core operating under sinusoidal and PWM voltage excitation

Increasing the energising flux density to 0.6T under sinusoidal and PWM waveforms under no-load and load conditions, again same results were obtained. Search coils position 1 and 13 have shown the highest values of localised power loss.

Comparing the results obtained under PWM with the result obtained under sinusoidal voltage excitation at 0.6T, the highest value of localised power loss induced in search coil position 1 and the smallest value was found to be in search coil position 8. Comparing the results under no-load and load conditions, the variation of localised power losses had values of 13% and 27% respectively, higher under PWM waveform.

Comparing the results obtained under PWM with the results obtained under sinusoidal at peak flux density of 1.0T, the highest value of localised power loss occurred in search coil position 1 under load and no-load conditions. As a result of comparison between PWM and sinusoidal waveforms it could be concluded that under no-load and load conditions localised power loss had values of 7% and 3% respectively higher under PWM waveform.

Fig. 4-13 shows the variation of localised power loss under sinusoidal and PWM waveform excitations under no-load condition and Fig. 4-14, shows variation of localised power loss under sinusoidal and PWM excitation under load condition at 50Hz. Highest values of localised power losses presented in tables 4-13, 4-14, 4-15. and 4-16 were chosen as reference.

Investigation of No-load and on-load performance of a model three-phase transformer core operating under sinusoidal and PWM voltage excitation

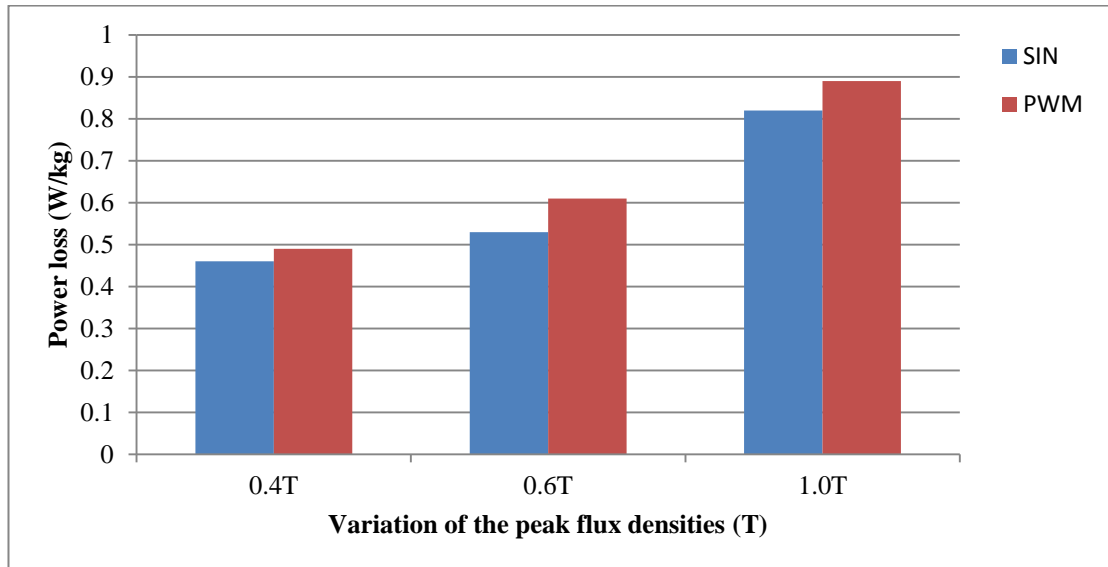


Fig. 4-13 Comparison of localised power loss under sinusoidal and PWM voltage excitation (No-load condition) central limb at various peak flux densities (T), 50 Hz

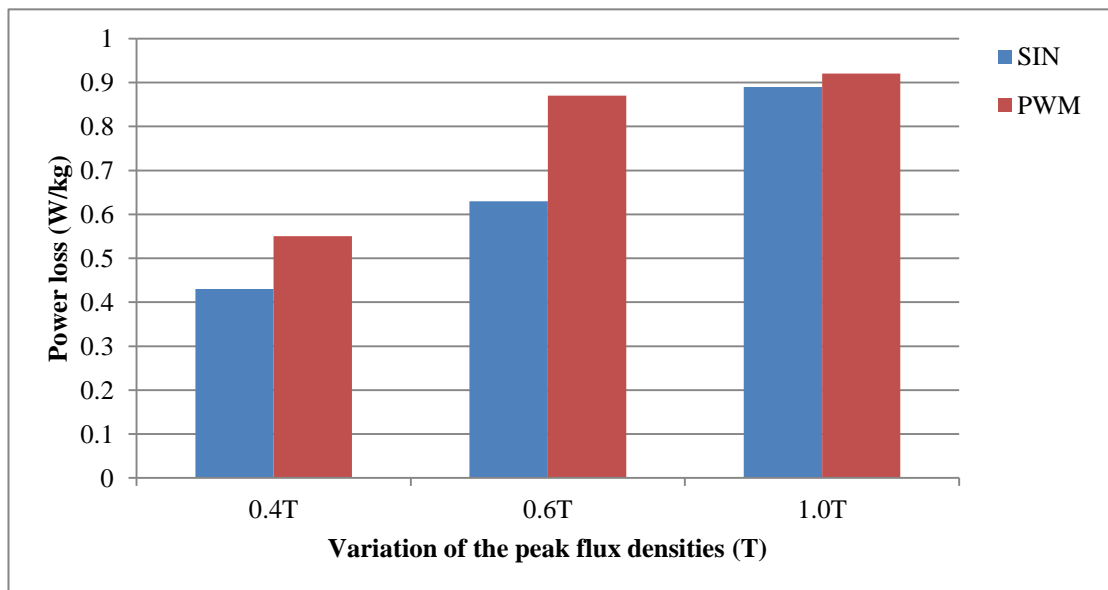


Fig. 4-14 Comparison of localised power loss under sinusoidal and PWM voltage excitation (Load condition) central limb at various peak flux densities (T), 50 Hz

4.3.4 Comparison between localised power loss obtained in the middle of the outer and central limbs of the model three-phase transformer core with various peak flux densities

Search coils were positioned in fifteen and fourteen regions in the same locations in the outer and central limbs as shown in Fig. 4-5 and 4-8 respectively. So comparison between sinusoidal and PWM flux conditions at various peak flux density at same position of the search coil can be made between central and outer limbs. Under sinusoidal voltage excitation at 0.4T under no-load conditions, localised power losses in the central limb were higher than those of the outer limb by the factor of 13%. Furthermore, under load condition central limb represents higher values of localised power loss than the outer limb by the factor of 16%. However, comparing the results obtained in the outer and central limbs when the core was energised by PWM voltage excitation under no-load and load conditions, central limb had shown higher localised power losses by factors of 14% and 16% respectively.

Comparing localised power loss when the core was energised at peak flux density of 0.6T under sinusoidal waveform under no-load and load conditions, central limb had higher localised power loss than the outer limb by factors of 18% and 6% respectively. Comparing the results obtained between outer at central limb when the core was energised by PWM voltage excitation at 0.6T under no-load and load conditions, central limb had shown higher value of localised power loss by the factor of 13% and 29% respectively.

Comparing localised power loss between outer and central limbs when the core was energised under peak flux density of 1.0T under sinusoidal no-load and load conditions, central limb has higher magnitudes of localised power loss than those in outer limb by 19% and 16% respectively. However, comparing the results obtained when the core was energised under PWM waveform under no-load condition, central limb had value of 19% higher than the outer limb whereas under load condition central limb had a value of 7% higher than the outer limb.

During all comparison between outer and central limb under load and no-load conditions, localised measurements were higher in the central limb than that in the

outer limb this due to the flux flowing in the central limb is higher than the flux flowing in the outer limb and could be due to the grain-oriented size.

4.3.5 Localised power loss obtained in the limb corner joints of the model three-phase transformer core with various peak flux densities

In order to investigate localised power loss in the joint areas, two search coils were placed, one search coil placed on the rolling direction (RD) and another search coil were placed on the transvers direction (TD). The reason why there were two search coils was because flux changes its direction and jumps from one lamination to the next lamination. Moreover, rotational flux occurs at the joint areas. However, search coil placed in the rolling direction was used to measure localised flux density in the rolling direction and the search coil placed in the transverse direction was used to measure localised flux density in the transvers direction. It was found that the flux in the rolling direction is three or four times larger than that of flux travelling in the transvers direction. The search coil holes were another factor on distribution the localised measurements on the transformer core, so they must be as small as possible in order to provide well balanced flux all over the areas. Large sized holes may cause disturbance of the magnetic flux in those areas. Fig. 4-6, 4-7, 4.9 and 4-10 show rolling and transvers directions of the search coils. Equation 4.8 was used to calculate the average value of localised magnetic flux occurring in the selected positions.

Localised power loss was calculated at the corner joint Fig. 4-6. When the core was energised at different peak flux densities of 0.4T, 0.6T and 1.0T, measurements were again taken under sinusoidal and PWM voltage excitations under no-load and load conditions. From tables 4-5, 4-6, 4-7 and 4-8, it can be seen that fifteen regions were chosen to measure localised power loss in which they have reached their saturation values at all energising peak levels. Furthermore, it can be seen that search coils at positions 1, 2 and 9 which were placed very close to the cutting edge have shown the highest value of localised power loss. This is because of high amount of the flux circulating in those areas. However, further away from the cutting edges localised power loss was found to be decreasing, search coil positions 6 and 10. This could be because high amount of localised magnetic flux density were still in the rolling direction.

Investigation of No-load and on-load performance of a model three-phase transformer core operating under sinusoidal and PWM voltage excitation

Comparing localised power loss when the core was energised under PWM and sinusoidal waveforms. At different peak flux density of 0.4T, 0.6T, and 1.0T under load and no-load conditions, localised power losses were higher under PWM voltage excitation. Fig 4.15 shows variation of localised distribution of power loss under sinusoidal and PWM voltage excitations under no-load condition and fig. 4-16 shows variation of localised power loss under sinusoidal and PWM voltage excitation under load condition at 50Hz. Highest values presented on table 4-5, 4-6, 4-7 and 4-8 were chosen as reference.

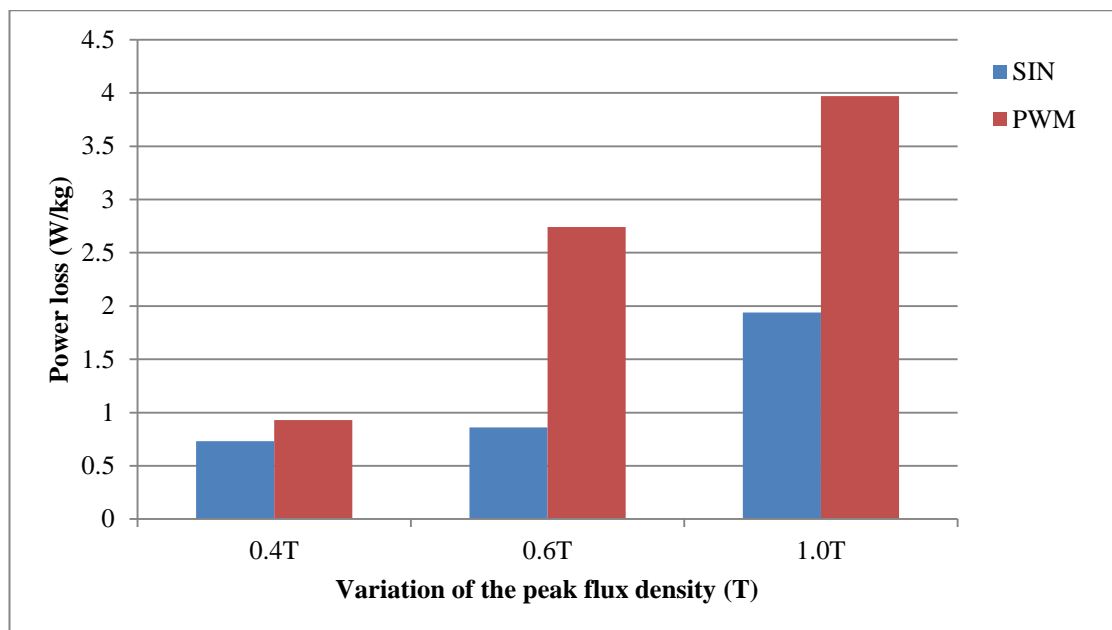


Fig. 4-15 Comparison of localised power loss under sinusoidal and PWM voltage excitation (No-load condition) at limb corner joints at various peak flux densities (T), 50 Hz.

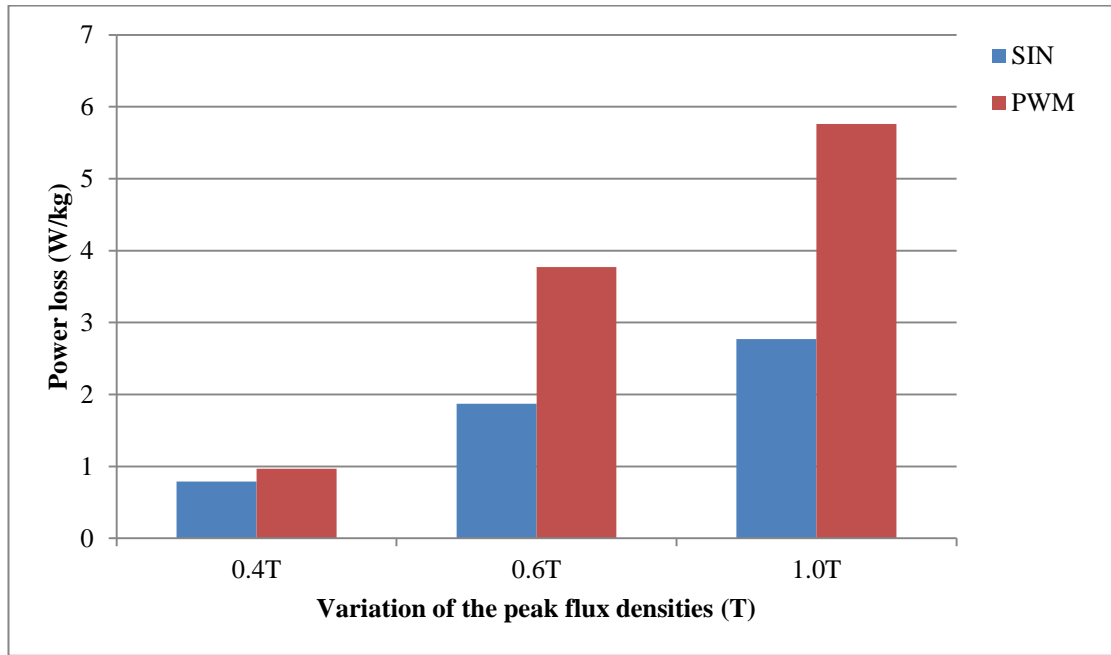


Fig. 4-16 Comparison of localised power loss under sinusoidal and PWM voltage excitation (Load condition) at limb corner joints at various peak flux densities (T), 50 Hz.

4.3.6 Localised power loss obtained in the yoke corner joints of the model three-phase transformer core with various peak flux densities

In order to compare localised power loss occurring at the limb and yoke on same positions, search coils were placed on the yoke joint as shown in fig. 4-7. Measurements were again taken under sinusoidal and PWM voltage excitations, under load-and no-load conditions. Fifteen search coils were chosen randomly to study localised power loss. Tables 4-9 and 4-10, show the values of localised power loss distribution under sinusoidal waveform and tables 4-11, and 4-12 show the magnitude of localised power losses under PWM waveform.

Firstly, measurements were taken under sinusoidal waveform at peak flux density 0.4T under no-load and load conditions, the average value of instantaneous localised power loss at the corner yoke joint was found to be in search coil position 1. Localised power loss was found to be decreasing away from the corner joint search coil position 10. Localised power loss at right corner search coil position 15 was compared with search coil position 1 near the cutting edge and it was found that

Investigation of No-load and on-load performance of a model three-phase transformer core operating under sinusoidal and PWM voltage excitation

localised power loss was found to be decreased in right corner under no-load and load conditions by factors of 1% and 14% respectively. However, when the core was energised under PWM waveform at peak flux density 0.4T under no-load and load conditions, search coils at all positions have reached their saturation value. Nevertheless, search coil position 6 has recorded the lowest value of localised power losses.

Highest magnitude value of localised power losses are shown in tables 4-9, 4-10, 4-11 and 4-12, were chosen as reference to compare the results obtained under PWM with the results obtained under sinusoidal voltage excitation. Comparing the results obtained with the core energised at peak flux density of 0.4T, localised power loss was found to be increased near the cutting edge joint and decreased further away from the cutting-edge joint, search coil position 10. Moreover, localised power loss was found to be higher with the core energised under PWM voltage excitation under no-load and load conditions, by factors of 14% and 16% respectively.

Increasing the energising flux to 0.6T under sinusoidal waveform, no-load condition highest magnitude value of loci power loss was recorded to be in search coil position 1, and lowest magnitude value of loci power loss was recorded to be in search coil positions 6, 10 and 15. When the core was energised under load condition, highest value of loci power loss was found to be in positions 1, 2 and 9 and the lowest value of loci power loss was found to be in search coil position 6. Energising the core with same peak flux density under PWM voltage excitation under no-load and load conditions, all search coils have reached their saturation value and search coil position 1 has shown the highest value of localised power loss.

Comparing the results obtained under PWM with the results obtained under sinusoidal voltage excitation at 0.6T, localised power loss was found to be increased under PWM voltage excitation under no-load and load conditions by factors of 60% and 43%, respectively higher than sinusoidal voltage excitation.

More comparisons were made with the core energised at peak flux density of 1.0T. Firstly, measurements were taken under sinusoidal no-load and load conditions, the highest magnitude value of localised power loss was found to be near corner joint and inside outer edge joint search coil positions 1, 2 and 15. And the lowest

Investigation of No-load and on-load performance of a model three-phase transformer core operating under sinusoidal and PWM voltage excitation

magnitude value of the localised power loss was found to be in search coil positions 6 and 10. Nevertheless, all search coils have reached their saturation value.

When the core was energised under PWM voltage excitation at peak flux density of 1.0T under no-load and load conditions, the highest magnitude value of localised power loss was again found to be near corner joint and inside outer edge search coil positions 1, 9 and 15. And the lowest magnitude value of localised power loss was kept in search coil positions 6 and 10.

Comparing the results obtained under PWM with the results obtained under sinusoidal voltage excitation at peak flux density of 1.0T. Localised power loss was found to be increased under PWM voltage excitation under no-load and load conditions by factors of 41% and 53 % higher than sinusoidal voltage excitation.

Fig. 4-17, shows variation of localised power loss under sinusoidal and PWM voltage excitations under no-load condition and Fig. 4-18, localised power loss under sinusoidal and PWM voltage excitations under load condition at 50Hz. Highest values presented on table 4-9, 4-10, 4-11 and 4-12 were chosen as reference.

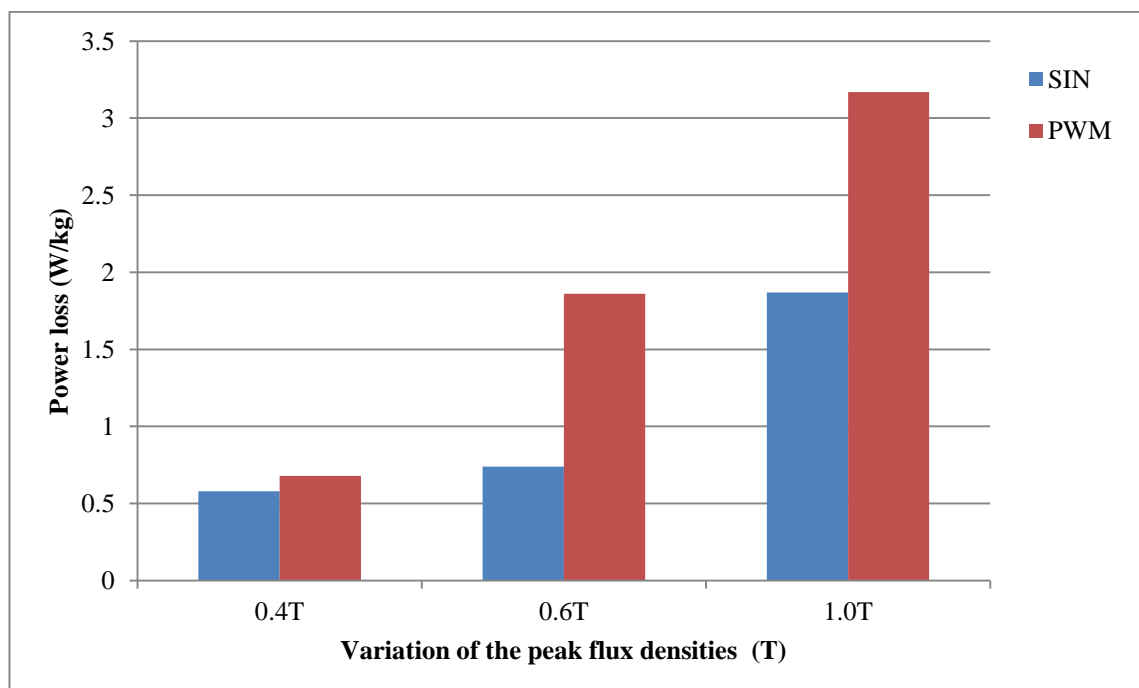


Fig. 4-17 Comparison of localised power loss under sinusoidal and PWM voltage excitation (no-load condition) at yoke corner joints at various peak flux densities (T), 50 Hz.

Investigation of No-load and on-load performance of a model three-phase transformer core operating under sinusoidal and PWM voltage excitation

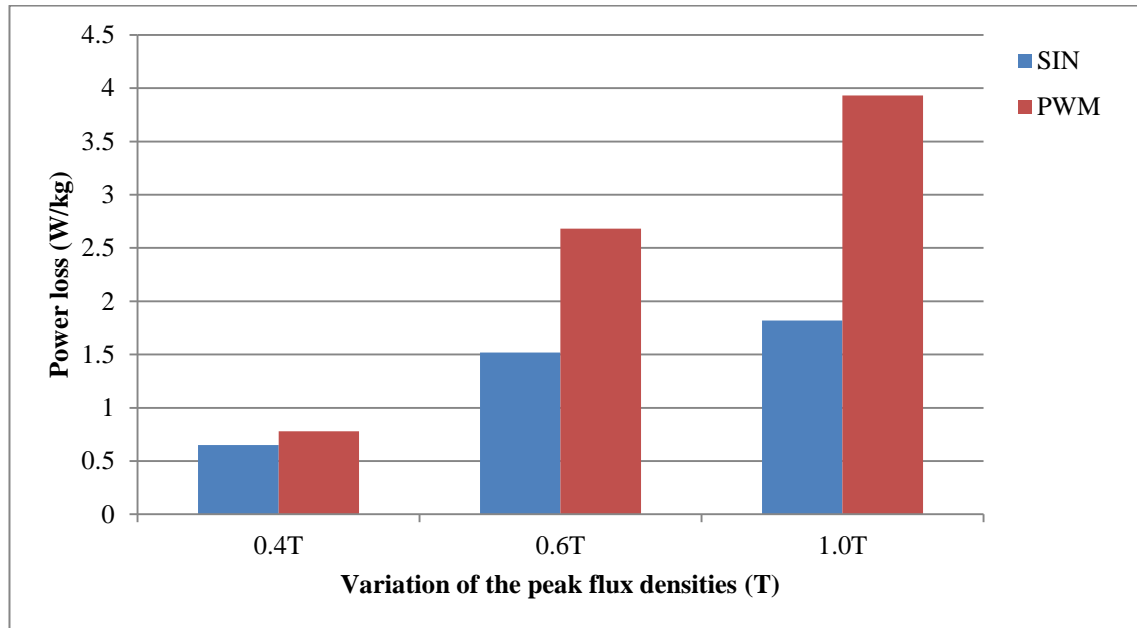


Fig. 4-18 Comparison of localised power loss under sinusoidal and PWM voltage excitation (Load condition) at various peak flux densities (T), 50 Hz.

4.3.7 Comparison between localised power loss obtained in the limb and yoke corner joints of the model three-phase transformer core with various peak flux densities

Highest magnitude values of localised power loss presented on tables 4-5, 4-6, 4-7, 4-8, 4-9, 4-10, 4-11 and 4-12 were analysed to study the difference of magnitude value of localised power loss between the limb and the yoke. Comparing the results obtained under sinusoidal waveform across the limb and yoke at the corner joints, with the core energised at peak flux density of 0.4T under no-load and load conditions, localised power loss was found to be higher in the limb than that of the yoke by factors of 20% and 17% respectively. Furthermore, with the core energised under PWM voltage excitation with the peak flux density of 0.4T under no-load condition, localised power loss in the limb had a value of 26% higher than that in the yoke, while under load condition localised distribution in the limb had a value of 19% higher than that in the yoke.

Comparing the results obtained under sinusoidal waveform between the limb and yoke with the core energised at peak flux density of 0.6T under no-load and load

Investigation of No-load and on-load performance of a model three-phase transformer core operating under sinusoidal and PWM voltage excitation

conditions, localised power losses were found to be 13% and 18% respectively higher in the limb than those of the yoke. However, comparing the result obtained between the limb and yoke when the core energised under PWM voltage excitation with the peak flux density of 0.6T under no-load and load conditions, localised power losses in the limb had values of 32% and 28% higher than those in the yoke,

Increasing the energising flux to 1.0T hence more comparisons between localised power loss occurred in the limb and in the yoke had been obtained. By comparing the results obtained when the core was energised under sinusoidal waveform under no-load and load conditions, localised power losses were found to be 3% and 34% higher in the limb than those of the yoke. However, comparing the results obtained between the limb and yoke when the core energised under PWM voltage excitation with the peak flux density of 1.0T under no-load and load conditions, localised power losses in the limb had values of 20% and 31% higher than those in the yoke.

It could be concluded that localised power loss was higher in the limb than that of the yoke. This was due to the flux density inside the yoke being less than that in the limb at all magnetising levels under no-load and load conditions.

4.3.8 Localised power loss obtained in the yoke- 45° joints with various peak flux densities

Fifteen localised search coils were mounted on the yoke- 45° at the T-joint as shown in fig. 4-9. Localised power loss was measured as shown in tables 4-17, 4-18, 4-19 and 4-20. Firstly, measurements were taken at peak flux density of 0.4T under sinusoidal and PWM waveforms under no-load and load conditions, search coil positions 1, 5 and 8 show the highest value of localised power loss, whereas search coil positions 3, 10 and 16 have shown the lowest magnitude value of loci power loss.

Same results were obtained when the core energised at 0.6T under sinusoidal and PWM waveforms under load and no-load conditions. Search coil positions 1 and 8 have kept the highest value of localised power loss.

Investigation of No-load and on-load performance of a model three-phase transformer core operating under sinusoidal and PWM voltage excitation

Further increasing of the energised flux density to 1.0 T under sinusoidal and PWM waveforms under load and no-load conditions give same result obtained from search coil positions 1 and 8 as they kept the highest magnitude values of localised power loss while search coil position 3 and 16 show the lowest magnitude values of localised power loss.

Comparing the results obtained in search coil position 1 at the top of the left corner with result obtained by search coil position 13 at the top right corner, search coil position 1 has shown the highest value of localised power loss under both sinusoidal and PWM waveforms. Further comparisons have been obtained away from the cutting edges, search coil position 3 was compared with the search coil position 16 under all levels of the magnetising peak flux density. Search coil position 3 has shown highest value of localised power loss under sinusoidal and PWM voltage excitations. This could be due to the size of the grain boundary.

Fig. 4-19 shows the variation of localised power loss under sinusoidal and PWM voltage excitations under no-load condition, and Fig 4-20, has shown the variation of localised power loss under sinusoidal and PWM voltage excitations under load condition at 50Hz. Highest values presented on table 4-17, 4-18, 4-19 and 4-20 were chosen as reference.

Investigation of No-load and on-load performance of a model three-phase transformer core operating under sinusoidal and PWM voltage excitation

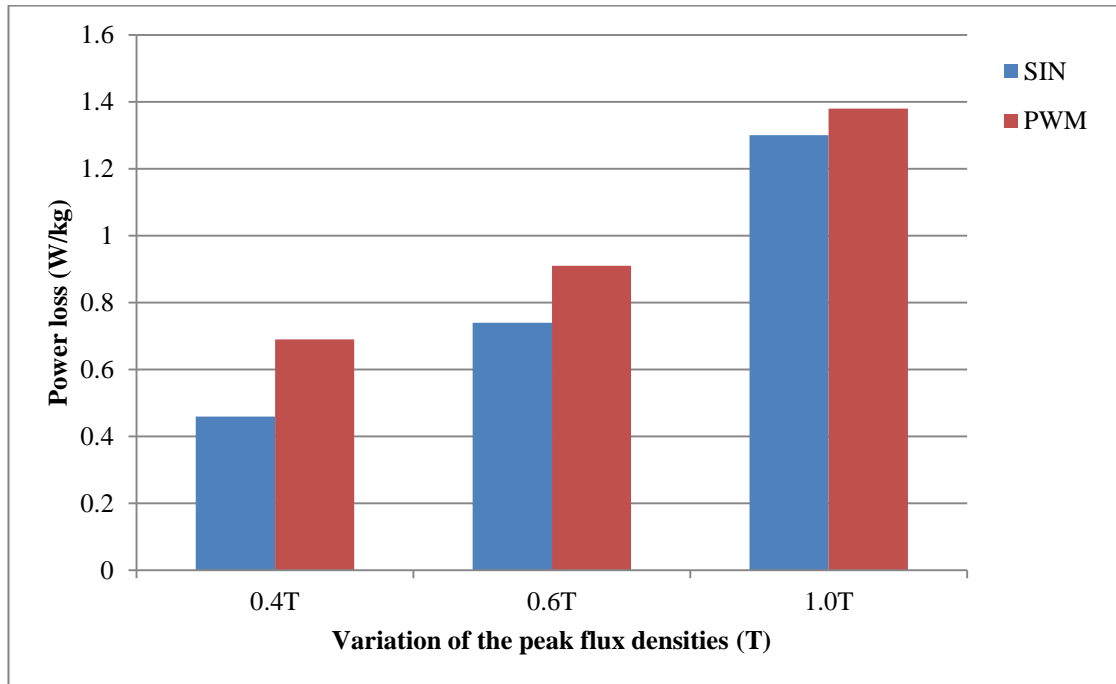


Fig. 4-19 Comparison of localised distribution of power loss under sinusoidal and PWM voltage excitation (No-load condition) at various peak flux densities (T), 50 Hz

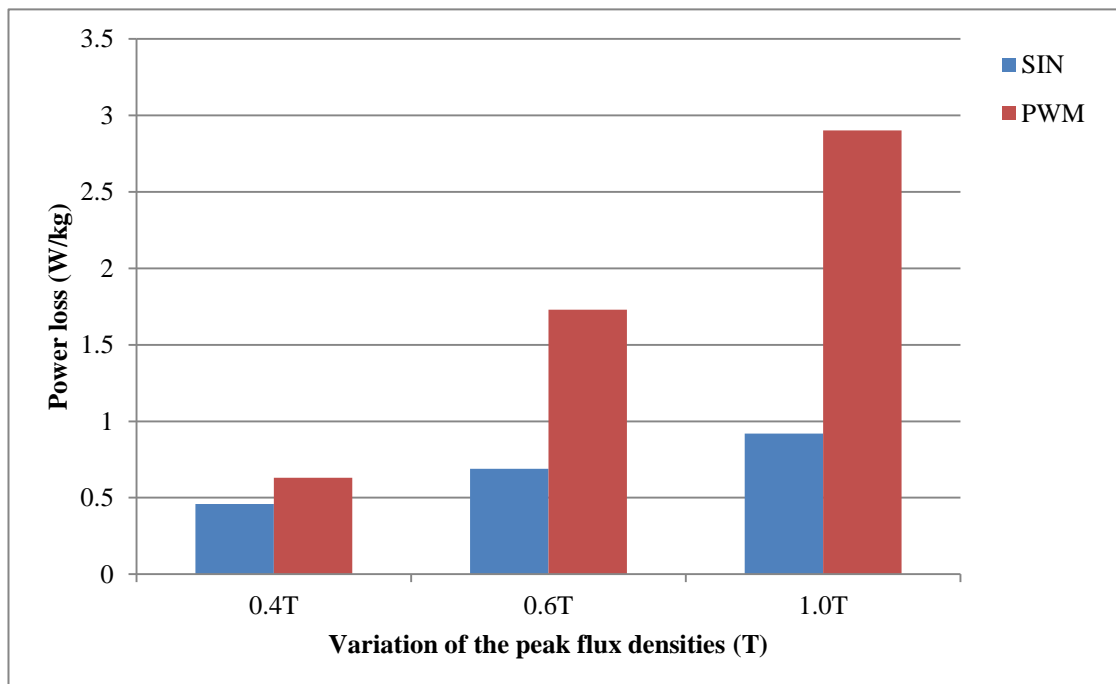


Fig. 4-20 Comparison of localised power loss under sinusoidal and PWM voltage excitation (Load condition) at various peak flux densities (T), 50 Hz

Investigation of No-load and on-load performance of a model three-phase transformer core operating under sinusoidal and PWM voltage excitation

The average value of localised power loss under sinusoidal waveform in the yoke-45° T-joint, Fig 4-9, was recorded to be increased near the joint, for instance at 0.4T under no-load and load conditions. Search coil position 1 and search coil position 3 were compared. The magnitude of localised power loss was increased by the factor of 19% and 15% respectively in search coil position 1. More comparisons have been obtained between the positions of the search coil at 0.6T under no-load and load conditions, the magnitude of localised power loss at search coil position 13 at the right top corner near the edge was compared with search coil position 8. The average value of the localised power loss was 9% and 3% higher in search coil position 8. Further comparisons have been obtained at core peak flux density 1.0T under no-load and load conditions, comparing top left corner search coil position 1 with the top left corner search coil position 13, the magnitude of localised power loss in search coil position 1 under no-load and load conditions had a value of 18% and of 34% higher than search coil position 13.

More comparisons of the results have been made, with the core energised under PWM voltage excitation, same search coil positions were compared. For example, under no-load condition at 0.4T the average value of localised power loss in search coil position 1 was 30% higher than search coil position 3. While under load condition it was again higher in search coil position 1 by a factor of 28%. However, with the core energised at 0.6T search coil positions 13 was compared with search coil position 8 under no-load and load conditions. The magnitude of localised power loss was higher in position 8 by factors of 4% and 25% respectively. Increasing the energising flux to 1.0T search coil position 1 was compared with search coil position 13 under no-load and load conditions. The magnitude of localised power losses were higher in search coil position 1 at the left top corner by factors of 5% and 32% respectably.

4.3.9 Localised power loss obtained in the limb T joints with various peak flux densities

At limb T-joint, 14 search coils were chosen to study localised power loss as shown in fig 4-10, and tables 4-21, 4-22, 4-23 and 4-24 show the variation of localised power loss against time under sinusoidal and PWM waveforms under load and no-load conditions. With the core energised under sinusoidal waveform at peak flux density of 0.4T under no-load and load conditions, search coil positions 13 and 1 have shown the highest value of localised power loss. Away from the cutting joint search coil positions 6 and 7 have shown the lowest value of localised power loss. However, comparing search coil position 5 with search coil position 8 under no-load and load conditions, localised power loss had a value of 5% and 2% respectively higher in search coil position 8.

Increasing the energised flux to 0.6T, search coil position 13 has shown the highest magnitude value of localised power loss. Whereas, search coil position 5 has shown the lowest value of localised power loss. Comparing the variation of localised power loss under no-load and load conditions, between the highest and lowest value induced in the search coil position 13 and search coil position 5, the results obtained had shown that under no-load condition search coil position 5 had a value of 33% higher localised power loss than search coil position 13, while under load condition it was 50% higher in search coil position 13.

Increasing the energised flux to 1.0T when measurements were taken under no-load condition, search coil positions 13, 1 and 16 have shown the highest value of localised power loss, and search coil position 8 has shown the lowest value of localised power loss. Comparing the result has been obtained between the highest and lowest induced power loss distribution under no-load and load conditions, so hence localised power loss in search coil position 13 was compared with localised power loss in search coil position 8. Localised power loss in search coil position 13 had a value of 16% and 37% respectively, higher than the localised power loss in search coil position 8.

When the core was energised at peak flux densities of 0.4T, 0.6T and 1.0T, under PWM voltage excitation under no-load and load conditions, same result of highest

Investigation of No-load and on-load performance of a model three-phase transformer core operating under sinusoidal and PWM voltage excitation

and lowest induced localised power loss was obtained at the same position of the search coils as those have been obtained under sinusoidal voltage excitation. At all magnetising peak value search coil position 13 kept the highest value of localised power loss. And search coil position 8 kept the lowest value of localised power loss. Comparing the result between the highest and lowest localised power loss, under no-load condition at 0.4T, 0.6T and 1.0T, search coil position 9 had values of 32%, 38% and 50% respectively, higher than search coil position 13. While under load condition at magnetising flux of 0.4T, 0.6T and 1.0T, localised power loss of search coil position 13 was higher than the localised power loss in search coil position 8 by 37%, 41% and 28% respectively.

Comparing the highest value of localised power loss under sinusoidal and PWM voltage excitation at peak flux density 0.4T under no-load condition, the highest value of localised power loss was recorded at search coil position 13 which has a value of 37% higher under PWM voltage excitation. However, with the core energised under load condition, localised power loss was 22% higher under PWM voltage excitation. Further comparing of the highest result of localised power loss detected by the search coils has been obtained with the core energised under sinusoidal and PWM waveforms at peak flux density of 0.6T under no-load condition, localised power loss had a value of 56% higher under PWM waveform, whereas under load condition it was higher by factors of 31% under PWM voltage excitation. However, more comparing of localised power loss has been obtained with the core energised under PWM and sinusoidal waveforms. Increasing the energising flux to 1.0T the highest localised power loss under PWM waveform was compared with the highest value of localised power loss with the core energised under sinusoidal waveform. Under no-load and load conditions localised power loss had a value of 63% and 30% respectively higher under PWM voltage excitation.

It can be concluded that localised power loss was higher under PWM voltage excitation in the T-joint (limb-joint) under all levels of magnetising peak flux density under load and no-load conditions.

Fig. 4-21 shows the variation of localised power loss under sinusoidal and PWM voltage excitation under no-load condition, and Fig. 4-22, shows the variation of

Investigation of No-load and on-load performance of a model three-phase transformer core operating under sinusoidal and PWM voltage excitation

localised power loss under sinusoidal and PWM voltage excitation under load condition at 50Hz. Highest variation values presented on tables 4-21, 4-22, 4-23 and 4-24 were chosen as reference.

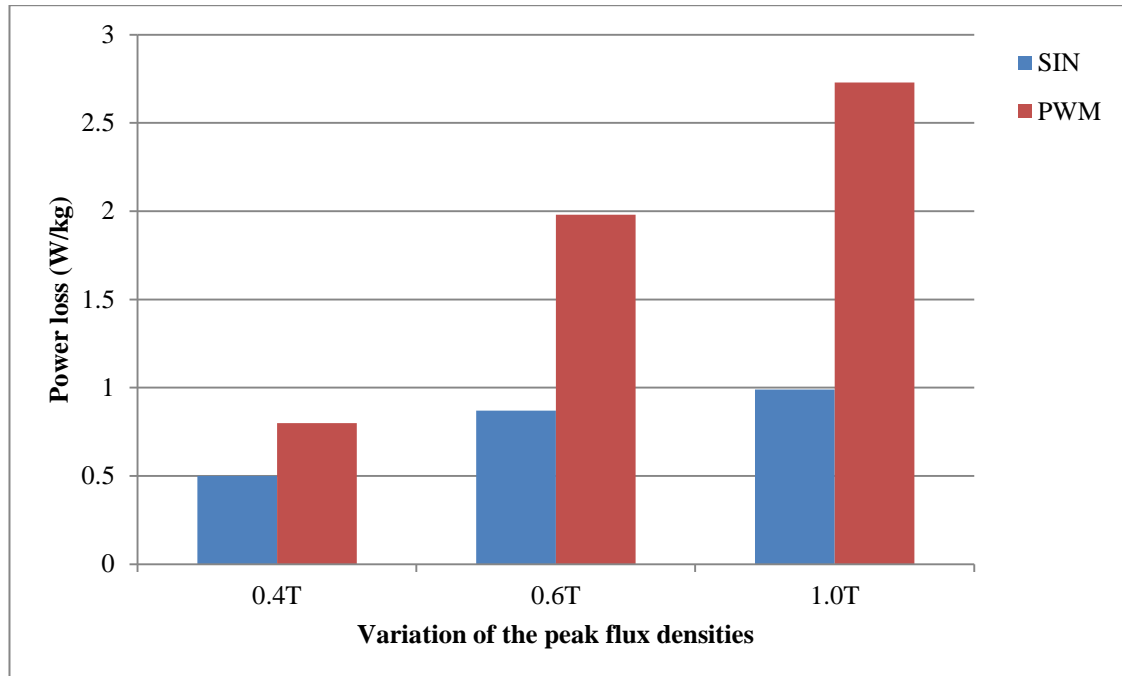


Fig. 4-21 Comparison of localised power loss under sinusoidal and PWM voltage excitation (No-load condition) at limb T-joints at various peak flux densities (T), 50 Hz.

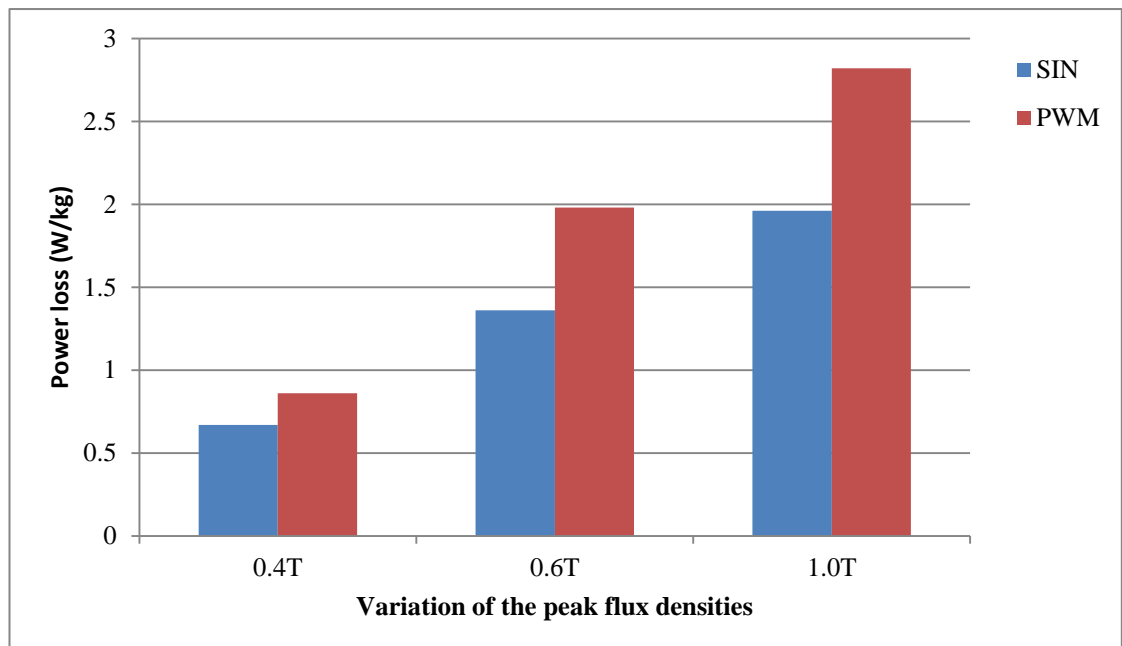


Fig. 4-22 Comparison of localised power loss under sinusoidal and PWM voltage excitation (Load condition) at limb T-joints at various peak flux densities (T), 50 Hz.

4.3.10 Comparison between power loss obtained in the limb and yoke T joints with various peak flux densities

Comparing localised power loss obtained in the T-joint and yoke-45° joint under sinusoidal waveform at peak flux density of 0.4T under no-load condition. Search coil position 13 in the limb T-joint, Fig. 4-10, was compared with the search coil position 8 in the yoke-45° joint, Fig. 4-9. Magnitude of comparisons value occurred during the measurements was taken from tables 4-17 and 4-21. It shows that the average of localised power loss in the limbs was 10% higher than that of the yoke-45° joint. Whereas under load condition comparing search coil position 8 in the 45°-yoke with the search coil position 13 in the limb T-joint, the maximum produced localised power loss remained higher in the limb by the factor of 32%.

Comparing localised power loss obtained in the T-joint and yoke-45° joint when the core energised by PWM voltage excitation at 0.4T under no-load condition, tables 4-19 and 4-23, comparing search coil position 16 in the yoke-45° joint with the search coil position 16 in the limb T-joint, it shows that localised power loss in the limb T-joint had value of 19% higher than that of the yoke-45° joint. However, comparing same search coil positions under load condition, tables 4-20 and 4-24, localised power loss found to be increased in the limb by 30%, than that of the yoke-45° joint. Search coil position 16 in the limb T-joint has shown higher value of localised power loss than search coil position 16 in the 45°-yoke joint at all magnetising levels under load and no-load condition.

Comparing localised power loss obtained in the T-joint and yoke-45° joint when the core energised under sinusoidal waveform at peak flux density 0.6T under no-load condition. Comparing search coil position 3 in the yoke-45° joint, with the search coil position 3 in the limb T-joint, tables 4-17 and 4-21 show maximum and minimum of localised power loss distribution. The variation of the localised power loss in the limb T-joint was 32% higher than that in the yoke. However, comparing the result obtained under load condition with the same search coil positions, tables 4-20 with 4-24. Localised power loss was higher by 37% in the limb joint than that of the yoke joint.

Investigation of No-load and on-load performance of a model three-phase transformer core operating under sinusoidal and PWM voltage excitation

Comparing the result obtained when the core energised by PWM voltage excitation at 0.6T under no-load condition. Localised power loss in the limb T-joint was 56% higher than that in the yoke-45° joint. However, comparing the result obtained under load condition tables 4-20 and 4.24. Localised power loss in the limb T-joint was 51% higher than that in the 45°-yoke joint.

Comparing the result obtained in the limb T-joint with the result obtained in the 45°-yoke joint, when the core energised at peak flux density of 1.0T under sinusoidal waveform no-load condition. Search coil position 3 in the limb was compared with search coil position 3 in the yoke-45° joint. Tables 4-17 and 4-21, localised power loss in the limb joint had value of 32%, higher than that in the yoke 45°- joint. However, comparing the result obtained under load condition tables 4-18 and 4-22, localised power loss in the limb joint has shown higher value than that of the yoke joint by the factor of 54%.

Comparing the result obtained when the core energised by PWM voltage excitation, at peak flux density 1.0T under no-load condition tables 4-19 and 4-23. Comparing search coil position 7 in the limb T-joint with the search coil position 3 in the yoke 45°-joint, localised power loss in the limb joint had a value of 48% higher than that of the yoke 45°- joint. However, comparing localised power loss under load condition with the same search coil positions, the result have shown that localised power loss in the limb T-joint has higher value than localised power loss in the yoke 45°- joint by the factor of 24%.

In conclusion with the core energised under sinusoidal and PWM voltage excitations at all magnetising level of peak flux density 0.4T, 0.6T and 1.0T, under load and no-load conditions, localised power loss in the limb T-joint have shown higher value than yoke-45° joint, that is due to the amount of the localised flux flow in the limb T-joint is higher than the amount of the localised flux flows in the yoke-45° joint.

Study of the rotational flux was also covered throughout this experiment. Most of the flux in the middle of the limb areas remained in the rolling direction, rotational flux was found to be very small in this area. However, T-joint areas had high concentration of rotational flux, especially near the cutting edge when the flux is

Investigation of No-load and on-load performance of a model three-phase transformer core operating under sinusoidal and PWM voltage excitation

expected to be jumping from one side to another side. The major axes of the localised flux density in the middle of the lamination and the outer joint were mainly along the rolling direction.

4.3.11 Influence of modulation index and switching frequency on total power loss in three-phase transformer core.

A secondary winding was connected to a power analyser “Norma D6000 (S/N: ND 58172 RR)”, so the secondary induced voltage was calculated using Fast Fourier Transform (FFT). Fig. 4-27, 4-28 and 4-29, show assigned value of modulation index m_a in the range of 0.5, 0.7, 0.8 and 1.2 with assigned value of switching frequency f_s varied in the range 1 kHz, 2 kHz and 3 kHz respectively. Transformer core was energised at peak flux density of 1.0T.

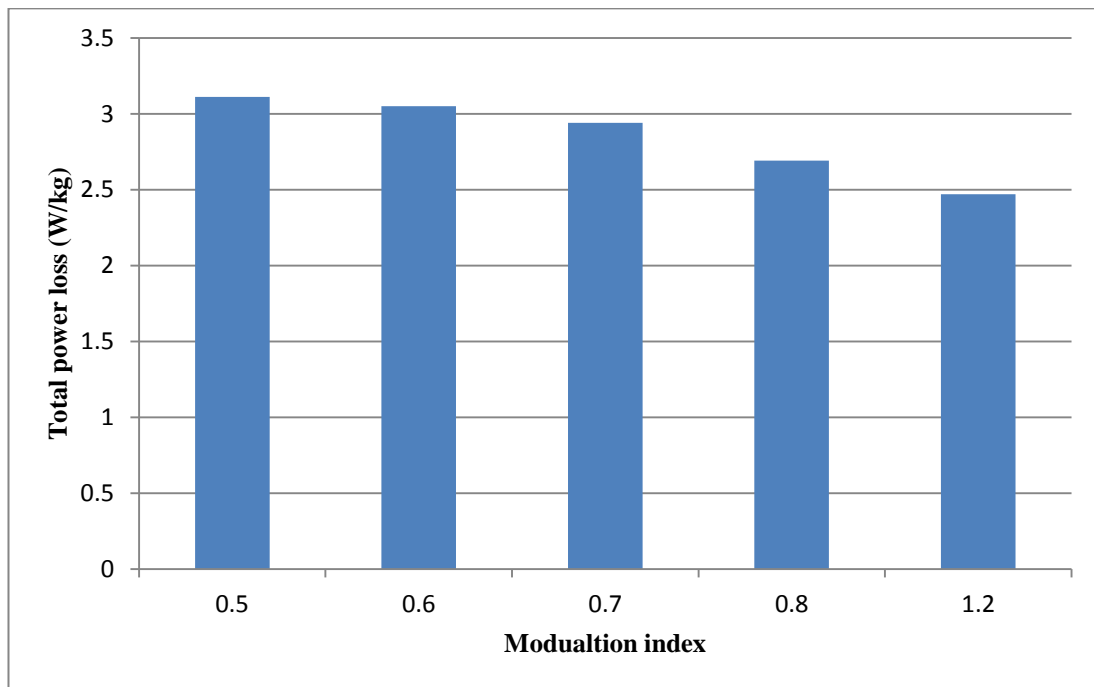


Fig. 4-23 Total power loss under PWM voltage excitation with assigned value of modulation index at f_s 3 kHz

Investigation of No-load and on-load performance of a model three-phase transformer core operating under sinusoidal and PWM voltage excitation

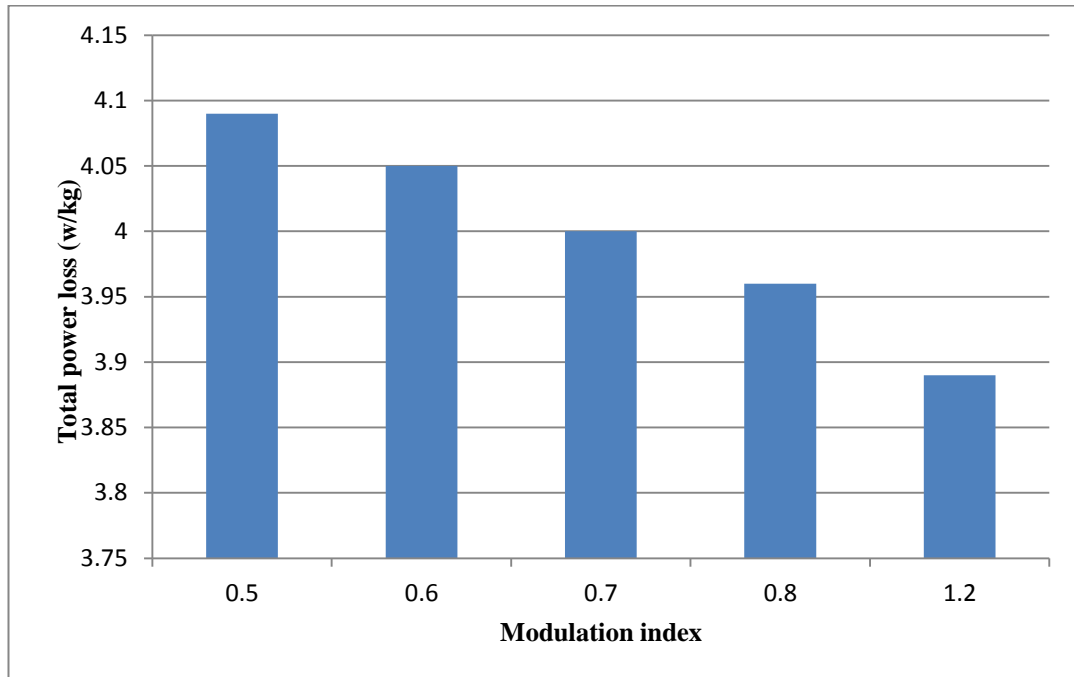


Fig. 4-24 Total power loss under PWM voltage excitation with assigned value of modulation index at f_s 2 kHz

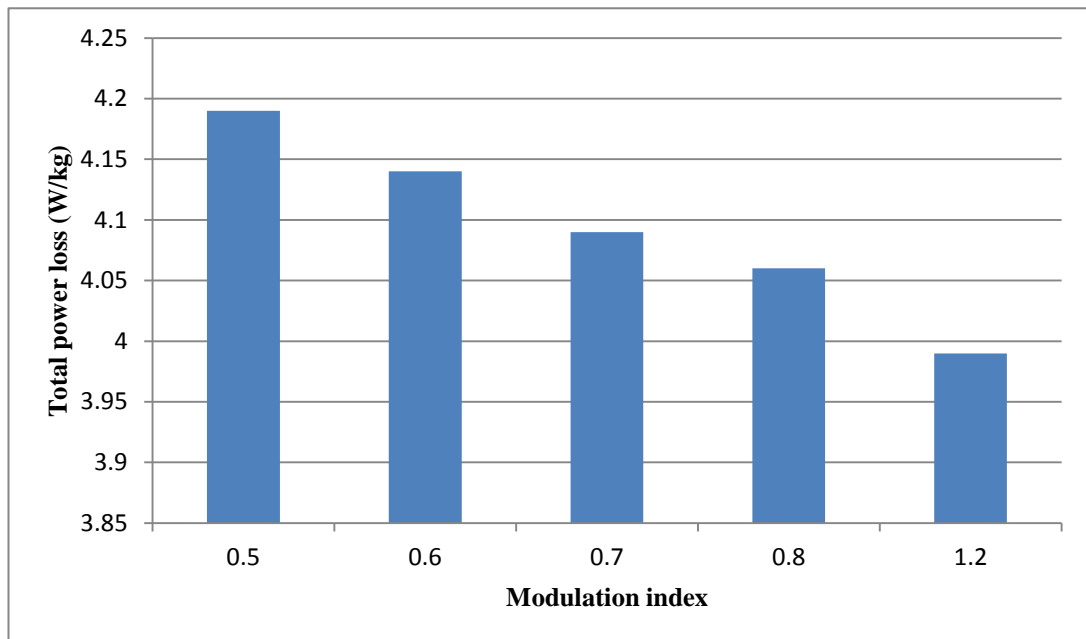


Fig. 4-25 Total power loss under PWM voltage excitation with assigned value of modulation index at f_s 1 kHz

4.3.12 Analysis and discussion

From Fig. 4-23 to Fig. 4-25, the highest loss of the transformer core occurred at the lowest value of modulation index = 0.5 and 0.6. Nevertheless, it was notice that total losses were decreased with the increase of modulation index and with increase of switching frequency f_s . This was caused by higher harmonic contents in the voltage waveforms produced by PWM inverter at lower values of $m_a = 0.5$ and 0.6.

The highest total losses were seen to be at the lowest values of modulation index m_a and at the lowest value of switching frequency f_s . An increase of the switching frequency under PWM voltage excitation caused a reduction in total loss for example, when m_a 0.5 at switching frequency of 1 kHz were compared to m_a 0.5 at switching frequency of f_s 3 kHz, the reduction in total power loss were 35 % W/kg.

It can be concluded that low value of m_a and low value of f_s results in increase in the total losses in transformer core. Beneficial effect was observed with increase of the modulation index to 1.2 and increase of switching frequency to 3 kHz which led to reduced total power loss under PWM voltage excitation.

CHAPTER 5

5. Introduction

Magnetostriction of core lamination is one of the main sources of transformer acoustic noise. A measurement system using strain gauge has been designed and built. This was optimized for magnetostriction measurements under sinusoidal and PWM voltage excitations.

Historically Five different methods were used to measure magnetostriction properties of electrical steel which are, Piezoelectric displacement transducer, linear variable differential transformer, capacitive displacement sensors, laser doppler techniques and resistance strain gauge. Results show reasonable correlation between those methods.

In this study the influence of localised magnetostriction of 3% grain-oriented silicon steel was investigated under sinusoidal and PWM waveforms under on load and no-load conditions, with the different peak flux densities.

5.1.1 Magnetostriction λ

In 1842 James Joule had discovered that ferromagnetic material changes its length when subjected to external magnetising field. He proved that by magnetising iron bar the length of the iron bar increases due to the change in the domain wall position as it starts to move from its original position to a new position [23]. He also discovered that magnetostriction can be positive or negative. If the length of the iron bar increases with increasing the external magnetising field, then magnetostriction is termed as positive λ . Whereas, if the length of the bar decreases with increasing the external magnetic field, magnetostriction is termed negative λ . However, after reversing the direction of external applied magnetizing field the sign of λ does not reverse. This results in magnetostriction having fundamental frequency of twice that of the excitation frequency.

5.1.2 Domain wall and spontaneous magnetostriction

Discorded magnetic moments interaction produce force between atoms that tends to strain lattice anisotropically, a magnetic material is deformed due to the magnetic interaction. This deformation is explained by an asymmetric tensor of elastic distortion, this effect can be observed under microscope [55]. When ferromagnetic material is heated above its Curie temperature and then cooled, domain wall will have completely random alignment of magnetisation which ensures that the bulk magnetisation within the whole volume is zero as shown in Fig. 5-1 (a). Whereas, when material goes below the Curie temperature it becomes ferromagnetic. As solid cooled below the Curie temperature, spontaneous magnetisation occurs within the domains and this produces spontaneous magnetostriction along particular direction as shown in Fig. 5-1 (b). At this point the amplitude of the magnetostriction is independent of crystallographic direction within each domain.

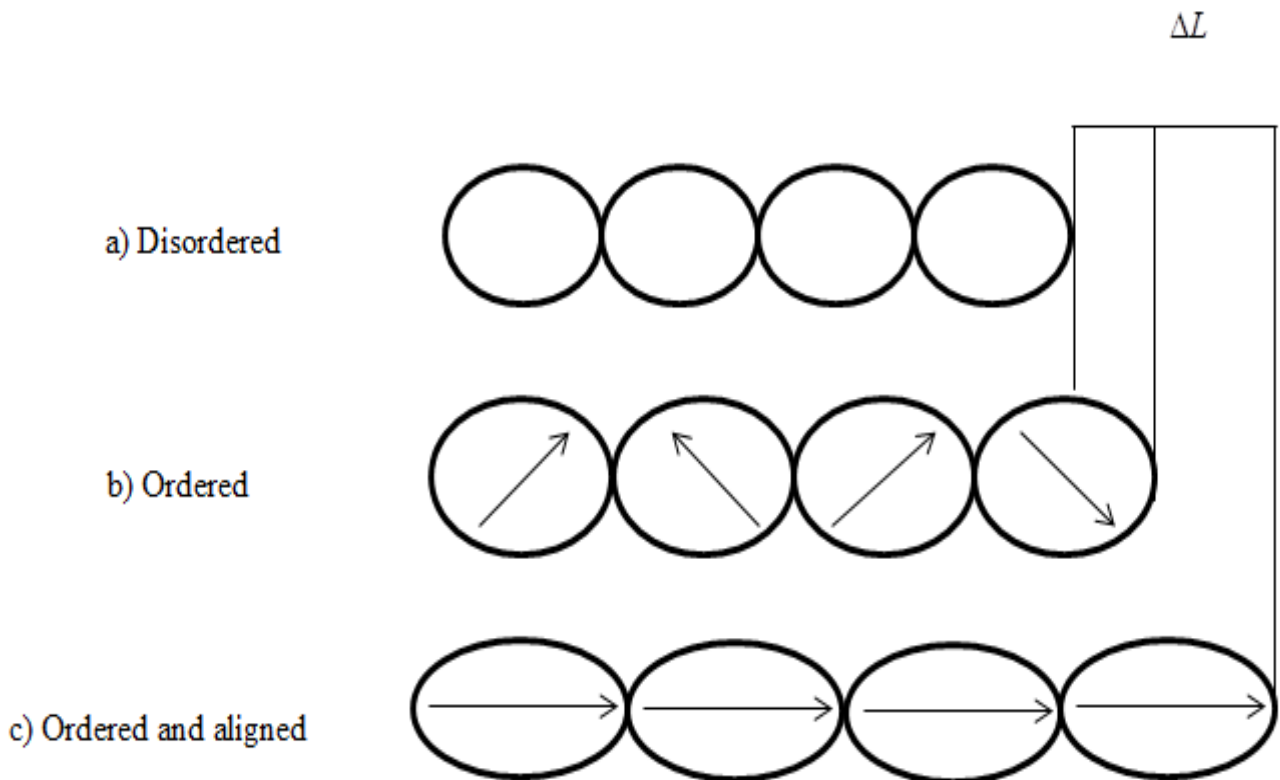


Fig. 5-1 Mechanism of magnetostriction

Investigation of No-load and on-load performance of a model three-phase transformer core operating under sinusoidal and PWM voltage excitation

The spontaneous magnetostriction along the direction of the domain magnetisation is equal to the saturation magnetostriction ' λ_s ' and will cause magnetoelastic energy ' E_λ ', this can be calculated using the following equation:

$$E_\lambda = -\frac{3}{2} \lambda_s \sigma \sin^2 \theta \quad (5.1)$$

Where θ is the angle between the direction of magnetisation and direction of the applied stress σ .

The average deformation throughout the cubic crystal such as silicon iron can then be obtained by using following equation which is widely known as Becker-Doring equation [56] assuming that the domains are oriented in random:

$$\lambda = \frac{3}{2} \lambda_{100} (\alpha_1^2 + \alpha_2^2 \beta_2^2 + \alpha_3^2 \beta_3^2 - \frac{1}{3}) + 3 \lambda_{111} (\alpha_1 \alpha_2 \beta_1 \beta_2 + \alpha_2 \alpha_3 \beta_2 \beta_3 + \alpha_1 \alpha_3 \beta_1 \beta_3) \quad (5.2)$$

Where α_1 , α_2 and α_3 are the directional of cosines of the magnetisation direction and β_1 , β_2 and β_3 are the directional cosines of the strain-measurement direction with respect to the cube edges. λ_{100} and λ_{111} are the saturation magnetisation constants in the [100] and [111] directions respectively [56].

5.1.3 Saturation magnetostriction

Saturation magnetostriction is the fractional change in length between a demagnetised ferromagnetic solid and the same solid in a magnetic field. In order to obtain saturated value in ferromagnetic material magnetic, field needs to be sufficiently strong to saturate the magnetic material along the direction of the applied field as shown in Fig. 5-1 (c). The applied magnetic field causes the domains to align in parallel and hence the strain are parallel as shown in Fig. 5-1 (c) [2].

5.1.4 Transformer noise

Recent study to develop transformer core efficiency are not restricted to lower losses but are also focused on lower noise. The increasing energy demand brings transformers closer to the population which makes the noise problem more and more important. Transformer core noise is emitted from winding noise, magnetic core vibration and core construction and core design [57].

5.2 Winding noise

Winding noise is classified as load noise or current noise because it is caused by the current passing through the winding and the total current of the other winding. Winding noise can be reduced by having good guilty winding wrapped precisely around the core [58].

5.2.1 Fans and pump noise

The other source of the noise in transformers is generated from cooling fans or pumps, as transformer loss will mostly have converted into heat. As a result, insulating medium inside the transformer, usually oil is used to remove the heat from winding and transformer core [59].

5.2.2 Magnetic core vibration

Core vibration is produced by magnetostriction and magnetic force which is known as the (Maxwell force). Due to the extension and contraction taking place all over the laminations each lamination behaves unpredictably with respect to its neighbour. Magnetic core vibration is identified as the biggest sources of noise [60].

5.2.3 Core construction and design

Transformer core is assembled by using many laminations having a distributed mass, with different movements occurring all over the core. Each lamination has different association mode. Nevertheless, mitred joints which introduce mechanical problems are hard to analyse [61].

Investigation of No-load and on-load performance of a model three-phase transformer core operating under sinusoidal and PWM voltage excitation

Present study shows that strain of the core is the primary source of the core noise, nevertheless, strain occurs in the core resulting from magnetostriction. The magnitude of the magnetostrictive properties depends on the type of material and applied magnetic field.

5.2.4 Magnetostriction characteristic under applied field

Magnetic domains in ferromagnetic material are strained in the direction of spontaneous magnetisation as result of applying external field, any rearrangement of the domain structure will change the net strain of the material. Nevertheless, this would cause the direction of the internal field within the domains to rotate to the direction of the applied field. Fig. 5-2 [62].

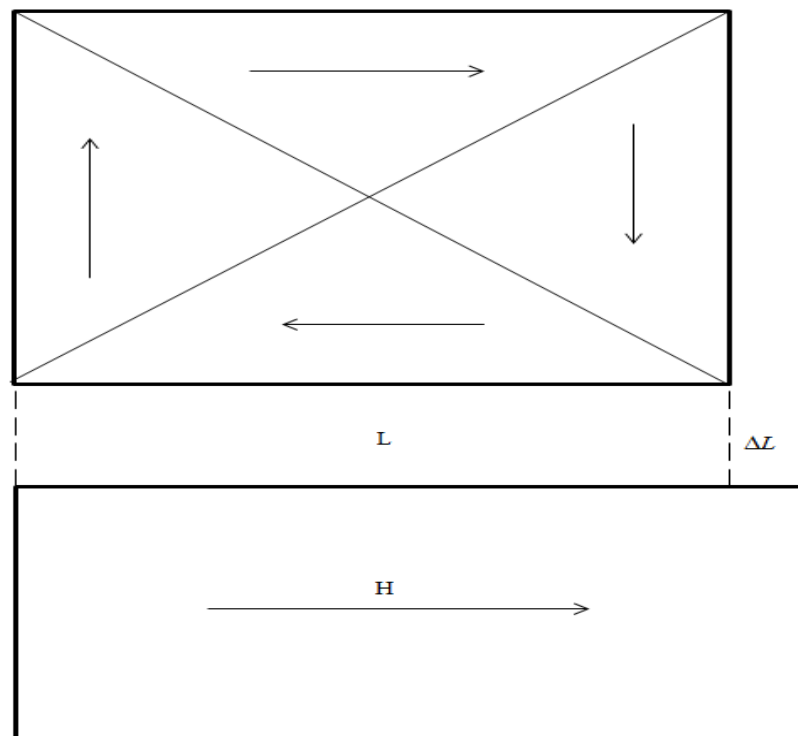


Fig. 5-2 Domain walls rotate to the applied field

Investigation of No-load and on-load performance of a model three-phase transformer core operating under sinusoidal and PWM voltage excitation

So, it can be noticed that domain wall is the primary reason for magnetostriction in the ferromagnetic materials.

5.3 Method used to measure magnetostriction

There are several methods used to measure magnetostriction which are: Piezoelectric displacement transducer, linear variable differential transformers, capacitive displacement sensors and laser Doppler techniques.

5.3.1 Piezoelectric displacement transducer

Piezoelectric displacement transducer consists of stylus pin mechanically linked to the piezoelectric bi-morph. Attaching the leads of the pin on the lamination surface. Fig. 5-3, changes of the charge being developed in the element. This method is used to measure well defined point and it is impossible to measure all areas simultaneously [63].

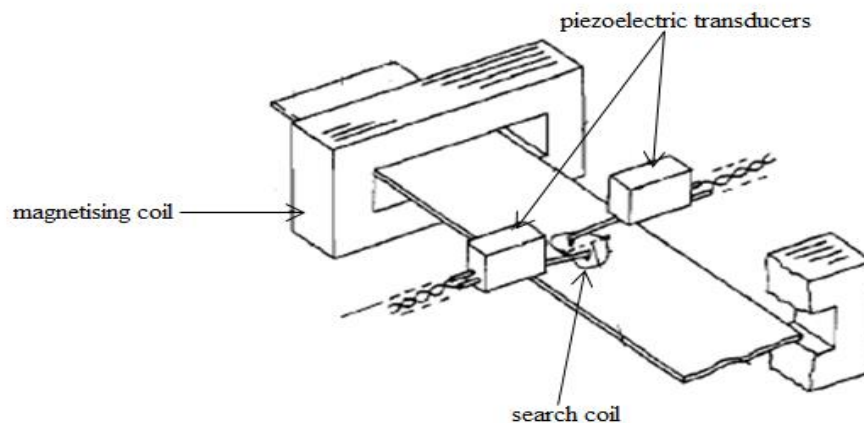


Fig. 5-3 Magnetostriction measurement systems using piezoelectric transduces technique

5.3.2 Linear variable differential transformer

Linear variable differential transformers (**LVDT**) can be used to measure magnetostriction, it consists of movable core with one primary coil and two secondary coils. The core is placed inside the coils at the centre. Fig. 5-4 and then sinusoidal excitation current applied to the primary winding which is coupled to the secondary winding by the movable core. The two secondary coils are identical. Movement of the core would cause a flux leakage in the secondary coils. When the core is moved away from the centre position, a differential voltage appears across the secondary coils then the displacement can be measured with the use of phase sensitive detector. Detecting of magnetostriction occurs when the core moves from its position, then sensitive detector gives an output proportional to the change which has occurred [64].

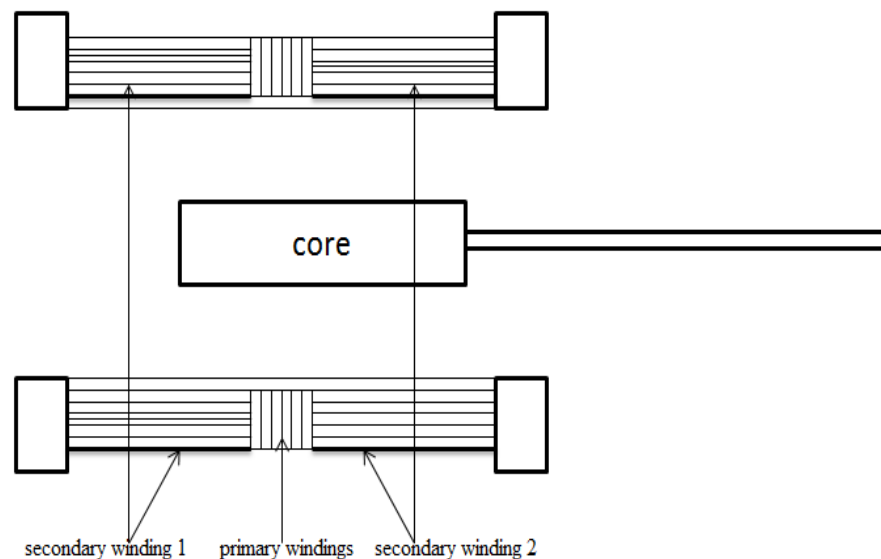


Fig. 5-4 Schematic diagram of LVDT

5.3.3 Capacitive displacement sensors

Capacitive displacement sensors generate an electrical signal as a result of the elastic deformation of a membrane and consist of an oscillator circuit and two plates separated by distance usually air. One of the plates is attached to the free end of the lamination whilst the other one is fixed. Vibration in the lamination produces a voltage signal proportional to the change in length of the specimen [65].

5.3.4 Laser Doppler techniques

Laser Doppler techniques was first presented by Nakata [66]. The magnetostriction displacement is measured by two mirrors mounted on the sample. Fig. 5-5. The laser beam is divided into two beams by the half mirror HM_1 . The beam a_1 has its frequency shifted by an amount Δf . Beam a_2 is reflected from mirror fixed on the sample, the output current is produced from a photoelectric detector. FM decoder gives a signal proportional to the velocity of sample vibration.

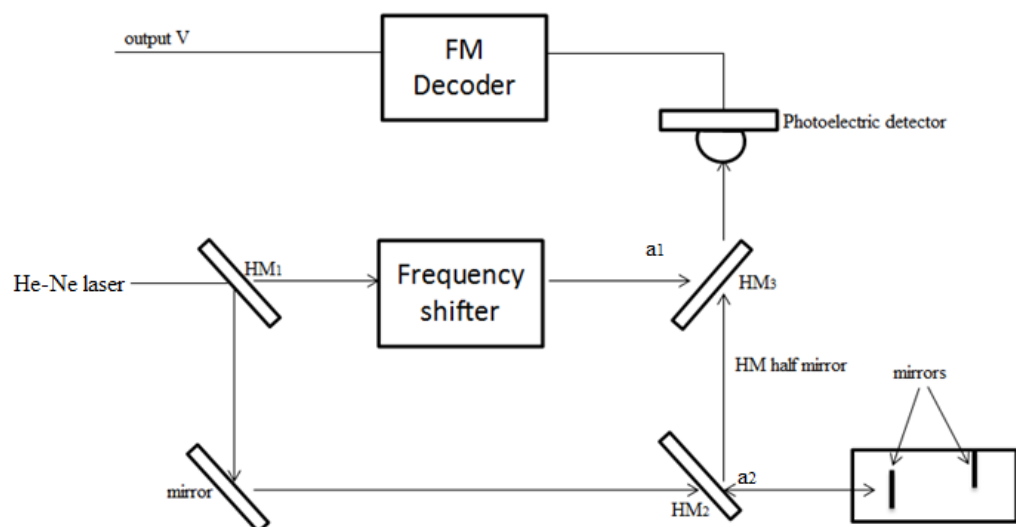


Fig. 5-5 Block diagram of a laser doppler velocimeter

Investigation of No-load and on-load performance of a model three-phase transformer core operating under sinusoidal and PWM voltage excitation

In this project strain gauges were used to study localised magnetostriction in the transformer core. Strain gauges were employed in the middle of the transformer core where the stress is highly present. And hence magnetostriction was measured due to the change occurred in the electrical resistance of strain gauge. There are two types of strain gauge used to measure localised magnetostriction, pro foil strain gauge and three-wire strain gauge.

5.4 Pro foils strain gauges

Type of strain gauge used to measure localised magnetostriction has a gauge length of 8 mm wound with gauge width of 4 mm, its gauge factor was approximately 2.1 and gauge resistance of 120Ω . The strain gauge is usually cemented to the polyimide backing which has a withstand temperature of up to 180°C , making them ideal for higher temperature applications and gives excellent bonding as shown in Fig. 5-6.

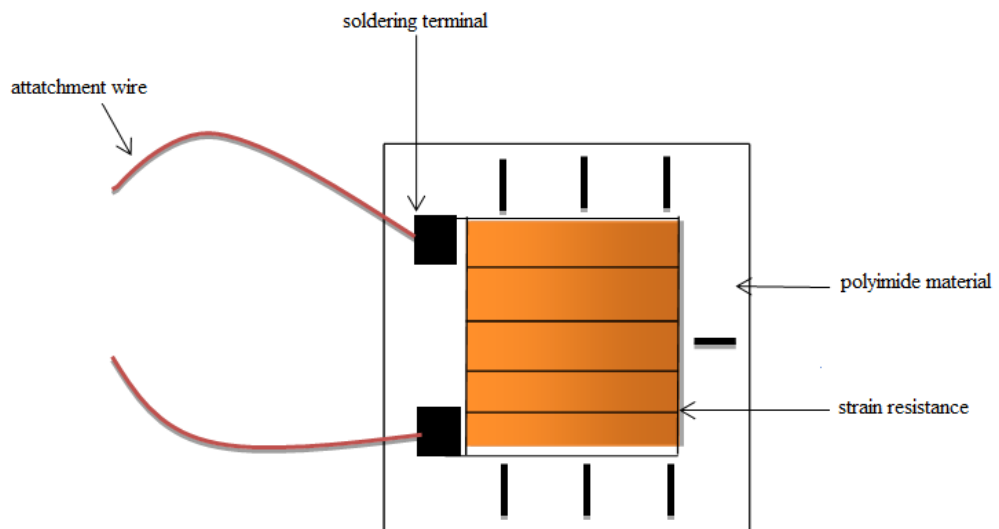


Fig. 5-6 Pro Foil strain gauge used to Measure magnetostriction

5.4.1 Three-wire strain gauge rosettes pre-wired

In order to study the strain in the core and bending effect of the lamination, pre-wired strain gauge was glued on both sides of the lamination. It was used to cover more area in the plane of the lamination as it was bigger than Pro Foil Strain Gauge as shown in Fig. 5-7.

Pre-wired strain gauge has three measuring electrical wire positioned in different axes which is composed on polyimide film. With gauge length of 10 mm, gauge width of 20 mm, gauge factor of 2.10 and gauge resistance of 120Ω .

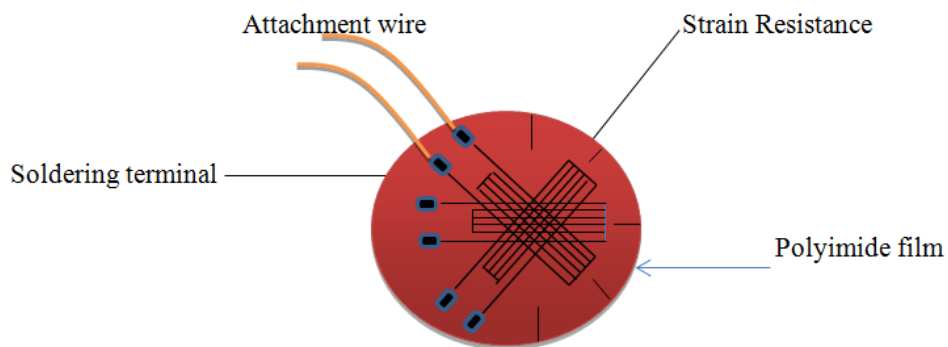


Fig. 5-7 Shows 3-Wire Strain Gauge Rosettes Pre-wired

Transformer core was energised by three-phase sinusoidal supply and PWM inverter with different peak flux densities under load and no-load conditions. Measurements were taken simultaneously with respect to the energising condition, data logger “700-128-SM” was used to measure and store localised magnetostriction.

5.4.2 Strain data logger

Localised magnetostriction was measured by, strain data logger “700-128-SM” when the core was energised by PWM inverter and sinusoidal voltage excitation. Figure 5.8 shows the measurement system, after carefully building the transformer core, strain gauge soldering attachment wires were connected to the data logger via terminal connector as shown in Fig. 5-8. Insulation of the attachment wires at the ends were removed very carefully. Moreover, attachment wires were twisted separately to avoid picking up any stray noise voltage.

Strain data logger has 80 channels which is can be used to measure large numbers of strain gauges simultaneously and also helps to connect specimen attachment wires straight to the channels.

After connecting attachment wires to the channel, it would be necessary to highlight selected channel this is can be done through the personal computer. However, strain data logger has unique advantages which allow you to know which is fault and active strain gauges by pressing the calibrate bottom. After calibrating strain gauges, it would be necessary to obtain initial balance of the specimen for each experiment and this obtained by potentiometer inserted between active and dummy gauges this is also known as the “apex resistance”.

After selecting desired channel and checking all strain gauges are calibrated. A galvanometer is tapped into the resistance, at the balance point reading of measurement can be taken by pressing alarm bottom which would record any change occur in the resistance. However, monitoring and collecting data can be done through personal computer which would indicate any changes occur in the electrical resistance, for each measuring circuit it is necessary to calibrate and rebalancing strain gauges repeatable.

Investigation of No-load and on-load performance of a model three-phase transformer core operating under sinusoidal and PWM voltage excitation

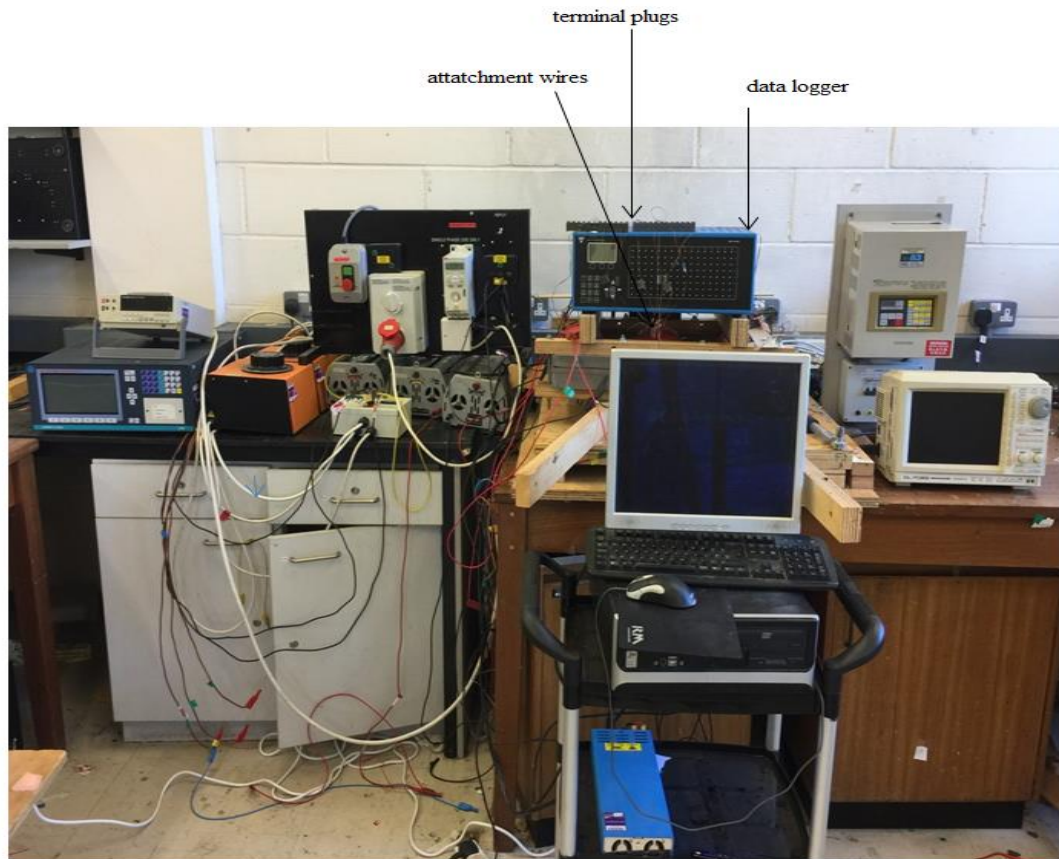


Fig. 5-8 Strain gauges measurement system

5.4.3 Strain gauge sample preparation

Firstly, locations of strain gauges were marked on the laminations on both rolling RD and TD directions (limbs, yokes, corners and T-joint) then, insulating coating on these areas was removed very carefully to avoid any stress or roughness on the surface which was then cleaned by using acetone. A drop of strain gauge special adhesive was applied on the surface, and then a gauge was stuck by pressing its whole area uniformly for a few minutes, until the adhesive was dry.

Nevertheless, wires used in this experiment were 0.08mm^2 paralleled vinyl lead wire with a very low resistance of $0.44\ \Omega$. The ends of the wires were soldered to the strain gauges through soldering terminal and then they were terminated to the logger through the input of the terminal connector. The output of the terminal connector was connected to RJ45 plugs and then the output voltage was passed to the logger through the logger measuring channel. Fig. 5-9 shows strain gauge measurement procedures connection. The soldered points were flattened as much as possible. The gauges and their leads were completely insulated from the lamination surface.

Investigation of No-load and on-load performance of a model three-phase transformer core operating under sinusoidal and PWM voltage excitation

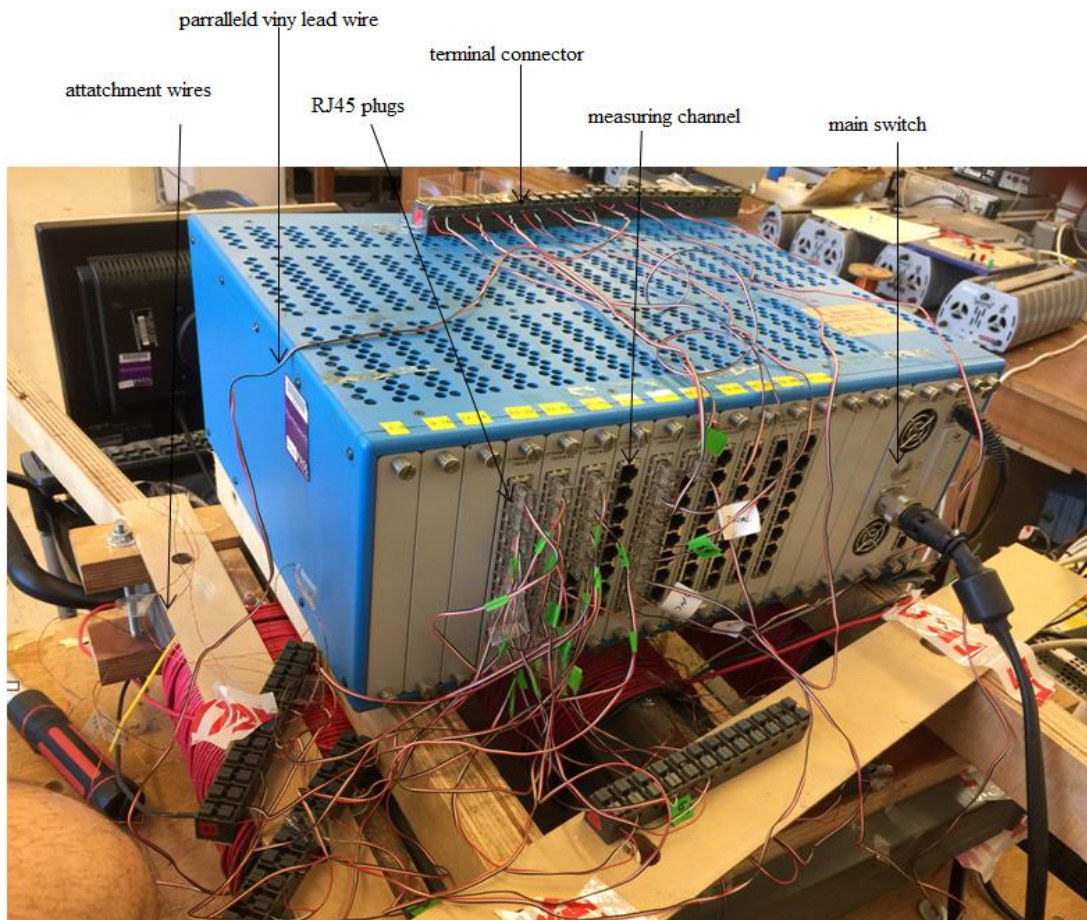


Fig. 5-9 Strain gauges measurement connection

As two type of strain gauges were employed in this work, transformer core was carefully mantled and dismantled twice. Nevertheless, position of strain gauges were varied Pro Foil Strain Gauges were cultivated on one side of the lamination on the other hand three Element Strain Gauges were cultivated on both sides of the lamination so that the bending effect due to the building factor and clamping pressure could be measured. Fig. 5-10 and 5-11 show position of Pro Foil Strain Gauges and Three-Wires Strain Gauges respectively.

Investigation of No-load and on-load performance of a model three-phase transformer core operating under sinusoidal and PWM voltage excitation

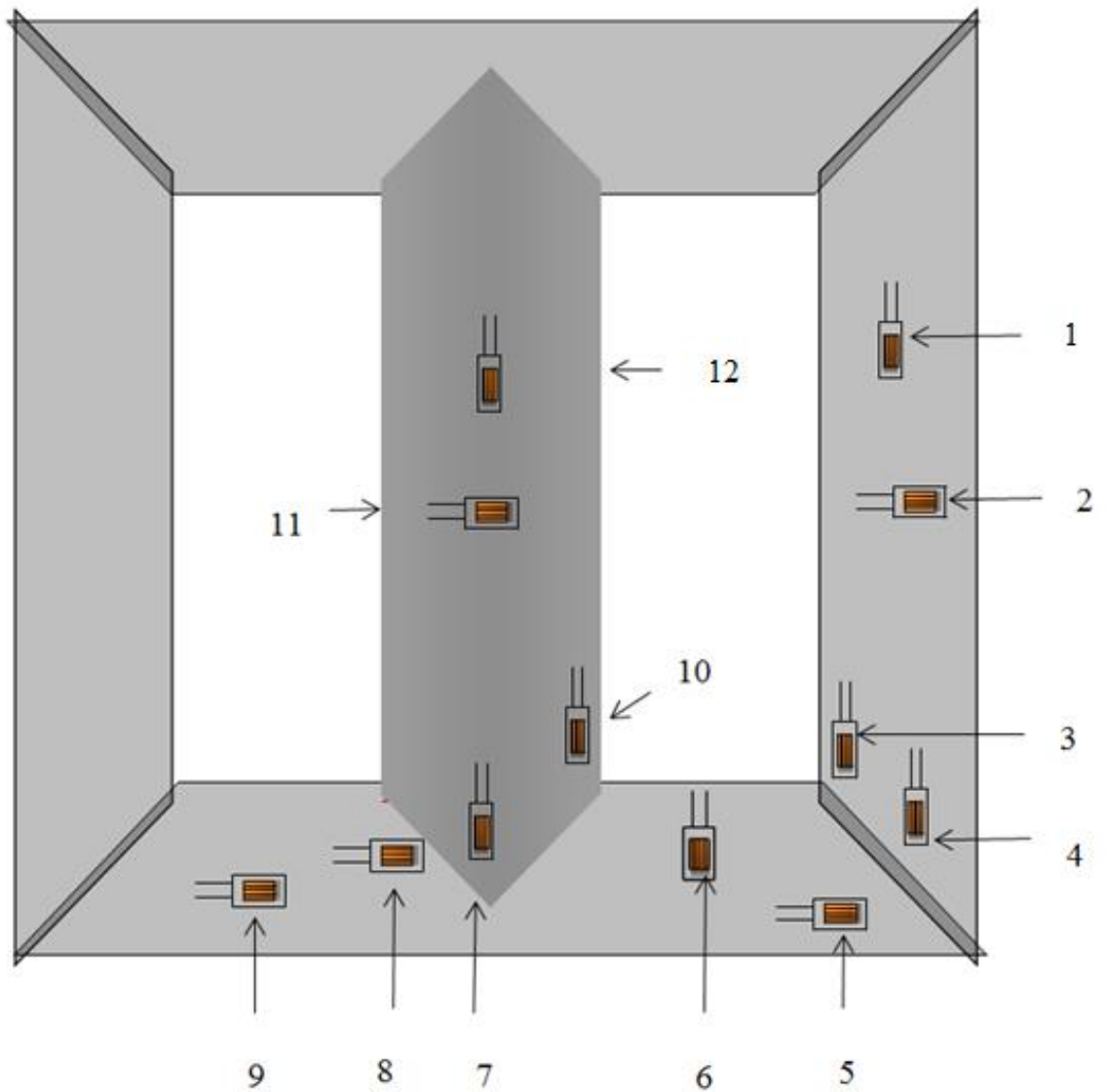


Fig. 5-10 Positions of pro foil strain gauges selected position

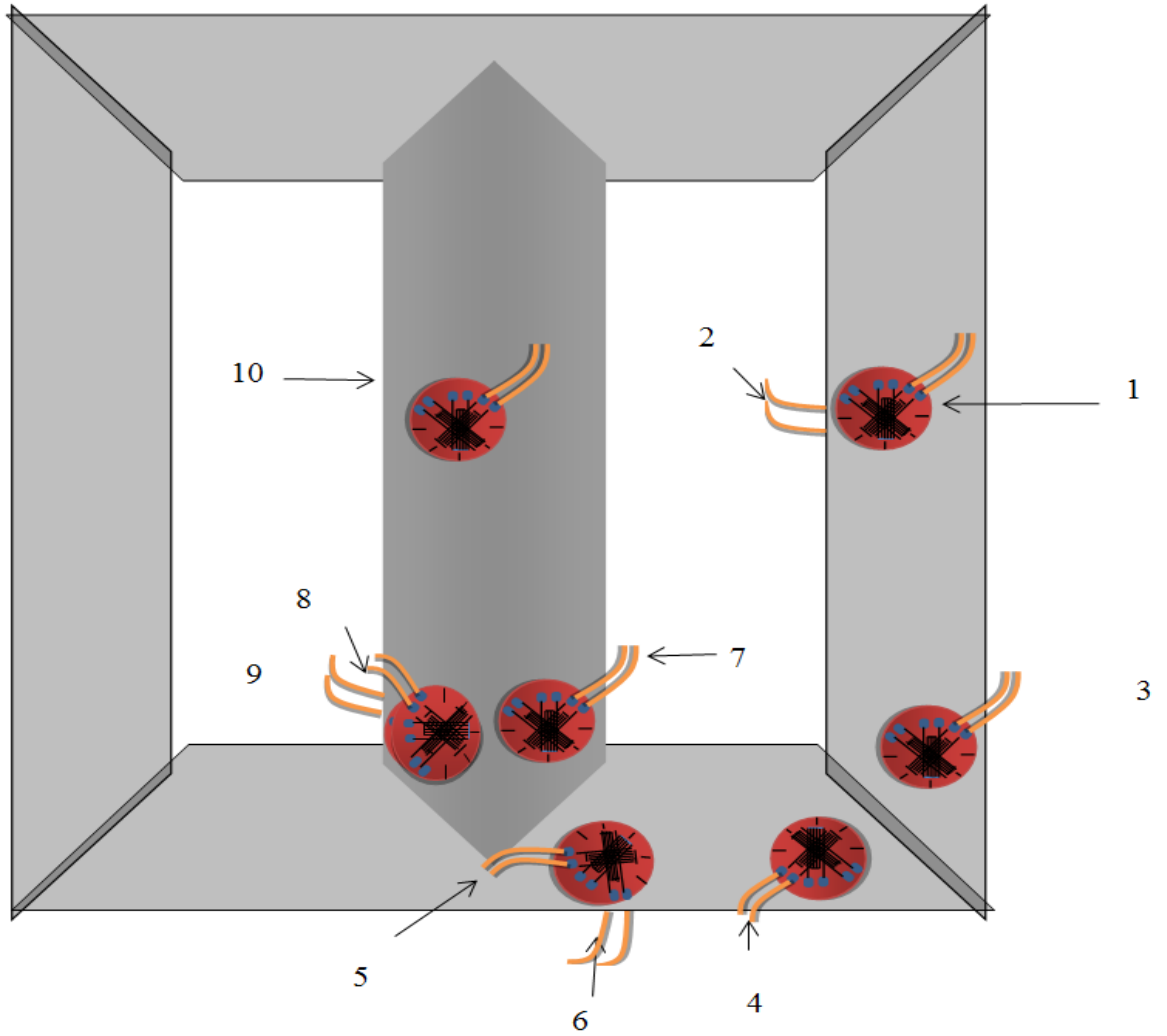


Fig. 5-11 Positions of three-wire strain gauges Roesttes pre-wired

Investigation of No-load and on-load performance of a model three-phase transformer core operating under sinusoidal and PWM voltage excitation

Strain gauges were glued on both sides of the lamination and in both directions, rolling and transvers directions (RD and TD), to measure localised magnetostriction and to measure the bending effect in the transformer core as shown in Fig. 5-11. The small length of the conductor in the direction at right angles to the axis of the gauge impart some degree of sensitivity to transvers strain, but this effect is small enough to be neglected. However, the resolution of the strain gauges is always in the range of 0.1×10^{-6} , which is reasonably sensitive for magnetostriction measurement. Strain gauge has advantages and disadvantages over the other techniques.

Advantages

1. Low cost
2. Localised measurement
3. High resolution measurement

Disadvantages

1. Time consuming
2. Preparation arrangement
3. Hard to place the gauge in required direction

In order to avoid any change of the strain electrical resistance (due to normal pressure), pieces of tough rubber (15 mm × 5 mm × 1 mm) were glued around each strain gauge and all over the test lamination. These pieces of rubber did not introduce any additional stress because of their flexibility. Fig. 5-12 and 5-13 show schematic diagram of the arrangement [67].

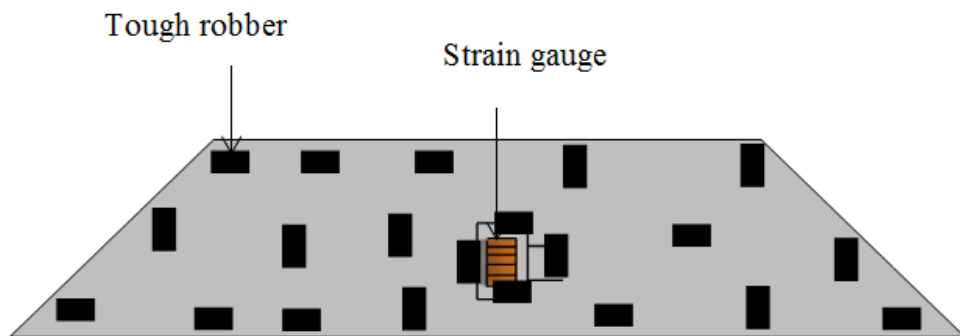


Fig. 5-12 Position of the robber placed around Pro-foil strain gauges

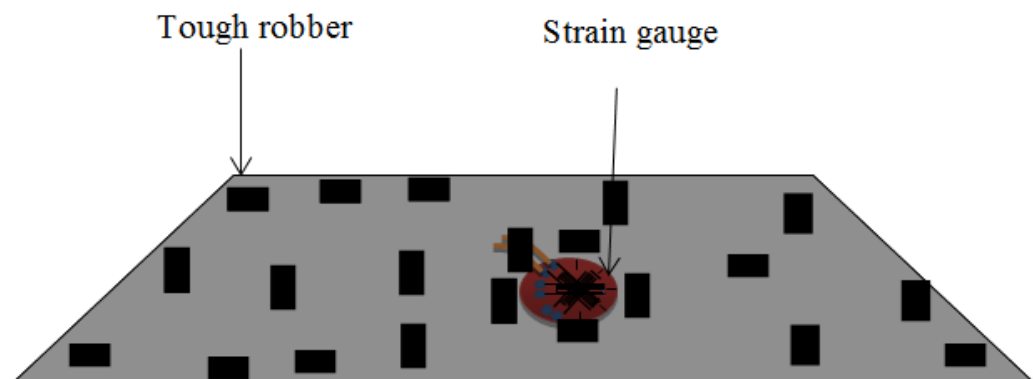


Fig. 5-13 Position of the robber placed around three- wire strain gauges Rosettes pre-wired

5.4.4 Magnetostriction calculation

Pro foil strain gauges and three-wire strain gauges rosettes pre-wired are placed on material in which they allow their electrical resistance to measure localised magnetostriction. As the test specimen extends or contracts under stress, a corresponding increase or decrease in electrical resistance. The alteration in resistance is, within wide limits, proportional to the strain in the specimen, that is:

$$\epsilon = \frac{1}{K} \cdot \frac{\Delta R_0}{R_0} \quad [67] \quad (5.3)$$

Where ϵ is the strain

K is the gauge factor and R_0 is the gauge resistance (120Ω). Strain can be calculated by altering the resistance of the gauge. So hence the change in resistance produces a change in the output voltage.

On the basis of change of length and cross-sectional area only, it can be shown that the gauge factor is $(1 + 2\nu)$, where ν is Poisson's ratio [68]. For most materials the specific resistance of the conductor changes with strain and the gauge factor is usually about 2.0. Tables 5-1 to 5-8 show the direction of the strain gauges and calculated values of the strain within the transformer core.

5.5 Investigation of localised magnetostriction within transformer core

Investigation of magnetostriction within the core has been carried out when the core was placed horizontally. Transformer core was energised with different peak flux densities under sinusoidal and PWM voltage excitations. Strain gauges were positioned in the middle of the core, assembled on several test laminations. As top half of the core has been removed then layers of the prepared laminations have been placed in the middle of the core over the lower half and then the top half has been put back very carefully. The corner joint was precisely adjusted with a Vernier, the core was then clamped together at a pressure of 0.5 Nm. Table 5-1 to table 5-4 shows magnetostriction measurement using Pro foil strain gauge when transformer core was energised by sinusoidal and PWM waveforms respectively.

To obtain wide knowledge about the operation of transformer core it is necessary to determine the strain that occurs in the laminations, as the transformer laminations are very stress sensitive. Furthermore, as the transformer core was mantled and dismantled for couple of times, the bending affect was unavoidable.

To study the bending effect of transformer core Three-Wire Strain Gauge Rosettes Pre-wired were cultivated on both side of the lamination as shown in fig. 5-11. Data logger was again used to monitor the changing value occurred in the electrical resistance of the strain gauges. Table 5-5 to table 5-8 show the value of bending effect occurring in the transformer core.

Investigation of No-load and on-load performance of a model three-phase transformer core operating under sinusoidal and PWM voltage excitation

Table 5-1 Localised Pro foil strain gauges strain measurements with the core placed in horizontal position under sinusoidal waveform with various peak flux densities, at 0.5Nm clamping pressure

Core flux Densities (T)	Strain gauges positions							Strain (ppm)				
	R1	2T	3R	4R	5R	6T	7R	8R	9R	10R	11T	12T
0	0.02	0.02	0.06	0.04	0.4	0.04	1.3	1.5	0.02	0.6	0.02	0.02
0.4	0.4	0.3	1.1	0.9	1.5	0.8	2.1	2.9	0.7	1.9	0.4	0.6
0.6	0.9	0.5	1.9	1.4	2.2	1.3	2.8	3.4	1.2	2.5	1.0	1.1
1.0	1.5	1.2	2.4	2.2	2.9	2.1	3.9	4.5	2.0	3.2	1.6	1.8

Table 5-2 Localised Pro foil strain gauges strain measurements with the core placed in horizontal position under PWM waveform with various peak flux densities, at 0.5Nm clamping pressure

Core flux Densities (T)	Strain gauges positions							Strain (ppm)				
	R1	2T	3R	4R	5R	6T	7R	8R	9R	10R	11T	12T
0.4	1.3	3.6	3.6	3.4	3.9	2.9	4.3	6.4	2.4	4.1	2.1	2.3
0.6	2.7	1.9	5.3	5.1	5.7	4.5	6.4	6.6	4.3	6.1	3.3	3.8
1.0	2.7	2.2	5.5	5.5	6.2	5.1	7.3	7.7	5.3	7.8	5.9	4.7

Investigation of No-load and on-load performance of a model three-phase transformer core operating under sinusoidal and PWM voltage excitation

Table 5-3 Localised Pro foil strain gauges strain measurements with the core placed in vertical position under sinusoidal waveform with various peak flux densities, at 0.5Nm clamping pressure

Core flux Densities (T)	Strain gauges positions							Strain (ppm)				
	R1	2T	3R	4R	5R	6T	7R	8R	9R	10R	11T	12T
0.4	2.7	2.6	0.5	0.5	1.7	1.5	5.2	3.3	1.6	4.8	3.5	4.3
0.6	3.6	3.7	1.3	1.4	2.8	1.8	6.3	1.8	1.5	7.6	4.6	5.6
1.0	4.7	4.5	1.7	1.7	3.2	3.2	7.8	4.6	3.6	9.7	5.2	7.5

Table 5-4 Localised Pro foil strain gauges strain measurements with the core placed in vertical position under PWM waveform with various peak flux densities, at 0.5Nm clamping pressure

Core flux Densities (T)	Strain gauges positions							Strain (ppm)				
	R1	2T	3R	4R	5R	6T	7R	8R	9R	10R	11T	12T
0.4	4.7	4.8	1.4	1.6	4.8	3.8	6.9	4.8	3.4	6.8	5.3	6.6
0.6	5.5	6.6	2.5	2.8	6.2	5.5	8.9	6.8	6.3	9.3	7.3	8.5
1.0	9.3	7.8	3.4	3.6	7.8	5.8	12.6	7.8	7.3	13.9	9.6	12.3

Investigation of No-load and on-load performance of a model three-phase transformer core operating under sinusoidal and PWM voltage excitation

Table 5-5 Three-wire strain gauges strain Rosettes Pre-wired measurements with the core placed in horizontal position under sinusoidal waveform with various peak flux densities, at 0.5Nm clamping pressure

Core flux Densities (T)	Strain gauge positions					strain (ppm)				
	1	2	3	4	5	6	7	8	9	10
0	0.02	0.02	0.4	0.6	3	4	1	2	2	0.08
0.4	0.4	0.7	1.8	2.6	6.7	7.3	4.3	4.3	5.8	0.7
0.6	0.9	1.3	4.0	5.4	8.5	9.4	6.7	6.7	7.8	1.7
1.0	1.6	2.4	5.1	7.5	14.6	15.1	11.7	11.1	13.8	2.8

Table 5-6 Localised Pro foil strain gauges strain measurements with the core placed in horizontal position under PWM waveform with various peak flux densities, at 0.5Nm clamping pressure

Core flux Densities (T)	Strain gauge positions					strain (ppm)				
	1	2	3	4	5	6	7	8	9	10
0.4	1.5	2.3	5.3	5.8	8.4	9.3	7.2	7.5	8.1	3.1
0.6	1.9	2.8	8.2	9.5	10.7	12.1	11.7	11.2	14.3	4.9
1.0	2.6	3.4	10.8	12.7	15.6	15.3	15.8	15.3	16.1	4.9

Investigation of No-load and on-load performance of a model three-phase transformer core operating under sinusoidal and PWM voltage excitation

Table 5-7 Three-wire strain gauges strain Rosettes Pre-wired measurements with the core placed in vertical position under sinusoidal waveform with various peak flux densities, at 0.5Nm clamping pressure

Core flux Densities (T)	Strain gauge positions					strain (ppm)				
	1	2	3	4	5	6	7	8	9	10
0.4	4.3	5.5	1.3	4.8	7.6	6.8	6.9	8.3	8.8	6.6
0.6	6.3	6.5	3.2	6.8	9.7	8.3	12.7	12.3	12.6	13.6
1.0	10.4	9.6	4.8	9.7	15.5	14.9	16.3	15.2	16.9	15.2

Table 5-8 Localised Pro foil strain gauges strain measurements with the core placed in vertical position under PWM waveform with various peak flux densities, at 0.5Nm clamping pressure

Core flux Densities (T)	Strain gauge positions					strain (ppm)				
	1	2	3	4	5	6	7	8	9	10
0.4	5.5	5.9	4.2	6.7	6.9	6.7	9.5	9.4	9.5	13.7
0.6	7.7	8.3	6.8	9.8	11.8	12.3	13.1	13.7	13.8	16.2
1.0	9.4	9.6	8.3	13.8	17.8	16.8	17.3	17.5	17.9	18.6

5.5.1 Stress

Stress is the internal forces reacting to external force exerted at a body's surface [5.1]. As it has been known, magnetic properties of ferromagnetic materials such as permeability, magnetostriction and power loss are sensitive to mechanical stress. The ferromagnetic domain pattern of a crystal, which is an indicator of its magnetic properties, changes with changes of strain of the crystal due to the applied stress. As long as the applied stress is within the elastic range of the material, the original pattern returns after unloading the applied stress.

Depicts a slice of material with infinitesimal thickness in equilibrium when external force is applied, the internal force will react to the applied external force and that would cause stresses normal and tangential to the material.

5.5.2 Stress calculation

The measured strains were converted to stresses by using theoretical Young's modulus [69] values. The commonly used Young's modulus for perfectly grain oriented steel are:

$$\epsilon_{\perp} = 1.17 \times 10^5 \quad \text{MN/m}^2 \quad (5.2)$$

$$\epsilon_{\tau} = 2.14 \times 10^5 \quad \text{MN/m}^2 \quad (5.3)$$

Where ϵ_{\perp} and ϵ_{τ} are the Young's modulus in rolling and transverse directions respectively. Tables 5.1 to 5.8 show the direction of the strain gauge and calculated values of the strain within the transformer core.

5.5.3 Noise and vibration phenomena in transformer core

The causes of transformer core vibration are magnetic force between laminations and lamination deformation due to magnetostriction. If a transformer core has homogenous structure, there is only in-plane vibration due to magnetostriction. However, as the transformer core is usually built from stack of lamination, there is a vibration in an out-plane direction due to the magnetic force [70]. If transformer core lamination is magnetised and magnetic flux flows uniformly along the rolling direction, the deformation due to transverse magnetostriction is neglected by approximately 5 times and magnetostriction in the rolling direction is higher than in the transverse direction when flux flows uniformly along the rolling direction [71].

Considering the dimensions of the three-phase transformer core, there are three different shapes for three-phase flux densities as shown in Fig. 5-14 [72]. Each limb of a three-phase core is magnetised with 120° phase shift [73]. Top and bottom yokes which are interlaced to the limbs have associated magnetic flux with the limbs.

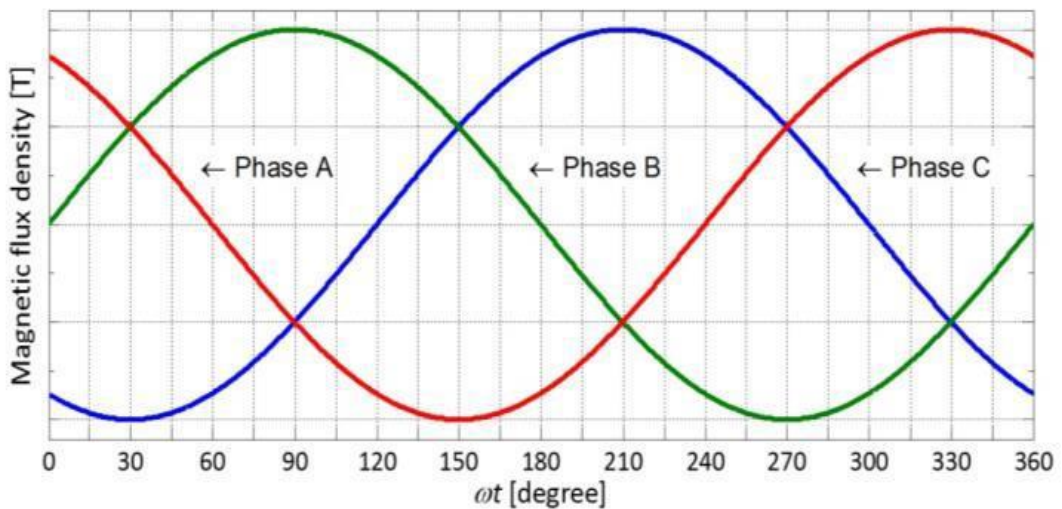


Fig. 5-14 Three-phase magnetic flux density waveforms [20]

Investigation of No-load and on-load performance of a model three-phase transformer core operating under sinusoidal and PWM voltage excitation

As each phase is magnetised with 120° angle phase difference so hence different movement take place in the core and hence magnetostriction is resulted all over the core as magnetostriction is proportional to induced voltage.

5.5.4 Influence of magnetic flux density on transformer core magnetostriction and vibration

Magnetic flux density was set with different peak flux densities in order to study its effect on magnetostriction and core vibration. Localised magnetostriction increased when the magnetic flux is increased from 0.4T, to 0.6T and 1.0T. The significant increase of localised magnetostriction is due to the effect of change in the domains structure due to the applied voltage. This affects the magnetic force and vibration to increase, and increases localised magnetostriction as shown in tables 5.1 to 5.8.

It could be concluded that when operating the core at low magnetic flux density, the noise and vibration are less than operating at high flux density. This can reduce the core noise and vibration. However, this leads to an increase in cost and larger core size.

5.6 Core vibration and sound level measurement (SPL)

Sound is defined as any pressure variation that human ear can detect, which is created when objects vibrate, the range of magnitude from the faintest to the loudest sound the ear can hear is so large that sound pressure is expressed on a logarithmic scale in units called decibels (*dB*). The decibel as used in acoustic is a measurement comparing the pressure generated by a noise against some standard level [74].

In order to make measurements of a acoustic noise generated at particular point in transformer core stress was converted to sound pressure level by using equation 5.4. Therefore, the sound pressure level (SPL) is given as

$$SPL = 20 \log_{10} \left(\frac{P_{meas}}{P_{ref}} \right) \quad [dBA] \quad [74] \quad (5.4)$$

Investigation of No-load and on-load performance of a model three-phase transformer core operating under sinusoidal and PWM voltage excitation

Where P_{meas} is the measured A-weighted sound pressure level, and P_{ref} is the reference sound pressure level and equal to $20\mu Pa$. Standard measurements use the A-weighted sound pressure level as a measured variable and measurements on transformers are made under no-load condition.

5.6.1 Analysis and Discussion

Magnetostriction distribution in the grain-oriented material is almost independent of the type of material, applied magnetic field and type of magnetization. Attempt has been made to analyse localised magnetostriction within the core under sinusoidal and PWM voltage excitations. Experiments were accomplished on a three-limb model transformer core with different peak flux densities of 0.4T, 0.6T and 1.0T. The core was stacked of HGO material which was built with laminations of 100 mm wide, 0.3 mm thick. These experiments have been carried out with the core placed in a horizontal position and then measurements were repeated with the core placed in the vertical position.

5.6.2 Localised magnetostriction under PWM and sinusoidal voltage excitation in three-phase transformer core in horizontal position

As the core was assembled and dismantled few times the bending of the yoke and limb was unavoidable. Tables 5.1 to 5.8 shows localised strain in central layer of the core. These measurements were taken under sinusoidal and PWM conditions when the core was placed horizontally and vertical. Torque wrench was used to set the clamping pressure of $0.50MN/m^2$.

Under Pro Foil Strain Gauges table 5.1 shows the localised distribution of peak to peak values for the total of 12 strain gauges, placed in different regions nine in the RD and three in TD. At 0.4T under sinusoidal and PWM voltage excitation the highest compressive strain of 2.9 and 6.4 ppm was obtained at strain gauge number (8) in the RD near the T-joint in the yoke. However, when the flux density was increased to 0.6T, compressive strain of 3.4 ppm under sinusoidal voltage excitation was observed in strain gauge number 8, with the core energised under PWM compressive strain of 6.6 ppm was observed in strain gauge number 8. Increasing the flux density to 1.0T, same trend of result was obtained, strain gauge number 8

Investigation of No-load and on-load performance of a model three-phase transformer core operating under sinusoidal and PWM voltage excitation

represents large magnitude of localised strain. It was increased to be 4.5ppm under sinusoidal and 7.7ppm under PWM voltage excitation.

Further away from yoke T-joint strain gauge position 7 was compared with strain gauge position 8 at peak flux densities of 0.4T, 0.6T and 1.0T under sinusoidal voltage excitation, their strains reduced by approximately 27%, 17% and 13% respectively.

Comparing the result obtained at corner joint strain gauge position 4 with strain gauge position 5 under sinusoidal and PWM voltage excitations, under sinusoidal excitation at 0.4T, 0.6T and 1.0T strain gauge position 5 has higher values of localised strain by the factor of 40%, 36% and 24% respectively. However, result obtained under PWM voltage excitation shows higher value of localised strain occurred in strain gauge position 5, at 0.4T localised strain was higher by 12%. At 0.6T localised strain was higher by 10% and at 1.0T localised strain was higher in strain gauge position 5 by 11%.

Comparing the result obtained in the outer limb with the result obtained in the central limb, strain gauge position 1 with strain gauge position 12 in the rolling direction. Under sinusoidal and PWM voltage excitation strain gauge position 12 shows higher value of localised strain at all magnetisation levels. For example, with the core energised under sinusoidal voltage excitation at 0.4T, localised strain was higher by 33% in strain gauge position 12. Increasing the flux density to 0.6T and 1.0T strain gauge position 12 shows higher localised strain than strain gauge position 1 by the factor of 18% and 16% respectively. Comparing strain gauge position 1 with strain gauge position 12 under PWM voltage excitation at 0.4T, 0.6T and 1.0T strain gauge position 12 shows higher localised strain by factors of 43%, 28% and 42% higher than the localised strain occurred in strain gauge number 1.

In order to study the bending affect induced in the transformer core three-wire Rosettes Pre-wired strain gauges were employed on both sides of the lamination, tables 5.5 and 5.6 show the value of bending effect and the value of localised magnetostriction. However, higher bending value recorded near the T-joint in the yoke strain gauges number 5 and 6 whereas, smallest value of localised strain was obtained in the middle of the outer limb strain gauges number 1 and 2.

Investigation of No-load and on-load performance of a model three-phase transformer core operating under sinusoidal and PWM voltage excitation

Away from the middle limb and middle yoke, comparing localised strain measurements in the limb and yoke corner joints strain gauges position 4 and 5. When the core energised under sinusoidal voltage excitation at 0.4T, 0.6T and 1.0T, tables 5.1 and 5.2, it can be seen that yoke corner joint has shown large values of localised strain than the outer limb. For example, at 0.4T, yoke corner joint had a value of 40% higher than limb joint. Increasing the flux density to 0.6T and 1.0T again yoke corner joint shows larger value of localised strain by the factor of 36% and 24% respectively higher than the outer limb. Nevertheless, comparing the result obtained with the same strain gauges position when the core energised under PWM voltage excitation at peak flux densities of 0.4T, 0.6T and 1.0T same results were obtained strain gauge position 5 show higher localised strain than strain gauge position 4 for example at 0.4T strain gauge position 5 has higher value of 12% than strain gauge position 4. Increasing the flux densities to 0.6T 1.0T strain gauge position 5 had a value of 10% and 11% higher than strain gauge position 4.

Discussion on the result obtained under Three-Wire Rosettes Pre-wired strain gauge with that obtained under Pro Foil strain gauges is as follows. It can be concluded that the increase of localised strain in the T-joint may be due to the presence of clamps and also due to the joint-overlapping and imperfect positions of the lamination. The magnitude of the localised strain in the centre limb was higher than those in the outer central limb. This was due to the fact that the ends of the outer limbs were held more firmly than those of the central limb. Further away from the centre, strain gauge positions 3 and 4 in the limb corner joint at the inner side of lamination, localised strain was increased. This is mainly because of the clamps and the fact that the effect of clamping was much higher at the inner edge. Highest localised strain in the transverse direction was obtained in the strain gauge position 6, for example at 0.4T, 0.6T and 1.0T under sinusoidal voltage excitation it was higher than strain gauges at position 2 by 62%, 61% and 42%, table 5.1, this is mainly due the larger bending in that region.

Near the corner and T-joint, higher values of localised strain were obtained. This is because flux deviation occurred in all directions in the core joint whereas in the limb flux follows the easy axis, again same results were obtained under load and no-load conditions.

Investigation of No-load and on-load performance of a model three-phase transformer core operating under sinusoidal and PWM voltage excitation

Basically, strain occurred all over the area under PWM and sinusoidal waveforms. The average value of magnetostriction was higher in the yoke than that in the limb due to the alternating magnetization. The average of localised strain was higher at the T-joint than that in the corner joint, this is due to rotational magnetization and the main direction of strain which is given in RD. However, under the two types of strain gauges used, localised magnetostriction was higher when the core was energised by PWM waveform. This is due to the high harmonic contents and due to the shape of the waveform.

5.6.3 Localised magnetostriction under PWM and sinusoidal voltage excitation in three-phase transformer core in vertical position

Tables 5.3, 5.4, 5.7 and 5.8 show localised strain in the limbs, yokes and the joint areas when the core was held in a vertical position. Under sinusoidal voltage excitation, table 5.3, in the middle regions of the central limb strain gauge position 12, the average of localised strain at 0.4T, 0.6T and 1.0T was 4.3 ppm, 5.6 ppm and 7.5 ppm respectively. While under PWM voltage excitation at magnetising flux of 0.4T was 6.6 ppm, and at magnetising flux density of 0.6T was 8.5 ppm. Nevertheless, at magnetising flux density of 1.0T it was 12.3 ppm. Away from the middle region, strain gauge position 10 near the T-joint localised strain was decreased, for example at 0.4T under sinusoidal voltage excitation it was decreased by 11%. And under PWM voltage excitation at 0.4T was decreased by 3%. Results have shown same trend under all magnetising levels, strain gauge position 10 shows higher value than strain gauge position 12 under both sinusoidal and PWM voltage excitations. Localised strain was higher near the T-joints than that in the central limb, this was due to the weights of upper yokes and the weight of the limbs themselves.

In the outer limb localised strain was smaller than that in the central limb. This could be due to the fact that most of the weight of the yokes was carried by the central limb. However, comparing the results obtained in the T-joint with the results obtained in the corner joint under sinusoidal and PWM voltage excitations, the level of localised strain in the T-joint being much larger than that of the corner joint area.

The average value of the localised strain occurred at the corner limb and yoke joint was found to be higher in the yoke corner joint under both type of strain gauges and

Investigation of No-load and on-load performance of a model three-phase transformer core operating under sinusoidal and PWM voltage excitation

under both type of excitation conditions. For example, at 0.4T under sinusoidal waveform table 5.3, strain gauge position 5 shows higher value of localised strain than strain gauge position 4, it was larger by 70%. More increasing of the energising flux density under PWM voltage excitation and table 5.7, under three-wire strain gauge at 1.0T, strain gauge position 4 had large value of localised strain by 50% larger than strain gauge position 3. However, the localised strain of the yoke was observed to be higher when the core placed in vertical position than horizontal position. For example, at 1.0T under sinusoidal voltage excitation strain gauge position 9 had a value of localised strain by a factor of 44% larger when the core placed in vertical position tables 5.1 and 5.3. When the core energised under PWM voltage excitation at 1.0T, tables 5.6 and 5.8, strain gauge position 4 shows large value of localised strain when the core placed in vertical position than that when the core placed in horizontal position by 7%. Larger under vertical position hence localised strain was found to be higher than what was observed when the core was placed horizontally. This increase on localised strain was mainly due to the introduction of the weight of the upper part of the core.

At the corner joint area, localised strain was found to be higher with the core placed in horizontal position. Comparing result obtained when the core placed on horizontal with the result obtained when the core placed in vertical position, strain gauge 4 table 5.1, was compared with strain gauge 4 table 5.3. At 1.0T, under sinusoidal waveform horizontal position was higher than vertical position by 22%. Furthermore, when the core energised under PWM voltage excitation, strain gauge number 4 table 5.2 was compared with the same strain gauge in table 5.4 at 0.6T strain results show that horizontal position had a value of 45% larger then vertical position.

In general, when the core was placed vertically overall localised strain occurred all over the transformer core, localised strain was found to be higher in the central limb and outer limb and also localised strain was found to be higher in the T-joint area and in the yoke area. On the other hand, localised strain was found to be higher in the corner joint when the core was placed in the horizontal position so it could be concluded that the overall localised strain was higher in the yoke area when the core was placed in vertical position, because of the weight of the core.

CHAPTER 6

6. Measurement with the Epstein Frame

Epstein frame which is sometimes called Epstein square has been invented by Epstein in 1900, and it was made as 50 cm square. Later in 1936 Burgwin has invented smaller size of Epstein frame with 25 cm square. Nevertheless, Epstein technique works in such a way by placing the Epstein strips between the limb and the yoke. In this step, clamping pressures were obtained through the limbs and yokes. However, corner joint in four-lamination Epstein frame is always double-lapped joint because it provides good and reproducible flux enclosure. Schematically diagram of Epstein frame is shown in Fig. 6-1.

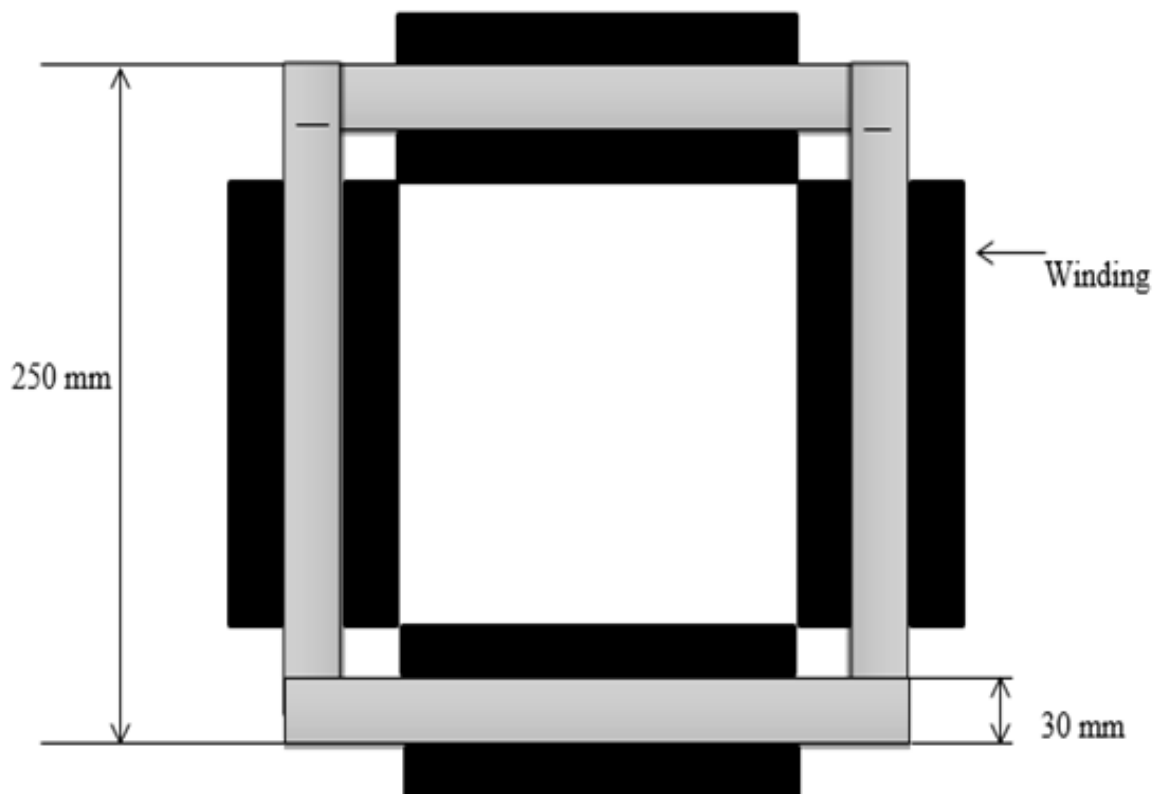


Fig. 6-1 Epstein frame and double overlapped joints

Investigation of No-load and on-load performance of a model three-phase transformer core operating under sinusoidal and PWM voltage excitation

There are four fixed windings connected in series. The primary winding is connected to the power source to provide magnetising current and the secondary winding is connected to a voltmeter to measure the induced voltage and hence peak flux density.

In the closed sample, the magnetic path length l_m is 0.94 m, as specified in standard IEC 60404-2, and the instantaneous magnetic field strength (H) was measured inside the labVIEW programme using equation (6.1).

$$H(t) = -\frac{NI(t)}{l_n} \quad (6.1)$$

Where $I(t)$ is the primary current, N is the number of turns on the primary winding and l_n is the magnetic path length. The instantaneous flux density B was obtained from equation (6.2)

$$B = -\frac{\int v dt}{AN_2} \quad (6.2)$$

Where A is the cross-sectional area, N_2 is the number of the secondary winding, $v(t)$ is the voltage measured across the secondary winding. By using this method there will be choice for selecting the most suitable material under different frequencies and different peak flux densities.

6.1.1 Single Strip Tester measurement

The experiment was carried out on single strip tester (SST) using HGO electrical steel material. Three strips were cut from the limb and two strips were cut from the yoke from the same batches used to construct the transformer core at (30 mm x 250 mm), and then annealed to relieve stress which occurred during the cutting process. Measurement of total power P_{tot} (W/kg) were taken under PWM and sinusoidal excitations. At core flux densities of 0.4T, 0.6T and 1T, both measurements were carried out under different peak of magnetising frequencies of 10, 25, 50, 100, 200 and 400 Hz. Using measurement controlled system as shown in Figs. 6-2. and 6.3 which consists of a computer, LabVIEW version 8.5 software, “NI PCI 6120” DAQ card, a power amplifier and a 1 Ω shunt resistance [75].

Each component of the measurement system has a specific different function, for example the magnetising voltage was generated by the LabVIEW programme via output voltage of the DAQ card. However, data was taken through LabVIEW programme which uses mathematical analysis in real time to process the measurement data and displays the desired output in real time.

In the magnetising core of the SST double vertical cores are used each core was made from GO steel laminations. A 250 turns of the secondary winding (N_2) was wound around a plastic former and 865 turns of primary winding (N_1) was wound around the secondary winding. Then sample was placed between the yokes as shown in Fig. 6-4.

Investigation of No-load and on-load performance of a model three-phase transformer core operating under sinusoidal and PWM voltage excitation

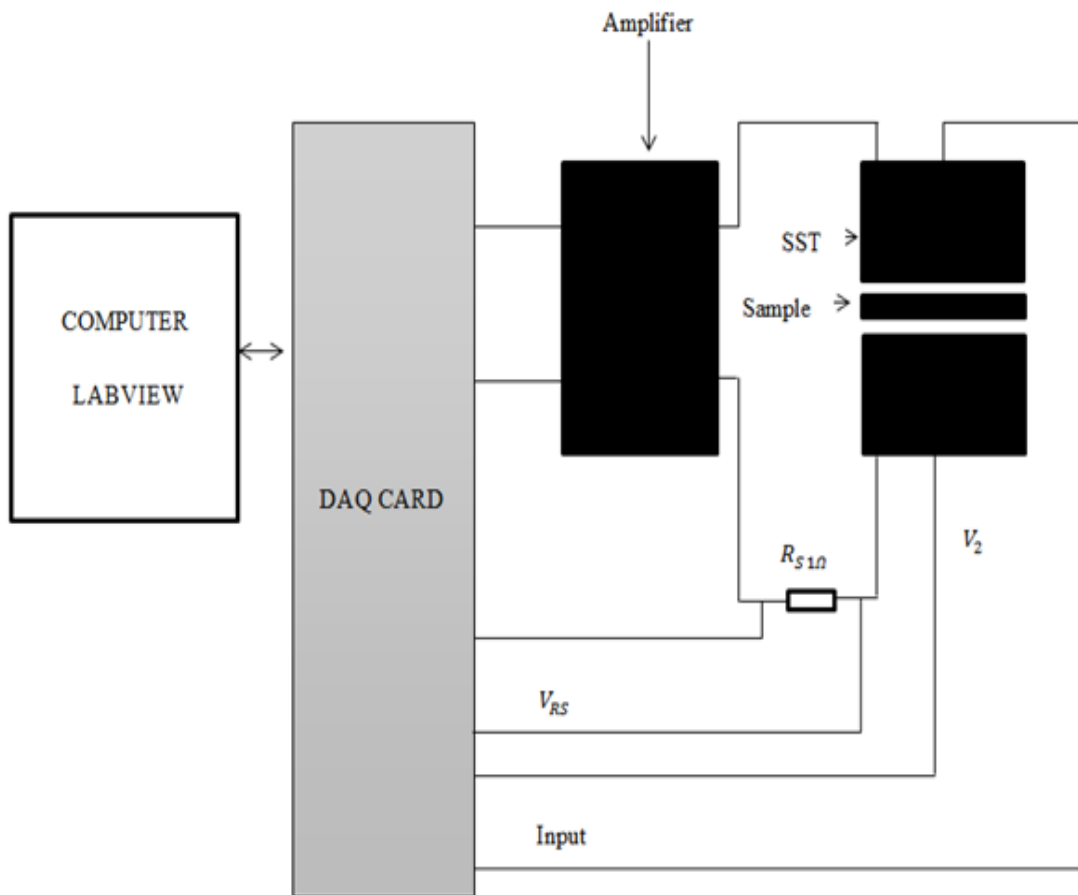


Fig. 6-2 Schematic diagram of computer-controlled Single Strip Tester (SST)

Investigation of No-load and on-load performance of a model three-phase transformer core operating under sinusoidal and PWM voltage excitation

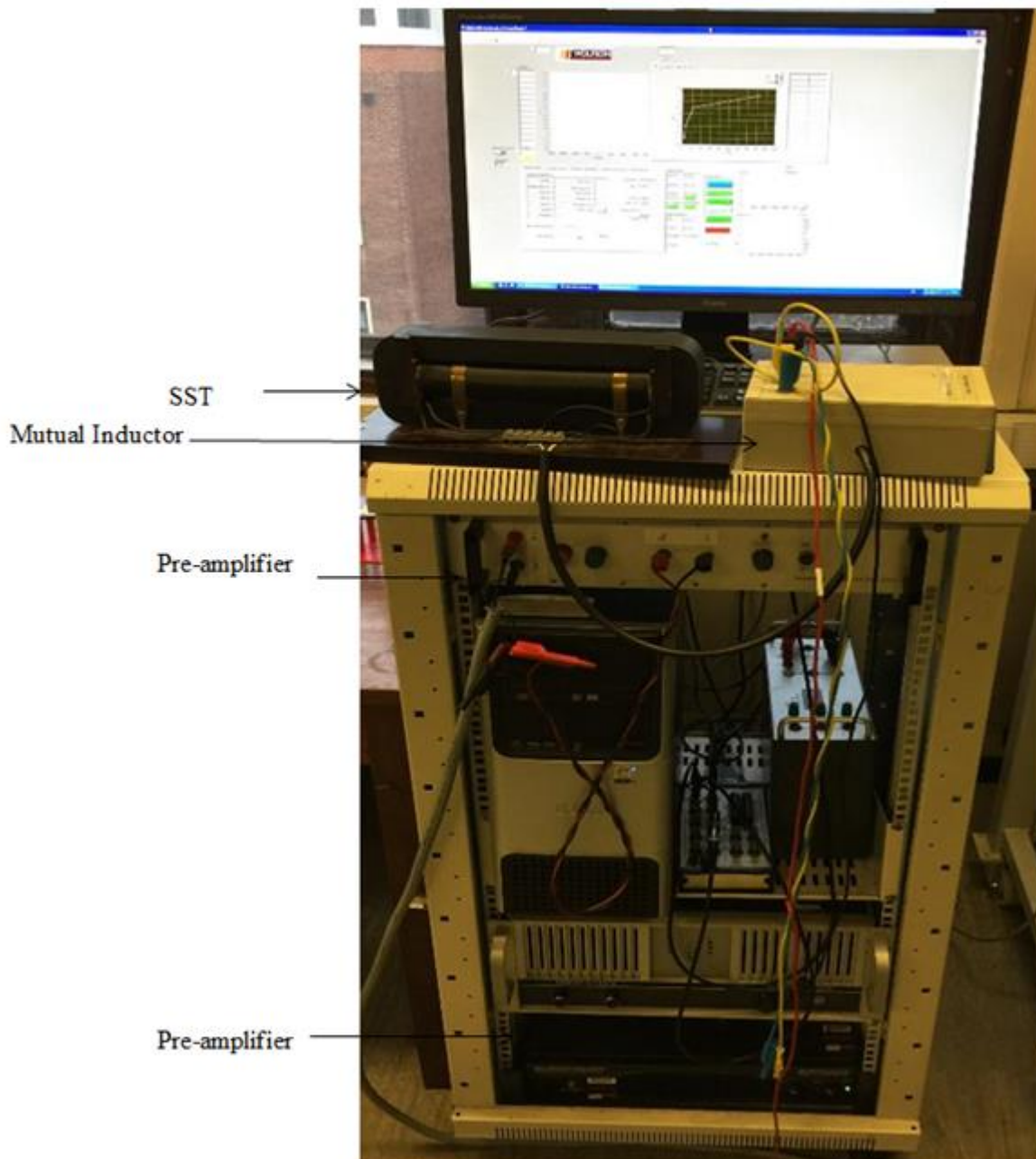


Fig. 6-3 Measurement system of single strip tester

Investigation of No-load and on-load performance of a model three-phase transformer core operating under sinusoidal and PWM voltage excitation

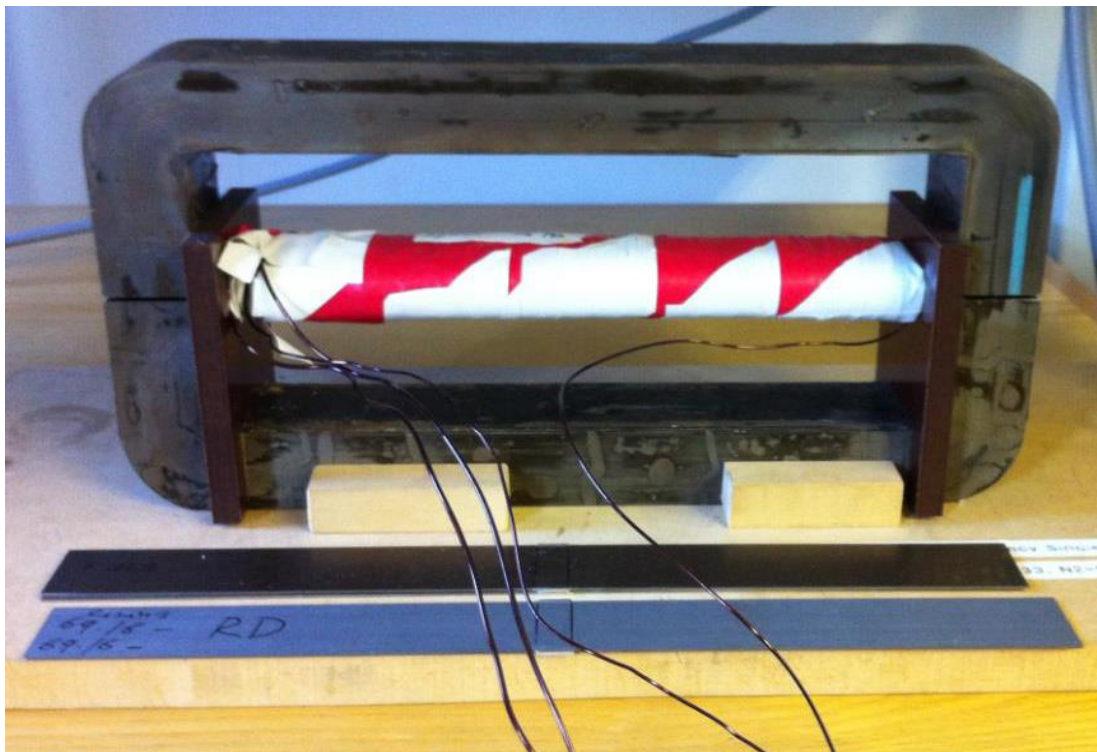


Fig. 6-4 Single strip tester

6.1.2 Power loss in electrical steel based on two-term formula

Power loss in electrical machine plays large role to determine the grades and the price of material. The power loss in magnetic material depends on four different parameters which are: frequency (f), peak flux density (B_{pk}), thickness of the material (d) and material resistivity (ρ).

Power loss due to time-varying magnetic field was separated into two main terms: hysteresis losses P_h (also referred to as static losses) and eddy current losses P_e which is also split into classical and anomalous losses (also called excess loss) [76] then the total loss is given by:

$$P_t = P_h + P_e = k_h f B_{pk}^n + k_e (f B_{pk})^2 \quad (\text{W/kg}^{-1}) \quad (6.3)$$

Where P_h is the hysteresis losses and is normally defined by the enclosed hysteresis loop as shown in Fig. 1-2 P_e is the eddy current loss which also known as (dynamic losses). k_h is the coefficient for hysteresis loss and k_e is the coefficient for eddy current loss. f is the magnetising frequency[Hz], B_{pk} is the peak flux density [T] and n is Steinmetz constant equal to 1.6.

This method is used when alternating magnetic field is applied to magnetic material, the area enclosed by hysteresis loop ($B - H$) represents a total core loss per cycle.

It is believed that hysteresis loss is due to energy dissipated when domain wall is moving through the material during magnetisation process. This loss is largely influenced by stress, impurities, dislocations, and surface roughness. Hence, these factors have a large impact on the magnitude of the material permeability.

It should be noted that hysteresis losses per cycle is frequency independent, hence this equation is only valid for low frequency, because at higher frequency magnetic field distribution is not uniform, maximum at the surface and minimum at the centre which is known as the skin effect [45].

6.1.3 Power loss in electrical steel based on three-term formula

Bertotti [45] explained excess losses based on statistical loss theory. The difference between two-term formula and three-term formula is that third term is added which represents excess loss, so the total core loss is expressed as

$$P_t = P_h + P_e + P_a = k_h f B_{pk}^n + k_e (f B_{pk})^2 + k_{ex} (f B_{pk})^{1.5} \quad (6.4)$$

The three coefficients (k_h , k_e , k_{ex}) given in equation (6-4) can be obtained from the measured core losses at different frequencies and flux density range. The excess losses are mainly related to the non-uniform distribution of the magnetic field inside the lamination, it depends on the material microstructure, conductivity and the cross-sectional area.

6.2 Loss separation using extrapolation method based on the two-term formulation

The extrapolation method is usually implemented to separate the core loss measurement at different frequencies, in this method the hysteresis loss is separated by extrapolating core loss per cycle versus magnetising frequency curves at different flux densities to zero frequency. Therefore, the power loss at zero frequency represents the static hysteresis loss per cycle. Dividing equation (6.3) by the magnetising frequency leads to [77].

$$\frac{P_t}{f} = \frac{P_h}{f} + \frac{P_e}{f} = k_h B_{pk}^n + k_e f B_{pk}^2 \quad (6.5)$$

This equation is a linear function of magnetising frequency at peak flux density B_{pk} and can be written as:

$$\frac{P_t}{f} = D + E f \quad (6.6)$$

Where $D = K_h B_{pk}^n$ is the hysteresis loss per cycle and $E = k_e B_{pk}^2$ eddy current loss. More detailed information for calculating these coefficients are available [78] [79] [80].

6.2.1 Loss separation using extrapolation method based on the three-term formulation

The extrapolation method is also applicable to separate loss components in the three-term formulation dividing (6.4) by the magnetising frequency leads to.

$$\frac{P_t}{f} = \frac{P_h}{f} + \frac{P_e}{f} + \frac{P_a}{f} = K_h B_{pk}^n + k_e f B_{pk}^2 + k_{ex} B_{pk}^{1.5} \sqrt{f} \quad (6.7)$$

The latter term is largely influenced by intricate phenomena related to microstructural interaction, magnetic anisotropy and non-homogenous. Locally induced eddy current [78] so that at constant coefficients of equation (6.7) can be written as:

$$\frac{P_t}{f} = D + E f + G \sqrt{f} \quad (6.8)$$

Where $D = K_h B_{pk}^n$, $E = k_e B_{pk}^2$ and $G = k_{ex} (B_{pk}^{1.5})$. More achievable method can be used to obtain the coefficients by plotting core loss per cycle versus the square root of the magnetising frequency (\sqrt{f}), for different value of peak flux density (B_{pk}) therefore equation (6.8) can be modified by [79]:

$$\frac{P_t}{f} = D + E(\sqrt{f})^2 + G \sqrt{f} \quad (6.9)$$

Where D, E and G are the coefficient of power loss components and can be obtained by nominal curve fitting. Using equations (6.7) and (6.8) we have:

$$D = K_h B_{pk}^n$$

$$E = K_e B_{pk}^2$$

$$G = K_{ex} B_{pk}^{1.5}$$

Therefore, applying this method for a given flux density, the loss coefficients K_h, K_e and K_{ex} can be obtained. In summary from equation (6.3) to (6.8), it can be concluded that in the extrapolation method, hysteresis loss per cycle is assumed to be

Investigation of No-load and on-load performance of a model three-phase transformer core operating under sinusoidal and PWM voltage excitation

frequency independent and eddy current power loss per cycle is assumed to be a linear function of frequency. Therefore, the total hysteresis loss can be calculated by multiplying the hysteresis power loss per cycle by the operating frequency f and the total eddy current power loss is calculated by multiplying the eddy current power loss per cycle by square root of the operating frequency \sqrt{f} .

6.2.2 Experimental results under PWM voltage excitation at 0.4 T

Power loss measurements were taken under sinusoidal and PWM voltage excitations on five strips (HGO) material using Epstein size laminations and were tested using the measurement system as described in part 5.3.4. The power loss results under PWM flux waveform were compared with those at the same peak flux densities under sinusoidal voltage excitation. Measurements of power loss of HGO were carried out at peak flux densities 0.4T and 1.0T respectively, table 6.1 shows total power loss per cycle with magnetising frequencies of 25, 50, 100, 200 and 400 Hz.

Table 6-1 Power loss per cycle under PWM voltage excitation at 0.4 T at different magnetising frequencies

Magnetising frequency Hz	Measured power loss (W/kg)	Power loss per cycle (W/kg). sec
25	0.098	0.0039
50	0.421	0.0084
100	1.229	0.0123
200	3.212	0.0160
400	6.753	0.0168

Specific power loss per cycle is plotted against the square root of frequency as shown in Fig. 6-5. On this graph, power loss components obtained by applying a polynomial curve fitting in Microsoft Excel are plotted.

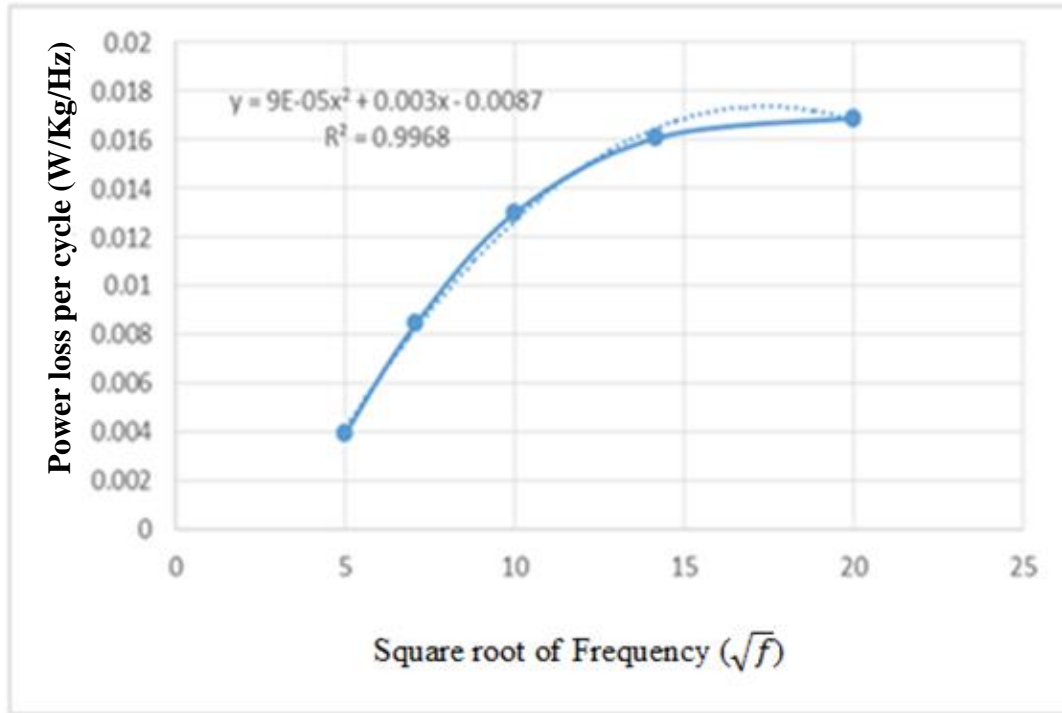


Fig. 6-5 Specific power loss per cycle versus square root of frequency at 0.4T under PWM voltage excitation

By applying the coefficients in equation (6.8), the power loss coefficients are automatically calculated as shown in table 6.1

$$D = K_e B^2 = 9E^{-5}$$

$$E = K_h B^2 = 0.003$$

$$G = K_{ex} B^{1.5} = 0.0087$$

Eddy current loss and hysteresis loss versus magnetising frequency are shown in Fig. 6-6. Hysteresis loss is deduced from the static hysteresis loops, and the value of eddy current power loss per cycle is a linear function of magnetising frequency and can be obtained using equation (6.10). However, the value of hysteresis and eddy current loss per cycle is shown in Fig. 6-6.

$$p_e = \frac{\pi^2}{6 \cdot \rho \cdot D} d^2 f^2 B_{pk}^2 W / kg / m^3 \quad (6.10)$$

Investigation of No-load and on-load performance of a model three-phase transformer core operating under sinusoidal and PWM voltage excitation

Where B_{pk} is the peak flux density (T): f is the frequency (Hz) ρ is the resistivity ($\Omega.m$). D is the density (kg/m^3) and d is the thickness of the lamination [80]. The thickness and the resistivity have significant impact on the eddy current power loss hence; small thickness and high resistivity will reduce the power loss.

Table 6-2 Measured and total power loss component of Epstein size lamination under PWM voltage excitation at 0.4T with different magnetising frequencies

Frequency (Hz)	Measured power loss per weight(W/kg)	P_e (W/kg)	P_h (W/kg)	P_a (W/kg)	$P_t = P_e+P_h+P_a$ (W/kg)
25	0.098	0.0562	0.217	0.375	0.648
50	0.421	0.225	0.435	1.060	1.720
100	1.299	0.9	0.87	3	4.77
200	3.212	3.6	1.74	8.485	13.825
400	6.753	14.4	3.48	24	41.88

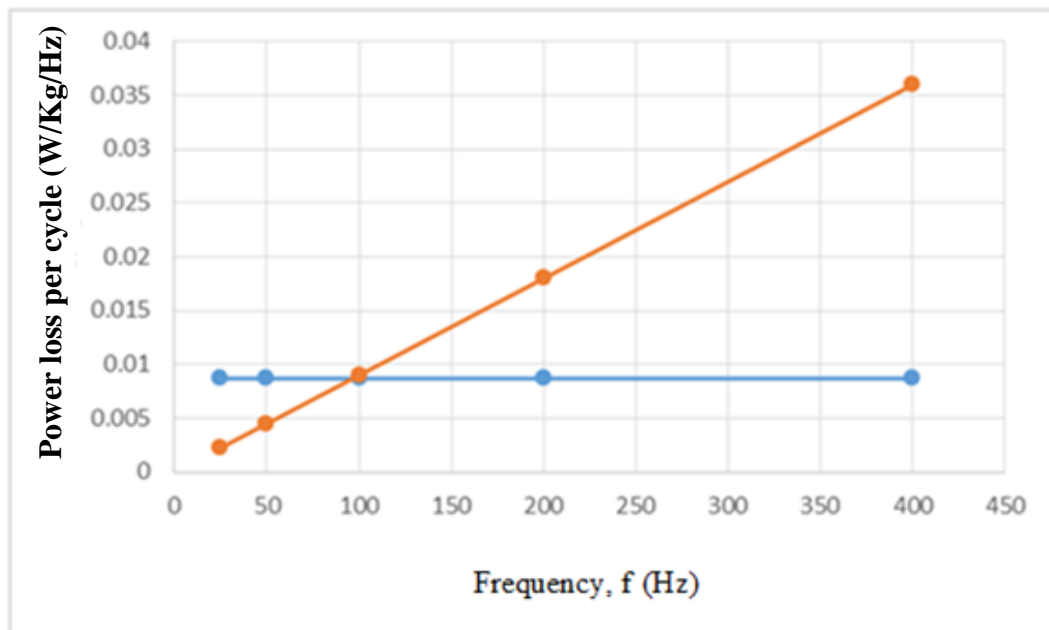


Fig. 6-6 Eddy current and hysteresis loss per cycle versus frequency (Hz) at 0.4T under PWM voltage excitation

Investigation of No-load and on-load performance of a model three-phase transformer core operating under sinusoidal and PWM voltage excitation

6.2.3 Experimental results under PWM voltage excitation at 1.0 T

Increasing the peak flux density to 1.0 T, the largest measured and total power losses were obtained as expected at 400 Hz they were 40.567 and 157.28 (W/kg) respectively. And the smallest measured and total power losses were obtained at (25 Hz). They were 0.634 and 2.405 W/kg respectively. Table 6.2 shows total power loss per cycle and table 6.3 summarises coefficient components of power loss when the core was energised at 1.0 T.

Table 6-3 Power loss per cycle under PWM voltage excitation at 1.0 T at different magnetising frequencies

Magnetising frequency Hz	Measured power loss Per weight (W/kg)	Power loss per cycle (W/kg). sec
25	0.634	0.025
50	2.335	0.046
100	6.719	0.067
200	17.173	0.085
400	40.567	0.101

Table 6-4 Measured and total power loss component of Epstein size lamination under PWM voltage excitation at 1.0 T with different magnetising frequencies

Frequency (Hz)	Measured power loss per weight(W/kg)	P_e (W/kg)	P_h (W/kg)	P_a (W/kg)	$P_t =$ $P_a+P_h+P_a$ (W/kg)
25	0.634	0.187	0.68	1.537	2.405
50	2.335	0.75	1.36	4.348	6.458
100	6.719	3	2.72	12.3	18.02
200	17.173	12	5.44	34.789	52.229
400	40.567	48	10.88	98.4	287.704

A specific power loss per cycle is plotted against the square root of frequency as shown in Fig. 6-7. By applying the coefficients in equation 6.8 the power loss components are automatically calculated,

$$D = K_e B^2 = 0.0003$$

$$E = K_h B^2 = 0.0123$$

$$G = K_{ex} B^{1.5} = 0.0272$$

Investigation of No-load and on-load performance of a model three-phase transformer core operating under sinusoidal and PWM voltage excitation

The value of hysteresis and eddy current power loss per cycle versus magnetising frequency is shown in Fig. 6-8.

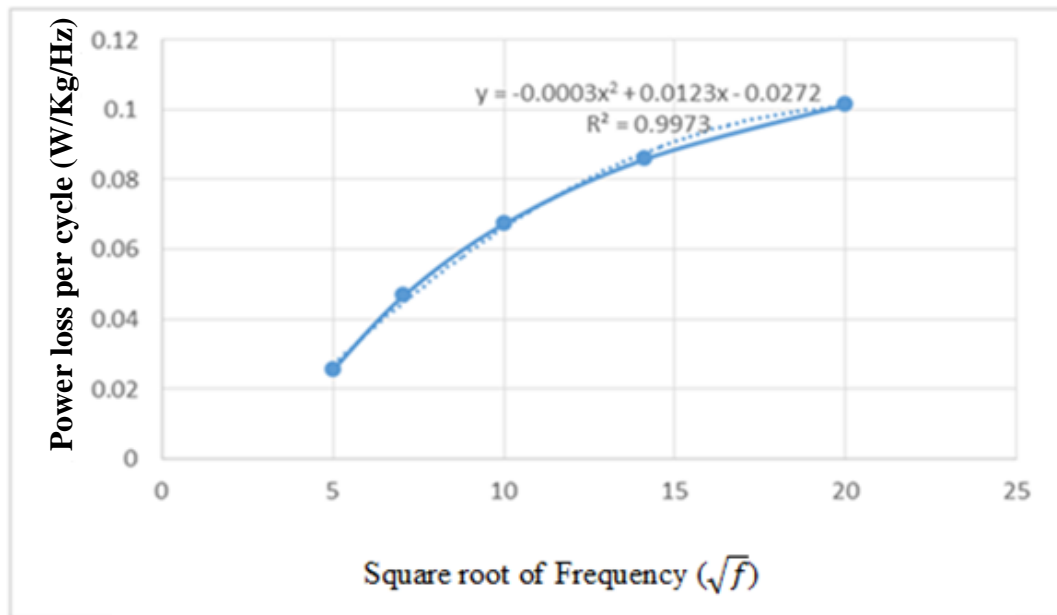


Fig. 6-7 Specific power loss per cycle versus root of frequency at 1T under PWM voltage excitation

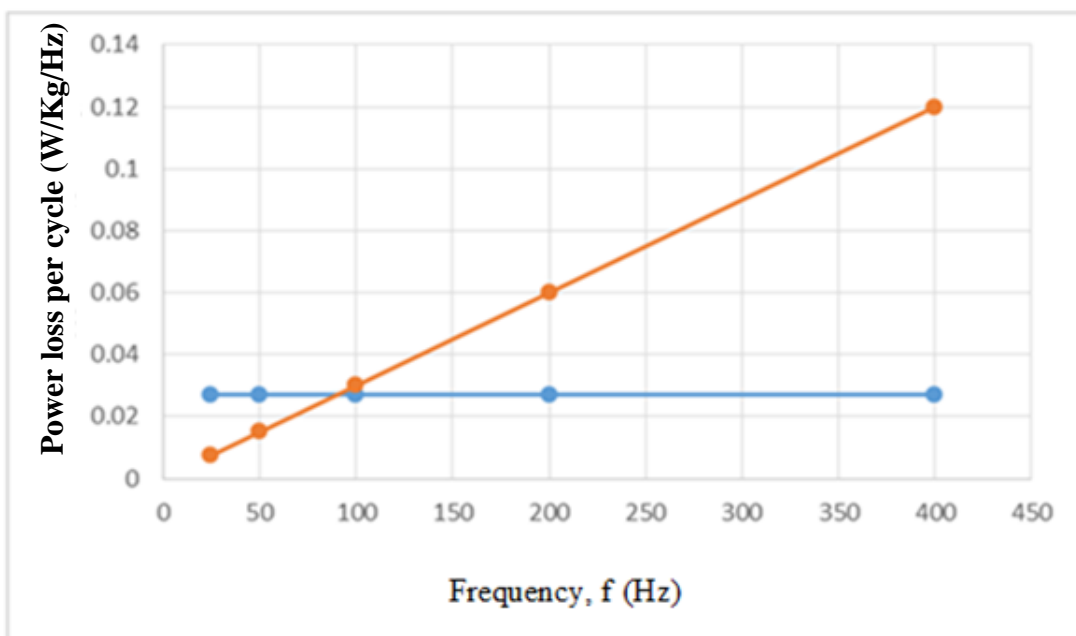


Fig. 6-8 Eddy current and hysteresis loss per cycle versus frequency (Hz) at 1T under PWM voltage excitation

Investigation of No-load and on-load performance of a model three-phase transformer core operating under sinusoidal and PWM voltage excitation

6.2.4 Experimental results under sinusoidal voltage excitation at 0.4T

Measurement of Epstein size lamination was again taken under sinusoidal flux condition using a measurement system as shown in Fig. 6-1, and 6-2. All measurements were taken at the same peak flux density and same magnetising frequency as that under PWM voltage excitation. Table 6.5 shows specific power losses per cycle and table 6.6 shows overall total losses at 0.4T as resulted under sinusoidal excitation.

Table 6-5 Power loss per cycle under sinusoidal voltage excitation at 0.4 T at different magnetising frequencies

Magnetising frequency Hz	Measured power loss per weight (W/kg)	Power loss per cycle (W/kg). sec
25	0.073	0.0029
50	0.241	0.0048
100	0.758	0.0075
200	2.043	0.010
400	4.665	0.011

Table 6-6 Specific and total power loss of an Epstein size lamination under sinusoidal voltage excitation at 0.4T and different magnetising frequencies

Frequency (Hz)	Measured power loss per weight(W/kg)	P_e (W/kg)	P_h (W/kg)	P_a (W/kg)	$P_t =$ $P_a+P_h+P_e$ (W/kg)
25	0.073	0.025	0.092	0.187	0.305
50	0.241	0.1	0.185	0.530	0.815
100	0.758	0.4	0.37	1.5	2.27
200	2.043	1.6	0.74	4.24	6.582
400	4.665	6.4	1.48	12	19.88

Total power loss per cycle versus square root of frequency is shown in Fig. 7-9. The polynomial function of this curve was obtained by using the polynomial curve fitting function in Microsoft Excel.

Investigation of No-load and on-load performance of a model three-phase transformer core operating under sinusoidal and PWM voltage excitation

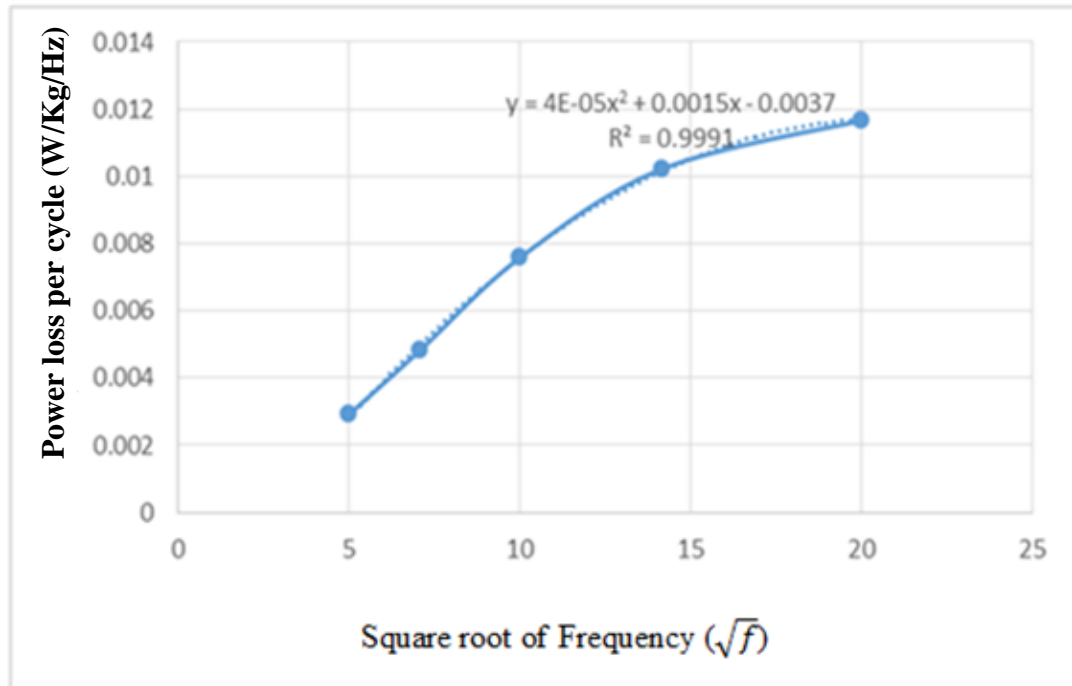


Fig. 6-9 Specific power loss per cycle versus square root of frequency at 0.4T under sinusoidal voltage excitation

By applying coefficients given below those obtained from Fig. 6-9. The eddy current power loss, hysteresis power loss and anomalous power can be calculated using equation 6.8.

$$D = K_e B^2 = 4E^{-5}$$

$$E = K_h B^2 = 0.0015$$

$$G = K_{ex} B^{1.5} = 0.0037$$

Investigation of No-load and on-load performance of a model three-phase transformer core operating under sinusoidal and PWM voltage excitation

Eddy current and hysteresis power losses per cycle versus magnetising frequency at 0.4T are shown in Fig. 6-10.

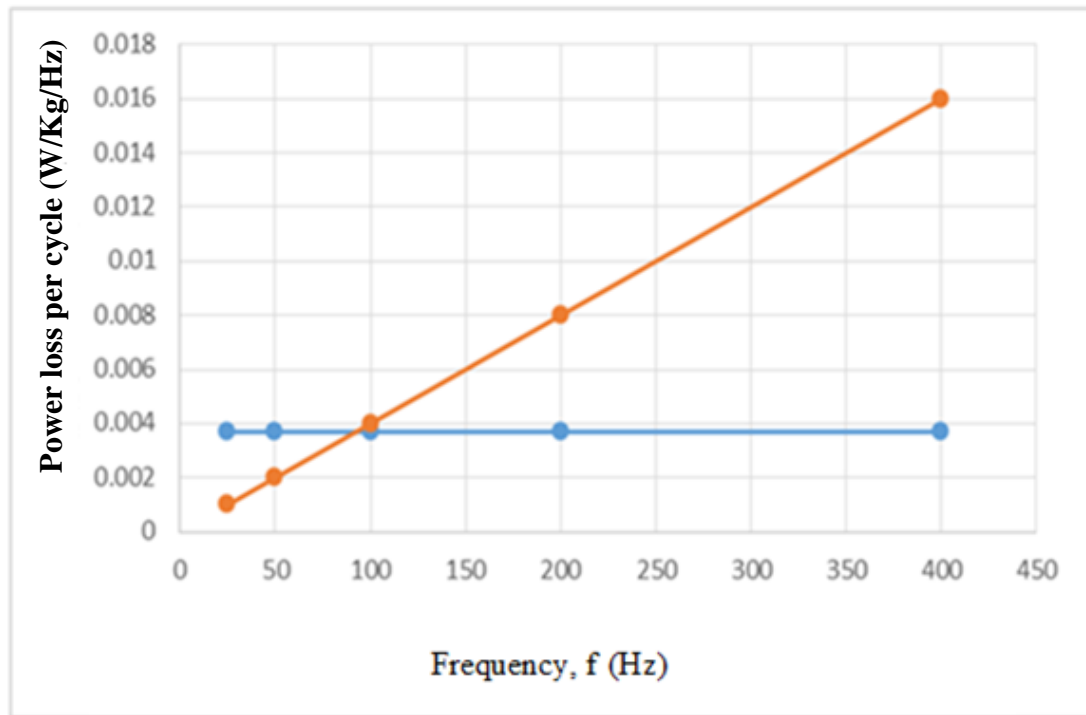


Fig. 6-10 Eddy current and hysteresis loss per cycle versus frequency (Hz) at 0.4T under sinusoidal voltage excitation

6.3 Experimental results under sinusoidal voltage excitation at 1.0 T

Magnetising the core with peak flux density at 1.0 T, the largest measured and total power losses were obtained as expected at 400 Hz they were 26.346 and 111.12 (W/kg) respectively. And the smallest measured and total power losses were obtained at (25 Hz). They were 0.436 and 1.77 W/kg respectively. Table 6.7 shows total power loss per cycle and table 6.8 summarise coefficient components of power loss with the core energised at 1.0 T.

Investigation of No-load and on-load performance of a model three-phase transformer core operating under sinusoidal and PWM voltage excitation

Table 6-7 power loss per cycle at 1.0 T at different magnetising frequencies

Magnetising frequency Hz	Measured power loss per weight (W/kg)	Power loss per cycle (W/kg). sec
25	0.436	0.017
50	1.409	0.028
100	4.435	0.044
200	11.801	0.059
400	26.346	0.065

Table 6-8 Specific and total power loss of an Epstein size lamination under sinusoidal voltage excitation at 1.0 T at different magnetising frequencies

Frequency (Hz)	Measured power loss per weight(W/kg)	P_e (W/kg)	P_h (W/kg)	P_a (W/kg)	$P_t =$ $P_e+P_h+P_a$ (W/kg)
25	0.436	0.125	0.545	1.1	1.77
50	1.409	0.5	1.09	3.111	4.701
100	4.435	2	2.18	8.8	12.98
200	11.801	8	4.36	24.890	37.250
400	26.346	32	8.72	70.4	111.12

Total power loss under sinusoidal voltage excitation per cycle versus square root of frequency is shown in Fig. 6-11.

Investigation of No-load and on-load performance of a model three-phase transformer core operating under sinusoidal and PWM voltage excitation

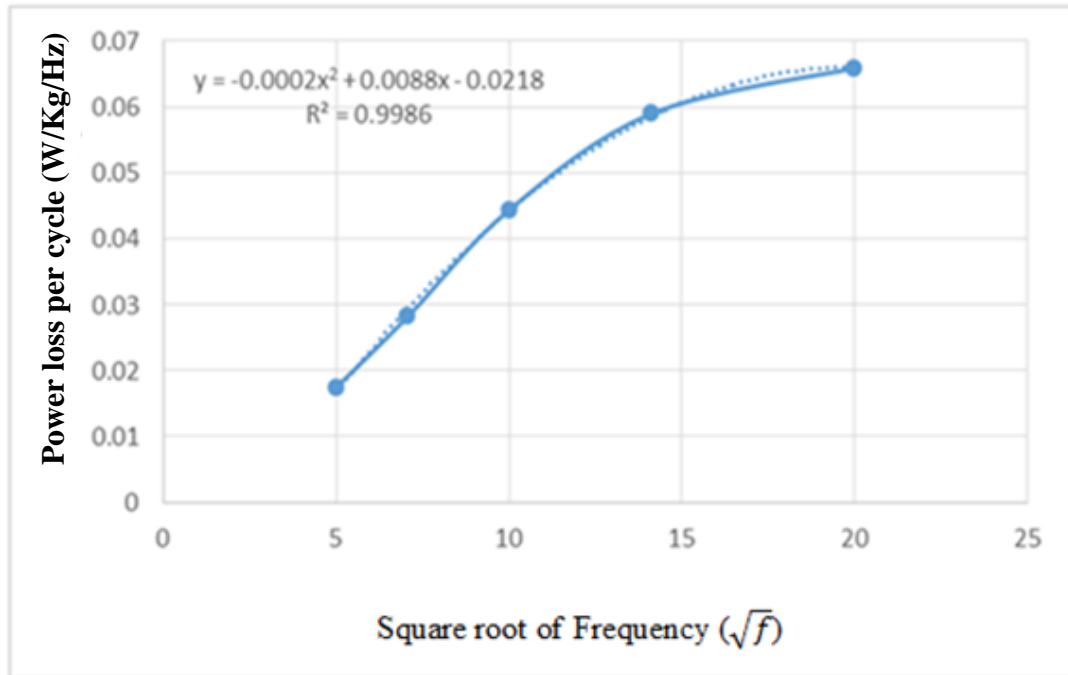


Fig. 6-11 Specific power loss per cycle versus square root of frequency at 1T under sinusoidal voltage excitation

By applying the coefficient given below, those obtained from Fig. 6-11. The eddy current power loss, hysteresis power loss and anomalous power loss can be calculated using equation 6-8.

$$D = K_e B^2 = 0.002$$

$$E = K_h B^2 = 0.0088$$

$$G = K_{ex} B^{1.5} = 0.0218$$

Where $D = K_e B^2$ is the eddy current losses per cycle, $E = K_h B^2$ is the hysteresis loss per cycle and $K_{ex} B^{1.5}$ is the anomalous loss per cycle. By applying equation (6.8) the eddy current power loss, hysteresis power loss and are shown in Fig. 6-12.

Investigation of No-load and on-load performance of a model three-phase transformer core operating under sinusoidal and PWM voltage excitation

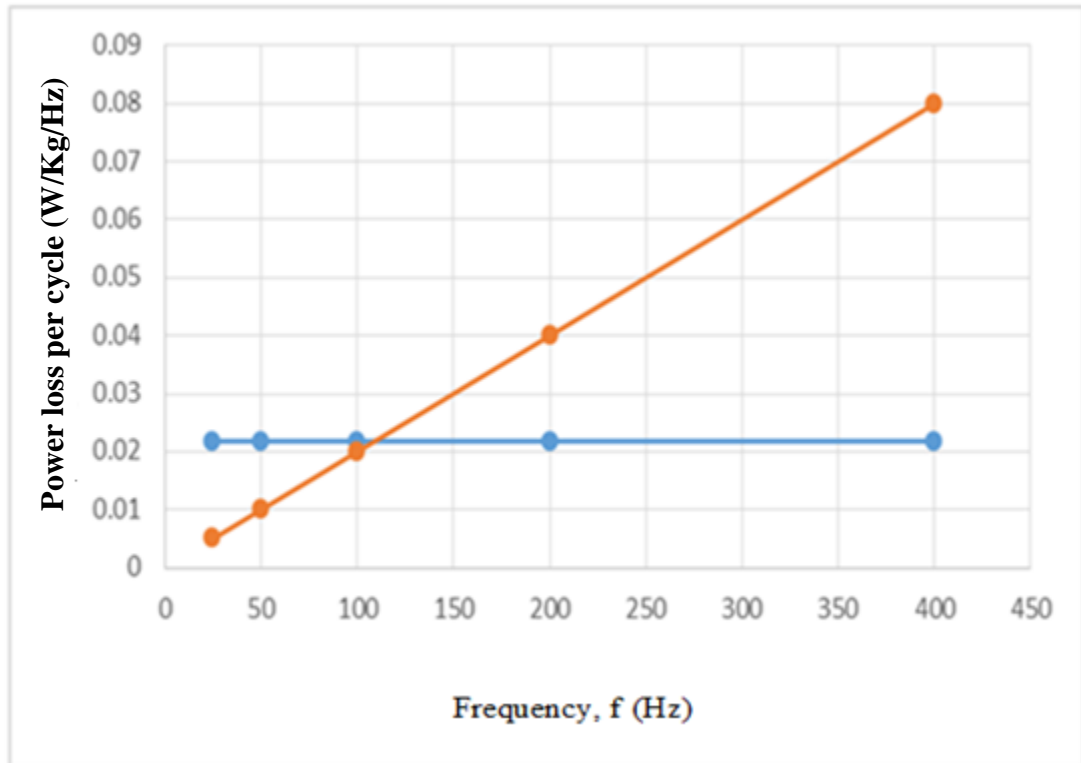


Fig. 6-12 Eddy current and hysteresis loss per cycle versus frequency (Hz) at 1T under sinusoidal voltage excitation

6.3.1 Comparison of the results

Specific and total power losses were measured under sinusoidal and PWM excitations using Epstein size laminations. Power loss was measured at various flux densities of 0.4T and 1.0T. Both measurements were conducted under magnetising frequencies of 25, 50, 100, 200, and 400 Hz.

At 0.4 T measured and total power loss results variation with flux density under PWM and sinusoidal voltage excitation are shown in tables 6.2 and 6.6. The total of measured power loss was higher as expected under PWM waveform. Comparing the total power loss and measured power loss under PWM waveform with the total and measured power loss occurred under sinusoidal waveform with varied magnetising frequency, it be seen that the total power loss results at 25 Hz magnetising frequency under PWM waveform were found to be 52% higher than that under sinusoidal. Increasing the magnetising frequency to 400 Hz, the loss difference between sinusoidal and PWM voltage excitation at 400 Hz was found to be 88%, higher under PWM voltage excitation. Furthermore, measured power loss under sinusoidal waveform was varied between 0.073 to 4.665 W/kg, whereas measured power loss under PWM waveform were varied between 0.098 and 6.753 W/kg.

Comparing the results obtained when Epstein frame energised at 1.0 T. as shown in tables 6.4 and 6.8, total power loss at 25 Hz magnetising frequency was again higher under PWM voltage excitation by 26%. And it was higher at 400 Hz magnetising frequency under PWM voltage excitation by 61%. Furthermore, measured power loss under PWM voltage excitation was varied between 0.634 to 40.56 W/kg and it was varied under sinusoidal waveform between 0.436 to 26.34 W/kg.

The loss difference between PWM and sinusoidal voltage excitation was found to be higher under PWM. Lowest loss occurred at low magnetising frequency 25 Hz and highest loss occurred at higher magnetising frequency 400 Hz. The results of total, measured power loss was found to be higher under PWM voltage excitation this is due to the high harmonic distortion occurring when the Epstein size sample was energised by PWM waveform.

7. CHAPTER 7

7.1.1 MATLAB block diagram contents

“MATLAB Simulink” is a powerful tool for modelling, simulating and analysing various electrical blocks data. Therefore, the simulation of three-phase transformer core was modelled by using the Simulink of “MATLAB 2015”. The Simulink blocks including following:

1. Three voltage sources were used to feed the transformer with electrical power
2. Three-phase breaker used to control the braking operation
3. Three-phase voltage and current measurements were used to measure the instantaneous DC voltage or current between two nodes
3. Three-phase transformer
4. Load switch
5. Three-phase parallel RLC load
6. Receiver signal used to receive signal from power GUI
7. Multimeter used to measure emf to calculate flux density
4. PWM Generator (2-level)
5. Universal bridge used to convert current
7. Scope used to monitor the signals
8. Bus selector used to separate signals
9. Fast Fourier Transformer FFT used to collect voltage and current harmonic
11. Power GUI block used to solve the circuit

Investigation of No-load and on-load performance of a model three-phase transformer core operating under sinusoidal and PWM voltage excitation

These blocks are combined to produce sinusoidal signal measurement and PWM signal measurement.

7.1.2 Simulation under sinusoidal voltage excitation

Three-phase transformer core was energised by three (AC) sinusoidal supplies. To obtain desired flux density equation 2.16 was used to set flux density to 0.4T, 0.6T and 1.0T respectively. And the frequency was set to 50 Hz,

Fig.7.1 and Fig. 7-2 show the overall circuit under sinusoidal excitation with load and the overall circuit with no-load condition.

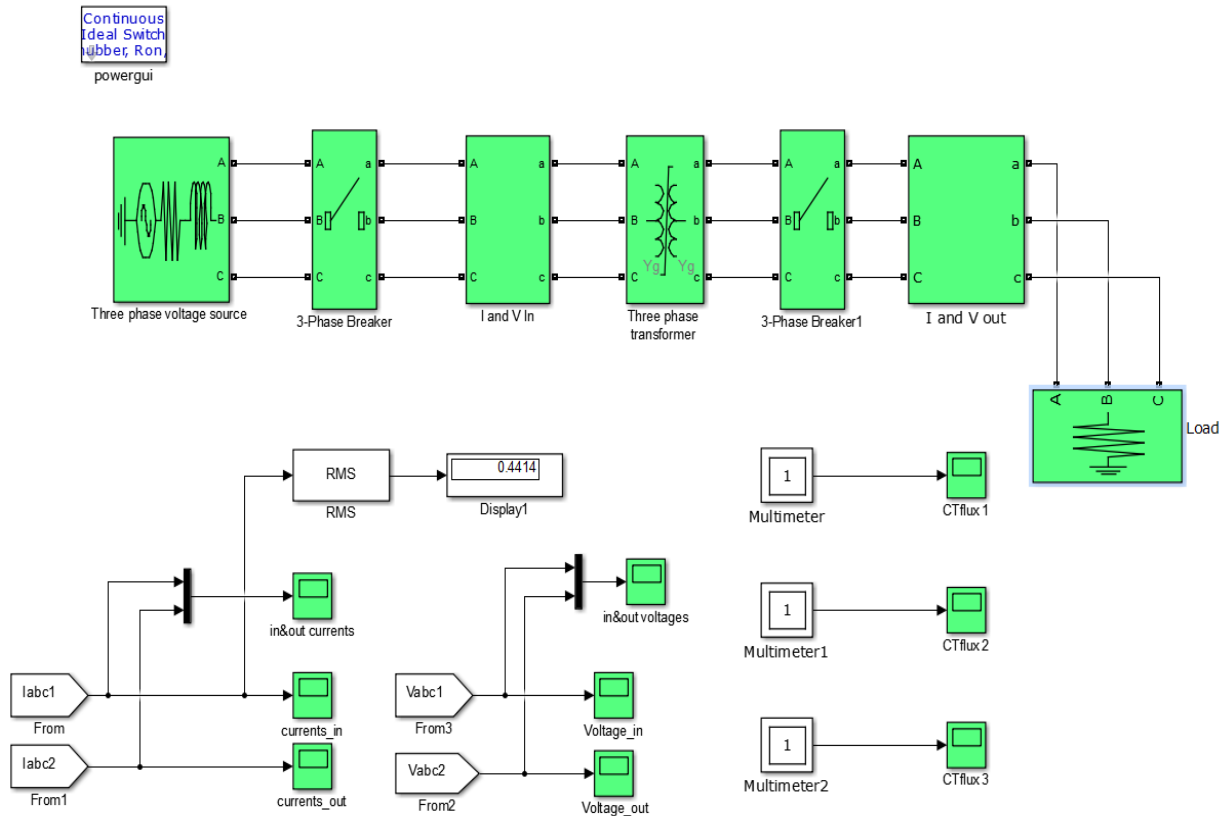


Fig. 7-1 Sinusoidal voltage excitation circuit under load condition

Investigation of No-load and on-load performance of a model three-phase transformer core operating under sinusoidal and PWM voltage excitation

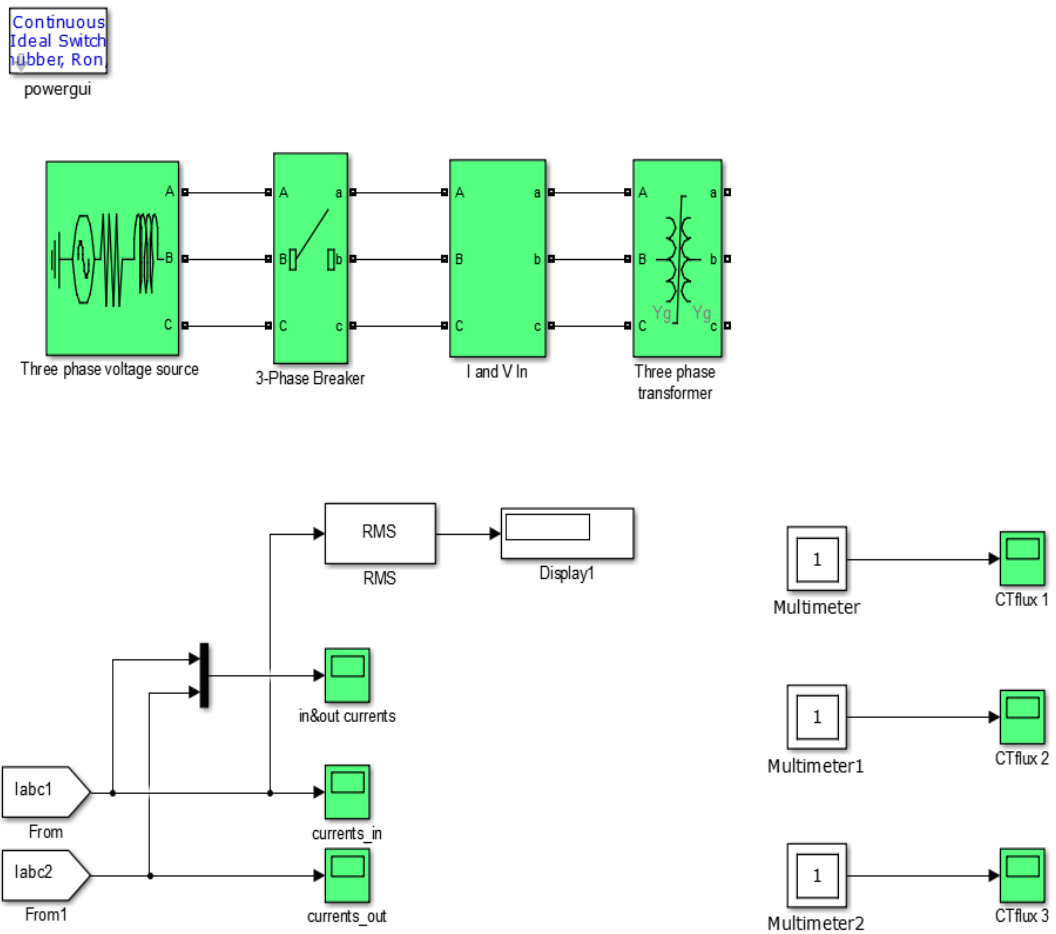


Fig. 7-2 Sinusoidal voltage excitation circuit under no-load condition

Investigation of No-load and on-load performance of a model three-phase transformer core operating under sinusoidal and PWM voltage excitation

7.1.3 Simulation under PWM voltage excitation

In order to study the difference between three-phase sinusoidal voltage excitation and three-phase PWM voltage excitation, PWM circuit was designed. Fig. 7-3 and Fig. 7-4 show the overall PWM circuit under load and no-load conditions.

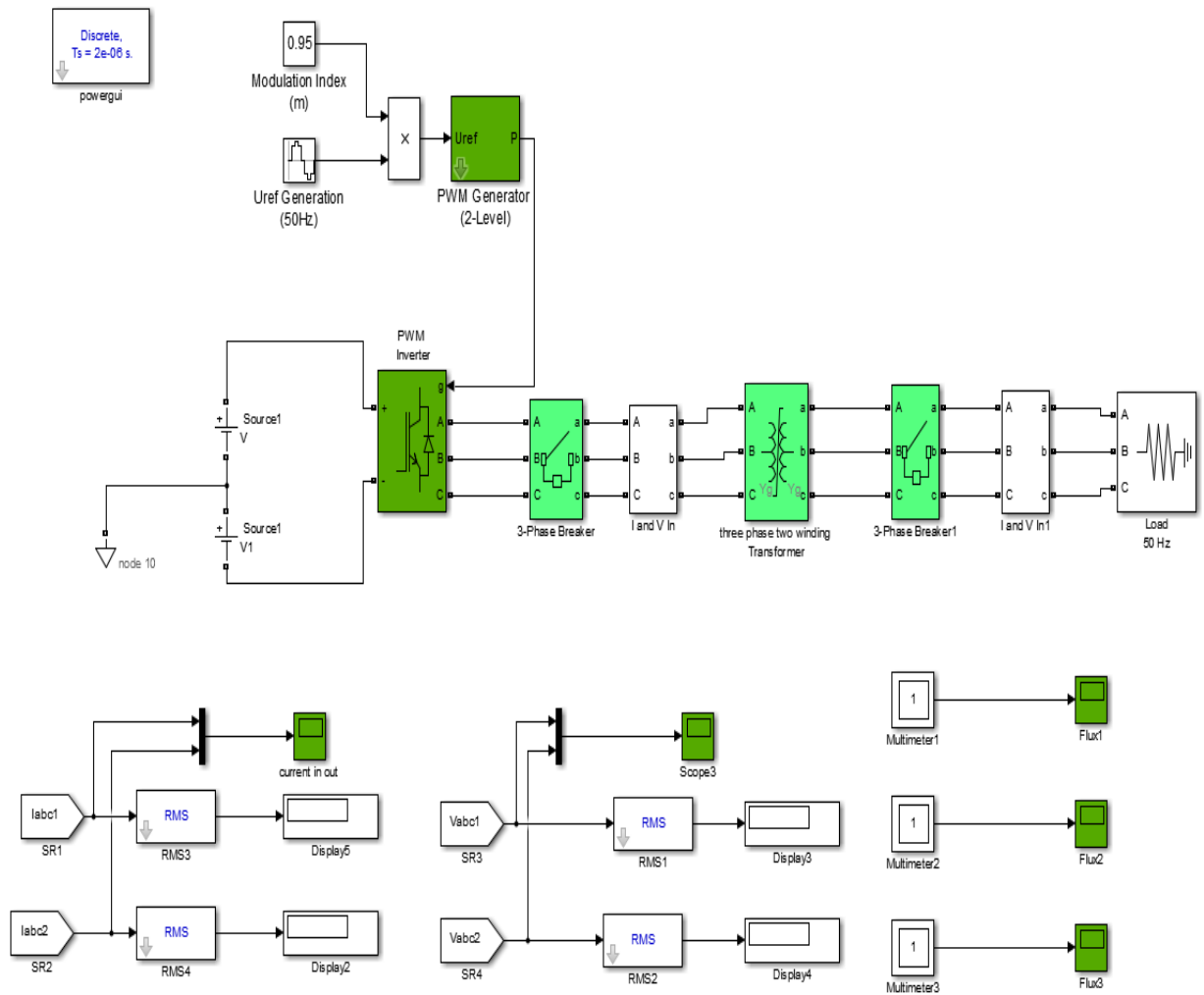


Fig. 7-3 PWM voltage excitation circuit under load condition

Investigation of No-load and on-load performance of a model three-phase transformer core operating under sinusoidal and PWM voltage excitation

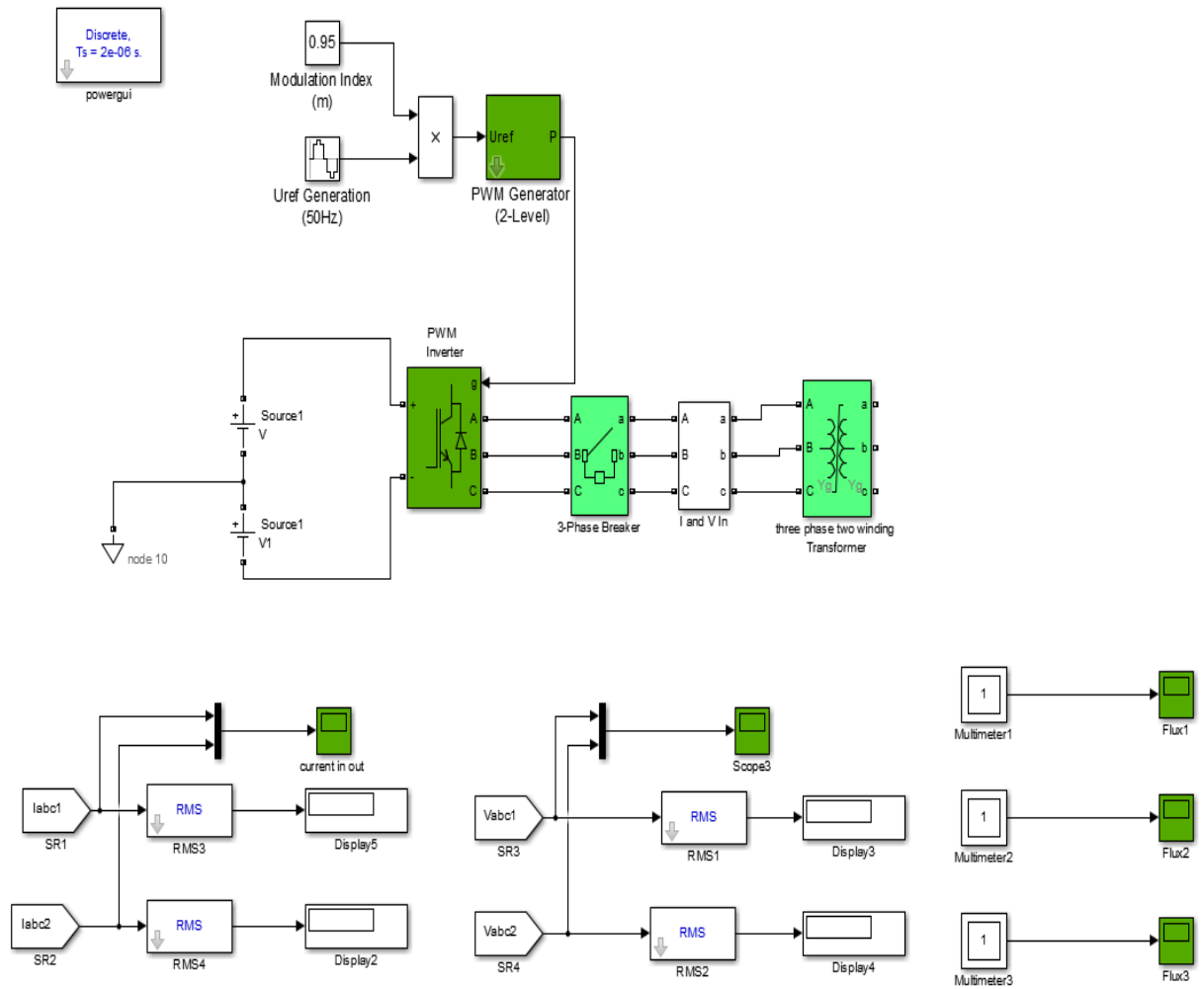


Fig. 7-4 PWM voltage excitation circuit under no-load condition

Investigation of No-load and on-load performance of a model three-phase transformer core operating under sinusoidal and PWM voltage excitation

7.1.4 Total harmonic distortion under sinusoidal voltage excitation

The harmonic content of primary current for the peak flux density of 0.4T, 0.6T and 1.0T was measured throughout the simulation under both load and no-load conditions. The result of the harmonic analysis for the primary current can be seen in Figs. 7-5 and Fig. 7-6. Furthermore, harmonics existing in the primary voltage under load and no-load conditions can be seen in Fig. 7-7 and 7-8.

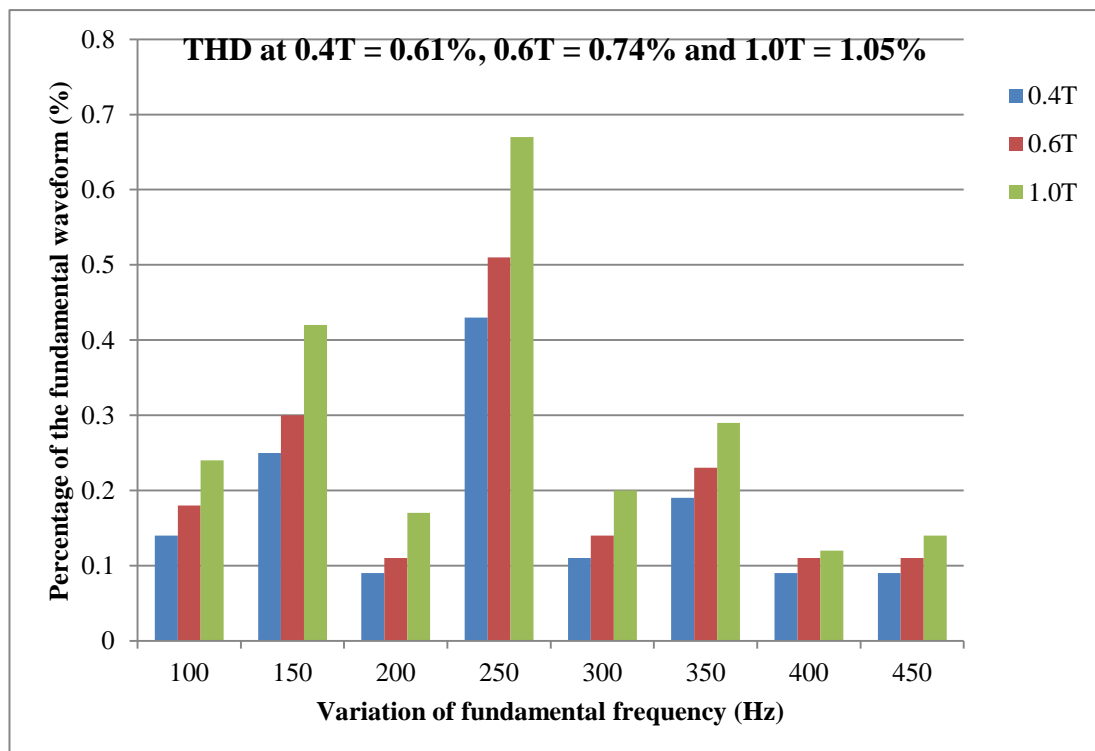


Fig. 7-5 Harmonic order content of primary current for sinusoidal supply voltage under no-load condition with different peak flux density (T)

Investigation of No-load and on-load performance of a model three-phase transformer core operating under sinusoidal and PWM voltage excitation

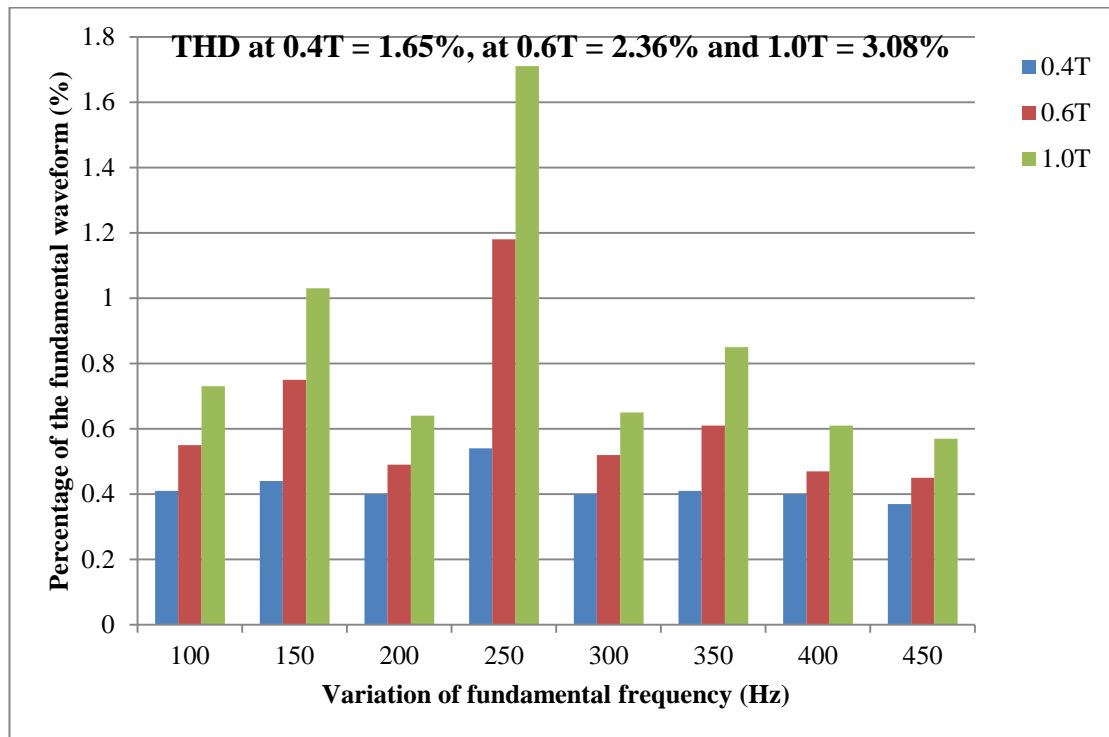


Fig. 7-6 Harmonic order content of primary current for sinusoidal supply voltage under on-load condition with different peak flux density (T)

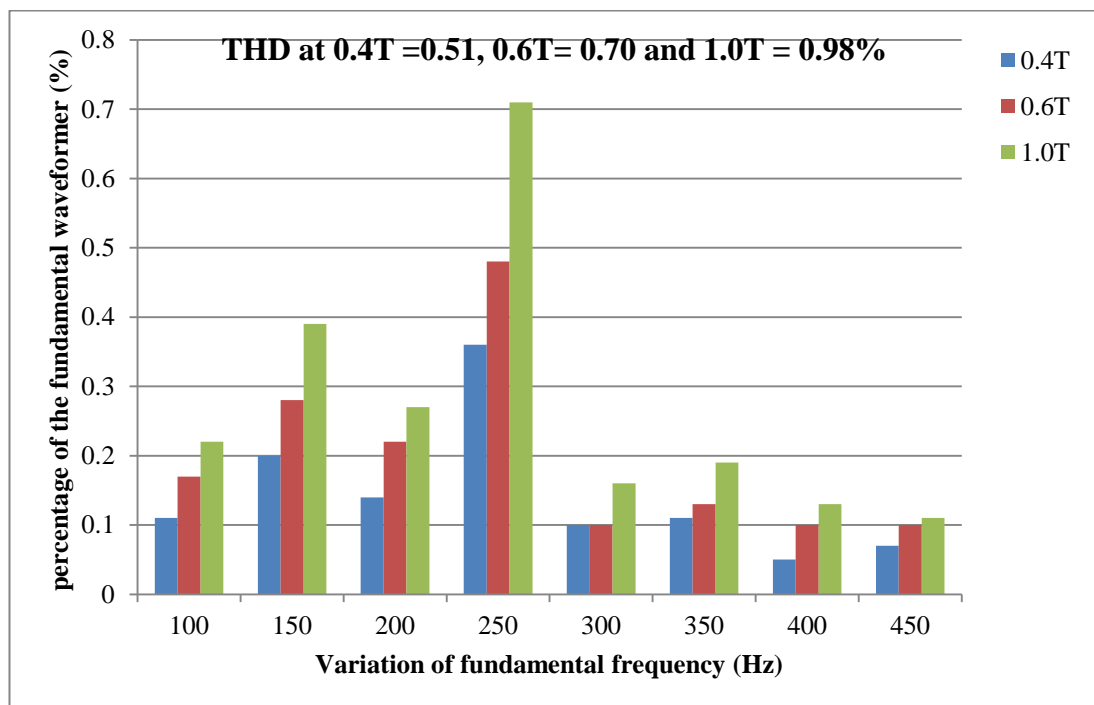


Fig. 7-7 Harmonic order content of primary voltage for sinusoidal supply voltage under no-load condition with different peak flux density (T)

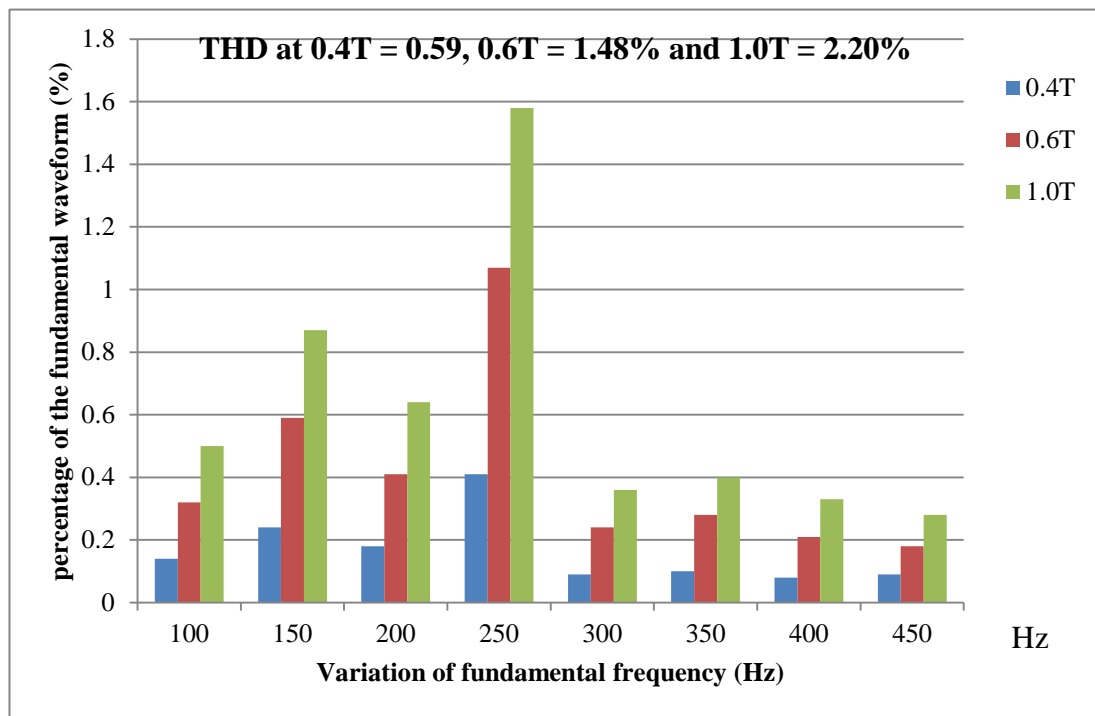


Fig. 7-8 Harmonic order content of primary voltage for sinusoidal supply voltage under on-load condition with different peak flux density (T)

7.2 Total Harmonic Distortion, THD under PWM Voltage Excitation

THD of primary current and primary voltage was computed throughout the simulation under both load and no-load conditions. Fig 7-9 and 7-10 show THD of the primary current under load and no-load conditions, and Fig 7-11 and 7-12 shows THD in secondary voltage under load and no-load conditions with different peak flux density under load condition.

Investigation of No-load and on-load performance of a model three-phase transformer core operating under sinusoidal and PWM voltage excitation

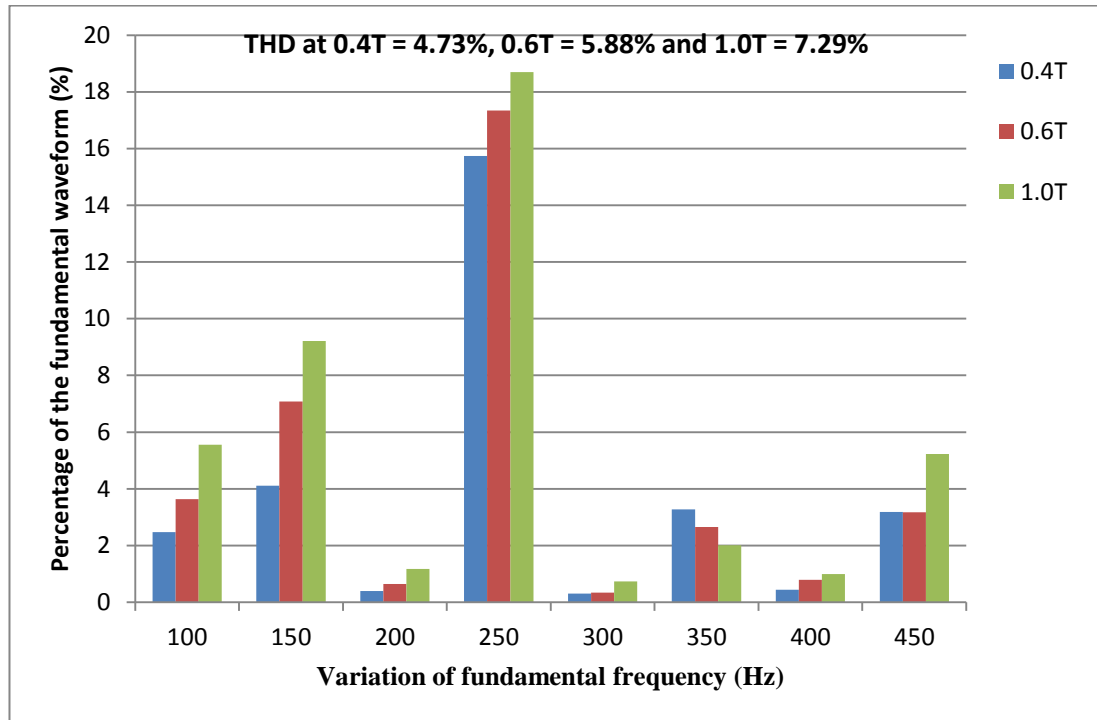


Fig. 7-9 Harmonic order content of primary current for PWM supply voltage under on-load condition with different peak flux density (T)

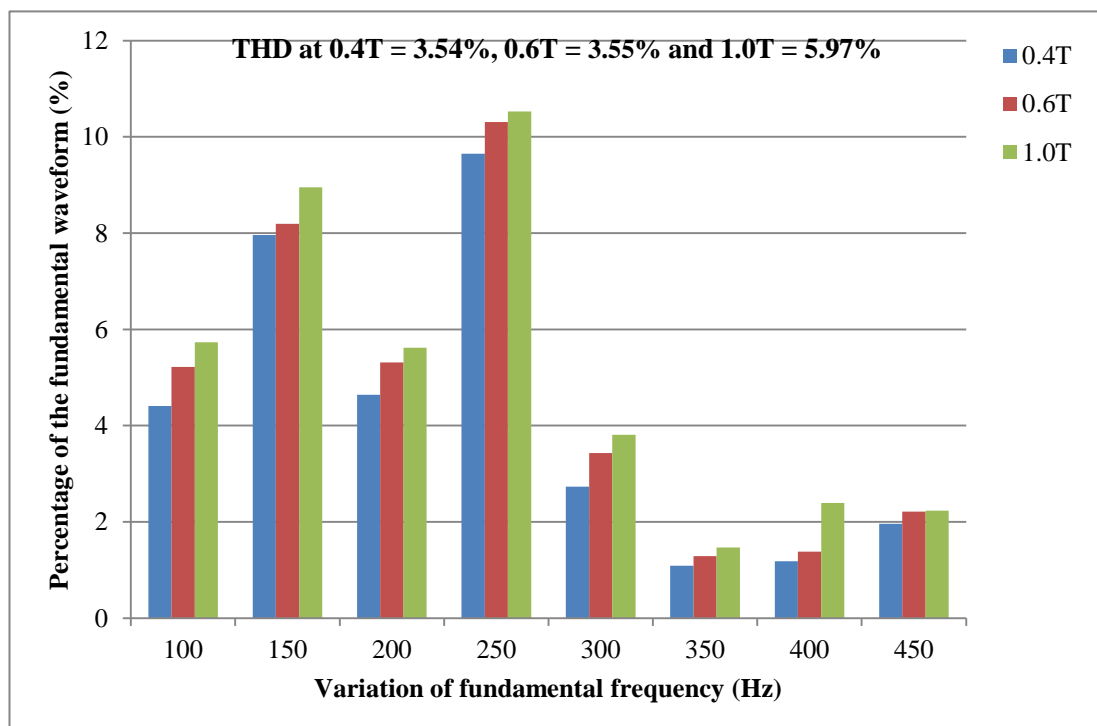


Fig. 7-10 Harmonic order content of primary current for PWM supply voltage under no-load condition with different peak flux density (T)

Investigation of No-load and on-load performance of a model three-phase transformer core operating under sinusoidal and PWM voltage excitation

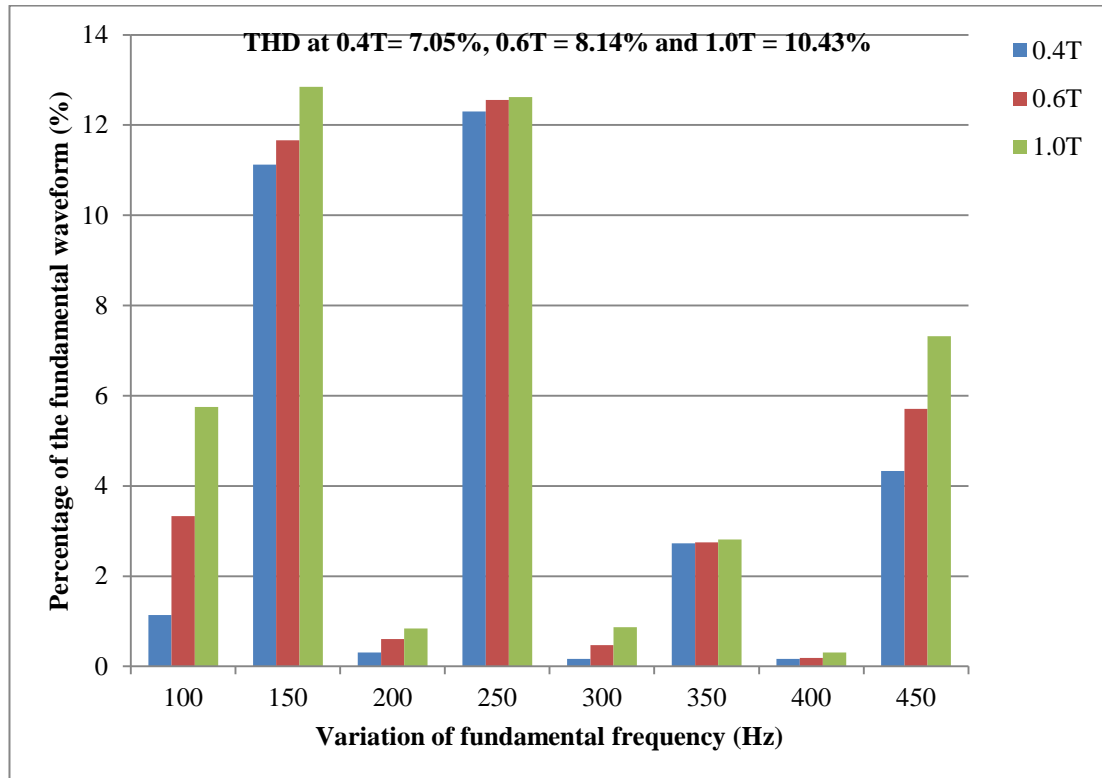


Fig. 7-11 Harmonic order content of secondary voltage for PWM supply voltage under on-load condition with different peak flux density (T)

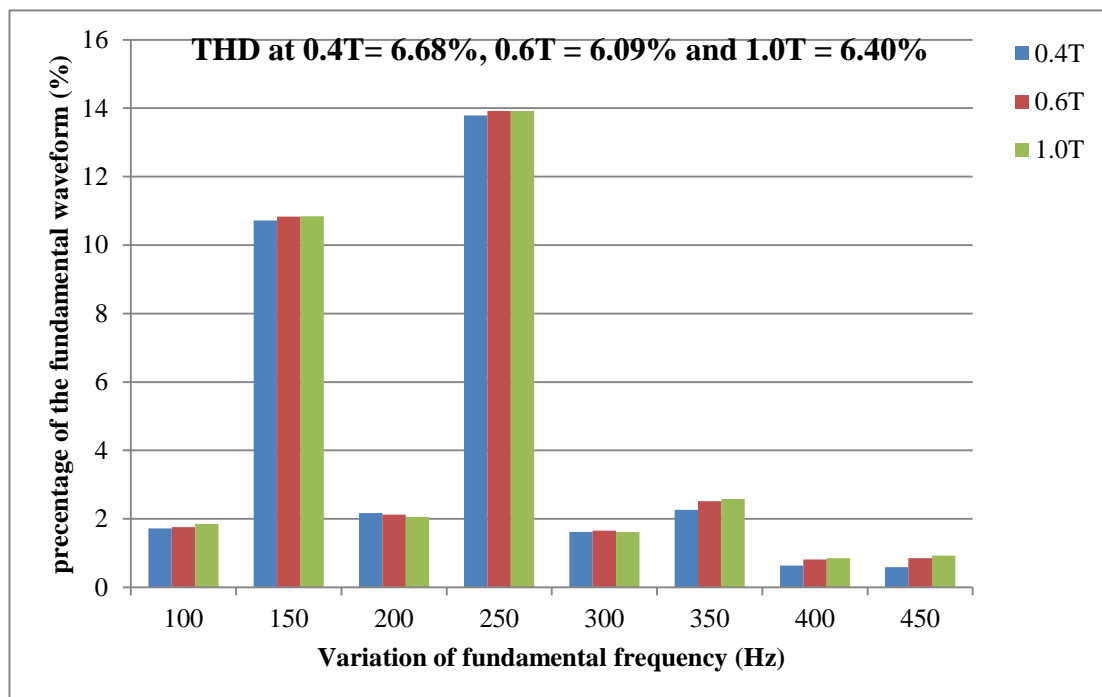


Fig. 7-12 Harmonic order content of secondary voltage for PWM supply voltage under no-load condition with different peak flux density (T)

Investigation of No-load and on-load performance of a model three-phase transformer core operating under sinusoidal and PWM voltage excitation

7.2.1 Total harmonic contents with a change in switching frequency

Fig. 7-12, 7-13, 7.14 and 7.15 below show how total harmonics of primary and secondary current and voltage are affected by switching frequency.

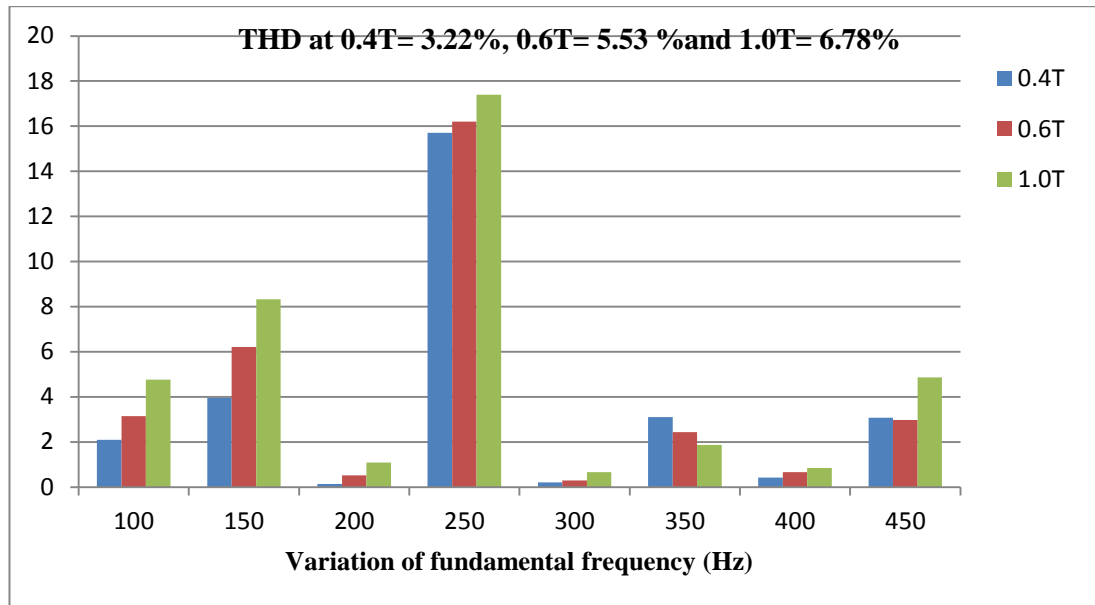


Fig. 7-13 Harmonic order contents of primary current for PWM supply voltage under on-load condition at switching frequency 3 kHz

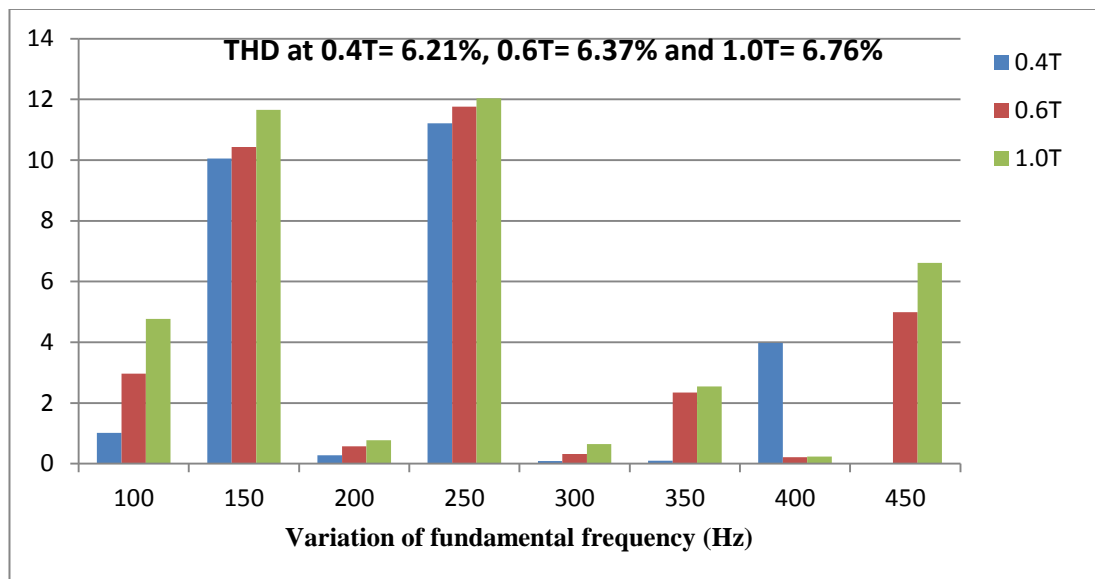


Fig. 7-14 Harmonic order contents of secondary voltage for PWM supply voltage under on-load condition at switching frequency 3 kHz

Investigation of No-load and on-load performance of a model three-phase transformer core operating under sinusoidal and PWM voltage excitation

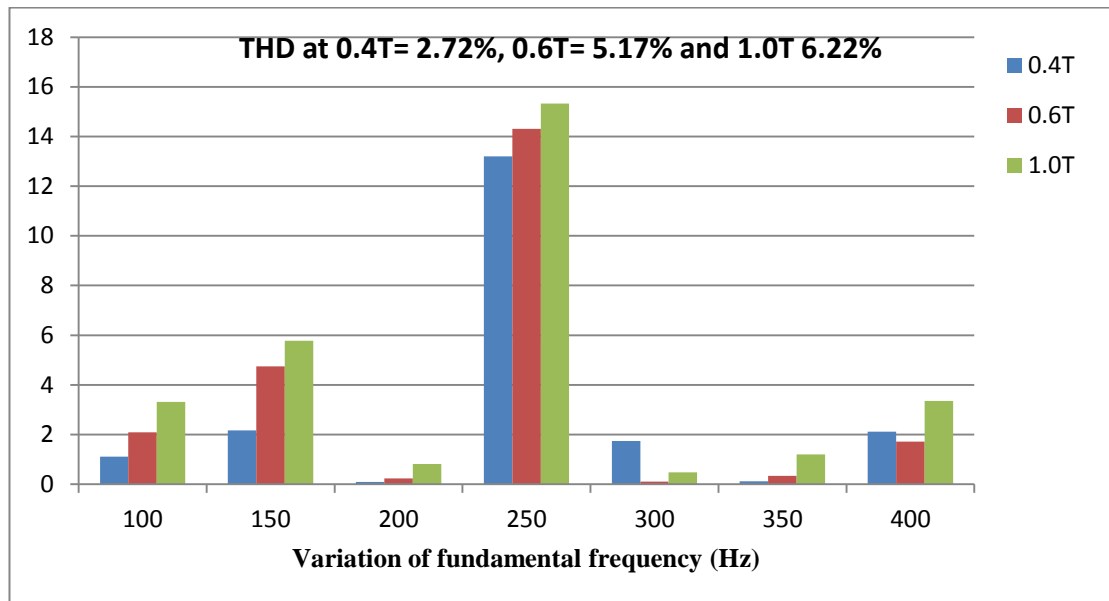


Fig. 7-15 Harmonic order contents of primary current for PWM supply voltage under on-load condition at switching frequency 5 kHz

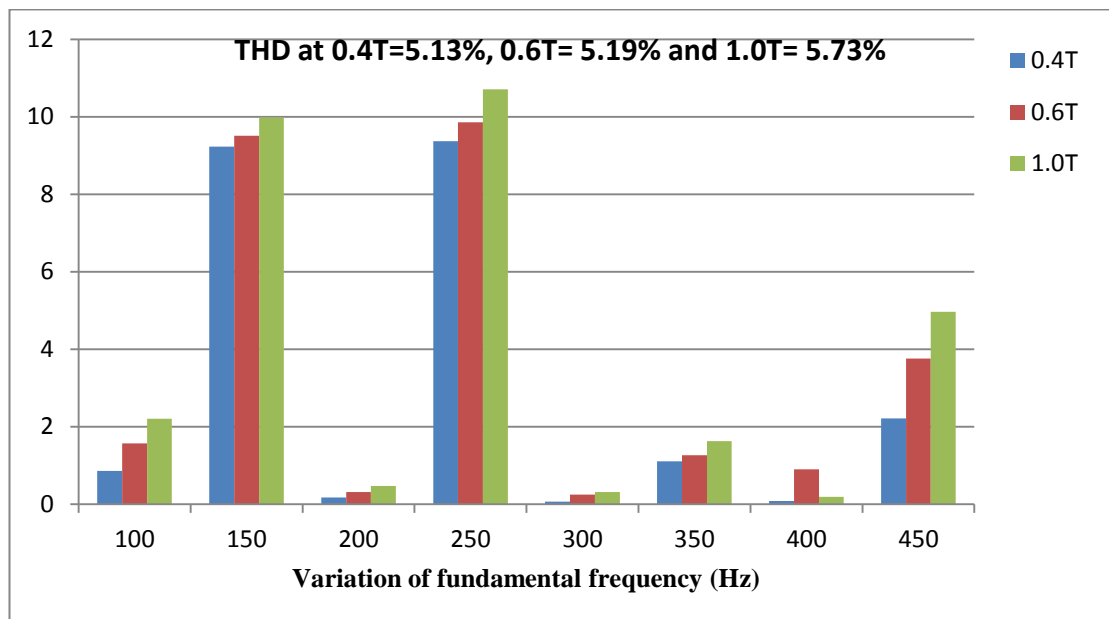


Fig. 7-16 Harmonic order contents of secondary voltage for PWM supply voltage under on-load condition at switching frequency 5 kHz

7.2.2 Harmonic analysis

Fig. 7-5 to Fig. 7-8 show that the sinusoidal supply has an insignificant amount of harmonic present. The most predominant harmonic of the primary and secondary currents and voltage under load and no-load condition is the 5th. This harmonic becomes more distorted on the output of the core when the core operated under load condition compared to the others when the core operated under no-load condition. Fig. 7-9 to Fig. 7-12 shows that the most predominant harmonic distortion caused by PWM waveform is the 5th. It is clearly shown that there is a higher harmonic content under PWM waveform compared to the sinusoidal excitation. This may suggest that PWM will create higher harmonic contents in the core producing higher losses compared to a sinusoidal input.

The odd harmonic rises proportionally with the peak flux density within the core under sinusoidal and PWM excitation, therefore the harmonic content is a factor leading to the increase in losses. A comparison of the Figs. 7-5, 7-6, 7-7, and 7-8 illustrates that little distortion occurs in the core when the core is excited by a sinusoidal input, the main distortion harmonics are in 3rd and 5th. The slight harmonics distortion may account for some of the losses incurred by the sinusoidal excitation.

From Fig. 7.13 to Fig. 7.16 show the PWM primary current waveform shows slightly lower magnitude on all harmonic components across the whole range of different peak flux densities compared to the secondary voltage. And also it can be observed that the amplitude of total harmonic component at low switching frequency were higher than that at a high switching frequency. For example the reduction in total harmonic distortion in the primary current Fig. 7-13 and Fig. 7-15 at 0.4T, 0.6T and 1.0T were 15%, 6.5% and 8.2% respectively lower at higher switching frequency of 5 kHz.

Comparing the effect of switching frequency on total harmonic distortion occurred in the secondary voltage Fig. 7-14 and Fig. 7-16 it can be obtained that at 0.4T, 0.6T and 1.0T the reduction in total harmonic components were 17%, 18% and 15% respectively lower at higher switching frequency, this was due to the reduction of

Investigation of No-load and on-load performance of a model three-phase transformer core operating under sinusoidal and PWM voltage excitation

Amplitude of harmonic components and reduction of harmonic contents in the core flux density waveform with increased switching frequency. These results confirmed the validity of the analysis carried out at other measurements. It was found the power loss and vibration of the core was decreased with increase in switching frequency. So these results present the benefit on the performance of the transformer core at high switching frequency.

7.2.3 Power loss analysis

Transformer loss can be categorized into two major groups no-load and load loss. The losses measured under no-load conditions in transformers consist of hysteresis and eddy current losses in core laminations and it is manifested as the heat generated in the core for example, when there is no current flowing in the secondary coil then transformer said to be on no-load. Even when the transformer is on no-load, current known as the exciting current flows in the primary winding because of the core losses and the finite permeability of any practical transformer core. The exciting current can be considered as having two components, the core losses current and the magnetising current. The no-load core loss was measured by using a “Scope” through multiplying the primary phase currents, I_1 , I_2 and I_3 by the primary phase voltage, V_1 , V_2 and V_3 . Dividing the component losses by the weight of the transformer core gives the value of power loss/weight.

On the other hand, when the transformer is operated under load condition, the no-load core loss per weight can be calculated through multiplying the three-phase primary currents I_1 , I_2 and I_3 by the three-phase secondary voltage V_4 , V_5 and V_6 and then dividing and then divides the product by the weight of the transformer core.

Fig.7-19. Shows the change in total losses of the transformer core with a change in peak flux density under sinusoidal and PWM voltage excitations under no load conditions.

Investigation of No-load and on-load performance of a model three-phase transformer core operating under sinusoidal and PWM voltage excitation

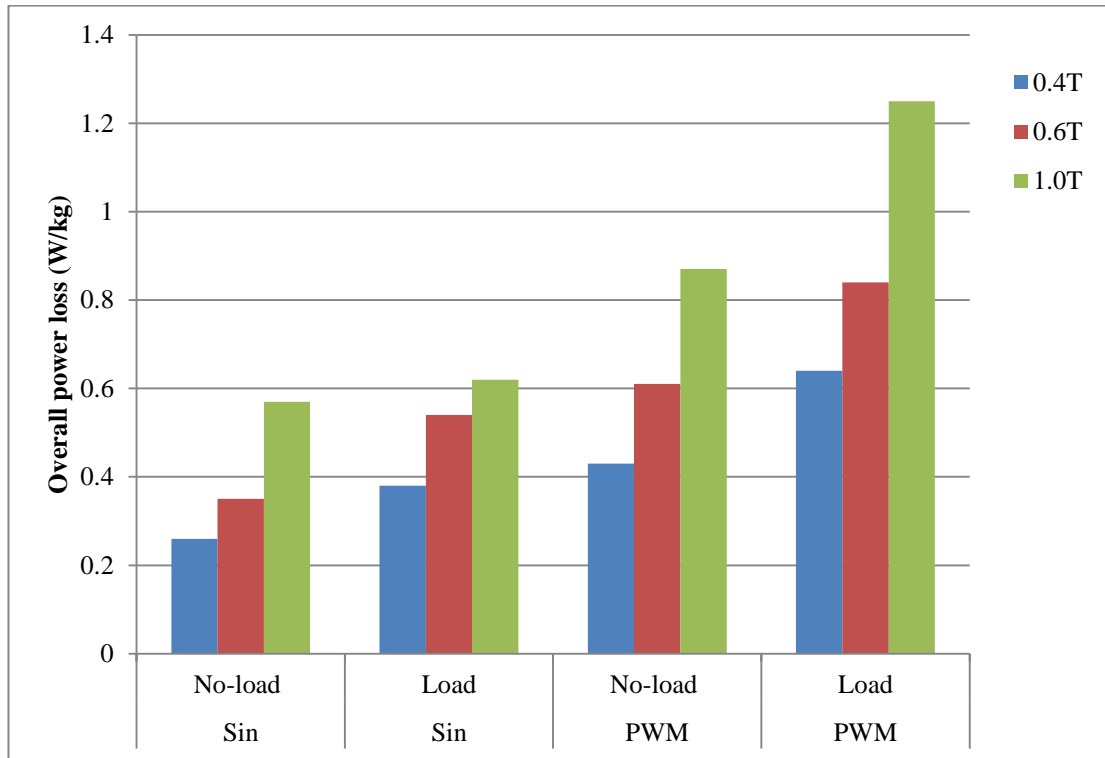


Fig. 7-17 Overall power loss of three-phase transformer core supplied by sinusoidal and PWM waveforms with change in the peak flux density (T) at 50 Hz at $M_i=0.5$ and $F_s=3\text{kHz}$

From Fig. 7-19 result shows that total power losses produced by various excitations. And increased under all excitations as the peak flux density increases, nevertheless all the excitation displays more increase in losses when the core was excited under load condition, for example. At the peak flux density of 1.0T the difference in losses with each excitation becomes most apparent. The sinusoidal excitation demonstrates the lowest increase losses through the whole range of peak flux densities, but this excitation still suffers from 54 W/kg rise in losses from 0.4T to 1.0T. However, under no-load condition power losses suffers from 38W/kg. All PWM modes tested show higher total losses compared to sinusoidal excitation. The most significant increase in losses from those graphs occurred when the PWM inverter was set with low modulation index and low switching frequency.

Investigation of No-load and on-load performance of a model three-phase transformer core operating under sinusoidal and PWM voltage excitation

7.2.4 Specific losses with a change in PWM modulation index

Fig. 7-20 Shows how the total power losses of the core change with change in the modulation index at varying core flux density at $f_s = 3$ kHz. Fig. 7-21 Shows how change in modulation index affects the total power losses of the core at $f_s = 2$ kHz. Fig. 7-22 shows how a change in modulation index affects the total power loss of the core at $f_s = 1$ kHz.

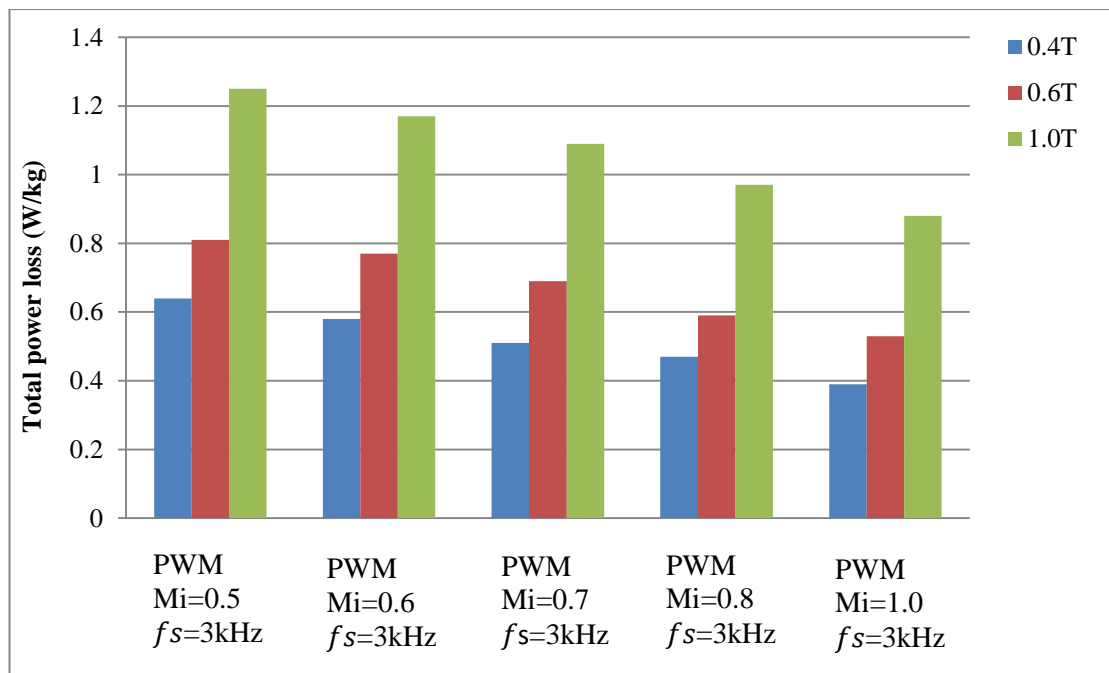


Fig. 7-18 Total power losses of the three-phase transformer core supplied by PWM waveform with change in the modulation index at 3kHz switching frequency.

Investigation of No-load and on-load performance of a model three-phase transformer core operating under sinusoidal and PWM voltage excitation

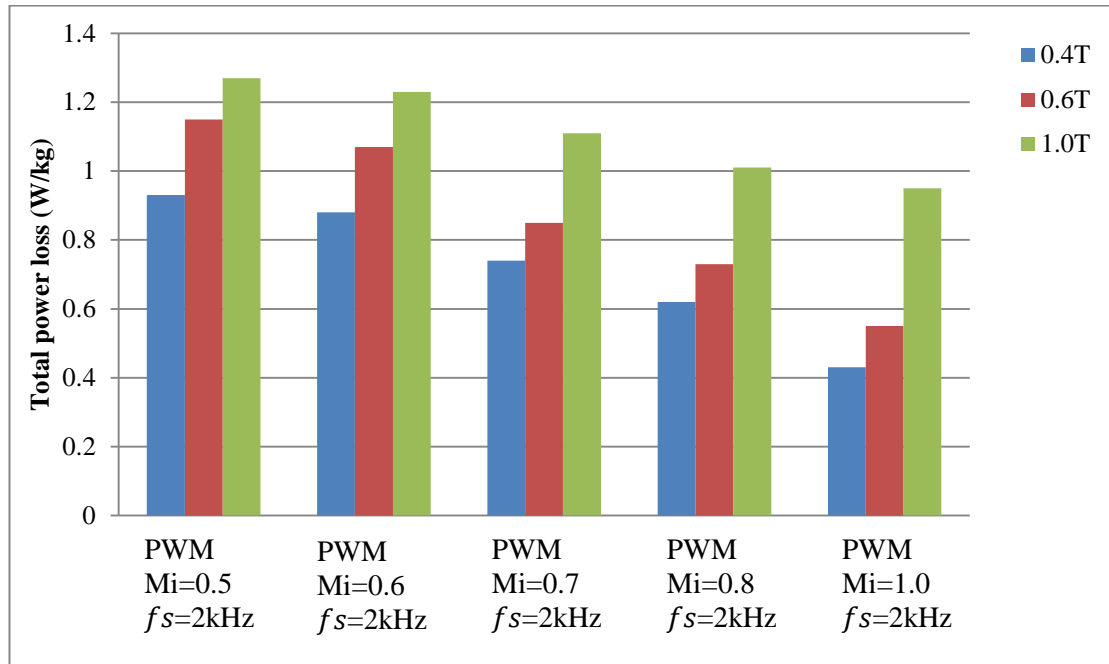


Fig. 7-19 Total power losses of the three-phase transformer core supplied by PWM waveform with change in the modulation index at 2kHz switching frequency

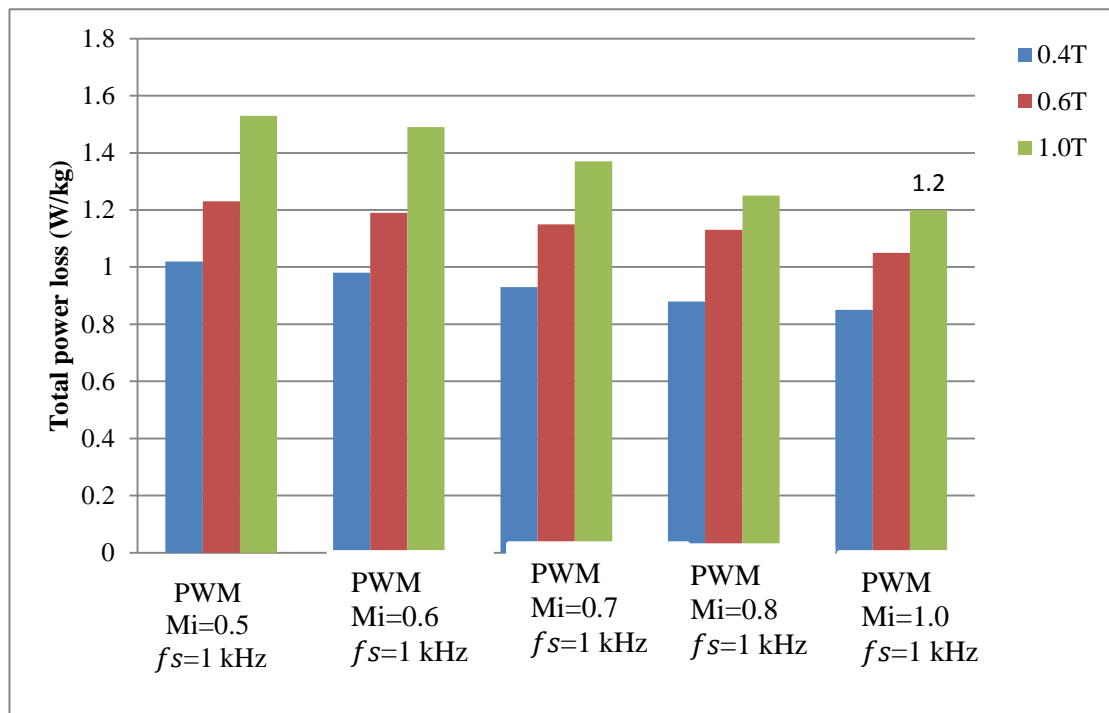


Fig. 7-20 Total power losses of the three-phase transformer core supplied by PWM waveform with change in the modulation index at 1 kHz switching frequency

Investigation of No-load and on-load performance of a model three-phase transformer core operating under sinusoidal and PWM voltage excitation

Fig. 7-20 to Fig 7-22 demonstrate that the total power loss increases with peak flux density. It also illustrates that as the modulation index of the PWM input waveform increases the losses from the core decrease. The highest total power losses when the modulation index is equalled to 0.5, the difference in losses as the modulation index increases becomes less apparent as the core peak flux density was reduced and it could conclude that even at the lower switching frequency of 1 and 2 kHz an increase in excitation modulation index gives rise to a decrease in the core losses.

7.2.5 Total losses with a change in PWM switching frequency

This assortment of graphs show how switching frequency affects the total power loss at various modulation index and peak flux densities at 50Hz fundamental. The graphs showing the effects of switching frequency with changing of modulation index of 0.5, 0.7, and 1.0 can be seen in Fig. 7-23 to Fig 7-24.

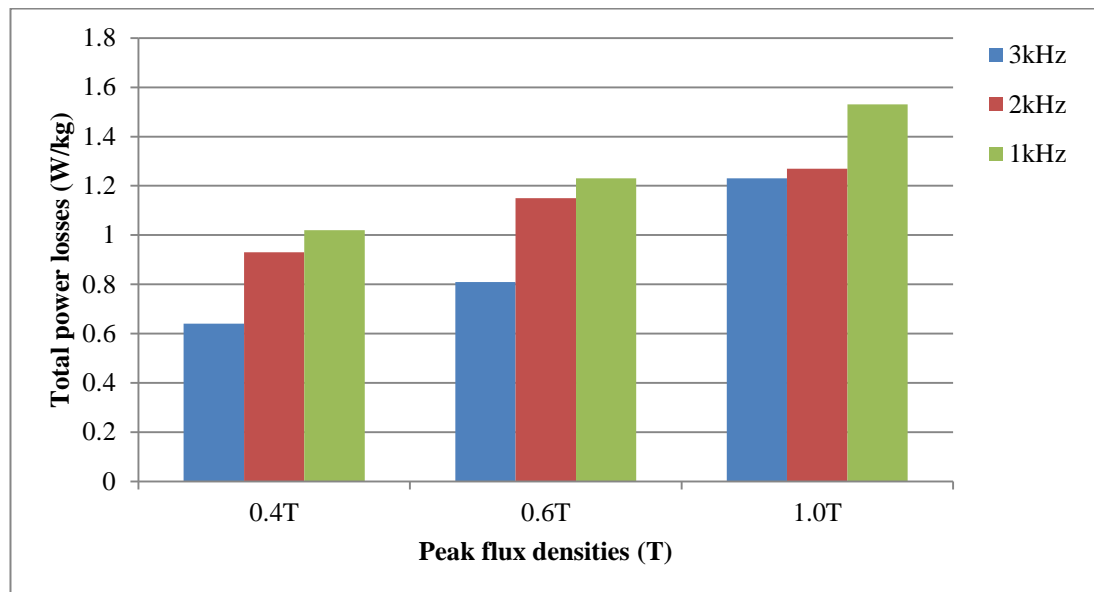


Fig. 7-21 Total power loss of the three-phase transformer core with change in switching frequency at constant modulation index of 0.5

Investigation of No-load and on-load performance of a model three-phase transformer core operating under sinusoidal and PWM voltage excitation

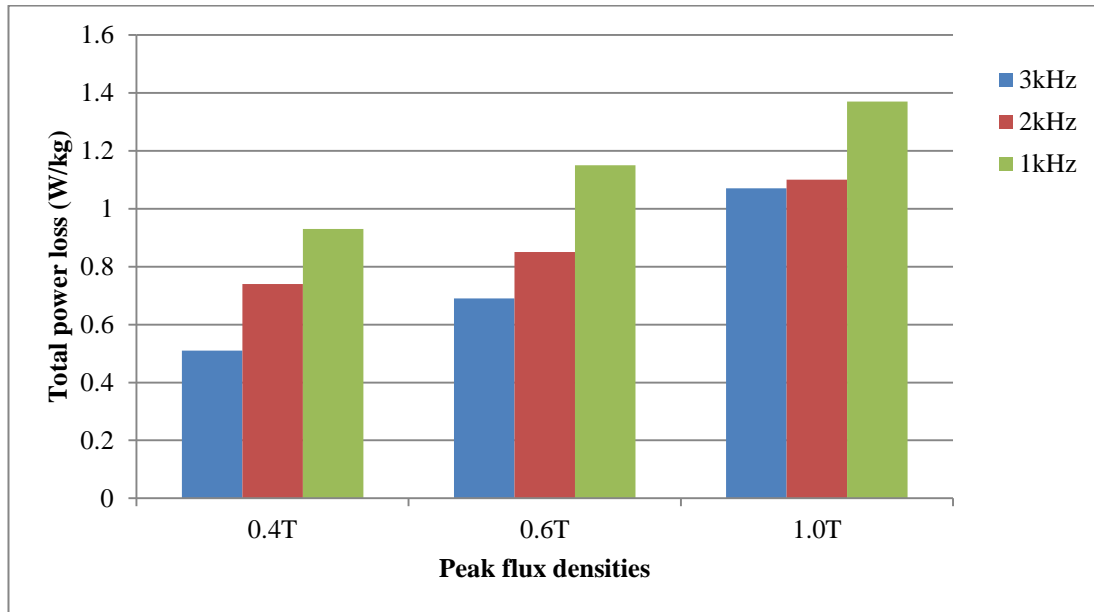


Fig. 7-22 Total power loss of the three-phase transformer core with change in switching frequency at constant modulation index of 0.7

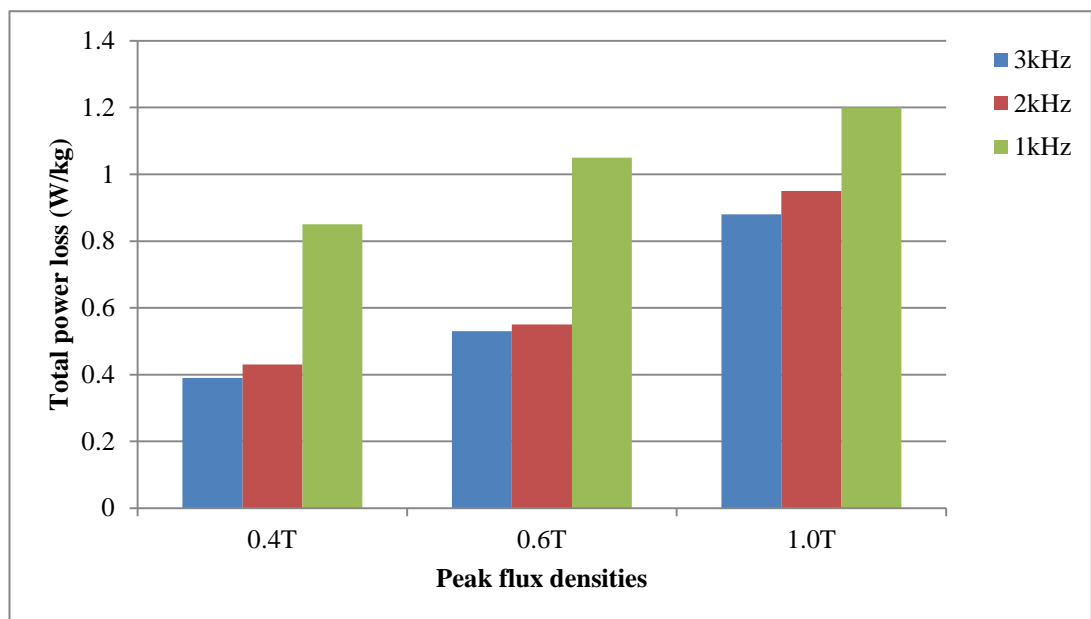


Fig. 7-23 Total power loss of the three-phase transformer core with change in switching frequency at constant modulation index of 1.0

Investigation of No-load and on-load performance of a model three-phase transformer core operating under sinusoidal and PWM voltage excitation

From Fig. 7-23 to Fig. 7-25, the effect of the switching frequency was compared. These graphs show that as the switching frequency is increased the losses of the core are reduced. At the peak flux density of 1.0T, $F_s = 1$ kHz, the loss is 1.20 W/kg this is then reduced by 22% when the switching frequency increased to 2 kHz. Further reduction in losses can be seen when the switching frequency is increased from 2 kHz to 3 kHz. When the flux density is reduced, the losses of the core decrease this could demonstrates that the effect of changing the switching frequency on the core losses is reduced when the peak flux density is reduced. Furthermore, figures exhibit that the core losses with changing switching frequency. The losses are reduced as switching frequency is increased.

By comparing all the graphs, it can be seen that by increasing the switching frequency the losses of the core are decreased. The effect of increasing switching frequency to reduce the core losses, the greatest difference in losses between the sinusoidal excitation and PWM excitation occurs when the lowest switching frequency is applied. The highest switching frequency for a PWM excitation exhibits the least difference in losses compared to the sinusoidal excitation.

7.2.6 Summary

It was found that the modulation index contributed to the largest variation in total power loss caused by PWM excitation. This distorted voltage condition led the three-phase transformer losses of 1.53 W/kg fig 7.22 at the lowest modulation index of 0.5 and a switching frequency of 1 kHz. This occurred when the core was saturated at a peak flux density of 1.0T.

When the modulation index was increased to 1.0 at switching frequency of 3 kHz fig. 7.20 these losses are reduced to 7%. The experimentation shows that as the switching frequency increased from 1 kHz to 3 kHz, the losses decreased.

This chapter has shown that application using transformer excited by PWM inverter can be improved to reduce total power losses, it appears selecting a PWM setting with a modulation index of 1.0 at switching frequency 3 kHz is given the best results.

CHAPTER 8

8. Conclusion and suggestion for future work

8.1.1 Conclusion

In this thesis, magnetic properties of the electrical steel laminations such as flux density distribution, localised and overall power losses, and localised magnetostriction distribution were studied over a wide range of magnetisation. The investigations have shown that these properties strongly depend on the material properties, especially at high frequencies, where localised magnetostriction and flux density along the laminations of the transformer core is distributed almost uniformly. Increasing the magnetising frequency leads to the distribution of the flux density to be non-uniform which increases the core noise. Further, the results showed that the distribution pattern of flux density and localised magnetostriction has strong dependence on the magnetising frequency and relative permeability of the material. Further observations from this investigation are as follows:

1. PWM causes power loss to increase in electrical steels compared to sinusoidal excitation due to the increase in both magnetostriction and vibration of the core. The ratio of loss increase is dependent on operating flux density, and PWM voltage excitation parameters. For example losses of three-phase transformer increased under low switching frequency and low modulation index.
2. Preliminary measurements of P/f against frequency seem to show that hysteresis and eddy current components of loss changes under PWM excitation. The reason for this is expected to be related to the very rapid domain switching which occurs at certain times in the PWM excitation cycle. The variation of specific power losses under PWM flux waveform with different peak flux densities show quadratic relation same as those under sinusoidal excitation.
3. It has been shown that increasing the magnetic flux density causes an increase in power loss and in strain of the core due to the increase in magnetostriction.

Investigation of No-load and on-load performance of a model three-phase transformer core operating under sinusoidal and PWM voltage excitation

4. The result from this investigation suggests that transformer energised by PWM inverter can be improved by selecting a PWM setting with high modulation and high switching frequency which will lead to reduction in power loss.
5. Localised magnetostriction is more significant when a core is operated at high flux density due to increased air gap in the joints.
6. When the core energised under PWM voltage excitation at low flux density, higher core strain is generated from in-plan direction of the lamination on its side surface than from the front and the top surface. However, at high flux density, higher strain is generated from the out of plan direction of the laminations due to an increase of both magnetostriction and magnetic force.
7. The highest strain levels were obtained at the joint and corner areas due to the out of the rolling direction magnetisation that results in high rolling direction of magnetostriction.
8. This research demonstrated that when a transformer core is operated at low 0.4T and 0.6T then higher core noise is generated from in-plan direction of the lamination on its side surface than from the front and the top surface. Whereas, at high flux density of 1T, higher noise is generated from the out-of-plan direction of the laminations due to an increase of both magnetostriction and magnetic force.

8.1.2 Suggestion for future work

The present investigation has given rise to a number of specific areas worthy of future investigation.

1. Further comparison of magnetostriction measurement system would be very useful in order to develop recognised methods to measure magnetostriction. For example, measurement of magnetostriction in the form of Epstein strips under PWM voltage excitation with stress should be carried out. After analysing measurement results, would be good to investigate the PWM parameters, for example modulation index and switching frequency effects on magnetostriction under stress condition.
2. A future study may consider ways in which to reduce the power losses created at higher flux density.
3. Verifying magnetic process under PWM voltage excitation by magnetic domain observation in order to optimise the performance of the transformer core under such complex waveform could be beneficial.
4. Investigation on how magnetic circuit geometries affect power loss under PWM voltage excitation could be considered.
5. Additional study of the core flux distribution is needed to look into the exact effect of the core strain distribution.
6. Geometry-dependent magnetostriction should be investigated because the demagnetisation factor affects magnetostriction, which may cause high errors in calculation of deformation and vibration in transformer core.
7. The performance of magnetostriction and power losses has been investigated on a bare model transformer core operating under PWM voltage excitation. Therefore, if

Investigation of No-load and on-load performance of a model three-phase transformer core operating under sinusoidal and PWM voltage excitation

practically possible future research should continue to determine the influence of windings, oil and tanks etc.

8. Multi- physics model simulating the magnetostriction distribution and magnetic flux density distribution is necessary in order to estimate the effect of magnetostriction on the flux waveform. If the material characteristics are known then specific losses can be estimated from the flux waveforms.

REFERENCES

- [1] D. Jiles, *Introduction to magnetism and magnetic materials*, Third edition. ed.: Boca Raton : CRC Press, Taylor & Francis Group, 2016.
- [2] B. D. Cullity, *Introduction to magnetic materials*, 2nd ed. ed., Hoboken, N.J.: Hoboken, N.J. : Wiley, 2008.
- [3] A. J. Moses, "Opportunities for exploitation of magnetic materials in an energy conscious world," 2002.
- [4] S. E. Zirka, Y. I. Moroz, P. Marketos, and A. J. Moses, "Viscosity-based magnetodynamic model of soft magnetic materials," *IEEE Transactions on Magnetics*, vol. 42, no. 9, pp. 2121-2132, 2006.
- [5] P. Brissonneau, "Non-oriented electrical sheets," *Journal of magnetism and magnetic materials*, vol. 41, no. 1-3, pp. 38-46, 1984.
- [6] P. Baudouin, M. De Wulf, L. Kestens, and Y. Houbaert, "The effect of the guillotine clearance on the magnetic properties of electrical steels," *Journal of Magnetism and Magnetic Materials*, vol. 256, no. 1, pp. 32-40, 2003/01/01/, 2003.
- [7] W. F. Barrett, "On the electrical conductivity and magnetic permeability of various alloys of iron," *Sci. Trans. Royal. Dublin Society*, vol. 67, 1900.
- [8] N. Goss, "New development in electrical strip steels characterized by fine grain structure approaching the properties of a single crystal," *Trans. Amer. Soc. Metals*, vol. 23, no. 1, pp. 511-531, 1935.
- [9] R. Bozorth, "The orientation of crystals in silicon iron," *Trans Am Soc Met*, vol. 23, pp. 1107-1111, 1935.
- [10] K. Detert, "Untersuchungen über eine neue art der sekundärrekristallisation in Fe-3% SI-legierungen," *Acta Metallurgica*, vol. 7, no. 9, pp. 589-598, 1959.
- [11] R. Bozorth, "Basic research and applications in magnetism," *IEEE Transactions on Magnetics*, vol. 5, no. 4, pp. 692-700, 1969.
- [12] F. Assmus, K. Detert, and G. Ibe, "Iron-silicon alloy with cubic structure. II," *Z. Metalik.*, vol. 48, pp. 344-349, 1957.
- [13] S. Taguchi, and A. Sakakura, "Characteristics of Magnetic Properties of Grain-Oriented Silicon Iron with High Permeability," *Journal of Applied Physics*, vol. 40, no. 3, pp. 1539-1541, 1969.
- [14] P. Banks, and E. Rawlinson, "Dynamic magnetostriction and mechanical strain in oriented 3% silicon-iron sheet subject to combined longitudinal and transverse stresses." pp. 1537-1546.

Investigation of No-load and on-load performance of a model three-phase transformer core operating under sinusoidal and PWM voltage excitation

- [15] W. Corner, and J. Mason, "The effect of stress on the domain structure of Goss textured silicon-iron," *British Journal of Applied Physics*, vol. 15, no. 6, pp. 709, 1964.
- [16] E. I. Amoiralis, M. A. Tsili, and A. G. Kladas, "Transformer design and optimization: a literature survey," *IEEE Transactions on Power Delivery*, vol. 24, no. 4, pp. 1999-2024, 2009.
- [17] J. Hodnette, and C. Horstman, "HIPERSIL A NEW MAGNETIC STEEL AND ITS USE IN TRANSFORMERS," *Westinghouse Engineer (East Pittsburgh, Pa.)*, pp. 52-56, 1941.
- [18] W. Swift, and G. Wolfe, "Influence of compressive stress on magnetic properties of a," *IEEE Transactions on Magnetics*, vol. 12, no. 3, pp. 244-248, 1976.
- [19] A. Moses, "Effects of stresses on magnetic properties of silicon-iron laminations," *Journal of materials science*, vol. 9, no. 2, pp. 217-222, 1974.
- [20] B. Thomas, "Flux paths and flux transfer mechanism in the T joints of three phase transformer cores," *IEEE Transactions on Magnetics*, vol. 11, no. 1, pp. 65-71, 1975.
- [21] R. A. Kievit, S. W. Davis, D. J. Mitchell, J. R. Taylor, J. Duncan, L. K. Tyler, C. Brayne, E. Bullmore, A. Calder, and R. Cusack, "Distinct aspects of frontal lobe structure mediate age-related differences in fluid intelligence and multitasking," *Nature communications*, vol. 5, pp. 5658, 2014.
- [22] M. Jones, and A. Moses, "Comparison of the localized power loss and flux distribution in the butt and lap and mitred overlap corner configurations," *IEEE Transactions on Magnetics*, vol. 10, no. 2, pp. 321-326, 1974.
- [23] J. P. Joule, "XVII. On the effects of magnetism upon the dimensions of iron and steel bars," *Philosophical Magazine Series 3*, vol. 30, no. 199, pp. 76-87, 1847.
- [24] F. Wilkins, and A. Drake, "Measurement and interpretation of power losses in electrical sheet steel." pp. 771-785.
- [25] A. Moses, and B. Thomas, "The spatial variation of localized power loss in two practical transformer T-joints," *IEEE Transactions on Magnetics*, vol. 9, no. 4, pp. 655-659, 1973.
- [26] A. Moses, and B. Thomas, "Problems in the design of power transformers," *IEEE Transactions on Magnetics*, vol. 10, no. 2, pp. 148-150, 1974.
- [27] M. H. Kheraluwala, D. Novotny, and D. M. Divan, "Design considerations for high power high frequency transformers." pp. 734-742.

Investigation of No-load and on-load performance of a model three-phase transformer core operating under sinusoidal and PWM voltage excitation

- [28] G. Swift, "Excitation current and power loss characteristics for mitered joint power transformer cores," *IEEE Transactions on Magnetics*, vol. 11, no. 1, pp. 61-64, 1975.
- [29] A. Boglietti, P. Ferraris, M. Lazzari, and F. Profumo, "Iron losses in magnetic materials with six-step and PWM inverter supply (induction motors)," *IEEE Transactions on Magnetics*, vol. 27, no. 6, pp. 5334-5336, 1991.
- [30] K. Overshott, "The use of domain observations in understanding and improving the magnetic properties of transformer steels," *IEEE Transactions on Magnetics*, vol. 12, no. 6, pp. 840-845, 1976.
- [31] F. Brailsford, and V. Mazza, "The alternating magnetic flux distribution in right-angled corners of transformer laminations. An Experimental Investigation," *Proceedings of the IEE-Part A: Power Engineering*, vol. 109, no. 44, pp. 173-180, 1962.
- [32] A. Piercy, "The changing shape of magnetostriction," *Physics Education*, vol. 32, no. 3, pp. 160, 1997.
- [33] A. Moses, and N. Tutkun, "Investigation of power loss in wound toroidal cores under PWM excitation," *IEEE Transactions on Magnetics*, vol. 33, no. 5, pp. 3763-3765, 1997.
- [34] A. Basak, and A. Moses, "Harmonic losses in a three phase transformer core," *IEEE Transactions on Magnetics*, vol. 14, no. 5, pp. 990-992, 1978.
- [35] A. Basak, and A. Qader, "Fundamental and harmonic flux behaviour in a 100 KVA distribution transformer core," *IEEE Transactions on Magnetics*, vol. 19, no. 5, pp. 2100-2102, 1983.
- [36] P. Neurath, "Magnetostriction and domain structure of materials for use in low-noise equipment," *Electrical Engineering*, vol. 73, no. 11, pp. 991-994, 1954.
- [37] C. Brownsey, and G. Maples, "Magnetostriction characteristics of 3.1% grain-oriented silicon-iron transformer steel." pp. 1859-1862.
- [38] P. I. Anderson, A. J. Moses, and H. J. Stanbury, "Assessment of the stress sensitivity of magnetostriction in grain-oriented silicon steel," *IEEE transactions on magnetics*, vol. 43, no. 8, pp. 3467-3476, 2007.
- [39] B. Cullity, and C. Graham, "Ferrimagnetism," *Introduction to Magnetic Materials, Second Edition*, pp. 175-195, 2008.
- [40] M. Bereźnicki, "The influence of skin effect on the accuracy of eddy current energy loss calculation in electrical steel sheets." pp. 1-4.
- [41] N. Imai, "Synchronous motor with permanent magnets and motor system," Google Patents, 1999.

Investigation of No-load and on-load performance of a model three-phase transformer core operating under sinusoidal and PWM voltage excitation

- [42] M. Amar, R. Kaczmarek, and F. Protat, "Prediction of power losses in silicon iron sheets under PWM voltage supply," *Journal of magnetism and magnetic materials*, vol. 133, no. 1-3, pp. 140-143, 1994.
- [43] G. Bertotti, *Hysteresis in magnetism: for physicists, materials scientists, and engineers*: Academic press, 1998.
- [44] D. Jiles, *Introduction to magnetism and magnetic materials*: CRC press, 2015.
- [45] G. Bertotti, "General properties of power losses in soft ferromagnetic materials," *IEEE Transactions on magnetics*, vol. 24, no. 1, pp. 621-630, 1988.
- [46] T. Nakata, Y. Kawase, and M. Nakano, "Improvement of measuring accuracy of magnetic field strength in single sheet testers by using two H coils," *IEEE transactions on magnetics*, vol. 23, no. 5, pp. 2596-2598, 1987.
- [47] T. L. Mthombeni, and P. Pillay, "Lamination core losses in motors with nonsinusoidal excitation with particular reference to PWM and SRM excitation waveforms," *IEEE Transactions on Energy Conversion*, vol. 20, no. 4, pp. 836-843, 2005.
- [48] R. Liu, C. C. Mi, and D. W. Gao, "Modeling of eddy-current loss of electrical machines and transformers operated by pulsewidth-modulated inverters," *IEEE Transactions on Magnetism*, vol. 44, no. 8, pp. 2021-2028, 2008.
- [49] N. Mohan, T. M. Undeland, and W. P. Robbins, "Power Electronics, Converters, Applications, and Design, Hoboken: John Wiley & Sons," Inc, 1989.
- [50] A. Boglietti, P. Ferraris, M. Lazzari, and M. Pastorelli, "Change of the iron losses with the switching supply frequency in soft magnetic materials supplied by PWM inverter," *IEEE Transactions on Magnetism*, vol. 31, no. 6, pp. 4250-4252, 1995.
- [51] B. D. Cullity, and C. D. Graham, *Introduction to magnetic materials*: John Wiley & Sons, 2011.
- [52] R. Albir, and A. Moses, "Improved dc bridge method employed to measure local power loss in electrical steels and amorphous materials," *Journal of Magnetism and Magnetic Materials*, vol. 83, no. 1-3, pp. 553-554, 1990.
- [53] A. Moses, B. Thomas, and J. Thompson, "Power loss and flux density distributions in the T-joint of a three phase transformer core," *IEEE Transactions on Magnetism*, vol. 8, no. 4, pp. 785-790, 1972.
- [54] N. Tutkun, and A. J. Moses, "Measurements of power loss distribution in a typical stator core under PWM voltage excitation," *Journal of magnetism and magnetic materials*, vol. 262, no. 2, pp. 230-234, 2003.

- [55] J. Liu, M. Strangwood, C. L. Davis, and A. J. Peyton, "Magnetic evaluation of microstructure changes in 9Cr-1Mo and 2.25 Cr-1Mo steels using electromagnetic sensors," *Metallurgical and Materials Transactions A*, vol. 44, no. 13, pp. 5897-5909, 2013.
- [56] J. Shilling, and G. Houze, "Magnetic properties and domain structure in grain-oriented 3% Si-Fe," *IEEE Transactions on Magnetics*, vol. 10, no. 2, pp. 195-223, 1974.
- [57] B. Weiser, H. Pfutzner, and J. Anger, "Relevance of magnetostriction and forces for the generation of audible noise of transformer cores," *IEEE Transactions on Magnetics*, vol. 36, no. 5, pp. 3759-3777, 2000.
- [58] S.-T. Wu, S.-C. Mo, and B.-S. Wu, "An LVDT-based self-actuating displacement transducer," *Sensors and actuators A: Physical*, vol. 141, no. 2, pp. 558-564, 2008.
- [59] S. Borucki, T. Boczar, and A. Cichoń, "Technical possibilities of reducing the sound pressure level emitted into the environment by a power transformer," *Archives of Acoustics*, vol. 36, no. 1, pp. 49-56, 2011.
- [60] G. Krishnan, and G. Ananthasuresh, "Evaluation and design of displacement-amplifying compliant mechanisms for sensor applications," *Journal of Mechanical Design*, vol. 130, no. 10, pp. 102304, 2008.
- [61] R. Henshell, P. Bennett, H. McCallion, and M. Milner, "Natural frequencies and mode shapes of vibration of transformer cores." pp. 2133-2139.
- [62] H. Williams, and W. Shockley, "A simple domain structure in an iron crystal showing a direct correlation with the magnetization," *Physical Review*, vol. 75, no. 1, pp. 178, 1949.
- [63] D. Mapps, and C. White, "Magnetostriction harmonics measurement using a double piezoelectric transducer technique," *Journal of Physics E: Scientific Instruments*, vol. 17, no. 6, pp. 472, 1984.
- [64] H. Tariq, A. Takamori, F. Vetrano, C. Wang, A. Bertolini, G. Calamai, R. DeSalvo, A. Gennai, L. Holloway, and G. Losurdo, "The linear variable differential transformer (LVDT) position sensor for gravitational wave interferometer low-frequency controls," *Nuclear Instruments and Methods in Physics Research Section A: Accelerators, Spectrometers, Detectors and Associated Equipment*, vol. 489, no. 1-3, pp. 570-576, 2002.
- [65] R. Birss, G. Keeler, P. Pearson, and R. Potton, "A capacitive instrument for the measurement of a large range of magnetostriction at low temperatures and high magnetic fields," *Journal of Physics E: Scientific Instruments*, vol. 11, no. 9, pp. 928, 1978.
- [66] T. Nakata, N. Takahashi, M. Nakano, K. Muramatsu, and P. Miyake, "Magnetostriction measurements with a laser Doppler velocimeter," *IEEE Transactions on Magnetics*, vol. 30, no. 6, pp. 4563-4565, 1994.

Investigation of No-load and on-load performance of a model three-phase transformer core operating under sinusoidal and PWM voltage excitation

- [67] H. Takaki, and T. Tsuji, "The Measurement of Magnetostriction by means of Strain Gauge," *Journal of the Physical Society of Japan*, vol. 11, no. 11, pp. 1153-1157, 1956.
- [68] A. A. Pitsillides, S. Rawlinson, R. Suswillo, S. Bourrin, G. Zaman, and L. Lanyon, "Mechanical strain-induced NO production by bone cells: a possible role in adaptive bone (re) modeling?," *The FASEB Journal*, vol. 9, no. 15, pp. 1614-1622, 1995.
- [69] P. Joslin, A. Moses, and J. Thompson, "Some aspects of effects of longitudinal and normal stress on power loss and flux distribution within a transformer core." pp. 709-716.
- [70] P. Cooke, M. G. Uranga, and G. Etxebarria, "Regional systems of innovation: an evolutionary perspective," *Environment and planning A*, vol. 30, no. 9, pp. 1563-1584, 1998.
- [71] D. C. Jiles, *Introduction to the electronic properties of materials*: CRC Press, 2001.
- [72] A. Lundgren, "On measurement and modelling of 2D magnetization and magnetostriction of SiFe sheets," Institutionen för elkraftteknik, 1999.
- [73] Z. Wang, B. Deng, and K. Yao, "Physical model of plastic deformation on magnetization in ferromagnetic materials," *Journal of Applied Physics*, vol. 109, no. 8, pp. 083928, 2011.
- [74] B. Truax, "Handbook for Acoustic Ecology. Burnaby," *British Columbia: Cambridge Street Publishing*, 1999.
- [75] M. Balehosur, "Prediction of no-load losses of stacked 3-phase, 3-limb transformer cores," Cardiff University, 2013.
- [76] P. Beckley, "Modern steels for transformers and machines," *Power Engineering Journal*, vol. 13, no. 4, pp. 190-200, 1999.
- [77] T. L. Mthombeni, and P. Pillay, "Physical basis for the variation of lamination core loss coefficients as a function of frequency and flux density." pp. 1381-1387.
- [78] Y. Chen, and P. Pillay, "An improved formula for lamination core loss calculations in machines operating with high frequency and high flux density excitation." pp. 759-766.
- [79] M. Ibrahim, and P. Pillay, "Advanced testing and modeling of magnetic materials including a new method of core loss separation for electrical machines," *IEEE Transactions on Industry Applications*, vol. 48, no. 5, pp. 1507-1515, 2012.

Investigation of No-load and on-load performance of a model three-phase transformer core operating under sinusoidal and PWM voltage excitation

- [80] D. M. Ionel, M. Popescu, S. J. Dellinger, T. Miller, R. J. Heideman, and M. I. McGilp, "On the variation with flux and frequency of the core loss coefficients in electrical machines," *IEEE transactions on industry applications*, vol. 42, no. 3, pp. 658-667, 2006.